New Structure for Moving Horizon Estimators. Application to Space Debris Tracking during the Atmospheric Re-entries

Rata Suwantong

N° d'ordre : 2014-23-TH

SUPELEC

ECOLE DOCTORALE STITS
« Sciences et Technologies de l'Information des Télécommunications et des Systèmes »

THÈSE DE DOCTORAT

DOMAINE : STIC
Spécialité : Automatique

Soutenue le 2 décembre 2014

par :

Rata SUWANTONG

Nouvelle Structure d'Estimateurs à Horizon Glissant. Application à l'Estimation de Trajectoires de Débris Spatiaux Pendant la Rentrée Atmosphérique

Directeur de thèse :	Didier DUMUR	Professeur (SUPELEC)
Co-encadrant de thèse :	Dominique BEAUVOIS	Professeur (SUPELEC)
Co-encadrant de thèse :	Sylvain BERTRAND	Ingénieur de Recherche (ONERA)

Composition du jury :

Président :	Michel ZASADZINSKI	Professeur (Université de Lorraine)
Rapporteurs :	Frédéric KRATZ	Professeur (ENSI de Bourges)
	Nicolas LANGLOIS	Docteur, HDR (ESIGELEC/IRSEEM)
Examinateurs :	Angelo ALESSANDRI	Professore Associato (Università di Genova)
	Hugues MOUNIER	Professeur (LSS-Supélec)

Publications and Communications

Here are the list of the publications and the communications on the results of this work

International Conferences with Proceedings

- Rata Suwantong, Sylvain Bertrand, Didier Dumur, Dominique Beauvois,"Space Debris Trajectory Estimation During Atmospheric Re-entries Using Moving Horizon Estimator," 2012 IEEE 51st Annual Conference on Decision and Control (CDC), p. 1764-1769, Maui, Hawaii, USA, 10-13 December 2012

- Rata Suwantong, Paul Bui Quang, Dominique Beauvois, Didier Dumur, Sylvain Bertrand, "Robustness Analysis of a Moving Horizon Estimator for Space Debris Tracking During Atmospheric Re-entries," 2013 IEEE 52nd Annual Conference on Decision and Control (CDC), p. 5522-5527, Florence, Italy, 10-13 December 2013

- Rata Suwantong, Sylvain Bertrand, Didier Dumur, Dominique Beauvois, "Stability of a Nonlinear Moving Horizon Estimator with Pre-Estimation," American Control Conference (ACC), 2014 , p. 5688-5693, Portland, Oregon, USA, 4-6 June 2014

- Rata Suwantong, Sylvain Bertrand, Didier Dumur, Dominique Beauvois, "Moving Horizon Estimation with Pre-Estimation (MHE-PE) for 3D Space Debris Tracking during Atmospheric Re-entries," 2014 IEEE 53rd Annual Conference on Decision and Control (CDC), Los Angeles, California, USA, 15-17 December 2014

Other Conferences

The author also gave a talk on the results of this work in the following conferences

- "Performance of a Moving Horizon Estimator for Space Debris Tracking during Atmospheric Re-entries," Journée de doctorants de l'ONERA, l'ONERA, Palaiseau, February 2012 and February 2013

- "Performance of a Moving Horizon Estimator for Space Debris Tracking during Atmospheric Re-entries," Journée de doctorants de SUPELEC, SUPELEC, Gif-sur-Yvette, December 2011, December 2012

- "Performance of a Moving Horizon Estimator for Space Debris Tracking during Atmospheric Re-entries," Nonlinear Model Predictive Control (CPNL) Research Group's Meeting, l'ENSTA, Paris, October 2013

- "Development of a Moving Horizon Estimator with Pre-Estimation," Journée de doctorants de SUPELEC), SUPELEC, Gif-sur-Yvette, December 2013

- "Development of a Moving Horizon Estimator with Pre-Estimation. Application to 1D Space Debris Tracking during Atmospheric Re-entries," Journée de doctorants de l'ONERA, l'ONERA, Palaiseau, February 2014

- "Development of a Moving Horizon Estimator. Application to 3D Space Debris Tracking during Atmospheric Re-entries," SUPELEC Commission Automatique, SUPELEC, Gif-sur-Yvette, March 2014

They won't listen. Do you know why? Because they have certain fixed notions about the past. Any change would be blasphemy in their eyes, even if it were the truth. They don't want the truth; they want their traditions.

Isaac Asimov (Pebble in the sky)

To my parents

Remerciements

Je tiens tout d'abord à remercier mon directeur de thèse, Didier Dumur pour ses idées et ses commentaires judicieux et ses compétences théoriques qui m'ont énormément guidée au cours de la thèse. Je remercie également mon co-directeur de thèse, Dominique Beauvois pour toutes ses remarques sur tous les détails auxquels je n'avais jamais pensé et pour ses compétences en filtrage et en applications qui m'ont ramenée aux situations réelles et non purement académiques. Je remercie aussi mon encadrant de l'Onera, Sylvain Bertrand, pour tout son soutien académique et moral, pour sa disponibilité et toutes les heures passées à réfléchir ensemble qui m'ont beaucoup aidée à clarifier mes idées. Je tiens ensuite à remercier mes rapporteurs, Nicolas Langlois et Frédéric Kratz, pour leurs commentaires, qui ont grandement participé à l'amélioration de mon manuscrit. Je remercie aussi les autres membres de mon jury, Angelo Alessandri, tout d'abord pour ses travaux qui m'ont inspirée pour la preuve de la stabilité dans la thèse et Michel Zasadzinski et Hugues Mounier pour leurs commentaires ouvrant d'autres pistes de réflexion pour l'avenir et pour leur gentillesse.

Je remercie aussi mes chers amis spécialistes dans le filtrage particulaire à l'Onera, Christian Musso, Paul Bui Quang et Achille Murangira pour leur amitié, leur écoute et leur soutien non seulement en filtrage mais aussi dans la vie. Je suis aussi reconnaissante envers Mathieu Baslesdent et Loïc Brevault mes amis spécialistes en optimisation pour leur amitié et leur aide. Je remercie aussi Hélène Piet-Lahanier et Julien Marzat pour tous leurs conseils. Je souhaite ensuite à remercier tous mes autres amis de l'Onera sans qui ces trois ans auraient été beaucoup moins sympathiques. Je tiens aussi à remercier ma famille en Thaïlande pour tout son soutien. Enfin, je voudrais remercier Damien Jacquemart, professionnellement pour toute son aide en mathématique et pour son lemme 1 sans lequel je n'aurais pas pu finir la preuve de la stabilité du MHE-PE et non professionnellement pour m'avoir donné une vie de thésarde heureuse et pour ses pâtes carbo, ses daubes et ses crumbles poire-chocolat qui m'ont donné de l'énergie pour la thèse au cours de ces trois années.

Contents

Nomenclature

Résumé en Français

Introduction

Contexte : Intérêts de l'Estimation de Trajectoires de Débris Spatiaux pendant la Rentrée Atmosphérique

Les orbites terrestres sont de nos jours très polluées par de nombreux débris spatiaux venant de nos activités spatiales. D'après une évaluation récente [NASA, 2012], on comptabilise en orbite terrestre environ 23000 débris d'un diamètre supérieur à 10 cm, 500000 entre 1 et 10 cm et plus de 100 millions plus petits qu'un centimètre. Les dangers relatifs aux débris spatiaux sont les suivants:

1. Si la densité de débris en orbite terrestre dépasse un seuil critique [Kessler et al., 2010], une cascade de collisions entre débris est à prévoir. Cette cascade de collision, appelée "effet de Kessler", induira une croissance exponentielle du nombre de débris et créera une ceinture de débris qui empêchera d'utiliser l'espace pendant plusieurs générations. Ce phénomène affectera alors de façon dramatique les technologies de navigation, la télécommunication, la surveillance, l'observation terrestre et la météorologie.

2. Les débris spatiaux peuvent détruire les satellites opérationnels, les vaisseaux spatiaux et la station spatiale internationale, du fait de leurs grandes vitesses de l'ordre de 10 km/s.

3. Il y a des risques de rentrées de grands objets dans l'atmosphère terrestre. En effet, de plus en plus de débris pénètrent dans l'atmosphère. D'une part à cause des projets liés à l'enlèvement de débris et, d'autre part, à cause de la politique des agences spatiales internationales demandant aux satellites en orbite basse de dévier leurs trajectoires en fin de vie et de rentrer dans l'atmosphère.

Pour éviter tous ces dangers relatifs aux débris spatiaux, il s'avère nécessaire d'enlever des débris, de prédire et d'éviter de nouvelles collisions et de prédire la rentrée des grands objets. Pour cela, les trajectoires de débris doivent être estimées précisément.

Ces travaux ont pour objectifs d'estimer les trajectoires de débris pendant la rentrée atmosphérique, ce qui est un problème réputé difficile. En effet, pendant la rentrée, la dynamique des débris n'est pas précisément connue [Mehrholz et al., 2002][Klinkrad, 2006]. Dans cette étude, l'estimation des trajectoires de débris est réalisée à partir de mesures radar sur la distance et les angles d'élévation et d'azimut entre le débris et la station radar.

Difficultés liés à l'Estimation des Trajectoires de Débris pendant la Rentrée Atmosphérique

Les difficultés liées à l'estimation des trajectoires de débris pendant la rentrée sont les suivantes:

1. Les mesures disponibles pour l'estimation des trajectoires sont bruitées. De ce fait, il est nécessaire d'avoir recours à un estimateur afin d'obtenir une meilleure précision des estimées.

2. Pour implémenter un estimateur, un modèle de la dynamique du débris (modèle d'estimation) doit être défini. Cependant, la dynamique du débris est mal connue due à l'évolution inconnue de son coefficient balistique, décrivant la résistance du débris contre la trainée. Cette dynamique inconnue du débris peut induire une erreur de modèle potentiellement importante. Ainsi, tout estimateur choisi pour ce problème doit être robuste vis-à-vis d'erreurs de modèle.

3. Il est possible que le débris se désintègre en plusieurs morceaux pendant la rentrée. Dans ce cas, il est impossible de prédire les caractéristiques du débris (masse, taille) à l'avance, induisant une erreur non négligeable lors de l'initialisation des algorithmes. Un estimateur choisi pour ce problème doit donc être robuste vis-à-vis d'une mauvaise initialisation également.

État de l'Art portant sur l'Estimation de Trajectoires pendant la Rentrée Atmosphérique

Les travaux existants sur l'estimation des trajectoires pendant la rentrée atmosphérique concernent uniquement des objets militaires [Farina et al., 2002][Austin and Leondes, 1981][Liu et al., 2005][Ristic et al., 2003]. Dans [Ristic et al., 2003], les performances de trois estimateurs classiques, à savoir le filtre de Kalman étendu (EKF), le filtre de Kalman sans odeur (UKF) et le filtre particulaire régularisé (RPF) ont été étudiées pour l'estimation de trajectoires d'objets militaires pendant la rentrée atmosphérique dont le coefficient balistique est inconnu mais quasi-constant en réalité. Le modèle d'estimation utilisé dans [Farina et al., 2002] suppose que le coefficient balistique d'objets militaire est constant durant une période d'échantillonnage. Ce modèle a donc n'a pas d'erreur de modèle important dans le cas d'un objet militaire.

Dans les travaux précédemment cités, l'EKF et l'UKF donnent des erreurs d'estimation importantes tandis que le RPF donne des erreurs d'estimation égales aux bornes de Cramer-Rao a posteriori qui sont les plus petites valeurs possibles pour un estimateur non biaisé. Néanmoins, le filtre particulaire est connu pour être sensible à une mauvaise initialisation et aux erreurs de modèle [Rawlings and Bakshi, 2006]. Par conséquent, l'EKF, l'UKF et le RPF ne semblent pas adaptés à l'estimation de trajectoires de débris pendant la rentrée, phase durant laquelle une erreur de modèle importante peut être présente. De ce fait, un autre estimateur doit être développé pour notre problème. L'estimateur à horizon glissant (MHE) [Rao et al., 2003][Alessandri et al., 2010] pourrait être un candidat potentiel pour l'estimation de trajectoires de débris pendant la rentrée du fait de sa robustesse vis-à-vis d'une mauvaise initialisation et d'une erreur de modèle [Haseltine and Rawlings, 2005][Ungarala, 2009].

Estimateur à Horizon Glissant (MHE)

Le MHE calcule une estimée à l'instant courant en résolvant un problème d'optimisation fondé sur la connaissance d'un certain nombre de mesures les plus récentes. La fenêtre de mesures est appelée "horizon". La fonction coût du MHE est traditionnellement décrite par une norme de la différence entre les mesures réelles et les mesures prédites sur l'horizon, une norme du bruit d'état sur l'horizon et une norme de la différence entre l'estimée au début de l'horizon et une estimée a priori au début de l'horizon. Le dernier terme de la fonction coût est souvent appelé "coût d'arrivée" [Haseltine and Rawlings, 2005][Liu, 2013][Zavala, 2008]. Dès qu'une nouvelle mesure est disponible, la mesure la plus ancienne sur l'horizon est éliminée et l'horizon est décalé d'un pas de temps en avance.

Comme le MHE fait intervenir une méthode d'optimisation, il n'est pas nécessaire de linéariser le système et le MHE permet la prise en compte de contraintes directement lors de l'optimisation. De plus, la stabilité de la dynamique de l'erreur d'estimation du MHE a été démontrée dans le cas du MHE pour des systèmes linéaires et non linéaires [Alessandri et al., 2008][Alessandri et al., 2010]. Néanmoins, le MHE peut nécessiter un temps de calcul important à cause du grand nombre de paramètres à optimiser qui sont l'estimée initiale au début de l'horizon et les estimées des bruits d'état sur l'horizon. De ce fait, le MHE n'est pas encore adapté à l'estimation de trajectoires de débris en temps réel. Nous allons nous focaliser sur la diminution du temps de calcul dans le contexte de la stratégie à horizon glissant.

Estimateur à Horizon Glissant avec Pré-Estimation (MHE-PE)

Nous nous intéressons alors au développement d'une stratégie à horizon glissant nécessitant moins de temps de calcul par rapport à la stratégie classique. Pour ce faire, nous allons modifier sa formulation plutôt que de modifier la méthode d'optimisation. L'interêt de la nouvelle stratégie développée est qu'elle pourra être combinée avec des méthodes d'optimisation rapides et adaptées pour le MHE pour réduire encore plus le temps de calcul. De telles méthodes sont exposées dans la littérature dans [Ferreau et al., 2012][Zavala, 2008].

Une telle stratégie a été proposée pour un système linéaire à temps discret dans [Sui et al., 2010]. Elle a été baptisée Estimateur à Horizon Glissant avec un Observateur Pré-Estimant (Moving Horizon Estimator with a Pre-Estimating Observer). Dans cette stratégie, l'erreur de modèle est compensée par l'utilisation d'un observateur auxiliaire. Un observateur désigne ici un estimateur dont les erreurs d'estimation convergent asymptotiquement vers zéro pour un système sans bruit. De plus, si un observateur est initialisé avec l'état vrai alors son erreur d'estimation est nulle à tout instant. L'Estimateur à Horizon Glissant avec un Observateur Pré-Estimant n'a pas besoin d'estimer la séquence de bruits d'état sur l'horizon comme le MHE classique. L'estimée initiale au début de l'horizon devient le seul paramètre à optimiser. Il utilise donc moins de temps de calcul par rapport au MHE classique et semble intéressant pour notre problème d'estimation de trajectoires de débris.

Cependant, la dynamique de débris pendant la rentrée est fortement non linéaire. Il est donc nécessaire de développer une stratégie similaire à celle proposée dans [Sui et al., 2010] pour un système non linéaire à temps discret. Il est également intéressant d'étendre les travaux de [Sui et al., 2010] à une stratégie qui utilise un estimateur auxiliaire, comme par exemple l'EKF, plutôt qu'un observateur auxiliaire sachant qu'il n'est toujours pas possible de trouver un estimateur au problème. Pour généraliser, nous appellerons notre

structure MHE avec estimateur auxiliaire, que nous nommerons “Estimateur à Horizon Glissant avec Pré-Estimation” (MHE-PE).

Objectifs de la Thèse

Les travaux de cette thèse consistent donc à :

1. Développer un estimateur à horizon glissant avec pré-estimation (MHE-PE) pour un système non linéaire permettant d'obtenir des estimées de grande précision, robuste vis-à-vis d'une mauvaise initialisation et d'une erreur de modèle et moins coûteux en temps de calcul par rapport à une stratégie classique du MHE. Nous allons également démontrer la stabilité de la dynamique de l'erreur d'estimation du MHE-PE.
2. Valider la nouvelle stratégie MHE développé dans le cadre de l'estimation de trajectoires de débris spatiaux pendant la rentrée.

Plan du Résumé de la Thèse

Le résumé de la thèse est structuré de la façon suivante :

Partie 1 Description de la dynamique des débris pendant la rentrée, de l'équation de mesures radar et des modèles d'estimation.

Partie 2 Formulation de l'estimateur à horizon glissant (MHE) classique est énoncé du théorème assurant la stabilité de la dynamique de l'erreur d'estimation.

Partie 3 Étude des performances du MHE classique dans le cadre de l'estimation de trajectoires de débris pendant la rentrée dans un cas à 1 dimension, en termes de précision des estimées, temps de calcul et robustesse vis-à-vis d'une erreur de modèle et d'une mauvaise initialisation, afin d'analyser si la stratégie à horizon glissant est adaptée au problème.

Partie 4 Développement d'une nouvelle stratégie d'estimation à horizon glissant conservant la robustesse et la précision des estimées du MHE classique mais nécessitant moins de temps de calcul.

Partie 5 Étude des performances de la stratégie à horizon glissant développée pour l'estimation des trajectoires de débris pendant la rentrée à 3 dimensions.

Partie 6 Conclusions et perspectives.

0.1 Contexte de l'estimation de trajectoires de Débris pendant la Rentrée Atmosphérique

Cette partie a pour objectif de décrire la dynamique des débris pendant la rentrée atmosphérique ainsi que l'équation de mesures radar. Nous y détaillons également les modèles d'estimation qui seront utilisés.

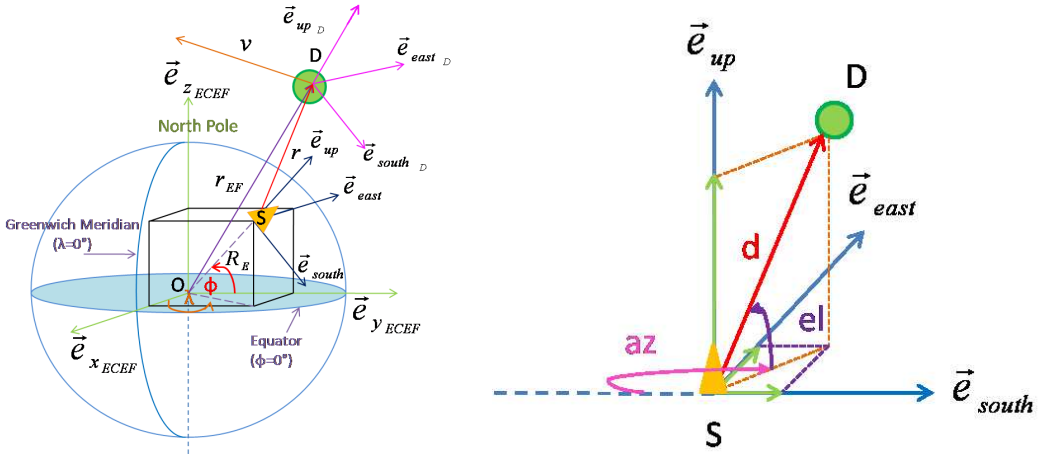

Figure 0.1: *Coordonnées ECEF, SEU et SEU_D en vert, bleu et rose respectivement. S: station radar, D: débris, O: centre de la Terre (gauche). Illustration des mesures radar (droite).*

0.1.1 Difficultés de l'Estimation des Trajectoires de Débris pendant la Rentrée Atmosphérique

0.1.1.1 Dynamique des Débris

Considérons un débris lorsqu'il rentre directement sur Terre. Dans cette étude, nous supposons que :

1. la rentrée est suffisamment rapide pour pouvoir négliger la rotation de la Terre,
2. les seules forces s'exerçant sur le débris sont la force gravitationnelle et la trainée, correspond à la force aérodynamique dans la direction opposée de la vitesse de l'objet. Cette hypothèse est réaliste pour un débris ayant un axe de symétrie, d'où la force aérodynamique se réduit à la seule composante opposée à la vitesse (trainée), et évoluant à une altitude plus petite que 120 km.

Définissons les coordonnées ECEF centrées au centre de la Terre O, la Terre étant fixe, et ayant les axes $\vec{e}_{x_{ECEF}}$, $\vec{e}_{y_{ECEF}}$ et $\vec{e}_{z_{ECEF}}$ comme vecteurs unitaires, voir figure 0.1. Soient D le centre de masse du débris, $\vec{OD}$ le vecteur, traduisant la distance entre le débris et le centre de la Terre et $\mathbf{r}_{EF}$ le vecteur $\vec{OD}$ décrit dans les coordonnées ECEF:

$$\mathbf{r}_{EF} = \vec{OD} = r_{x_{ECEF}} \cdot \vec{e}_{x_{ECEF}} + r_{y_{ECEF}} \cdot \vec{e}_{y_{ECEF}} + r_{z_{ECEF}} \cdot \vec{e}_{z_{ECEF}} \tag{1}$$

Soient $\mathbf{v}_{EF}$ et $\mathbf{a}_{EF}$ les vecteurs vitesse et accélération du débris dans les coordonnées ECEF respectivement. On a alors :

$$\mathbf{a}_{EF} = \dot{\mathbf{v}}_{EF} = \ddot{\mathbf{r}}_{EF} \tag{2}$$

Définissons H l'altitude du débris qui est une fonction de la position du débris $\mathbf{r}_{EF}$ et du rayon terrestre R_E, de la forme suivante :

$$H(\mathbf{r}_{EF}(t)) = \|\mathbf{r}_{EF}(t)\| - R_E \tag{3}$$

La dynamique du débris est donnée par la relation :

$$\mathbf{a}_{EF}(t) = -\frac{GM}{\|\mathbf{r}_{EF}(t)\|^3}\mathbf{r}_{EF}(t) - \frac{\rho(H(\mathbf{r}_{EF}(t)))C_D(t)A(t)}{2m(t)}\|\mathbf{v}_{EF}(t)\|\mathbf{v}_{EF}(t) \tag{4}$$

Le premier terme du membre de droite de (4) représente la gravité et le deuxième terme représente l'accélération due à la trainée. G est la constante gravitationnelle de la Terre, M est la masse de la Terre, m, a et C_D sont la masse, la section et le coefficient de trainée du débris respectivement. La densité atmosphérique ρ dépend de l'altitude H et est modélisée par :

$$\rho(H(t)) = \mathsf{c}_1 e^{-\mathsf{c}_2 H(t)} \tag{5}$$

$\mathsf{c}_1 = 1,227\ kg/m^3$, $\mathsf{c}_2 = 1,093 \cdot 10^{-4}\ m^{-1}$ pour $H < 9144\ m$ et $\mathsf{c}_1 = 1,754\ kg/m^3$, $\mathsf{c}_2 = 1,490 \cdot 10^{-4}\ m^{-1}$ pour $H \geq 9144\ m$ [Farina et al., 2002].

Les variations de m, a et C_D dans le temps sont complexes et généralement difficiles à calculer. Il est donc intéressant de définir une nouvelle variable rassemblant ces trois inconnues. Cette variable est appelée "le coefficient balistique" de l'objet $\beta \in \mathbb{R}^{+*}$, défini par :

$$\beta(t) = \frac{m(t)}{A(t) \cdot C_D(t)}, \tag{6}$$

En combinant (5) et (6), la dynamique du débris s'écrit sous la forme:

$$\mathbf{a}_{EF}(t) = -\frac{GM}{\|\mathbf{r}_{EF}(t)\|^3}\mathbf{r}_{EF}(t) - \frac{\rho(H(\mathbf{r}_{EF}(t)))}{2\beta(t)}\|\mathbf{v}_{EF}(t)\|\mathbf{v}_{EF}(t) \tag{7}$$

Les seuls travaux existant sur l'estimation de trajectoires d'objets pendant la rentrée atmosphérique concernent des objets militaires [Farina et al., 2002][Liu et al., 2005][Ristic et al., 2003]. Le coefficient balistique β d'un objet militaire est presque constant pendant la rentrée. En revanche, pour un débris, β a une évolution inconnue et une hypothèse sur sa dynamique doit être faite dans le modèle d'estimation. Ceci peut engendrer une erreur de modèle importante, ce qui constitue la première difficulté dans l'estimation de trajectoire de débris pendant la rentrée.

0.1.1.2 Mesures Radar Bruitées

Soient λ et ϕ la longitude et la latitude de la station radar respectivement, S le centre de la station radar, $\vec{SD}$ le vecteur caractérisant la distance entre le débris et la station radar et $\vec{e}_{south}$, $\vec{e}_{east}$, $\vec{e}_{up}$ les vecteurs unitaires suivants les directions sud, est et verticale dirigée vers le haut respectivement, voir figure 0.1. Définissons également les coordonnées SEU qui sont des coordonnées locales liées à la station radar avec les axes $\vec{e}_{south}$, $\vec{e}_{east}$, $\vec{e}_{up}$ comme vecteurs unitaires, et $\mathbf{r}$ le vecteur $\vec{SD}$ dans les coordonnées SEU de la façon suivante:

$$\mathbf{r} = \vec{SD} = r_x\vec{e}_{south} + r_y\vec{e}_{east} + r_z\vec{e}_{up} \tag{8}$$

ou de façon équivalente $\mathbf{r} = \begin{pmatrix} r_x & r_y & r_z \end{pmatrix}^T$. La relation entre $\mathbf{r}$ et $\mathbf{r}_{EF}$ est décrite comme suit :

$$\mathbf{r} = \begin{pmatrix} sin\phi cos\lambda & sin\phi sin\lambda & -cos\lambda \\ -sin\lambda & cos\lambda & 0 \\ cos\phi cos\lambda & cos\phi sin\lambda & sin\phi \end{pmatrix} \mathbf{r}_{EF} - \begin{pmatrix} 0 \\ 0 \\ R_E \end{pmatrix} \tag{9}$$

Définissons $\mathbf{v}$ et $\mathbf{a}$ comme étant la vitesse et l'accélération du débris dans les coordonnées SEU respectivement. Ces vecteurs peuvent être calculés à partir de $\mathbf{v}_{EF}$ et $\mathbf{a}_{EF}$ en dérivant (9).

La trajectoire de débris sera estimée à partir de mesures radar bruitées de la distance d entre le débris et la station, de l'angle el d'élévation (angle entre le vecteur $\vec{SD}$ et le plan du sol) et de l'angle az d'azimuth (angle entre la direction du nord $-\vec{e}_{south}$ et la projection

du vecteur $\vec{SD}$ sur sol). Les mesures radar sont supposées être disponibles toutes les T_s secondes. Définissons $\mathbf{r}_k = \mathbf{r}(t = kT_s)$, $k \in \mathbb{N}$. Le vecteur de mesures en temps discret à l'instant k s'écrit :

$$y_k = \begin{pmatrix} d_k^m \\ el_k^m \\ az_k^m \end{pmatrix} = \begin{pmatrix} d_k \\ el_k \\ az_k \end{pmatrix} + v_k = \begin{pmatrix} \sqrt{r_{x_k}^2 + r_{y_k}^2 + r_{z_k}^2} \\ \arcsin(\frac{r_{z_k}}{d_k}) \\ \arctan(\frac{r_{y_k}}{-r_{x_k}}) \end{pmatrix} + v_k \tag{10}$$

où l'exposant m signifie "mesuré", et où :

$$d_k = \sqrt{r_{x_k}^2 + r_{y_k}^2 + r_{z_k}^2} \tag{11}$$

$$el_k = \begin{cases} \arcsin(\frac{r_{z_k}}{d_k}) & \text{si } r_{z_k} \neq d_k \\ \frac{\pi}{2} & \text{sinon} \end{cases} \tag{12}$$

$$az_k = \arctan(\frac{r_{y_k}}{-r_{x_k}}) \tag{13}$$

el_k doit être égal à $\pi/2$ lorsque $r_{z_k} = d_k$ pour que l'équation de mesure h soit $\mathcal{C}^2$. Cette propriété de régularité sera nécessaire pour la suite. v_k est un bruit de mesure modélisé par un bruit blanc borné de moyenne nulle et de matrice de covariance:

$$R = \begin{pmatrix} \sigma_d^2 & 0 & 0 \\ 0 & \sigma_{el}^2 & 0 \\ 0 & 0 & \sigma_{az}^2 \end{pmatrix} \tag{14}$$

où σ_d, σ_{el} et σ_{az} sont les écart types associés au bruit de mesures.

0.1.1.3 Fragmentation d'un Débris pendant la Rentrée

Il se peut que pendant la rentrée les débris se fragmentent en plusieurs morceaux du fait de la chaleur. Ce phénomène, appelé "breakup" en anglais, se produit à une altitude d'environ 80 km. Dans ce cas, certaines caractéristiques des débris, comme par exemple la masse et la section, ne pourront pas être prédites à l'avance. De ce fait, le coefficient balistique initial peut être mal connu et l'algorithme d'estimation peut être mal initialisé.

Pour résumer, l'estimateur qui sera utilisé lors de l'estimation des trajectoires de débris pendant la rentrée doit donc être robuste non seulement à l'erreur de modèle mais aussi à une mauvaise initialisation.

Considérons maintenant deux modèles d'estimation qui seront utilisés pour l'estimation de trajectoires de débris. L'un, proposé dans [Ristic et al., 2003], inclut le coefficient balistique dans le vecteur d'état. L'autre, que nous proposons dans cette étude, inclut l'accélération dans le vecteur d'état.

0.1.2 Modèles d'Estimation

Les deux modèles d'estimation considérés incluent la position et la vitesse du débris dans le repère SEU (le repère local lié à la station radar). On suppose que le débris est suffisamment proche de la station radar pour que la Terre puisse être considérée comme étant plate. De ce fait on a $H = r_z$ et la gravité est considérée constante pointée vers le sol avec une norme $g_E = 9.81\ m/s^2$. Examinerons tout d'abord le modèle incluant le coefficient balistique dans le vecteur d'état.

0.1.2.1 Modèle d'Estimation avec le Coefficient Balistique comme Variable d'Etat

Dans ce modèle le vecteur d'état en temps continu se définit au temps t par :

$$x(t) = \begin{pmatrix} \mathbf{r}(t)^T & \mathbf{v}(t)^T & \beta(t) \end{pmatrix}^T$$

On suppose que la dérivée de $\beta(t)$ est engendrée par un bruit blanc de moyenne nulle w_β de densité spectrale constante q_β. De ce fait :

$$\begin{aligned} \mathbf{a}(t) &= -\frac{1}{2}\frac{\rho(r_z(t))}{\beta(t)} \|\mathbf{v}(t)\| \mathbf{v}(t) - \begin{pmatrix} 0 \\ 0 \\ g_E \end{pmatrix} \\ \dot{\beta}(t) &= w_\beta(t) \end{aligned} \tag{15}$$

Il s'avère cependant plus simple d'implanter l'estimateur en discret sachant que les mesures sont disponibles en temps discret. Définissons $\mathbf{r}_k$, $\mathbf{v}_k$ et β_k les valeurs de $\mathbf{r}(t)$, $\mathbf{v}(t)$ et $\beta(t)$ aux instants $t = kT_s$, pour $k \in \mathbb{N}$. T_s est la période d'échantillonnage choisie égale à la période de mesures. Faisons alors l'hypothèse que $\forall t[kT_s, (k+1)T_s]$, on a $\dot{\mathbf{v}}(t) = \mathbf{a}_k + \mathbf{w}_a(t)$ où :

$$\mathbf{a}_k = -\frac{1}{2}\frac{\rho(r_{z_k})}{\beta_k} \|\mathbf{v}_k\| \mathbf{v}_k - \begin{pmatrix} 0 \\ 0 \\ g_E \end{pmatrix} \tag{16}$$

et $\mathbf{w}_a(t)$ est un vecteur de bruit blanc en temps continu, représentant l'erreur de discrétisation, de densité spectrale constante $\mathbf{q}_a$. On suppose également que les composantes de w_a sont non corrélés. De ce fait, $\mathbf{q}_a = \text{diag}\begin{pmatrix} q_{a_x} & q_{a_y} & q_{a_z} \end{pmatrix}$ où q_{a_x}, q_{a_y} et q_{a_z} sont des constantes. Le modèle d'estimation en discret s'écrit :

$$x_{k+1} = \begin{pmatrix} \mathbf{r}_{k+1} \\ \mathbf{v}_{k+1} \\ \beta_{k+1} \end{pmatrix} = \begin{pmatrix} \mathbf{r}_k + \mathbf{v}_k T_s + \mathbf{a}_k \dfrac{T_s^2}{2} \\ \mathbf{v}_k + \mathbf{a}_k T_s \\ \beta_k \end{pmatrix} + w_k \tag{17}$$

w_k est un vecteur de bruit blanc en temps discret de moyenne nulle et de matrice de covariance:

$$Q = \begin{pmatrix} \dfrac{T_s^3}{3}\mathbf{q}_a & \dfrac{T_s^2}{2}\mathbf{q}_a & \mathbf{0}_{3\times 1} \\ \dfrac{T_s^2}{2}\mathbf{q}_a & T_s\mathbf{q}_a & \mathbf{0}_{3\times 1} \\ \mathbf{0}_{1\times 3} & \mathbf{0}_{1\times 3} & q_\beta T_s \end{pmatrix} \tag{18}$$

0.1.2.2 Modèles d'Estimation avec l'accélération comme Variable d'Etat

Le vecteur d'état en continu pour ce modèle au temps t, $x(t)$, est défini par

$$x(t) = \begin{pmatrix} \mathbf{r}(t)^T & \mathbf{v}(t)^T & \mathbf{a}(t)^T \end{pmatrix}^T \tag{19}$$

Définissons le vecteur d'état en temps discret $x_k = x(t = kT_s)$. Supposons $\forall t \in [kT_s, (k+1)T_s]$, $\dot{\mathbf{a}}(t) = \mathbf{f}_k + \boldsymbol{\xi}(t)$ où $\mathbf{f}_k \triangleq \dot{\mathbf{a}}(t)|_{\beta=cte, t=kT_s}$. En écrivant $\mathbf{f}_k \triangleq \begin{pmatrix} f_{x_k} & f_{y_k} & f_{z_k} \end{pmatrix}^T$, on obtient :

$$f_{x_k} = -\mathsf{c}_2 a_{x_k} v_{z_k} + a_{x_k}\left[a_{x_k}\left(\frac{1}{v_{x_k}} + \frac{v_{x_k}}{\|\mathbf{v}_k\|^2}\right) + a_{y_k}\frac{v_{y_k}}{\|\mathbf{v}_k^2\|} + a_{z_k}\frac{v_{z_k}}{\|\mathbf{v}_k\|^2}\right] \tag{20}$$

$$f_{y_k} = -\mathsf{c}_2 a_{y_k} v_{z_k} + a_{y_k}\left[a_{x_k}\frac{v_{x_k}}{\|\mathbf{v}_k\|^2} + a_{y_k}\left(\frac{1}{v_{y_k}} + \frac{v_{y_k}}{\|\mathbf{v}_k\|^2}\right) + a_{z_k}\frac{v_{z_k}}{\|\mathbf{v}_k\|^2}\right] \tag{21}$$

$$f_{z_k} = \left(-\mathsf{c}_2 v_{z_k} + \left[a_{x_k}\frac{v_{x_k}}{\|\mathbf{v}_k\|^2} + a_{y_k}\frac{v_{y_k}}{\|\mathbf{v}_k\|^2} + a_{z_k}\left(\frac{1}{v_{z_k}} + \frac{v_{z_k}}{\|\mathbf{v}_k\|^2}\right)\right]\right)(a_{z_k} + g_E) \tag{22}$$

$\boldsymbol{\xi}(t)$ est un bruit blanc continu de moyenne nulle de densité spectrale $\tilde{\mathbf{q}}$ représentant non seulement l'erreur de discrétisation mais aussi l'erreur due au fait que β n'est pas constant en réalité. Cela implique que $E\{\boldsymbol{\xi}(t)\boldsymbol{\xi}^T(\tau)\} = \tilde{\mathbf{q}}(t)\delta(t-\tau)$. Supposons ensuite que $\tilde{\mathbf{q}}(t) = \tilde{\mathbf{q}}$, $\forall t$ et que les composantes de $\boldsymbol{\xi}$ sont décorrélées. $\tilde{\mathbf{q}}$ peut donc s'écrire sous la forme $\tilde{\mathbf{q}} = \text{diag}\begin{pmatrix}\tilde{q}_x & \tilde{q}_y & \tilde{q}_z\end{pmatrix}$ où $\tilde{q}_x$, $\tilde{q}_y$ et $\tilde{q}_z$ sont des constantes.

Le modèle d'estimation en temps continu pour $\forall t \in [kT_s, (k+1)T_s]$ est donc

$$\begin{aligned}\ddot{\mathbf{r}}(t) &= \dot{\mathbf{v}}(t) = \mathbf{a}(t) = -\frac{\mathsf{c}_1 e^{-\mathsf{c}_2 r_z(t)}\,\|\mathbf{v}(t)\|}{2\beta(t)}\mathbf{v}(t) + \begin{pmatrix}0\\0\\-g_E\end{pmatrix}\\ \dot{\mathbf{a}}(t) &= \mathbf{f}_k + \boldsymbol{\xi}(t)\end{aligned} \tag{23}$$

En intégrant (23) sur une période d'échantillonnage, on obtient le modèle d'estimation en temps discret sous la forme

$$x_{k+1} = \begin{pmatrix}\mathbf{I}_{3\times3} & T_s\mathbf{I}_{3\times3} & \frac{T_s^2}{2}\mathbf{I}_{3\times3}\\ \mathbf{0}_{3\times3} & \mathbf{I}_{3\times3} & T_s\mathbf{I}_{3\times3}\\ \mathbf{0}_{3\times3} & \mathbf{0}_{3\times3} & \mathbf{I}_{3\times3}\end{pmatrix}x_k + \begin{pmatrix}\frac{T_s^3}{6}\mathbf{f}_k\\ \frac{T_s^2}{2}\mathbf{f}_k\\ T_s\mathbf{f}_k\end{pmatrix} + w_k \tag{24}$$

où w_k est un bruit blanc discret de moyenne nulle et de matrice de covariance

$$Q = \begin{pmatrix}\frac{1}{20}T_s^5\mathbf{I}_{3\times3} & \frac{1}{8}T_s^4\mathbf{I}_{3\times3} & \frac{1}{6}T_s^3\mathbf{I}_{3\times3}\\ \frac{1}{8}T_s^4\mathbf{I}_{3\times3} & \frac{1}{3}T_s^3\mathbf{I}_{3\times3} & \frac{1}{2}T_s^2\mathbf{I}_{3\times3}\\ \frac{1}{6}T_s^3\mathbf{I}_{3\times3} & \frac{1}{2}T_s^2\mathbf{I}_{3\times3} & T_s\mathbf{I}_{3\times3}\end{pmatrix} \otimes \tilde{\mathbf{q}} \tag{25}$$

où $\otimes$ est le produit de Kronecker[1].

Dans cette partie on a vu qu'un estimateur robuste vis-à-vis d'erreurs de modèle et d'une mauvaise initialisation doit être choisi pour l'estimation des trajectoires de débris pendant la rentrée atmosphérique à cause de la dynamique inconnue des débris, des mesures radar bruitées et d'une mauvaise initialisation éventuelle.

L'estimateur à horizon glissant (MHE) [Rao et al., 2003][Alessandri et al., 2010] pourrait être un candidat potentiel pour ce problème du fait de ses robustesses vis-à-vis d'une

[1]Si a est une matrice de dimension $m \times n$ et B est une matrice de dimension $p \times q$, alors $a \otimes B$ est une matrice de dimension $mp \times nq$ telle que

$$a \otimes B = \begin{pmatrix}a_{11}B & \cdots & a_{1n}B\\ \vdots & \ddots & \vdots\\ a_{m1}B & \cdots & a_{mn}B\end{pmatrix} \tag{26}$$

mauvaise initialisation [Haseltine and Rawlings, 2005] et d'une erreur de modèle [Ungarala, 2009]. Dans la partie suivante, nous allons décrire la formulation du MHE classique ainsi que le théorème assurant la stabilité de la dynamique de l'erreur d'estimation, tels que détaillés dans la littérature.

0.2 Estimateur à Horizon Glissant (MHE)

Dans cette étude, on considère un système dynamique modélisé par les équations suivantes:

$$x_{k+1} = f(x_k) + w_k \tag{27a}$$

$$y_k = h(x_k) + v_k \tag{27b}$$

où $k \in \mathbb{N}$ est l'indice de temps en discret. $x_k \in \mathbb{R}^{n_x}$ est le vecteur d'état et w_k est le bruit d'état représentant non seulement les perturbations sur le système mais aussi une erreur de modèle [Ristic et al., 2004][Alessandri et al., 2008]. $y_k \in \mathbb{R}^{n_y}$ est le vecteur de mesures représentant la sortie du système et v_k est le bruit de mesures. w_k et v_k sont supposés être des bruits blancs non correlés de moyenne nulle. Notons Q_k et R_k les matrices de covariance de w_k et v_k respectivement. L'état initial x_0 est supposé inconnu.

Des contraintes sur l'état et sur les bruits peuvent être imposées et le MHE peut prendre en compte ces contraintes directement pendant l'optimisation. Les contraintes peuvent par exemple s'écrire sous la forme :

$$x_k \in \mathbb{X}_k \subset \mathbb{R}^{n_x},\ \ w_k \in \mathbb{W}_k \subset \mathbb{R}^{n_x},\ \ v_k \in \mathbb{V}_k \subset \mathbb{R}^{n_y} \tag{28}$$

où $\mathbb{X}_k$ est un ensemble convexe compact et $\mathbb{W}_k$ et $\mathbb{V}_k$ sont des ensembles compacts incluant l'origine.

La démarche consiste alors à estimer l'état x_k à chaque instant en utilisant les $N+1$ mesures les plus récentes regroupées dans une "fenêtre glissante" $[k-N, k]$. N est appelé longueur d'horizon du MHE. Soient $\hat{x}_{k-N|k}$ et $\{\hat{w}_{k-N+i|k}\}_{i=0}^{N-1}$ les estimées et l'état et des bruits d'état associés, calculées à l'instant k. On définit aussi y_{k-N}^{k} la collection des mesures sur l'horizon par $y_{k-N}^{k} = \begin{pmatrix} y_{k-N}^T & y_{k-N+1}^T & \dots & y_k^T \end{pmatrix}^T$ et w_{k-N}^{k-1} la séquence de bruit d'état sur l'horizon par $w_{k-N}^{k-1} = \begin{pmatrix} w_{k-N}^T & \dots & w_{k-1}^T \end{pmatrix}^T$. On note enfin $\hat{x}_{k-N|k}^{-}$ la valeur a priori de l'estimée $\hat{x}_{k-N|k}$.

0.2.1 Formulation du MHE

L'estimée de l'état à l'instant k calculée à l'instant $k \geq N$ est obtenue en résolvant :

$$\min_{\hat{x}_{k-N|k}, \{\hat{w}_{k-N+i|k}\}_{i=0}^{N-1}} \mathbf{J}_k(\hat{x}_{k-N|k}, \{\hat{w}_{k-N+i|k}\}_{i=0}^{N-1}, \hat{x}_{k-N|k}^{-}, y_{k-N}^{k}) \tag{29a}$$

$$\mathbf{J}_k = \left\| \hat{x}_{k-N|k} - \hat{x}_{k-N|k}^{-} \right\|_{\mathcal{P}}^2 + \sum_{i=0}^{N-1} \left\| \hat{w}_{k-N+i|k} \right\|_{\mathcal{Q}}^2 + \sum_{i=0}^{N} \left\| y_{k-N+i} - h(\hat{x}_{k-N+i|k}) \right\|_{\mathcal{R}}^2 \tag{29b}$$

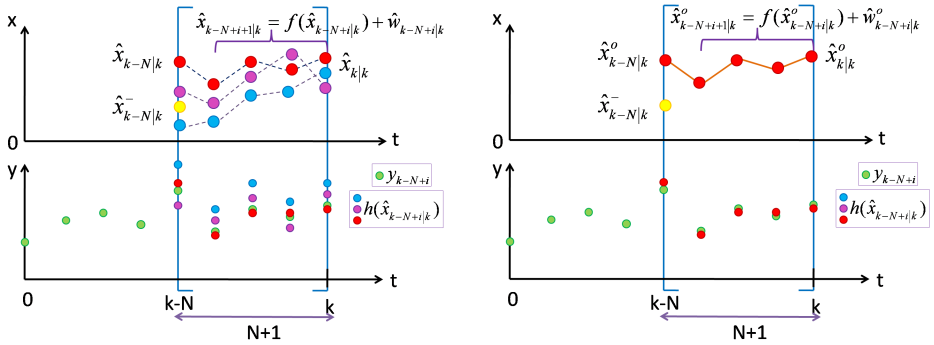

Figure 0.2: Illustration du MHE: à l'instant k, les $N+1$ mesures les plus récentes sont utilisées pour trouver la solution optimale de (29b): $(\hat{x}^{\circ}_{k-N|k}, \{\hat{w}^{\circ}_{k-N+i|k}\}_{i=0}^{N-1})$. $\hat{x}^{\circ}_{k|k}$ calculée en propageant $\hat{x}^{\circ}_{k-N|k}$ et $\{\hat{w}^{\circ}_{k-N+i|k}\}_{i=0}^{N-1}$ avec l'équation d'état (29c).

soumis aux contraintes

$$\hat{x}_{k-N+i+1|k} = f(\hat{x}_{k-N+i|k}) + \hat{w}_{k-N+i|k},\ \forall i \in [0, N-1] \tag{29c}$$

$$\hat{x}_{k-N|k} \in \mathbb{X},\ \ \hat{w}_{k-N+i|k} \in \mathbb{W},\ \ y_{k-N+i} - h(\hat{x}_{k-N+i|k}) \in \mathbb{V},\ \forall i \in [0, N-1] \tag{29d}$$

$\mathcal{P}$, $\mathcal{Q}$ et $\mathcal{R}$ sont des matrices de pondération définies positives. Les matrices $\mathcal{Q}$ et $\mathcal{R}$ peuvent être choisies égales respectivement à l'inverse des matrices de covariance de bruit d'état et de bruit de mesure, soit Q^{-1} et R^{-1}.

Soit $(\hat{x}^{\circ}_{k-N|k}, \{\hat{w}^{\circ}_{k-N+i|k}\}_{i=0}^{N-1})$ la solution optimale du problème (29) à l'instant k. L'estimée a priori au début de l'horizon $\hat{x}^{-}_{k-N|k}$ est calculée en utilisant la solution optimale de (29) à l'instant précédent $(\hat{x}^{\circ}_{k-N-1|k-1}, \hat{w}^{\circ}_{k-N-1|k-1})$ et (29c).

$\hat{x}_{k|k}$ désigne l'estimée de x_k calculée à l'instant k donnée par le MHE. $\hat{x}_{k|k}$ est calculée en propageant la solution optimale $(\hat{x}^{\circ}_{k-N|k}, \{\hat{w}^{\circ}_{k-N+i|k}\}_{i=0}^{N-1})$ en utilisant l'équation d'état (29c). Pour $k < N$, la formule (29) est toujours valable mais avec un horizon de longueur croissante égale à k à chaque instant. La figure 0.2 illustre le principe du MHE.

Le MHE peut s'envisager dans deux contextes particuliers : le cadre déterministe [Alessandri et al., 2008][Alessandri et al., 2010] et le cadre stochastique [Rao et al., 2003][Qu and Hahn, 2009]. Dans le cadre déterministe, l'état initial x_0, le bruit d'état w_k et le bruit de mesure v_k sont considérés comme des variables déterministes inconnues de caractéristiques inconnues qui prennent une valeur dans un ensemble compact connu. Dans le cadre stochastique, x_0, w_k et v_k sont considérés comme des variables aléatoires suivant des lois statistiques spécifiques.

Les formulations du MHE dans les deux cadres peuvent être utilisées pour un système bruité. Dans le cadre déterministe, la matrice de pondération $\mathcal{P}$ peut être choisie constante. Dans le cadre stochastique, en supposant que 1. l'état initial $x_0 \sim \mathcal{N}(\hat{x}^{-}_0, P^{-}_0)$ où $\hat{x}^{-}_0$ désigne l'estimée initiale a priori et P^{-}_0 désigne la matrice de covariance d'erreur initiale a priori, 2. $w_k \sim \mathcal{N}(0, Q)$, 3. $v_k \sim \mathcal{N}(0, R)$ et 4. la densité conditionnelle de l'état au début de l'horizon suit une loi normale $p(x_{k-N}|y_0^{k-N-1}) \sim \mathcal{N}(\hat{x}^{-}_{k-N|k}, P^{-}_{k-N|k})$ où $\hat{x}^{-}_{k-N|k}$

est l'estimée a priori de l'état au début de l'horizon et $P^-_{k-N|k}$ la matrice de covariance d'erreur a priori au début de l'horizon. La matrice de pondération $\mathcal{P}$ peut être choisie égale à l'inverse de $P^-_{k-N|k}$ et est calculée en utilisant l'équation de propagation de la matrice de covariance d'erreur de l'EKF :

$$\begin{aligned} P^-_{k-N|k} &= Q + \hat{F}_{k-N-1} P^-_{k-N-1|k-1} \hat{F}^T_{k-N-1} - \hat{F}_{k-N-1} P^-_{k-N-1|k-1} \hat{H}^T_{k-N-1} \cdots \\ &\quad (R + \hat{H}_{k-N-1} P^-_{k-N-1|k-1} \hat{H}^T_{k-N-1})^{-1} \hat{H}_{k-N-1} P^-_{k-N-1|k-1} \hat{F}^T_{k-N-1} \end{aligned} \tag{30}$$

où $\hat{F}_{k-N-1} = \dfrac{\partial f(x)}{\partial x}|\hat{x}^\circ_{k-N-1|k-1}$ et $\hat{H}_{k-N-1} = \dfrac{\partial h(x)}{\partial x}|\hat{x}^\circ_{k-N-1|k-1}$ sont les matrices jacobiennes de la fonction d'état f et de la fonction de mesure h respectivement.

Dans la partie suivante, nous discutons du théorème sur la stabilité de la dynamique de l'erreur d'estimation du MHE.

0.2.2 Stabilité de la Dynamique de l'Erreur d'Estimation du MHE

Il a été démontré dans [Alessandri et al., 2010] que la dynamique de l'erreur d'estimation du MHE dans le cadre déterministe est stable si la matrice de pondération $\mathcal{P}$ vérifie certaines conditions. Ceci peut être établi si le system (27) est tel que:

(A1) $\mathbb{X}$ est un ensemble convexe compact, $\mathbb{W}$ et $\mathbb{V}$ sont des ensembles compacts contenant l'origine.

(A2) L'état initial x_0 est tel que, pour toute séquence de bruits d'état $\{w_k\}$, la trajectoire du système $\{x_k\}$ reste dans l'ensemble $\mathbb{X}$, $\forall k$

(A3) f et h sont des fonctions $\mathcal{C}^2$ par rapport à x sur $\mathbb{X}$. De ce fait, f et h sont localement Lipschitz[2]. Nous noterons L^x_f et L^x_h respectivement les constantes de Lipschitz associées.

(A4) Le système est observable sur $N+1$ pas. Définissons l'application F portant sur des observations du système (27) sur l'horizon $[k-N, k]$ sous la forme :

$$F(x_{k-N}, w^{k-1}_{k-N}) \triangleq \begin{pmatrix} h(x_{k-N}) \\ h(f^{w_{k-N}}(x_{k-N})) \\ \vdots \\ h \circ f^{w_{k-1}} \circ \cdots \circ f^{w_{k-N}}(x_{k-N}) \end{pmatrix} \tag{31}$$

où $\circ$ représente la composition de fonctions et $f^{w_i}(x_i) \triangleq f(x_i) + w_i = x_{i+1}$ et

$$f^{w^{k-N+i}_{k-N}}(x_i) = f^{w_{k-N+i}} \circ \cdots \circ f^{w_{k-N}}(x_{k-N}),\ i \in [0, N-1] \tag{32}$$

Le système (27) est dit observable sur $N+1$ pas si au moins l'une de ces conditions, qui sont équivalentes [Hanba, 2010], est vérifiée:

(a) Pour un système sans bruit d'état, l'application $F(x_{k-N}, \mathbf{0}_{n_x N \times 1})$ est injective, c'est à dire si $F(x'_{k-N}, \mathbf{0}_{n_x N \times 1}) = F(x''_{k-N}, \mathbf{0}_{n_x N \times 1})$ alors $x'_{k-N} = x''_{k-N}$.

(b) $\forall x_{k-N} \in \mathbb{X}$, rang $\left(\dfrac{\partial F(x_{k-N}, \mathbf{0}_{n_x N \times 1})}{\partial x_{k-N}} \right) = n_x$

[2]Une fonction $f(x)$ est localement Lipschitz par rapport à son argument x s'il existe une constante positive L^x_f telle que $\|f(x') - f(x'')\| \leq L^x_f \|x' - x''\|$, pour tout x' et tout x'' dans une région donnée de l'espace d'état. L^x_f est la constante de Lipschitz associée.

(c) $\forall(x', x'') \in \mathbb{X}^2$, il existe une fonction de classe K^3 $\phi(\cdot)$ telle que

$$\phi(\|x' - x''\|^2) \leq \|F(x', \mathbf{0}_{n_x N \times 1}) - F(x'', \mathbf{0}_{n_x N \times 1})\|^2 \tag{33}$$

(A5) Le système (27) a une sensibilité finie, c'est à dire que le minimum de la fonction $\phi(\cdot)$ dans (33) existe. Définissons δ le paramètre de la sensibilité du système (27) par

$$\delta = \inf_{(x',x'')\in\mathbb{X}^2, x' \neq x''} \frac{\phi(\|x' - x''\|^2)}{\|x' - x''\|^2} > 0 \tag{34}$$

La condition (A5) assure qu'une variation de l'état au début de l'horizon implique une variation de l'application $F(x_{k-N}, w_{k-N}^{k-1})$. Dans ce cas, $F(x_{k-N}, w_{k-N}^{k-1})$ est équivalent à la séquence des mesures sur l'horizon y_{k-N}^{k} dans le cas sans bruit de mesure. Plus δ est grand, plus le système est "observable" [Alessandri et al., 2008] (nécessitant de fait un nombre de mesures plus faible pour construire une estimée).

Dans [Alessandri et al., 2010], il est démontré que si $\mathcal{P}$ de la forme $\mathcal{P} = p\mathbf{I}_{n_x}$ où $p \in \mathbb{R}^+$ est choisi tel que :

$$\alpha_{MHE} \triangleq c_1 p + \frac{(L_f^x)^2 c_2 p}{p + c_3 \delta} < 1 \tag{35}$$

alors la dynamique de l'erreur d'estimation du MHE est stable. Cela implique que l'erreur d'estimation du MHE converge vers une certaine borne.

c_1, c_2 et c_3 sont des constantes positives. Les expressions de ces constantes ne sont pas données dans [Alessandri et al., 2010] ni dans des travaux disponibles dans la littérature. Nous avons donc calculé ces constantes pour $\mathcal{Q}$ et $\mathcal{R}$ diagonalisables.

$$c_1 = \frac{6}{\lambda_{\mathcal{Q},min}},\ c_2 = 12,\ c_3 = \frac{2}{3}\lambda_{\mathcal{R},min} \tag{36}$$

où $\lambda_{\mathcal{Q},min}$ et $\lambda_{\mathcal{R},min}$ sont les plus petites valeurs propres de $\mathcal{Q}$ et $\mathcal{R}$ respectivement.

Des conditions sur la stabilité de la dynamique d'erreur d'estimation du MHE dans le cadre stochastique existent [Rao et al., 2003] mais sont difficiles à vérifier en pratique. Même si la stabilité du MHE dans ce cadre est difficile à garantir, il s'avère être plus robuste vis-à-vis d'une mauvaise initialisation et d'une erreur de modèle par rapport à l'EKF, à l'UKF et au RPF [Rao et al., 2003][Haseltine and Rawlings, 2005][Ungarala, 2009][Suwantong et al., 2012][Suwantong et al., 2013].

La partie suivante a pour objectif d'étudier les performances du MHE pour l'estimation des trajectoires des débris pendant la rentrée dans le but de vérifier si la stratégie à horizon glissant est adaptée à notre problème.

0.3 Etudes des Performances du MHE classique pour l'Estimation des Trajectoires des Débris pendant la Rentrée

Afin de vérifier si le MHE classique est adapté au problème d'estimation de trajectoire de débris pendant la rentrée, les performances du MHE sont évaluées dans le cas où le

[3]Une fonction $\sigma(s) : \mathbb{R}^+ \to \mathbb{R}^+$ est dite de classe K si elle est continue, strictement croissante et $\sigma(0) = 0$.

débris tombe verticalement sur la station radar. Le problème est donc réduit à un cas à une dimension sur l'axe $\vec{e}_z$. Les performances sont évaluées en termes de taux de non-divergence, précision des estimées et temps de calcul. Les performances des MHEs dans les deux cadres (stochastique et déterministe) sont comparées à celles de l'EKF, de l'UKF et du RPF. Les performances des estimateurs utilisant les deux modèles d'estimation, celui avec le coefficient balistique dans le vecteur d'état et celui avec l'accélération dans le vecteur d'état, sont également comparées.

Dans cette étude, l'horizon N des MHEs est choisi égal à $2n_x = 6$ qui est un choix recommandé dans [Rao, 2000]. Le paramètre de pondération p du MHE dans le cadre déterministe est choisi tel que la condition sur la stabilité (35) soit vérifiée.

0.3.1 Simulation des Trajectoires

Pour ces études, les trajectoires de 100 débris sphériques creux en Aluminium sont simulées sur une durée de 20 secondes. Cette forme est représentative des étages supérieurs et des réservoirs de gaz. Dans notre simulation, chaque débris a une épaisseur égale à 3 cm. L'altitude initiale r_{z_0}, la vitesse initiale v_{z_0} et le diamètre extérieur des débris D sont tirés aléatoirement suivant les lois uniformes suivantes: $r_{z_0} \sim \mathbf{U}(69, 70)$ km, $v_{z,0} \sim \mathbf{U}(-6500, -5500)$ m/s et $D \sim \mathbf{U}(20, 30)$ cm. Le diamètre des débris est supposé constant pendant la rentrée. Cette distribution de diamètre implique que la masse des débris soit dans l'intervalle $m \in [7.43, 18.63]$ kg. Le coefficient balistique β pour une sphère ne dépend que de l'altitude et de la norme de la vitesse de débris et peut être calculé en utilisant l'expression analytique [Morrison, 2010][Collins, 2012]. Ces trajectoires simulées sont considérées comme les "trajectoires réelles". Ensuite, les mesures de radar bruitées sont simulées à partir de ces trajectoires réelles et fournies comme données d'entrée aux estimateurs.

0.3.2 Robustesse vis-à-vis des Erreurs de Modèle

Une erreur de modèle peut être compensée par un bon choix des paramètres du bruit d'état qui représente bien le changement de l'état qui n'est pas pris en compte dans le modèle d'estimation sur une période d'échantillonnage [Bar-Shalom et al., 2004]. En revanche, dans la réalité, un bon choix des paramètres des bruits d'état ne peut pas être garanti sachant que l'état réel du système n'est pas connu. Il est donc impératif que l'estimateur utilisé pour l'estimation des trajectoires des débris pour la quelle une erreur de modèle importante peut être présente soit robuste vis-à-vis d'un mauvais choix de paramètres de bruit d'état.

Ainsi, pour un modèle d'estimation donné, la robustesse des estimateurs vis-à-vis d'une erreur de modèle sera étudiée en donnant aux estimateurs deux valeurs de paramètre de bruit d'état différentes et en observant ses performances. Ces deux valeurs sont choisies pour correspondre au comportement approprié pendant les 10 premières secondes de la rentrée, et au comportement lié aux 10 dernières secondes respectivement. Pour le modèle avec coefficient balistique, les valeurs de q_β telles que $\sqrt{q_\beta T_s} = 100$ kg/m^2 et $\sqrt{q_\beta T_s} = 1$ kg/m^2 sont choisies respectivement. Pour le modèle avec accélération, les valeurs de $\tilde{q}$ telles que $\sqrt{\tilde{q} T_s} = 15$ m/s^2 et $\sqrt{\tilde{q} T_s} = 1,5$ m/s^2 sont choisies respectivement.

0.3.3 Robustesse vis-à-vis d'une Mauvaise Initialisation

On suppose que le débris est connu, sphérique avec une épaisseur connue de 3 cm mais avec un diamètre extérieur D inconnu. Pour initialiser les estimateurs, on a besoin de

faire une hypothèse sur la distribution de D. Dans cette étude, on s'intéresse aux deux cas d'initialisation différents suivants :

1. On fait l'hypothèse que $D \sim \mathbf{U}(20, 30)$ cm. Ceci correspond au cas d'une bonne initialisation.

2. On fait l'hypothèse que $D \sim \mathbf{U}(80, 100)$ cm. Ceci correspond au cas d'une mauvaise initialisation.

Ces deux configurations permettent ainsi d'analyser la robustesse des estimateurs vis-à-vis d'une mauvaise initialisation est ainsi étudiée.

0.3.4 Pourcentages de Non-Divergence

On définit le pourcentage de non-divergence pour un estimateur comme étant le pourcentage des simulations Monte Carlo pour lesquelles les erreurs d'estimation de la position données par l'estimateur sont inférieures à 500 m à chaque instant.

Les pourcentages de non-divergence de chaque estimateur pour les deux modèles et pour les différents choix de paramètres du bruit d'état sont comparés dans le tableau 0.1.

Estimator	Modèle avec β		Modèle avec a_z	
	$\sqrt{q_\beta T_s} = 100$	$\sqrt{q_\beta T_s} = 1$	$\sqrt{\tilde{q} T_s} = 15$	$\sqrt{\tilde{q} T_s} = 1.5$
EKF	87	100	100	100
UKF	100	100	100	100
RPF	84	0	100	0
MHE deter.	100	100	100	100
MHE sto.	100	100	100	100

Tableau 0.1 : Pourcentages de non-divergence pour chaque estimateur

On peut observer que le modèle avec accélération donne de plus grands pourcentages de non-divergence. On peut observer également que le RPF est très sensible aux choix des paramètres du bruit d'état. Il n'est donc pas adapté au problème d'estimation de trajectoires de débris. Il convient cependant de noter qu'un estimateur peut être non-divergent tout en donnant une erreur d'estimation importante. La précision de ses estimées doit donc être prise également en compte.

0.3.5 Précisions des Estimées de Position

Les erreurs quadratiques moyennes (RMSE) des estimées de position données par chaque estimateur pour les simulations Monte Carlo pour lesquelles des erreurs sur la position sont plus petite que 500 m à chaque instant pour le cas d'une bonne initialisation sont présentées dans la figure 0.3. On peut remarquer que

- Le MHE dans le cadre déterministe est le plus robuste vis-à-vis du choix de paramètre du bruit d'état.

- Même si l'EKF et l'UKF donnent des erreurs d'estimation plus petites que le MHE déterministe lorsque les paramètres du bruit d'état sont bien choisis, ils peuvent donner des erreurs importantes lorsque les paramètres sont mal choisis. Etant

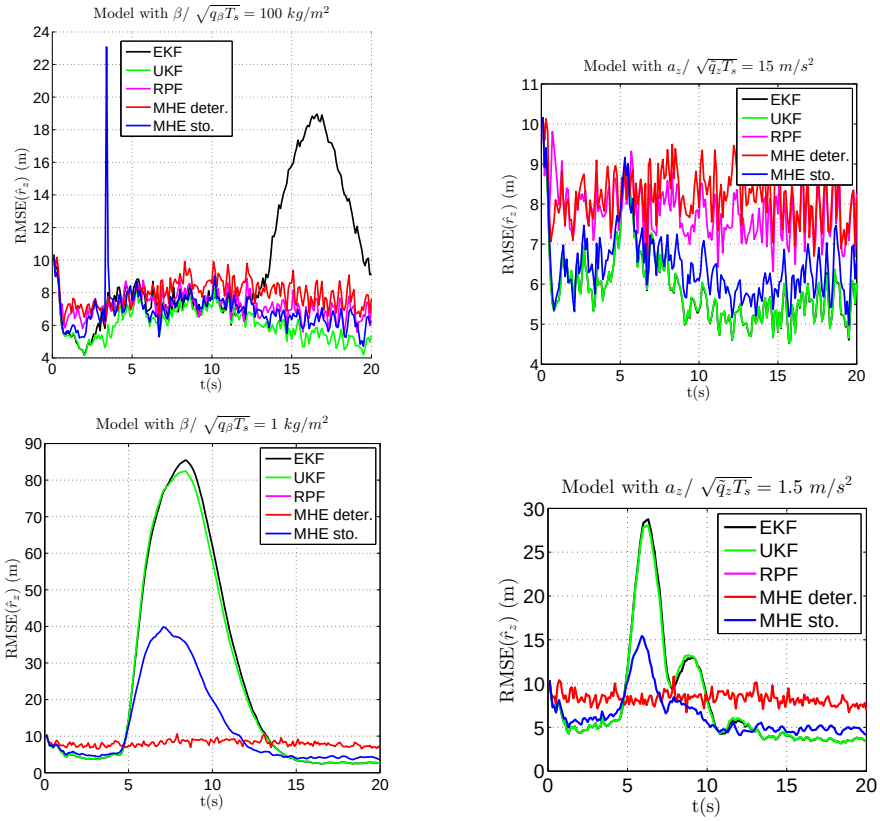

Figure 0.3: RMSE des estimées de position données par chaque estimateur

donné qu'un bon choix de paramètres du bruit d'état ne peut pas être garanti pour l'estimation des trajectoires des débris, l'EKF et l'UKF ne sont donc pas adaptés au problème.

- Les erreurs d'estimation sont plus petites globalement lorsque le modèle d'estimation avec accélération est utilisé.
- La précision du MHE dans le cadre stochastique est entre celle du MHE dans le cadre déterministe et l'EKF et l'UKF. Ceci est dû au fait que le MHE dans ce cadre met à jour sa matrice de pondération en utilisant l'EKF.

En comparant les précisions des estimées de position dans le cas d'une mauvaise initialisation avec celles dans le cas d'une bonne initialisation on constate que le modèle d'estimation avec l'accélération dans le vecteur d'état est plus robuste vis-à-vis d'une mauvaise initialisation de l'estimée par rapport au modèle avec le coefficient balistique.

0.3.6 Temps de Calcul Moyen par Itération

En comparant le temps de calcul moyen par itération constaté pour chaque estimateur pour les deux modèles et pour les deux valeurs des paramètres de bruit d'état en utilisant MATLAB sur un PC standard dans le tableau 0.2, on observe que les MHEs nécessitent un temps de calcul important. Ils ne sont pas encore utilisables pour l'estimation de trajectoires de débris en temps réel avec MATLAB. En revanche, ils sont les seuls estimateurs parmi ceux testés à être robustes vis-à-vis du choix de paramètre du bruit d'état. Il est donc intéressant de réduire le temps de calcul des MHEs.

De ce fait, l'étape suivant de la thèse a pour but de développer de l'estimateur à horizon glissant avec pré-estimation (MHE-PE). Ce dernier est censé nécessiter moins de temps de calcul que le MHE classique.

Estimateur	Temps de calcul moyen/ iteration (s)			
	Modèle avec β		Modèl avec a_z	
	$\sqrt{q_\beta T_s} = 2$	$\sqrt{q_\beta T_s} = 0.2$	$\sqrt{\tilde{q} T_s} = 20$	$\sqrt{\tilde{q} T_s} = 2$
EKF	$1.4 \cdot 10^{-4}$	$1.4 \cdot 10^{-4}$	$1.4 \cdot 10^{-4}$	$1.4 \cdot 10^{-4}$
UKF	$6.1 \cdot 10^{-4}$	$5.9 \cdot 10^{-4}$	$6.1 \cdot 10^{-4}$	$6.7 \cdot 10^{-4}$
RPF	0.43	0.27	0.43	0.27
MHE déter.	0.29	0.34	0.23	0.34
MHE sto.	0.48	0.20	0.23	0.20

Tableau 0.2 : Temps de calcul moyen par itération pour chaque estimateur

0.4 Estimateur à Horizon Glissant avec Pré-Estimation (MHE-PE)

Cette partie a pour objectif de développer l'estimateur à horizon glissant avec pré-estimation (MHE-PE) pour un système non-linéaire. La stabilité de la dynamique de l'erreur d'estimation du MHE-PE sera démontrée et une borne supérieure de l'erreur d'estimation du MHE-PE sera calculée. Grâce à la réduction du nombre de paramètre à optimiser, le MHE-PE utilisera moins de temps de calcul par rapport aux MHEs classiques. L'implantation du MHE-PE pour l'estimation des trajectoires des débris pendant la rentrée en 3D sera envisager à la partie 5.

0.4.1 Formulation du MHE-PE

Soit N l'horizon du MHE-PE. L'estimée $\hat{x}_k$ à l'instant k du MHE-PE pour $k \geq N$ est calculée en utilisant les $N+1$ mesures les plus récentes sur "l'horizon glissant" $[k-N, k]$. Pour $k < N$, $\hat{x}_k$ est estimé en utilisant toutes les mesures disponibles $\{y_j\}_{j=0}^{k}$. Nous rappelons que $y_{k-N}^{k} = \begin{pmatrix} y_{k-N}^T & y_{k-N+1}^T & \cdots & y_k^T \end{pmatrix}^T$ est la collection de mesures sur l'horizon. Soit $\hat{x}_{k-N|k}$ une estimée de l'état réel de l'instant $k-N$ calculé à l'instant k. Soit $\hat{x}^{\circ}_{k-N|k}$ la valeur optimale de $\hat{x}_{k-N|k}$. $\hat{x}^{-}_{k-N|k}$ est une valeur a priori de $\hat{x}_{k-N|k}$ calculée avant l'acquisition de la mesure y_k.

Définissons le *système nominal* comma la partie "sans bruit" du système réel modélisé dans (27). Le système nominal est modélisé par :

$$\begin{aligned} {}^{n}x_{k+1} &= f({}^{n}x_k) \\ {}^{n}y_k &= h({}^{n}x_k) \end{aligned} \tag{37}$$

où ${}^{n}x_k \in \mathbb{X}$ est l'état nominal et ${}^{n}y_k \in \mathbb{Y} \subset \mathbb{R}^{n_y}$ est la sortie dans le cas sans bruit. Ce modèle sera appelé "modèle d'estimation nominal".

Définissons (Σ) le système d'un pré-estimateur $g(\cdot,\cdot)$ tel que

$$\begin{aligned} \hat{x}_{k+1} &= g(\hat{x}_k, y_k) \\ \hat{y}_k &= h(\hat{x}_k) \end{aligned} \tag{38}$$

$\hat{y}_k$ est la mesure prédite donnée par le pré-estimateur g. On considère que $\hat{x}_k \in \hat{\mathbb{X}}$, $\forall k$.

Le MHE-PE est formulé de la façon suivante :

$$\hat{x}^o_{k-N|k} = \arg \min_{\hat{x}_{k-N|k} \in \hat{\mathbb{X}}} \mathbf{J}_k(\hat{x}_{k-N|k}, \hat{x}^-_{k-N|k}, y^k_{k-N}) \tag{39a}$$

$$\mathbf{J}_k = \mu \left\| \hat{x}_{k-N|k} - \hat{x}^-_{k-N|k} \right\|^2 + \sum_{i=0}^{N} \left\| y_{k-N+i} - h(\hat{x}_{k-N+i|k}) \right\|^2_{\mathcal{R}} \tag{39b}$$

$$\hat{x}_{k-N+i+1|k} = g(\hat{x}_{k-N+i|k}, y_{k-N+i}),\ \forall i \in [0, N-1] \tag{39c}$$

μ est un scalaire positif représentant la confiance dans la valeur a priori $\hat{x}^-_{k-N|k}$ et $\mathcal{R}$ est la matrice de pondération représentant la confiance dans la collection de mesures y^k_{k-N}. $\mathcal{R}$ peut être par exemple choisi égal à l'inverse de la matrice de covariance du bruit de mesure R^{-1}. L'estimée $\hat{x}^\circ_{k|k}$ de x_k donné par le MHE-PE est calculée en utilisant (39c) pour $i = 1, \ldots, N$ à partir de $\hat{x}^o_{k-N|k}$, et $\hat{x}^-_{k-N|k}$ est déterminée à partir de

$$\hat{x}^-_{k-N|k} = f(\hat{x}^\circ_{k-N-1|k-1}) \tag{40}$$

On note que dans le MHE-PE l'évolution de l'estimée à *tous les instants* sur l'horizon suit l'équation du pré-estimateur g au lieu du modèle d'estimation comme dans le MHE classique dans (29c). En effet, le MHE-PE implante localement le pré-estimateur g qui est ré-initialisé à chaque instant au début de l'horizon en résolvant le problème d'optimisation (39). g est appelé un "pré-estimateur" puisqu'il "pré-estime" en quelque sorte l'état avant que l'algorithme d'optimisation donne l'estimée optimale.

Dans le MHE-PE, l'erreur de modèle est prise en compte "approximativement" dans l'étape de la pré-estimation à travers la structure du pré-estimateur g. La séquence de bruit d'état sur l'horizon ne doit plus être estimée et l'estimée au début de l'horizon devient le seul paramètre à optimiser du problème (39). Le temps de calcul du MHE-PE sera donc logiquement réduit par rapport au MHE classique.

0.4.2 Conditions Garantissant la Stabilité de la Dynamique de l'Erreur d'Estimation du MHE-PE

Le modèle d'estimation est supposé vérifier les conditions (A1)-(A3) de la partie 0.2.2 et le pré-estimateur est supposé vérifier les conditions suivantes :

(C4) g est localement Lipschitz par rapport à ses arguments

(C5) $\forall {}^n\hat{x}_0 \in \hat{\mathbb{X}}$, $\forall {}^nx_0 \in \mathbb{X}$, il existe une fonction de classe K ψ telle que $\|{}^n\hat{x}_k - {}^nx_k\|^2 \leq \psi(\|{}^n\hat{x}_0 - {}^nx_0\|^2)$, $\forall k$.

ou

(C5a) g donne des erreurs d'estimation bornées dans le cas de bruits bornés

Un exemple d'estimateur g qui vérifie (C5) est un observateur déterministe.

Définissons le vecteur des mesures prédites sur l'horizon par le pré-estimateur g initialisée à l'instant $k-N$ par $\hat{x}_{k-N}$ et recevant les mesures y^{k-1}_{k-N} par

$$G(\hat{x}_{k-N}, y_{k-N}^{k-1}) \triangleq \begin{pmatrix} h(\hat{x}_{k-N}) \\ h \circ g(\hat{x}_{k-N}, y_{k-N}) \\ \vdots \\ h(g^N(\hat{x}_{k-N}, y_{k-N}^{k-1})) \end{pmatrix} = \hat{y}_{k-N}^{k} \tag{41}$$

$$g^i(\hat{x}_{k-N}, y_{k-N}^{k-N+i-1}) \triangleq \underbrace{g(g(\ldots g}_{\text{i fois}}(\hat{x}_{k-N}, y_{k-N}), \ldots), y_{k-N+i-1}), \;\; 2 \leq i \leq N \tag{42}$$

Une de ces trois conditions sur le système du pré-estimateur (Σ) est supposée d'être vérifié

(C6a) (Σ) est uniformément observable sur $\hat{\mathbb{X}}$ par rapport à toutes les mesures admissibles, c'est à dire $\exists N > 0$, $\forall y_{k-N}^{k-1} \in \mathbb{Y}^N$, la fonction $G(\hat{x}_{k-N}, y_{k-N}^{k-1})$ est injective en fonction de l'estimée initiale de l'horizon $\hat{x}_{k-N}$

(C6b) (Σ) vérifie la condition de rang pour une observabilité uniforme sur $\hat{\mathbb{X}}$ par rapport à toutes les mesures admissibles, c'est à dire $\exists N > 0$, $\forall \hat{x}_{k-N} \in \hat{\mathbb{X}}$, $\forall y_{k-N}^{k-1} \in \mathbb{Y}^N$,

$$\text{rang}\left(\frac{\partial G(\hat{x}_{k-N}, y_{k-N}^{k-1})}{\partial \hat{x}_{k-N}}\right) = n_x$$

(C6c) g est K-uniformément observable sur $\hat{\mathbb{X}}$ par rapport à toutes les mesures admissibles, i.e. $\exists N \geq n_x$, $\forall (\hat{x}', \hat{x}'') \in \hat{\mathbb{X}}^2$, $\forall y_{k-N}^{k-1} \in \mathbb{Y}^N$, il existe une fonction de classe K $\phi_g(\cdot)$ telle que :

$$\phi_g(\|\hat{x}' - \hat{x}''\|^2) \leq \|G(\hat{x}', y_{k-N}^{k-1}) - G(\hat{x}'', y_{k-N}^{k-1})\|^2 \tag{43}$$

Pour finir, g est supposée vérifier :

(C7) L'application $G(\cdot, \cdot)$ a une sensibilité finie à l'estimée, c'est à dire la K-fonction $\phi_g(\cdot)$ dans (43) vérifie

$$\delta_g = \inf_{(\hat{x}_1, \hat{x}_2) \in \hat{\mathbb{X}}^2, \hat{x}_1 \neq \hat{x}_2} \frac{\phi_g(\|\hat{x}_1 - \hat{x}_2\|^2)}{\|\hat{x}_1 - \hat{x}_2\|^2} > 0 \tag{44}$$

0.4.3 Théorème Garantissant la Stabilité de la Dynamique de l'Erreur d'Estimation du MHE-PE

Les travaux effectués dans le cadre de cette thèse ont permis d'aboutir à l'énoncé du théorème suivant

Théorème 1 (Stabilité de la Dynamique de l'Erreur d'Estimation du MHE-PE)**.** *Supposons que le modèle d'estimation vérifie (A1)-(A3) et que le pré-estimateur g du MHE-PE vérifie les conditions (C4)-(C7). La dynamique de l'erreur d'estimation du MHE-PE est stable si le paramètre de pondération μ est choisi tel que*

$$\alpha_{MHE-PE} \triangleq \frac{8\mu(L_f^x)^2}{(\mu + \frac{\lambda_{\mathcal{R},min}\delta_g}{2})} < 1 \tag{45}$$

Grâce au théorème 1, la stabilité de la dynamique de l'erreur d'estimation du MHE-PE pourra être garantie en choisissant une valeur de μ satisfaisant la condition (45). Ceci est faisable dès que L_f^x et δ_g sont calculés.

Pour un système sans bruit l'erreur d'estimation du MHE-PE tend asymptotiquement vers zéro.

Les performances de cet estimateur sont finalement analysés à la partie suivant.

0.5 Performances du MHE-PE pour l'Estimation des Trajectoires des Débris pendant la Rentrée Atmosphérique

Les performances du MHE-PE pour l'estimation des trajectoires des débris pendant la rentrée en 3 dimensions seront comparées à celles de l'EKF, l'UKF, le RPF et le MHE dans le cadre déterministe. Sachant que le modèle d'estimation avec l'accélération s'avère être plus performant au niveau de la précision des estimées et plus robuste vis-à-vis d'une mauvaise initialisation que le modèle avec le coefficient balistique, il sera le seul implanté pour la suite. Les robustesses des estimateurs vis-à-vis d'une mauvaise initialisation et d'un mauvais choix de paramètre du bruit d'état seront étudiées comme à la partie 3. Les valeurs du paramètre de bruit d'état $\tilde{q}$ sont choisies comme à la partie 3 également, c'est-à-dire $\tilde{q}$ tel que $\sqrt{\tilde{q}T_s} = 15\ m/s^2$ et $\sqrt{\tilde{q}T_s} = 1.5\ m/s^2$.

0.5.1 Simulation des Trajectoires et des Mesures

Comme à la partie 3, les trajectoires de 100 débris sphériques creux en Aluminium d'épaisseur égale à 3 cm sont simulées sur une durée de 20 secondes. L'altitude initiale H_0, la longitude initiale $\lambda_{D,0}$, la latitude initiale $\phi_{D,0}$, la pente initiale (l'angle entre le plan horizontal et la vitesse initiale) γ_0, le cap initial (l'angle entre la direction du nord et la projection de la vitesse initiale sur le plan horizontal) θ_0, la norme de la vitesse initiale $\|\mathbf{v}_0\|$ et le diamètre supérieure des débris D, supposé constant pendant la rentrée, sont tirés aléatoirement suivant les lois uniformes suivantes: $H_0 \sim \mathbf{U}(69, 70)\ km$, $\lambda_{D,0} \sim \mathbf{U}(2.284443°, 2.407881°)$, $\phi_{D,0} \sim \mathbf{U}(48.820315°, 48.897227°)$, $\gamma_0 \sim \mathbf{U}(-30°, -80°)$, $\theta_0 \sim \mathbf{U}(20°, 40°)$, $\|\mathbf{v}_0\| \sim \mathbf{U}(5000, 10000)\ m/s$ et $D \sim \mathbf{U}(20, 30)\ cm$.

Les mesures associées à chaque trajectoire sont simulées en utilisant (10) en supposant que la période d'acquisition de mesures $T_s = 0.1\ s$, la longitude de la station $\lambda = 2.336523°$, la latitude de la station $\phi = 48.836080°$, les écart types de bruits de mesures $\sigma_d = 10\ m$ et $\sigma_{el} = \sigma_{az} = 0.005°$. Ces valeurs de σ_d, σ_{el} et σ_{az} ont le même ordre de grandeur que la résolution de la station allemande TIRA et la station d'ESA ARMOR [Alarcón et al., 2005]. La période d'échantillonnage pour les estimateurs est choisie égale à T_s également.

0.5.2 Réglages du MHE-PE

L'horizon $N = 2n_x = 18$ est choisi. L'estimée $\hat{x}_k$ à chaque instant k du MHE-PE est supposée vérifier :

$$\begin{aligned} \hat{\mathbf{r}}_k &\in [-100, 100] \times [-100, 100] \times]0, 100]\ km \\ \hat{\mathbf{v}}_k &\in [-10000, 0[\times]0, 10000] \times [-10000, 0[\ m/s \\ \hat{\mathbf{a}}_k &\in [-2500, 2500]^3\ m/s^2 \end{aligned} \tag{46}$$

Ces contraintes sont choisis en considérant les plages de valeurs des positions, des vitesses et des accélérations des trajectoires simulées.

Un filtre de Kalman Etendu (EKF) est choisi pour le pré-estimateur g, c'est-à-dire

$$\hat{x}_{j+1|k} = g(\hat{x}_{j|k}, y_j) = f(\hat{x}_{j|k}) + K_j(y_j - h(\hat{x}_{j|k})) \tag{47}$$

$\forall j \in [k - N, k - 1]$ et K_j et le gain de Kalman. On suppose également qu'il existe un constant $c_{K,k} \in \mathbb{R}$ tel que

$$c_{K,k} \triangleq \max_{\varsigma \neq 0} \frac{\|K_k \varsigma\|}{\|\varsigma\|} < \infty \tag{48}$$

(48) est vérifié pour le EKF dans le MHE-PE puisque l'estimée $\hat{x}$ est bornée à chaque instant à cause des contraintes imposés lors de l'optimisation. Vérifions maintenant les conditions garantissant la stabilité de la dynamique de l'erreur d'estimation du MHE-PE, c'est-à-dire (A1)-(A3) dans la section 0.2.2 et (C4)-(C7) dans la section 0.4.2.

0.5.3 Vérifications des Conditions pour la Stabilité de la Dynamique de l'Erreur d'Estimation du MHE-PE

Commençons par les conditions (A1)-(A2):

(A1) $\mathbb{X}$ est un ensemble convexe compact, $\mathbb{W}$ et $\mathbb{V}$ sont des ensembles compacts contenant l'origine.

(A2) L'état initial x_0 est tel que, pour toute séquence de bruits d'état $\{w_k\}$, la trajectoire du système $\{x_k\}$ reste dans l'ensemble $\mathbb{X}$, $\forall k$

Les conditions (A1) et (A2) sont vérifiés puisque $\mathbb{X}$ peut être choisi comme $\hat{\mathbb{X}}$ dans (46) qui contient l'état réel de tout instant. Considérons maintenant (A3) :

(A3) f et h sont des fonctions $\mathcal{C}^2$ par rapport à x sur $\mathbb{X}$. De ce fait, f et h sont localement Lipschitz. Nous noterons L_f^x et L_h^x respectivement les constantes de Lipschitz associées.

Rappelons que les fonctions f et h sont décrites dans (23) et (10) respectivement. Sachant que f et h sont des compositions des fonctions $\mathcal{C}^2$ sur $\mathbb{X}$, elles sont donc également $\mathcal{C}^2$. Leurs constantes de Lipschitz peuvent être calculées en supposant égales à des normes de matrice de leurs matrices de Jacobien. Ceci est calculé numériquement où on trouve que $L_f^x = 1.2$ et $L_h^x = 1$ peuvent être choisies. Considérons maintenant (C4)-(C5)

(C4) g est localement Lipschitz par rapport à ses arguments

(C5) $\forall {}^n\hat{x}_0 \in \hat{\mathbb{X}}$, $\forall {}^nx_0 \in \mathbb{X}$, il existe une fonction de classe K ψ telle que $\|{}^n\hat{x}_k - {}^nx_k\|^2 \leq \psi(\|{}^n\hat{x}_0 - {}^nx_0\|^2)$, $\forall k$.

En utilisant le fait que f et h sont localement Lipschitz et (48) est vérifié, g défini dans (47) est donc localement Lipschitz. (C4) est donc vérifié. Nous pouvons voir que la condition (C5) est vérifié également en écrivant (27a) et (47) pour un système sans bruit et en utilisant le fait que f et h soient localement Lipschitz et (48). Considérons maintenant (C6b) et (C7).

(C6b) (Σ) vérifie la condition de rang pour une observabilité uniforme sur $\hat{\mathbb{X}}$ par rapport à toutes les mesures admissibles, c'est à dire $\exists N > 0$, $\forall \hat{x}_{k-N} \in \hat{\mathbb{X}}$, $\forall y_{k-N}^{k-1} \in \mathbb{Y}^N$,
$$\text{rang}\left(\frac{\partial G(\hat{x}_{k-N}, y_{k-N}^{k-1})}{\partial \hat{x}_{k-N}}\right) = n_x$$

(C7) L'application $G(\cdot,\cdot)$ a une sensibilité finie à l'estimée, c'est à dire la K-fonction $\phi_g(\cdot)$ dans (43) vérifie 44

(C6b) est vérifié en utilisant le calcul symbolique dans MATLAB. En conséquence, la fonction $G_{1:n_x}$ est inversible. En utilisant le théorème des accroissements finis pour les fonctions multivariables [Nachbar, 2013] et la définition de la norme inférieure d'une matrice dans [Von Neumann and Goldstine, 1947] sachant que $G_{1:n_x}$ est inversible, nous pouvons montrer que $\delta_g = (\|(\partial G_{1:n_x}/\partial \hat{x})^{-1}\|_2^{-1})^2$ peut être choisi. En utilisant le calcul

numérique en MATLAB, nous trouvons que $\delta_g = 1.6 \cdot 10^{-15}$ peut être choisi pour que (C7) soit vérifiée. Dans cette étude, $\mu = 5 \cdot 10^{-19}$, permettant de vérifier (45), est choisi.

Pour résumer, en choisissant l'EKF comme pré-estimateur pour le MHE-PE, les conditions garantissant la stabilité de la dynamique de l'erreur d'estimation du MHE-PE sont toutes vérifiées. Considérons maintenant les performances des estimateurs testés.

0.5.4 Pourcentages de Non-Divergence

Les pourcentages de non-divergence comme définit dans la partie 3 de chaque estimateur pour chaque cas d'étude sont comparées dans le tableau 0.3. Ce tableau permet de conclure que tous les estimateurs sauf le RPF ont 100% de pourcentage de non-divergence. Le RPF donne un pourcentage de non-divergence non nul uniquement lorsqu'il est bien initialisé et lorsque le paramètre de bruit d'état est bien choisi.

Estimateur	Bonne init.		Mauvaise initi	
	$\sqrt{\tilde{q}T_s} = 15$	$\sqrt{\tilde{q}T_s} = 1.5$	$\sqrt{\tilde{q}T_s} = 15$	$\sqrt{\tilde{q}T_s} = 1.5$
EKF	100	100	100	100
UKF	100	100	100	100
RPF	67	0	0	0
MHE-PE	100	100	100	100
MHE	100	100	100	100

Tableau 0.3 : Pourcentages de non-divergence dans les cas d'une bonne initialisation et d'une mauvaise initialisation et pour les deux valeurs du paramètre de bruit d'état

0.5.5 Précision des Estimées

Les normes sur les erreurs quadratiques moyennes (RMSE) des estimées de position pour les simulations Monte Carlo pour lesquelles des erreurs sur chaque composante de la position sont inférieures à 500 m à chaque instant sont affichées sur figure 0.4. On peut remarquer que :

1. L'EKF, l'UKF, le MHE-PE et le MHE donnent le même ordre de précision des estimées dans les deux cas d'initialisation. Ils sont donc robustes vis-à-vis d'une mauvaise initialisation.

2. L'EKF et l'UKF peuvent donner des erreurs d'estimation importantes lorsque le paramètre du bruit d'état n'est pas bien choisi. Dès lors qu'un bon choix de ce paramètre ne peut être garanti, l'EKF et l'UKF ne sont pas adaptés à l'estimation de trajectoires de débris pendant la rentrée.

3. Le MHE-PE est robuste vis-à-vis d'un mauvais choix du paramètre du bruit d'état.

4. Le MHE est aussi robuste vis-à-vis d'un mauvais choix du paramètre du bruit d'état dès qu'il converge. Les erreurs d'estimation initiales importantes peuvent être induites par des minima locaux, sachant que le nombre de paramètres à optimiser est très grand.

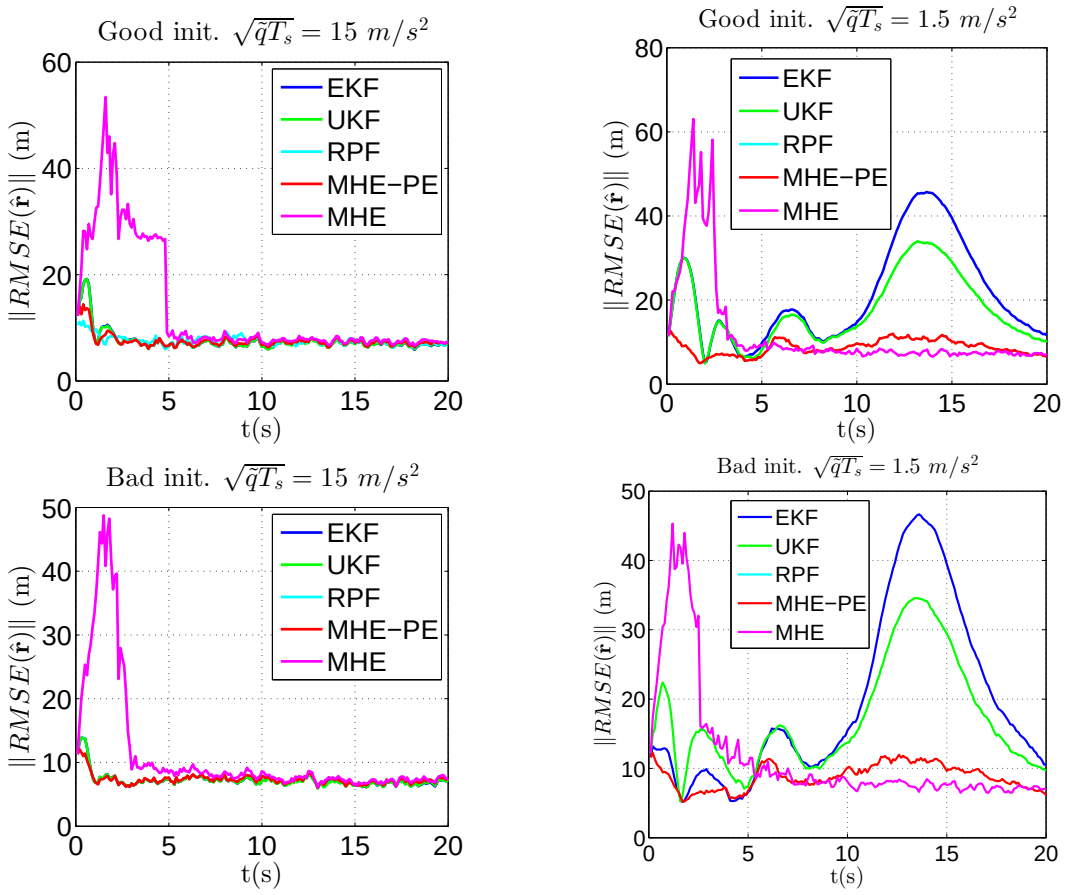

Figure 0.4: $\|RMSE(\hat{\mathbf{r}})\|$ donné par chaque estimateur dans les cas d'une bonne et d'une mauvaise initialisations pour deux valeurs de paramètre du bruit d'état $\tilde{q}$.

0.5.6 Temps de Calcul par Itération

Les temps de calcul par itération minimaux, moyens et maximaux donnés par chaque estimateur sont présentés dans le tableau 0.4. Les estimateurs sont implantés avec MATLAB sur un PC standard. On peut observer que l'EKF et l'UKF requièrent un temps de calcul faible. Néanmoins, on rappelle qu'ils peuvent donner des erreurs d'estimation importantes lorsque le paramètre du bruit d'état n'est pas bien choisi. Le RPF requiert un temps de calcul important et donne des erreurs d'estimation fortes. Il n'est donc pas adapté au problème non plus. Le MHE-PE nécessite environ 6 fois moins de temps de calcul que le MHE.

Estimateur	Temps de Calcul/ itération (s)		
	Min.	Moy.	Max.
EKF	$3 \cdot 10^{-4}$	$3 \cdot 10^{-4}$	$5 \cdot 10^{-5}$
UKF	0.002	0.002	0.011
RPF	0.045	1.578	2.195
MHE-PE	0.482	0.865	1.588
MHE	2.638	5.330	7.438

Tableau 0.4 : Temps de calcul par itération utilisé par chaque estimateur

0.5.7 Conclusions

Cette partie a permis de vérifier que le MHE-PE donne une bonne précision des estimées, est robuste vis-à-vis d'une mauvaise initialisation et d'un mauvais chois de paramètre du bruit d'état pour l'estimation de trajectoires de débris pendant la rentrée atmosphérique en 3D. De plus, il nécessite 6 fois moins de temps de calcul environ par rapport au MHE classique. On note que ce temps de calcul du MHE-PE sur MATLAB n'est pas encore applicable à l'estimation de trajectoires de débris en temps réel sachant que la période d'échantillonnage $T_s = 0.1\ s$. Cependant, son temps de calcul peut être encore réduit en le combinant avec des méthodes d'optimisation plus rapides ou en ayant recours à un langage de programmation plus rapide. Dans cette partie, nous avons également vu que l'EKF en tant que pré-estimateur pour le MHE-PE permet de garantir la stabilité de la dynamique de l'erreur d'estimation du MHE-PE pour l'estimation de trajectoires des débris.

0.6 Conclusions et Perspectives

Conclusions

Dans cette thèse nous avons

1. Etudié les performances du MHE classique pour l'estimation de trajectoires de débris spatiaux pendant la rentrée en 1D en les comparant à celles des estimateurs classiques utilisés dans l'estimation de trajectoire d'un objet militaire pendant la rentrée à savoir l'EKF, l'UKF et le RPF. Les performances ont été étudiées en termes de pourcentages de non-divergence, précision des estimées et temps de calcul. On a observé que le MHE est le seul parmi les estimateurs testés qui est robuste vis-à-vis d'un mauvais choix de paramètre du bruit d'état. Dès lors qu'un bon choix de paramètre du bruit d'état ne peut pas être garanti dans le cas de l'estimation de trajectoires de débris, le MHE s'avère le plus adapté au problème comparativement à l'EKF, l'UKF et le RPF. Cependant le MHE requiert un temps de calcul très important.

2. Développé une stratégie à horizon glissant qui demande moins de temps de calcul par rapport à la stratégie classique en modifiant sa formulation, consistant en un estimateur à horizon glissant avec pré-estimation (MHE-PE). Dans le MHE-PE, l'erreur de modèle est prise en compte "approximativement" lors de l'étape de la pré-estimation à travers la structure du pré-estimateur. La séquence de bruit d'état sur l'horizon ne doit plus être estimée et l'estimée au début de l'horizon devient le seul paramètre à optimiser. Le temps de calcul du MHE-PE est donc réduit par rapport au MHE classique. Nous avons également élaboré un théorème garantissant la stabilité de la dynamique de l'erreur d'estimation d'un estimateur à horizon glissant avec pré-estimation (MHE-PE) pour un système non linéaire avec bruits bornés.

3. Implanté le MHE-PE pour l'estimation de trajectoire de débris pendant la rentrée en 3D. Le MHE-PE offre une bonne précision des estimées, est robuste vis-à-vis d'une mauvaise initialisation et d'un mauvais choix de paramètre du bruit d'état. De plus, il requiert 6 fois moins de temps de calcul que le MHE.

Perspectives

Ce travail de thèse pourra se prolonger pour les perspectives suivantes :

1. Étudier l'effet de la longueur de l'horizon du MHE-PE sur ses performances.

2. Développer une méthode fournissant la longueur maximale de l'horizon qu'il convient de ne pas dépasser. Pour cela, on pourra s'inspirer des travaux de [Kratz et al., 1997][Graton et al., 2014] dans lesquels la longueurs maximale de l'horizon est calculée dans le cas d'un estimateur à mémoire finie pour un système linéaire.

3. Développer une stratégie permettant de prendre en compte des paramètres de bruit d'état adaptatifs.

4. Développer une stratégie permettant de prendre en compte avoir des paramètres de réglages du MHE-PE adaptatifs. Ceci pourra s'appuyer sur les travaux de [Mamboundou and Langlois, 2011] qui ont été réalisés dans le cadre de l'étude de la commande prédictive linéaire.

5. Etudier les performances du MHE-PE dans le cas d'un bruit multiplicatif. Récemment un observateur pour un système non linéaire avec bruit multiplicatif a été proposé dans [Barbata et al., 2014a] et [Barbata et al., 2014b]. Une combinaison du MHE-PE avec un tel observateur pourrait être intéressante.

6. Comparer les performances du MHE-PE avec celles du filtre de Kalman à horizon glissant (RNK) proposé récemment dans [Rengaswamy et al., 2013] même si la preuve de la stabilité du RNK pour un système non linéaire n'a pas encore été établie.

7. Étudier l'effet de la valeur du paramètre de pondération μ du MHE-PE.

8. Implanter le MHE-PE avec des techniques d'optimisation rapides proposées dans [Ferreau et al., 2012][Zavala, 2008] avec un langage de programmation rapide pour une application en temps réel pour l'estimation de trajectoires de débris pendant la rentrée.

Introduction

Context

Today, the Earth's orbit is highly polluted by space debris, resulting from human space activities. According to recent evaluation [NASA, 2012] there are approximately 23,000 objects larger than 10 centimeters orbiting around the Earth, 500,000 between 1 and 10 centimeters and more than 100 millions smaller than 1 centimeter. The dangers of space debris are the following:

First, if the density of space debris orbiting around the Earth reaches a critical threshold [Kessler et al., 2010], there will be a continual cascade of collision between debris. This cascade of collision will cause the number of space debris to increase exponentially and create a debris belt which will make space use impossible for generations. This consequence can have high effects in our daily life since space use is omnipresent in today's technologies such as in navigation, telecommunication, surveillance, Earth observation, and meteorology.

Second, space debris, even a small one, can destroy operational satellites by collisions due to its high impact velocity which is around 8-12 km/s.

Third, there are risks of large objects' re-entry on Earth.

To prevent dangers from space debris, space debris removal, new collision avoidance and large objects' re-entry prediction are needed. To do so, the trajectories of space debris have to be accurately estimated.

In this work, we focus on the space debris tracking problem during atmospheric re-entries which is known to be a very difficult problem since the dynamics of the debris during this phase is not accurately known [Mehrholz et al., 2002][Klinkrad, 2006]. Even though there are less than 20 large pieces of space debris that have reached the ground up to now, there will be more and more re-entries due to debris mitigation policy and possible debris removal projects. This results from debris mitigation guidelines established by Space Agencies worldwide requesting that satellites in Low Earth Orbits (LEOs) have to de-orbit at their end of operational life and re-enter the atmosphere. During the re-entries, it is possible that the debris disintegrates into many fragments due to high mechanical loads and heating rates. This phenomenon is called a "breakup". A breakup usually occurs at the altitude around 80 km. In this case, it is impossible to have the characterization of the debris, e.g. the mass and the cross section, in advance. This also makes the space debris tracking problem during the re-entries difficult.

The tracking in this study is done using measurements radar which are the distance, the elevation angle and the azimuth angle between the debris and the radar station.

Challenges in Space Debris Tracking during Atmospheric Re-entries

Since the dynamics of the debris is not accurately known, assumptions on the dynamics of the debris have to be made in the estimation model. This can result in high model errors. It is also possible that the estimation algorithm, i.e. the estimator, is badly initialized due to a lack of information on the debris' dynamics. As a consequence, an estimator to be used for space debris tracking during atmospheric re-entries must be proven to be robust against not only high model errors but also bad initialization.

The only available studies on re-entry object tracking concern military objects [Farina et al., 2002][Austin and Leondes, 1981][Liu et al., 2005][Ristic et al., 2003]. In [Ristic et al., 2003], the performances of the Extended Kalman Filter (EKF), the Unscented Kalman Filter (UKF) and the Regularized Particle Filter (RPF) are evaluated. The RPF is shown to be the most efficient in term of accuracy of the estimate while the EKF and the UKF fail to provide small estimation errors. However, the RPF is known to be sensitive to model errors and bad initialization [Rawlings and Bakshi, 2006][Ungarala, 2009]. To summarize, these classical estimators used in object tracking during the re-entries do not seem to be adapted for the case of space debris. An alternative estimator should therefore be implemented for the problem.

Moving Horizon Estimator (MHE): A Robust Estimator

An a priori good candidate estimator for space debris trajectory estimation could be the Moving Horizon Estimator (MHE) [Rao et al., 2003][Alessandri et al., 2010] which is shown to be robust against poor initialization [Haseltine and Rawlings, 2005] and against model errors [Ungarala, 2009]. The MHE computes an estimate at the current instant based on information from a fixed number of latest measurements collected over a finite horizon by solving an optimization problem. One of the advantages of the MHE is that it allows handling complex nonlinear models directly. Hence, there is no need for system linearization which can induce additional errors. Another advantage of the MHE is that constraints can be incorporated directly during the optimization. Besides, the stability of the dynamics of the estimation errors of the MHE has also been proven [Alessandri et al., 2008][Alessandri et al., 2010]. However, the MHE requires large computation time due to large number of its optimization variables. As a result, the MHE cannot be used yet for real-time space debris trajectory estimation. We are therefore interested in working on the computation time reduction of the MHE strategy.

Moving Horizon Estimation with Pre-Estimation (MHE-PE): A Fast Moving Horizon Strategy

We would like to develop a moving horizon strategy that reduces the computation time of the classical MHE by working on its formulation rather than changing the optimization method. What is interesting is that this kind of strategy can be combined with fast optimization methods adapted to the MHE in the literature [Ferreau et al., 2012][Zavala, 2008] to reduce even more computation time. An MH strategy of this kind has been proposed in [Sui et al., 2010] for discrete-time linear systems. It is called the Moving Horizon Estimator with Pre-Estimating Observer. In this case, model errors are compensated through

the use of an auxiliary observer without searching for estimates of process noise like in the classical MHE. The initial estimate at the beginning of the horizon hence becomes the only optimization variables. This strategy, therefore, requires less computation time than the classical one.

Thanks to its small computation time and robustness, this strategy seems interesting for the estimation problems for which the computation time of the MHE would be prohibitive such as space debris tracking during atmospheric re-entries. However, the dynamics of the debris during this phase is highly nonlinear. It is therefore interesting to develop an MH strategy similarly to the one proposed in [Sui et al., 2010] but for discrete-time nonlinear systems and then implement the developed strategy for space debris tracking during the re-entries. Since it would require the design of an observer which can be difficult especially for nonlinear systems, it is also interesting to extend the work of [Sui et al., 2010] to a strategy that would require an auxiliary estimator, such as an EKF for example, rather than an auxiliary observer. To make a generalization, we will refer to an MHE strategy using either an auxiliary estimator or an auxiliary observer as "the Moving Horizon Estimator with Pre-Estimation" (MHE-PE).

Objectives of this Work

The goals of this work are

1. To develop a nonlinear estimator which provides high accuracy of the estimates, is robust against bad initialization and model errors and requires less computation time compared to existing estimators with the same accuracy and robustness, and
2. To implement the developed estimator for space debris trajectory estimation during atmospheric re-entries.

Outline

The thesis is structured as follow

- **Chapter 1**: We review the state of the art on the object tracking during atmospheric re-entries.
- **Chapter 2**: We discuss the state of the art on the classical MHE.
- **Chapter 3**: We evaluate the performances of the classical MHE for a simplified 1D problem of space debris trajectory estimation in terms of accuracy of the estimates, computation time and robustness of the estimators against model errors and bad initialization, to verify if the MHE strategy is adapted for the problem.
- **Chapter 4**: We aim at reducing the computation time by developing an MHE-PE strategy for nonlinear systems preserving high robustness and accuracy of the estimates of the classical MHE but with less computation time.
- **Chapter 5**: We study the performances of the developed MH strategy for 3D space debris trajectory estimation.
- **Chapter 6**: We make a conclusion on the results of this work and discuss perspectives for future works.

CHAPTER 1

Introduction to Space Debris Tracking during Atmospheric Re-Entries

"It came to me when I tried to classify your species. I realized that you're not actually mammals. Every mammal on this planet instinctively develops a natural equilibrium with the surrounding environment but you humans do not. You move to an area and you multiply and multiply until every natural resource is consumed. The only way you can survive is to spread to another area. There is another organism on this planet that follows the same pattern. Do you know what it is? A virus. Human beings are a disease, a cancer of this planet. You are a plague, and we are the cure."

— Agent Smith, The Matrix

Objectives of this chapter

- To show the necessity of space debris tracking. For this, the potential threats of space debris will be discussed, followed by the presentation of on-going debris mitigations and why space debris tracking is needed.
- To show the difficulties of space debris tracking during atmospheric re-entries. For this, the real dynamics of the debris during the re-entries and the equations of radar measurements will be presented.
- To discuss the design of an estimation model and demonstrate the need of an estimator which is robust to model errors.
- To discuss the state of the art of the works on object tracking during the re-entries.

1.1 Space Debris Menace

1.1.1 What is Space Debris?

Space debris covers natural (meteoroid) and artificial (man-made) objects. Meteoroids are in orbits around the Sun, while most artificial objects are in orbits around the Earth. Man-made debris includes non-functional spacecrafts, abandoned launch object stages,

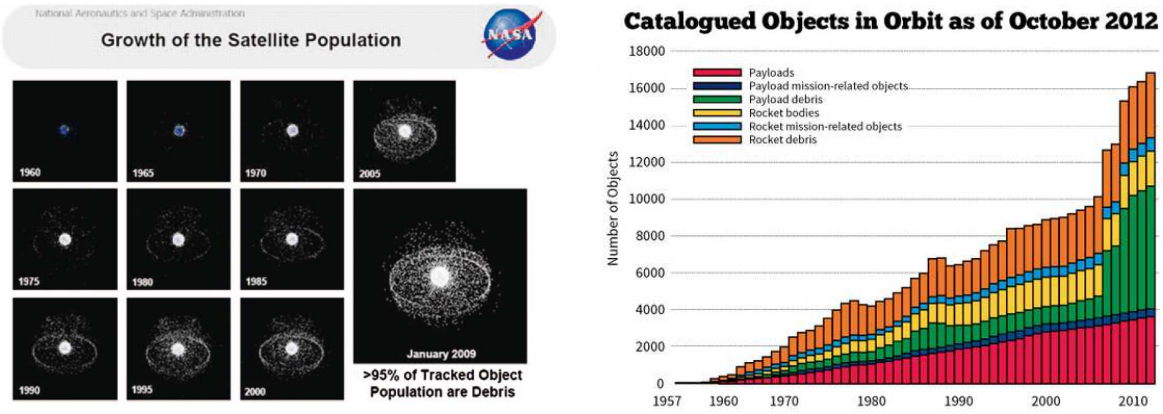

Figure 1.1: *Evolution of the satellite population in the Earth's orbit (left) and types of cataloged objects in orbit as of October 2012 (right). Credits: NASA (left), ESA (right)*

mission-related debris and fragments as a result of explosions and collisions in space, firings of satellite solid rocket motors, material aging effects, and leaking thermal-control systems.

Today, there are so many objects orbiting around the Earth that space debris has become a new hazard for space uses.

1.1.2 Space Debris Population

At the beginning of the age of space exploration, "The Big Sky Theory" was applied in space activities. This theory stipulates that orbits around the Earth are so immense that we could launch anything into them and the launched objects would not collide with anything else. Today, this is not true any more. Since Sputnik's launch in 1957, more than 4,000 satellites have been sent into space. Now, there are only around $1,000$ that are operational. More than 95 percent of all man-made objects in orbits around the Earth are debris [Imburgia, 2011].

In September 2012, the U.S. Space Surveillance Network tracked about $23,000$ orbiting objects larger than 10 *cm* using radars and optical telescopes. These tracked objects are referred to as cataloged objects. The evolution of the number of the cataloged objects and their types are shown in Fig. 1.1. Among these objects, approximately 6 % are operational spacecrafts, 21 % are old spacecrafts, 17 % are rocket upper stages, 13 % are mission-related debris, and 43 % are fragments from (mostly) explosions or collisions [Mehrholz et al., 2002]. The estimated population of particles between 1 and 10 *cm* in diameter is approximately $500,000$ and the number of particles smaller than 1 *cm* exceeds 100 million [NASA, 2012].

1.1.3 Dangers of Space Debris

This section discusses three types of dangers of space debris. The first one concerns the creation of debris belts that would prevent us from using space for generations due to high debris population in orbits. This phenomenon is called the Kessler syndrome. The second one concerns the collisions between debris and operational satellites or spacecraft and the third one concerns dangers from large object re-entries.

Kessler syndrome Proposed by the father of space debris, Donald Kessler, former Head of NASA's Orbital Debris[1] Program, in 1978, the Kessler syndrome is a cascading chain of collisions between space debris that would make space use impossible. It would happen when the population of the space debris exceeds a tipping point. In this situation, each collision would generate a swarm of debris fragments, and each of those fragments then goes on to trigger further collisions. In the hypothetical doomsday scenario, this runaway cascade continues until all satellites in orbit have been destroyed. That would dramatically impact our way of life back on Earth − no mobile phones, no GPS, no accurate weather forecasting, no satellite broadcasting [Burns, 2013].

NASA announced in 2013 that the Kessler syndrome has already begun in Low Earth Orbits (LEOs). However, according to D. Kessler, it is a decades-long process which will happen throughout the next 100 years. He also announced that the time between collisions is around 10 years at the moment and could be reduced to five years in 20 years' time [Burns, 2013]. Furthermore, LEOs are mainly used for weather forecasting, oil spill and bush fire detection, and polar ice monitoring. Communications satellites are mainly situated high up in Geosynchronous Orbits (GEOs).

Collisions with operational satellites and spacecraft In LEOs, space debris typically travels at speed between 8 and 12 km/s [Mehrholz et al., 2002], fast enough for a relatively small piece of debris to damage a satellite or a spacecraft. Figure 1.2 shows a test in which a 1.2 cm wide impactor struck a 18 cm Aluminum block at a speed of 6.8 km/s. The walls of spacecraft and rocket bodies are much thinner than this block. A 10 cm particle impacting a spacecraft will most likely result in a catastrophic disintegration. Moreover, more fragments will be generated and can induce further collisions.

Up to now, three majors collisions have been recorded. In 1996, a French reconnaissance satellite named Cerise has been hit by a fragment from the third stage of an Ariane launcher that had exploded ten years earlier (see figure 1.2). In 2007, China's anti-satellite test, which used a missile to destroy an old weather forecast satellite, added more than 3,000 pieces to the debris problem. In 2009, a defunct Russian satellite collided with a functioning U.S. Iridium commercial satellite and destroyed it. The collision added more than 2,000 pieces of trackable debris to the catalogue of space junk.

Space debris is also a threat for the International Space Station (ISS). In April 2014, the ISS, with 39 astronauts on board, narrowly avoided a collision with a part of Ariane 5 rocket launched by ESA, by approximately 0.8 km which is very small regarding the typical velocities of space debris (8-12 km/s). It was the second time in less than 3 weeks that the ISS had to sidestep debris. In fact, the ISS has had to consider sidestepping space junk dozens of times since it was launched in 1998, sometimes cancelling the orbital dodge at the last moment [Zolfagharifard, 2014].

Large object re-entry More than 32,000 tons of payloads, rocket bodies, and mission-related objects were injected into orbit since the beginning of space flight activities. Some 5,500 tons are still in space today. More than 17,000 cataloged objects have re-entered the Earth's atmosphere and most did burn up completely. However, in the case of compact and massive spacecraft, the melting and evaporation process will not be complete and fragments of the object may reach the ground. This usually occurs in an uncontrolled manner. Such uncontrolled re-entries may lead to elevated risk levels, either due to hazardous payloads (e.g. a reactor core of Cosmos 954 in 1978), or due to large masses (e.g. Skylab on 11-Jul-1979, with a mass of 74 tons and Salyut-7 on 07-Feb-1991, with a mass

[1] Orbital debris is defined as man-made space debris

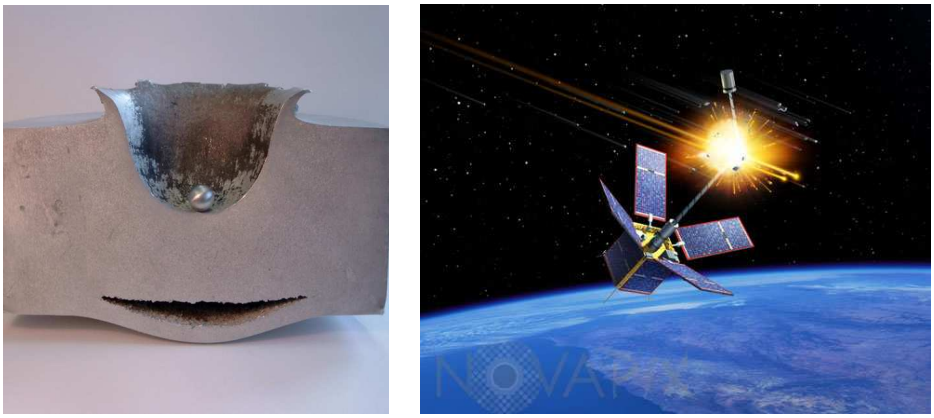

Figure 1.2: *Dangers from collisions with space debris: Supersonic impact test in which a 1.2 cm wide impactor struck a 18 cm Aluminum block at a speed of 6.8 km/s (left) and the French Cerise reconnaissance satellite being struck in 1996 by a fragment from the third stage of an Ariane launcher that had exploded ten years earlier (right). Credits: ESA*

Figure 1.3: *Large objects re-entries: the second-stage propellant tank of a Delta II launch object recovered in Texas in 1997, after orbiting Earth for nine months (left) and a 70 kg-titanium Delta 2 third stage, known as a PAM-D (Payload Assist Module - Delta), landed on Saudi Arabia in 2001 (right). Credits: NASA*

of 40 tons). [Klinkrad, 2005][Mehrholz et al., 2002]. Figure 1.3 shows two large re-entered objects.

In 2012, it is estimated that there were approximately 400 re-entering objects heavier than 800 kg per year [Morrison, 2012]. Up to now there were less than 20 large objects that have reached the ground [Aerospace.org, 2013]. Nonetheless, due to space debris mitigation guidelines established by Space Agencies worldwide, satellites in LEOs are requested to de-orbit at their end of operational life and re-enter the atmosphere. As a consequence, there will be more and more re-entries within 25 years [Klinkrad, 2005].

For controlled re-entries of recent satellites, the satellite must land on a safe area with daily casualty expectation lower than defined limit, e.g. 10^{-4} deaths for the U.S. However, many large objects in LEOs lack capability to control re-entry location. In this case, the time of the re-entry and the re-entry point must be predicted and the debris must be tracked during the re-entry. This is a very difficult task due to atmospheric and aerodynamic uncertainties [Morrison, 2012].

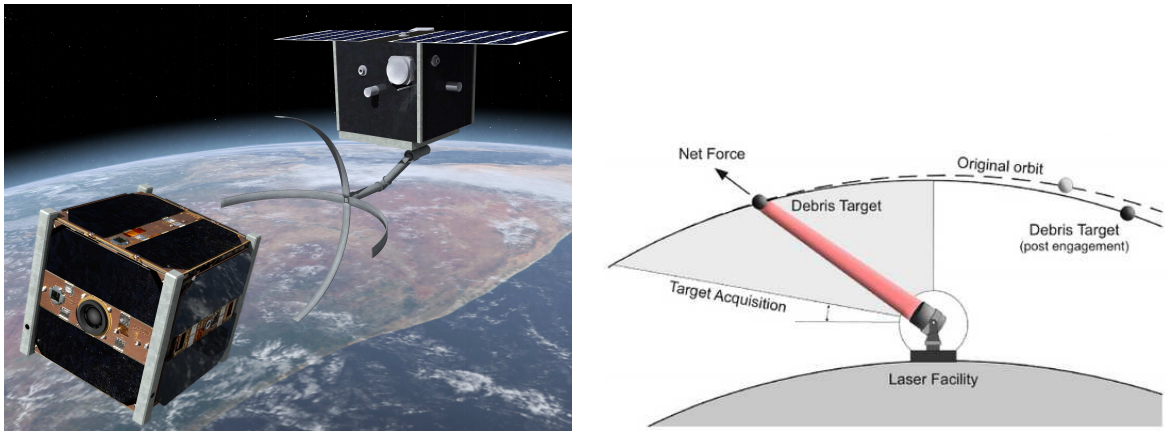

Figure 1.4: *Illustrations of the CleanSpace One Project (left) and the NASA's laser project for space debris de-orbiting (right). Credits: EPFL (left), NASA (right)*

1.1.4 Space Debris Mitigations

In order to overcome the Kessler syndrome and to guarantee space use in the future, the population of space debris must be controlled. This can be done by:

- Avoiding new collisions between debris and operational satellites and between debris and debris
- De-orbiting defunct satellites to a less densely populated orbit
- Doing active removal

Collision avoidance can be done by tracking space debris using radar measurements provided by ground stations, predicting the trajectories of large objects, calculating the probability of collisions with operational satellites and deviating the trajectory of the satellite at risk [Klinkrad, 2005]. For satellites in the high GEO region, they are recommended to de-orbit to a higher orbit, referred to as "graveyard orbit". This will keep them out of their previous densely populated orbits for at least a few hundred years.

Researchers are also looking seriously into active debris removal. The United States Department of Defense has launched Phoenix Program which aims at using a robot mechanic-like object to snag still-working antennas from the many retired and dead satellites in GEOs. The Japanese Aerospace Agency (JAXA) is working on magnetic nets that will use a specially generated magnetic field to reel-in the debris in LEOs. Once the debris is captured, the nets will be pulled down by Earth's gravity, incinerating the junk once the net enters the atmosphere. This mission is planned for 2019. L'Ecole Polytechnique Federale de Lausanne (EPFL) and the Swiss Space Systems have also launched the CleanSpace One Project in which a robotic spacecraft will be launched into orbit from an airplane. The spacecraft will chase down a target satellite, grab it and then jump back into the Earth's atmosphere, destroying itself along with the derelict satellite. The project is planned for 2018. NASA is also working on laser for removing space debris. The idea is to de-orbit a piece of debris by slowing it down using a ground-based laser. Then, the slowed down object will start to re-enter the atmosphere [Mason et al., 2011]. Figure 1.4 shows illustrations of the CleanSpace One Project and the NASA's laser project for space debris de-orbiting.

1.1.5 Space Debris Tracking

Space debris tracking is needed

- To avoid new collisions with operational satellites and spacecraft
- To do active removal
- To determine the re-entry window (time and location) of large objects

The tracking is mainly done using ground-based radars for debris in LEO altitudes and optical telescopes for debris whose altitude is above LEOs [Klinkrad, 2006]. The measurements from radar stations and telescopes are the distance, the elevation angle and the azimuth angle. Sometimes, Doppler measurements which are equivalent to the measurements of the object's velocity are also given. In our studies, we consider only distance and angles measurements which is the most difficult tracking problem since less information on the debris is given.

In [Mehrholz et al., 2002], the space debris tracking process is described as follows:

> There is generally a priori information available, such as some orbital elements and the approximate size of the object (radar cross-section). The radar beam is pointed to a pre-determined position in space and after detection the object is tracked and observation vectors are collected, from which its orbital parameters and radar signature can be computed. The latter provides clues as to the object's intrinsic motion (rotation or tumbling rate). This mode of observation is called "target directed" and is used when the uncertainty in the knowledge of an object's orbit is unacceptably high and more precise information is required, for instance for collision-avoidance manoeuvres for operational spacecraft and for re-entry predictions for potentially dangerous objects.

Nevertheless, the measurements given by radar are noisy due to the imperfection of the sensors and atmospheric perturbation. One can make use of knowledge in the dynamics of the debris to gain better accuracy using an estimation algorithm where the "state" of the system which is defined as "information required to describe the system under investigation" is estimated. This algorithm is called an "estimator" or a "filter". To estimate the state of a system, an estimator uses noisy measurements issued from the system, a model of evolution of the system over time (an estimation model) and a model relating the noisy measurements to the state (a measurement model).

If the dynamics of the system is not well known, an estimation model that fully describes the system cannot be derived. In this case, model errors are present and the used estimator must be robust to these errors. This is the case for space debris tracking during atmospheric re-entries due to the complexity in modeling aerodynamic forces acting on the debris [Mehrholz et al., 2002][Morrison, 2012]. The difficulties of this problem will be discussed in the next section.

1.2 Difficulties in Space Debris Tracking during the Re-Entries

During the re-entries (below 120 km of altitude [Gallais, 2007]), the dynamics of space debris is mostly poorly known. This is due to unknown variations of aerodynamic force

which is the most dominant force during the re-entries [Klinkrad, 2006]. Tracking space debris during the re-entries is therefore a very difficult problem for uncontrolled objects [Mehrholz et al., 2002]. Let us discuss the dynamics of space debris during the re-entries and the radar measurement equations to see the complexity of the tracking problem.

1.2.1 Unknown Dynamics of Space Debris During the Re-entries

Consider the trajectory of a piece of space debris during its atmospheric re-entry following these assumptions. First, we assume that:

(a1) The debris has a direct re-entry to the ground and that the re-entry is fast enough that the Earth's rotation can be neglected

As a consequence of (a1), the Earth-centered, Earth fixed (ECEF) coordinates can be considered as an inertial frame and are used to describe the dynamics of the debris. The ECEF coordinates have the center of the Earth O as the center and $\vec{e}_{x_{ECEF}}$, $\vec{e}_{y_{ECEF}}$ and $\vec{e}_{z_{ECEF}}$ as their unit vectors, see figure 1.5. Denote D as the point of the center of mass of the debris and $\vec{OD}$ the distance vector between the debris D from the center of the Earth O. Define $\mathbf{r}_{EF}$ the distance vector $\vec{OD}$ described in the ECEF coordinates as:

$$\mathbf{r}_{EF} = \vec{OD} = r_{x_{ECEF}} \cdot \vec{e}_{x_{ECEF}} + r_{y_{ECEF}} \cdot \vec{e}_{y_{ECEF}} + r_{z_{ECEF}} \cdot \vec{e}_{z_{ECEF}} \tag{1.1}$$

Denote $\mathbf{v}_{EF}$ and $\mathbf{a}_{EF}$ the velocity and the acceleration of the debris described in the ECEF coordinates respectively. We have

$$\mathbf{a}_{EF} = \dot{\mathbf{v}}_{EF} = \ddot{\mathbf{r}}_{EF} \tag{1.2}$$

We assume also that

(a2) The only major forces acting on the object are the gravitational force and the aerodynamic force. This assumption is realistic below altitudes of ~ 120 km [Klinkrad, 2006]

(a3) The object admits an axis of symmetry

The aerodynamic force can be decomposed in the drag component and the lift component for an object admitting an axis of symmetry. Denote $\mathbf{v}_{air}$ the velocity of the air in the ECEF coordinates. Define the velocity of the object relative to air $\mathbf{v}_{D/air}$ in the ECEF coordinates as

$$\mathbf{v}_{D/air} = \mathbf{v}_{EF} - \mathbf{v}_{air}$$

The drag component is the component along the direction of $\mathbf{v}_{D/air}$ but in the opposite direction. The Lift is defined as the component normal to $\mathbf{v}_{D/air}$ on the symmetry plane of the object, see figure 1.6.

For the sake of simplicity we assume that

(a4) The lift can be neglected

This assumption is realistic for the following types of objects:

- Spherical objects, such as most of meteors and the PAM-D upper stage in Fig.1.3

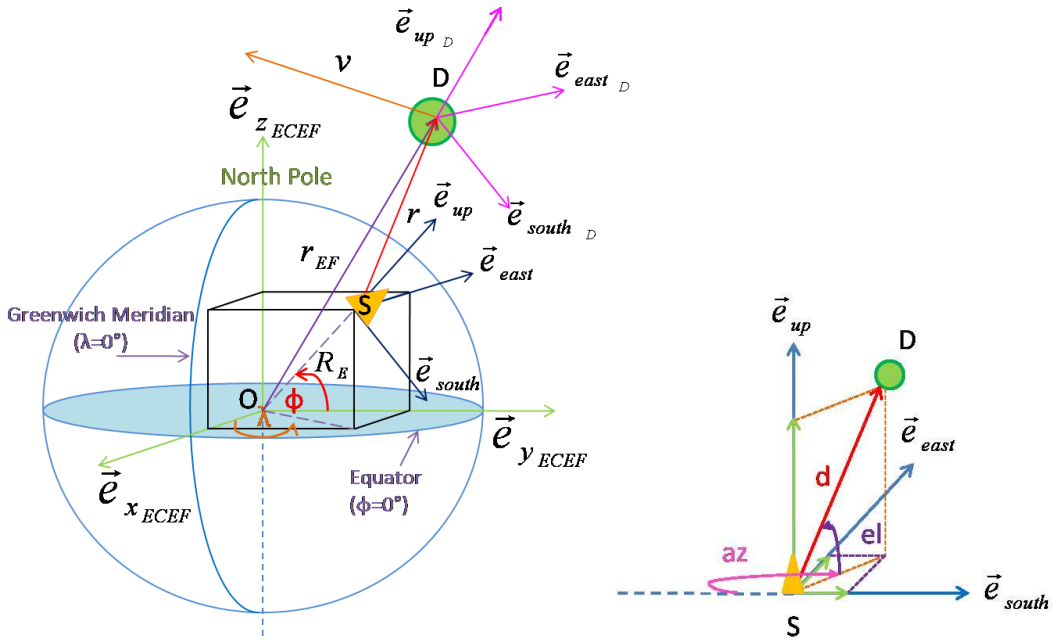

Figure 1.5: *ECEF, SEU and SEU_D coordinates in green, blue and magenta respectively. S: radar station, D: space debris, O: center of the Earth (left). Illustration of the radar measurements (right). The elevation angle el is defined as the angle between the distance vector between the object D and the radar station S and the ground. The azimuth angle az is defined as the angle between the north direction $-\vec{e}_{south}$ to the projection of the distance vector on the ground.*

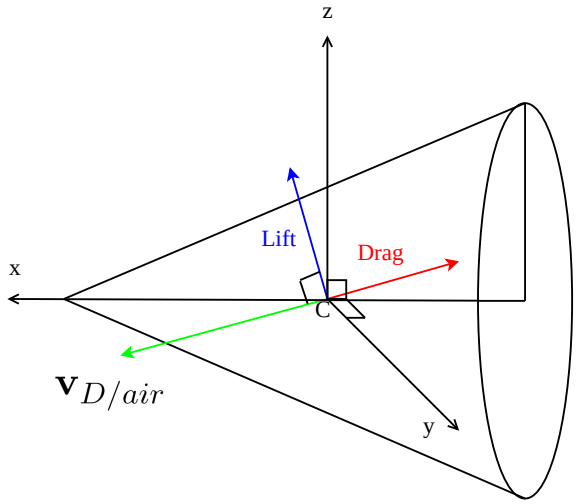

Figure 1.6: *Consider an object admitting a symmetry plane. Define C the center of mass of the object, axis Cx is chosen as the axis of symmetry of the object, Cz is chosen to be perpendicular to Cx and be in the plane of symmetry. Denote $\mathbf{v}_{D/air}$ the relative velocity of the object to the air. The aerodynamic force acting on the object can be decomposed in 2 components. The drag is defined as the component along the direction of $\mathbf{v}_{D/air}$ but in the opposite direction. The Lift is defined as the component normal to $\mathbf{v}_{D/air}$ in the symmetry plane*

- Unmanned re-entering objects, such as for Mars mission. These objects are generally designed to have small lift compared to drag for its aerodynamic stability during direct entry [Brown, 2008] [Schoenenberger et al., 2009]
- Axisymmetric objects (generally the case for planetary entry probes), with a negligible angle between the velocity of the object and the horizontal plane, also called a flight path angle, at the beginning of the re-entry [Gallais, 2007]
- Military re-entering objects thanks to their designs [Gallais, 2007]

Define H the altitude of the object which is function of the position of the object $\mathbf{r}_{EF}$ and R_E the mean Earth radius as

$$H(\mathbf{r}_{EF}(t)) = \|\mathbf{r}_{EF}(t)\| - R_E \tag{1.3}$$

The dynamics of the object is described by

$$\mathbf{a}_{EF}(t) = -\frac{GM}{\|\mathbf{r}_{EF}(t)\|^3}\mathbf{r}_{EF}(t) - \frac{\rho(H(\mathbf{r}_{EF}(t)))C_D(t)A(t)}{2m(t)}\|\mathbf{v}_{EF}(t)\|\mathbf{v}_{EF}(t) \tag{1.4}$$

The first term on the r.h.s. of the acceleration represents the gravity and the second term represents the acceleration due to the drag. G_E is the Earth's gravitational constant, M is the mass of the Earth, m is the mass of the object, A is the cross section and C_D is the drag coefficient of the object. The atmosphere density ρ depends on the altitude of the object H, modelled by

$$\rho(H(t)) = \mathsf{c}_1 e^{-\mathsf{c}_2 H(t)} \tag{1.5}$$

$\mathsf{c}_1 = 1.227\ kg/m^3$, $\mathsf{c}_2 = 1.093 \cdot 10^{-4}\ m^{-1}$ for $H < 9144\ m$ and $\mathsf{c}_1 = 1.754\ kg/m^3$, $\mathsf{c}_2 = 1.490 \cdot 10^{-4}\ m^{-1}$ for $H \geq 9144\ m$ [Farina et al., 2002].

Denote that m and A of the object can be time-varying since the object can be burnt up during the re-entry. C_D is also generally time-varying. Even when m and A are constant, the calculation of $C_D(t)$ can be very difficult. For an axisymmetric object, C_D depends on the altitude H, the velocity, the geometry and the angle of attack[2] of the object [Gallais, 2007]. For a sphere, C_D depends only on the Reynolds number which depends on the altitude, the velocity and the cross section of the object [Morrison, 2010].

Ballistic coefficient Since the variations in time of m, A and C_D are complex and generally difficult to compute, it is interesting to define a new variable assembling these three unknowns. This variable is called the ballistic coefficient of the object $\beta \in \mathbb{R}^{+*}$, defined as

$$\beta(t) = \frac{m(t)}{A(t) \cdot C_D(t)} \tag{1.6}$$

β characterizes the ability to resist the drag of the object. An object with a high β loses less speed due to the drag compared to an object with a low β.

Re-entry military objects are usually designed to maintain a high velocity. Their values of β are usually high. The typical values are $5000 - 10000\ kg/m^2$ [Gallais, 2007]. Moreover, β of a re-entry military object is nearly constant. On the other hand, planetary entry probes are generally designed to have high braking at high altitude and low atmosphere

[2]The angle between the relative velocity of the object to the air ($v_{D/air}$) and the axis of symmetry of the object

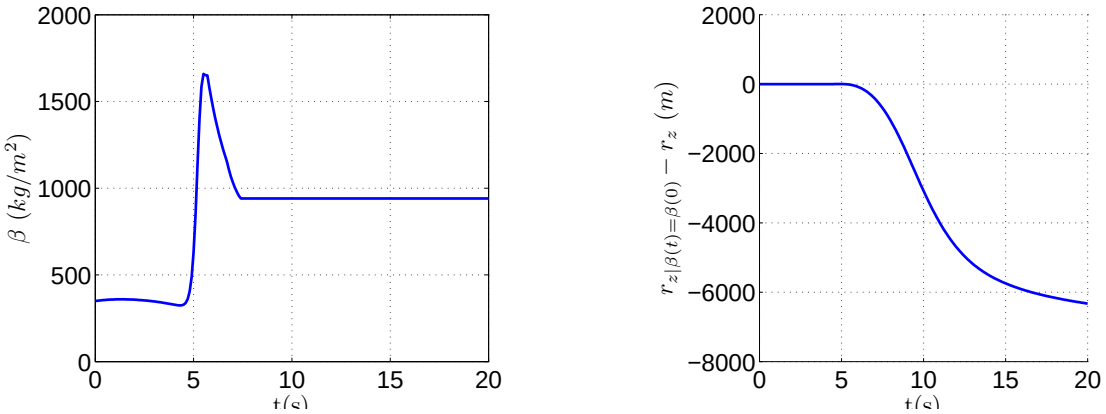

Figure 1.7: *Example of variation of β of a piece of space debris with time (left). Example of position difference with time between two cases: the one where β is constant equal to the initial value $\beta(0)$, e.g. a case of military vehicles, and the one where β varies with time starting from the value $\beta(0)$, e.g. a case of space debris (right).*

density to lessen heat stresses, and to allow soft landing. Their values of β are usually low. The typical values are $50 - 100\ kg/m^2$. Concerning space debris, if the debris is burnt during the re-entry, m and A may vary with time. The rotation of the debris also causes the variation of A. Moreover, C_D can have high variation with time. Hence, β of space debris during the re-entry is generally a time-varying function as described in (1.6).

To visualize the variation of β, the trajectory of an Aluminum hollow sphere debris during the re-entry is simulated. This shape can represent upper stages and pressure tanks of satellites or of launch vehicles. In the simulation, an outer diameter of 22.17 cm and a thickness of 3 cm are chosen. The mass and the diameter of the debris are supposed to be constant. The debris is assumed to fall down vertically to the ground. The initial altitude of 69.767 km and the initial speed of 5695.7 m/s are chosen. An analytical expression of C_D of a sphere in function of the altitude H, the speed of the debris $\|\mathbf{v}_{EF}\|$ and the diameter of a sphere can be found in section C.1. Figure 1.7 (left) shows the variation of β with time of the debris during 20 s of its re-entry. To compare the effect on the position of the debris due to the variation of β. The trajectory of the same sphere but whose β is constant equal to the initial value $\beta(0)$ during the re-entry, is also simulated, although this case is not realistic. Figure 1.7 (right) shows the difference of the positions r_z in time between the case where β is constant and the one where β varies starting from the value $\beta(0)$. An object whose β is nearly constant is a military vehicle for example.

Thanks to this figure, we see that it is important to take into account the variation of β to have an accurate prediction of the position of space debris.

Dynamic equation of an object during the re-entry Combine (1.4) and (1.6), the dynamic equation of the object becomes

$$\mathbf{a}_{EF}(t) = -\frac{G_E M}{\|\mathbf{r}_{EF}(t)\|^3}\mathbf{r}_{EF}(t) - \frac{\rho(H(\mathbf{r}_{EF}(t)))}{2\beta(t)}\|\mathbf{v}_{EF}(t)\|\mathbf{v}_{EF}(t) \tag{1.7}$$

To implement an estimator, a model of the dynamics of the debris, i.e. the estimation model, must be chosen. However, an estimation model that can fully describe the dynamics of the debris during the re-entries does not exist due to unknown evolution of the ballistic

coefficient. As a consequence, estimation errors due to the estimation model, called model errors, are present. This is the first difficulty in space debris tracking during the re-entries.

In this work, we consider a problem of space debris tracking using radar measurements which are the distance, the elevation angle and the azimuth angle of the debris from the radar station. These radar measurements may be noisy due to atmospheric perturbation and sensor imperfection. This is the second difficulty of the problem. The equation of the radar measurements as function of the position of the debris will be described in the next section.

1.2.2 Noisy Radar Measurements

Denote λ and ϕ the longitude and the latitude of the radar station respectively. Denote S as the point where the radar station locates, $\vec{SD}$ the distance between the debris and the radar station and $\vec{e}_{south}$, $\vec{e}_{east}$, $\vec{e}_{up}$ unit vectors along the south, east and up direction respectively (see Fig. 1.5). Define the SEU coordinates as the coordinates centered at the point S and whose axes are $\vec{e}_{south}$, $\vec{e}_{east}$, $\vec{e}_{up}$. Define $\mathbf{r}$ the vector $\vec{SD}$ described in the SEU coordinates as follows:

$$\mathbf{r} = \vec{SD} = r_x\vec{e}_{south} + r_y\vec{e}_{east} + r_z\vec{e}_{up} \tag{1.8}$$

Equivalently, we have

$$\mathbf{r} = \begin{pmatrix} r_x \\ r_y \\ r_z \end{pmatrix} \tag{1.9}$$

The position of the debris from the center of the Earth in the ECEF coordinates $\mathbf{r}_{EF}$ can be converted into the position of the debris from the radar station in the SEU coordinates $\mathbf{r}$ using:

$$\mathbf{r} = \begin{pmatrix} sin\phi cos\lambda & sin\phi sin\lambda & -cos\lambda \\ -sin\lambda & cos\lambda & 0 \\ cos\phi cos\lambda & cos\phi sin\lambda & sin\phi \end{pmatrix} \mathbf{r}_{EF} - \begin{pmatrix} 0 \\ 0 \\ R_E \end{pmatrix} \tag{1.10}$$

Denote $\mathbf{v}$ and $\mathbf{a}$ the velocity and the acceleration of the object in the SEU coordinates respectively. They can be calculated from $\mathbf{v}_{EF}$ and $\mathbf{a}_{EF}$ by differentiating (1.10). Remark that $\dot{\vec{SD}} = \underbrace{\dot{\vec{SO}}}_{=0} + \dot{\vec{OD}}$. As a consequence,

$$\|\mathbf{v}\| = \|\mathbf{v}_{EF}\| \tag{1.11}$$

$$\|\mathbf{a}\| = \|\mathbf{a}_{EF}\| \tag{1.12}$$

The trajectory of the object will be estimated from noisy radar measurements which are the measurements of the distance d, the elevation angle el and the azimuth angle az between the radar station (S) and the object (D). Consider figure 1.5. The elevation angle el is defined as the angle between the distance vector between the object D and the radar station S and the ground. The azimuth angle az is defined as the angle between the north direction $-\vec{e}_{south}$ to the projection of the distance vector on the ground. Denote d^m, el^m and az^m the measured distance, elevation and azimuth respectively.

The radar measurements are supposed to be available every T_s second. Define $\mathbf{r}_k = \mathbf{r}(t = kT_s)$, $k \in \mathbb{N}$. The discrete-time measurement vector at instant k is defined as

$$y_k = h(x_k) + v_k = \begin{pmatrix} d_k^m \\ el_k^m \\ az_k^m \end{pmatrix} = \begin{pmatrix} d_k \\ el_k \\ az_k \end{pmatrix} + v_k = \begin{pmatrix} \sqrt{r_{x_k}^2 + r_{y_k}^2 + r_{z_k}^2} \\ \arcsin(\frac{r_{z_k}}{d_k}) \\ \arctan(\frac{r_{y_k}}{-r_{x_k}}) \end{pmatrix} + v_k \tag{1.13}$$

where

$$d_k = \sqrt{r_{x_k}^2 + r_{y_k}^2 + r_{z_k}^2} \tag{1.14}$$

$$el_k = \begin{cases} \arcsin(\frac{r_{z_k}}{d_k}) & \text{if } r_{z_k} \neq d_k \\ \frac{\pi}{2} & \text{otherwise} \end{cases} \tag{1.15}$$

$$az_k = \arctan(\frac{r_{y_k}}{-r_{x_k}}) \tag{1.16}$$

The superscribe m stands for "measured". el_k is defined equal to $\pi/2$ when $r_{z_k} = d_k$ to make the measurement function (h) $\mathcal{C}^2$ which is one of the properties we need for the study afterwards.

v_k is a discrete-time measurement noise modelled by a zero-mean bounded white noise with covariance matrix.

$$R = \begin{pmatrix} \sigma_d^2 & 0 & 0 \\ 0 & \sigma_{el}^2 & 0 \\ 0 & 0 & \sigma_{az}^2 \end{pmatrix} \tag{1.17}$$

where σ_d, σ_{el} and σ_{az} are the standard deviations associated to the measurement noise.

Now, let us discuss the last difficulty of space debris tracking during the re-entries.

1.2.3 Unknown Initial Ballistic Coefficient due to a Breakup

It is possible that an object during the re-entry disintegrates into many fragments due to high mechanical loads and heating rates. This phenomenon is called a "breakup". Figure 1.8 shows the area in which debris generally spread after breakups. Most of the breakups occur at $\sim$ 80 km [Battie et al., 2012] [Ailor, 2012] so it is impossible to predict the size and the ballistic coefficient of each fragment in advance. An a priori value of the ballistic coefficient given to an estimator may, therefore, have high errors. This bad initialization of the estimator may lead to divergence or high estimation errors. This is the third difficulty of the space debris tracking during the re-entries.

1.2.4 Summary of Difficulties in Space Debris Tracking during the Re-entries

In this section, we have seen the following difficulties for the design of an estimation algorithm to solve a space debris tracking problem during the re-entries:

- The debris tracking is realized using radar measurements which are noisy. An estimator should therefore be implemented to gain better accuracy on the position of the debris

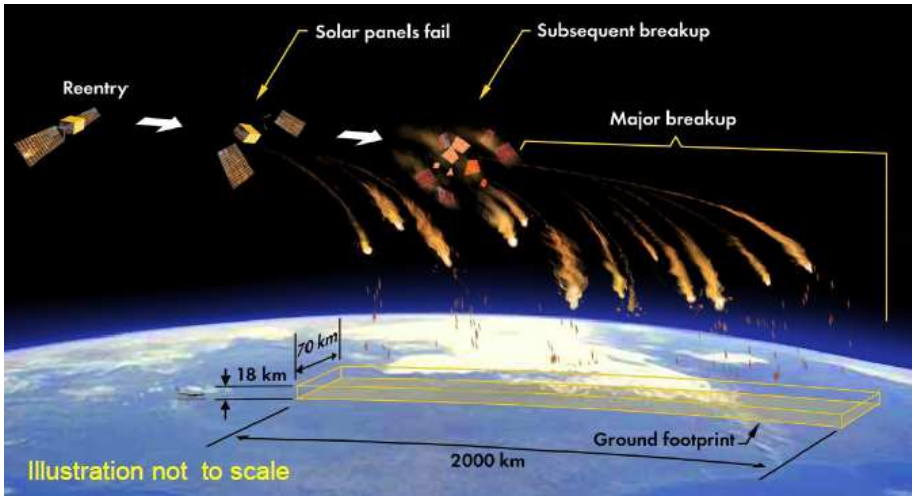

Figure 1.8: *Space hardware re-enters at very shollow angle ($< 1°$). Most of the breakups occur at ~ 80 km or lower. Debris spreads over long, narrow footprint ($\sim 2000 \times 70km$). 10 to 40 % of dry mass on orbit survives to the Earth's surface, posing potential hazard to people and property [Ailor, 2012]*

- To implement an estimator, a model of the dynamics of the debris must be chosen. This model is called an "estimation model". However, the dynamics of the debris is very complex. The mass and the diameter of the debris can vary in time and the drag force cannot be precisely described due to the unknown evolution of its ballistic coefficient. As a consequence, one can only have an estimation model that describes the real dynamics of the debris approximately. The used estimator should therefore be robust to these model errors
- High initial error on an a priori value of the ballistic coefficient estimate is possible if the debris is created during a breakup

Two estimation models will be proposed in the next section. The first one uses a hypothesis of a nearly constant ballistic coefficient and a nearly constant acceleration over a sampling period which is used in the existing work on military object tracking during the re-entry with unknown ballistic coefficient [Ristic et al., 2003]. The second one, proposed here for the first time, uses a hypothesis of a nearly constant acceleration derivative during a sampling period.

1.3 Estimation Models of Space Debris during the Re-entries

Before discussing the estimation models used in an estimator for space debris tracking during the re-entries, let us consider a general estimation problem.

1.3.1 General Estimation Problem

Let us introduce the state vector $x_k \in \mathbb{R}^{n_x}$ representing the real system. n_x is the dimension of the state vector and $k \in \mathbb{N}$ is a time index. The state is supposed to evolve according to an estimation model as follows:

$$x_k = f(x_{k-1}) + w_{k-1} \tag{1.18}$$

f is called a state function, and w_k is a process noise. The process noise w_k takes into account not only disturbances in the estimation model *but also model errors* [Ristic et al., 2004]. The state of the system will be estimated using the output of the system, referred to as the measurements. Denote $y_k \in \mathbb{R}^{n_y}$ the measurement vector at instant k. The measurements are supposed to be related to the state by a measurement model as follows:

$$y_k = h(x_k) + v_k \tag{1.19}$$

h is a measurement function and v_k is a measurement noise. w_k and v_k are assumed to be zero-mean non-correlated white noises. Denote Q_k and R_k the covariances of w_k and v_k respectively.

♠ The goal of the nonlinear estimation is to estimate the real state x_k based on the sequence of all available measurements $y_0^k = \begin{pmatrix} y_0^T & \dots & y_k^T \end{pmatrix}^T$. Denote $\hat{x}_k^- \triangleq \hat{x}_{k|k-1}$ the a priori estimate at instant k and $\hat{x}_k \triangleq \hat{x}_{k|k}$ the a posteriori estimate at instant k.

The estimation problems can be stated in two different frameworks: a deterministic one and a stochastic one, both can deal with systems under noises. The deterministic framework is deterministic in the sense that the initial state, the process and the measurement noise are considered to be unknown deterministic variables. The stochastic framework is stochastic in the sense that the initial state, the process and the measurement noise are considered to be unknown random variables.

Estimation in a deterministic framework In this framework, the initial state, the process and measurement noises are considered to be unknown deterministic variables [Alessandri et al., 2003]. An example of an estimator considering this framework is the Moving Horizon Estimator (MHE) in the deterministic framework [Alessandri et al., 2010] in which a least-squares criterion based on the measurements over the most recent time interval is used.

Estimation in a stochastic framework In this framework, the initial state, the process and measurement noise are considered to be random variables. The state x_k of the real system is therefore considered as a random variable as well. The problem consists in constructing the a posteriori probability density function (pdf), generally referred to as a posteriori density of the state x_k based on y_0^k, noted by $p(x_k|y_0^k)$. Then, the a posteriori estimate $\hat{x}_k$, supposed to be equal to the expectation of the random variable x_k, can be computed. Examples of estimators considering this framework are the Extended Kalman Filter (EKF), the Unscented Kalman Filter (UKF), the Particle Filter (PF) and the Moving Horizon Estimator (MHE) in the stochastic framework [Rao et al., 2003][Ungarala, 2009].

♠ Our objective is to estimate the trajectory of the debris during atmospheric re-entries using noisy radar measurements (distances, elevation angles, azimuth angles).

Constraints According to [Ristic et al., 2004], one can have constraints imposed either on the state vector or on the process and the measurement noises in some estimation problems. In the case of space debris tracking during the re-entries, we can have constraints on target position (positive altitude for example), speed (decreasing due to aerodynamics

drag) or ballistic coefficient (strictly positive). In general, the performance of an estimator is improved by incorporating constraints into the estimator.

Now, two estimation models of the debris during the re-entries which will be used in an estimator will be proposed. As mentioned before, it is impossible to model the dynamics of the space debris accurately due to the unknown variation of the ballistic coefficient $\beta(t)$ in (1.7). The estimation models we propose here are only simplified versions of the real dynamics of the debris in section 1.2.1.

1.3.2 Estimation Models used for Space Debris Tracking during the Re-entries

Two estimation models are considered:

- The first one includes the position, the velocity and the ballistic coefficient of the object in the state vector and assumes that the time derivative of $\beta(t)$ is driven by a zero-mean white noise. This model is used in the literature for military object tracking during the re-entries [Ristic et al., 2003][Minvielle, 2002].
- The second model includes the position, the velocity and the acceleration of the object in the state vector. In this model, it is assumed that the derivative of acceleration $\mathbf{a}(t)$ is driven by a zero-mean white noise where $\beta(t)$ is assumed to be constant during a sampling period in the computation of $\dot{\mathbf{a}}$. The second model therefore benefits from knowledge in the derivative of the acceleration while the first one does not. There exist works on re-entering object tracking considering acceleration in the state vector [Brooks, 2010][Cardillo et al., 1999]. However, in their works the derivative of the acceleration $\dot{\mathbf{a}}$ is chosen equal to zero unlike what we propose here.

An analysis of the advantages of the second model with respect to the first one will be provided later in chapter 3.

♠ We precise that our works focus on developing an estimator which can guarantee small estimation errors despite model errors that may be caused by simplified estimation models like in space debris tracking during the re-entries.

For our space debris tracking problem, the models will be presented first in continuous-time since assumptions on the dynamics of the debris are made in continuous-time. Since the measurements are available in discrete-time, discrete-time versions of the estimation models are easier to implement and a discrete-time version of the presented estimation models will be derived. Before discussing the estimation models, let us consider the common assumptions used in both estimation models: the flat Earth and constant gravity assumptions.

1.3.2.1 Flat Earth and Constant Gravity Assumptions

It is assumed that the debris is close enough to the radar station that the Earth can be considered flat in the observation space. To see the picture clearer, consider the local coordinates of the debris centered at the center of mass of the debris $(D, \vec{e}_{south_D}, \vec{e}_{east_D}, \vec{e}_{up_D})$ and the local coordinates of the radar station $(S, \vec{e}_{south}, \vec{e}_{east}, \vec{e}_{up})$ described in figure 1.5. If the debris and the station is close enough that the unit vectors of the SEU_D coordinates can be considered parallel to those of the SEU coordinates component by component, then

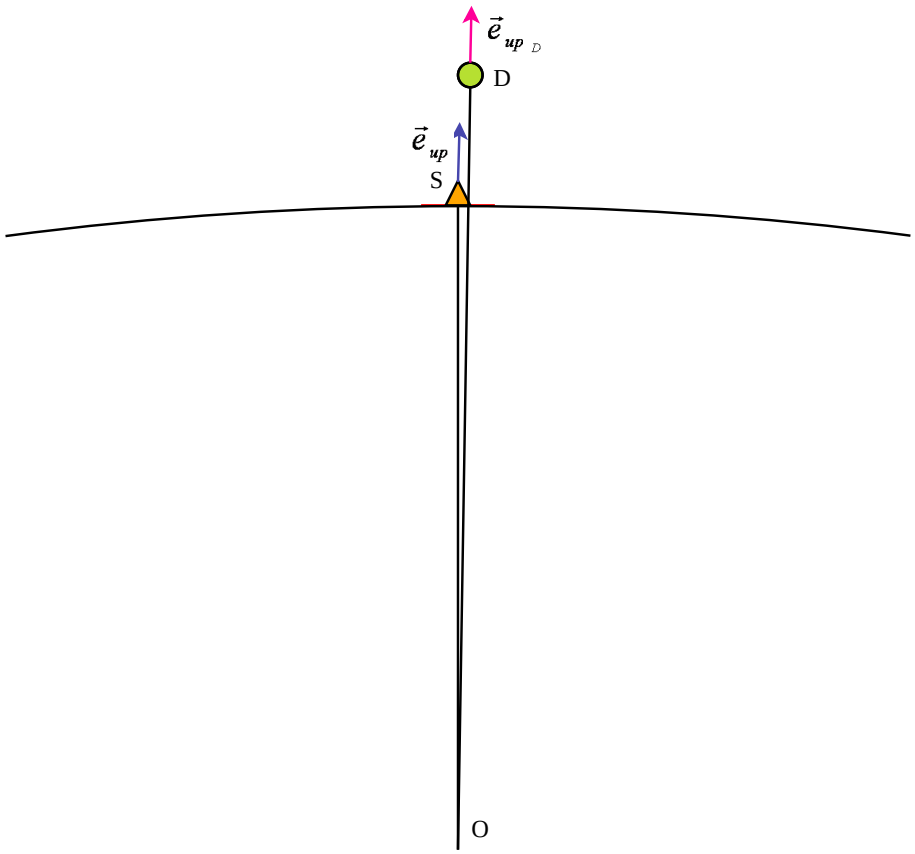

Figure 1.9: *Flat Earth assumption can be considered when the debris is close enough to the radar station that the coordinates SEU can be considered parallel to the coordinates SEU_D. In this case, it can be considered that $r_z = H$.*

the Earth is nearly flat in the observation space as presented in figure 1.9.

Thanks to this assumption, we have in both estimation models:

$$H = r_z \tag{1.20}$$

The gravity is considered constant and pointing downward. In our studies, only space debris not farer than 100 km from the station are considered. Hence, the flat Earth and the constant gravity assumptions are realistic.

Now, let us consider the first estimation model which is the one with ballistic coefficient as a state variable.

1.3.2.2 Estimation Model with Ballistic Coefficient as a State Variable

Continuous-time estimation model with ballistic coefficient This model includes the position $\mathbf{r}(t)$, the velocity $\mathbf{v}(t)$, both in SEU coordinates and the ballistic coefficient $\beta(t)$ of the object in the state vector and assumes that the time derivative of $\beta(t)$ is driven by a zero-mean white noise.

Denote $x(t)$ the state vector at time t. It is defined as

$$x(t) = \begin{pmatrix} \mathbf{r}(t)^T & \mathbf{v}(t)^T & \beta(t) \end{pmatrix}^T \tag{1.21}$$

It is assumed that the derivative of $\beta(t)$ is driven by a continuous-time zero-mean white noise $w_\beta(t)$ with a power spectral density $q_\beta(t)$. In other words,

$$E\{w_\beta(t)w_\beta(\tau)\} = q_\beta(t)\delta(t-\tau) \tag{1.22}$$

where $\delta(\cdot)$ is the dirac distribution. For the sake of simplicity, $q_\beta(t)$ is assumed to be constant and equal to q_β.

The estimation model is described by

$$\begin{aligned} \dot{\mathbf{r}}(t) &= \mathbf{v}(t) \\ \dot{\mathbf{v}}(t) &= -\frac{1}{2}\frac{\rho(r_z(t))}{\beta(t)}\|\mathbf{v}(t)\|\,\mathbf{v}(t) - \begin{pmatrix} 0 \\ 0 \\ g_E \end{pmatrix} \\ \dot{\beta}(t) &= w_\beta(t) \end{aligned} \tag{1.23}$$

where ρ is calculated using (1.5) and recall that $H(t) = r_z(t)$ as in (1.20).

The gravity term $\begin{pmatrix} 0 & 0 & g_E \end{pmatrix}^T$ is derived from (1.7) by assuming that the positions in SEU coordinates $r_{x,y,z}$ are much smaller than the Earth's radius R_E. In fact, the acceleration in SEU coordinates $\mathbf{a}$ can be derived from that in the ECEF coordinates $\mathbf{a}_{EF}$ using the transformation matrix in (1.10) as follows:

$$\mathbf{a} = \begin{pmatrix} sin\phi cos\lambda & sin\phi sin\lambda & -cos\lambda \\ -sin\lambda & cos\lambda & 0 \\ cos\phi cos\lambda & cos\phi sin\lambda & sin\phi \end{pmatrix} \mathbf{a}_{EF} = -\frac{G_E M}{\|\mathbf{r}_{EF}\|^3}\begin{pmatrix} r_x \\ r_y \\ r_z + R_E \end{pmatrix} - \frac{\rho(H)}{2\beta}\|\mathbf{v}\|\,\mathbf{v} \tag{1.24}$$

Using the fact that $r_{x,y,z} \ll R_E$, we have $\|\mathbf{r}_{EF}\| \sim R_E$ and

$$\begin{pmatrix} r_x \\ r_y \\ r_z + R_E \end{pmatrix} \sim \begin{pmatrix} 0 \\ 0 \\ R_E \end{pmatrix}$$

Therefore,

$$\mathbf{a} \sim -\begin{pmatrix} 0 \\ 0 \\ \frac{G_E M}{R_E^2} \end{pmatrix} - \frac{\rho(H)}{2\beta}\|\mathbf{v}\|\,\mathbf{v} \tag{1.25}$$

The Earth's gravity $g_E \triangleq \frac{G_E M}{R_E^2}$ varies depending on the location of the debris. The nominal "average" value at the Earth value at the Earth's surface, known as standard gravity is, by definition $g_E = 9.80664\ m/s^2$ [Mechtly, 1964]. This average value will be used in our study.

Discrete-time estimation model with ballistic coefficient In order to implement the estimators and since measurements from radar station will be available at discrete-time intervals, (1.23) is discretized. Denote $\mathbf{r}_k$, $\mathbf{v}_k$ and β_k the value of $\mathbf{r}(t)$, $\mathbf{v}(t)$ and $\beta(t)$ at time $t = kT_s$, for $k \in \mathbb{N}$, where T_s is the sampling period chosen equal to the measurement interval for the sake of simplicity. It is assumed that $\forall t \in [kT_s, (k+1)T_s]$

$$\dot{\mathbf{v}}(t) = \mathbf{a}_k + \mathbf{w}_a(t) \tag{1.26}$$

where

$$\mathbf{a}_k = -\frac{1}{2}\frac{\rho(r_{z_k})}{\beta_k}\|\mathbf{v}_k\|\,\mathbf{v}_k - \begin{pmatrix}0\\0\\g_E\end{pmatrix} \tag{1.27}$$

and $\mathbf{w}_a(t)$ is a continuous-time zero-mean white noise vector, accounting for discretization error with a power spectral density $\mathbf{q}_a(t)$. In other words,

$$E\{\mathbf{w}_a(t)\mathbf{w}_a^T(\tau)\} = \mathbf{q}_a(t)\delta(t-\tau) \tag{1.28}$$

For the sake of simplicity, we assume $\mathbf{q}_a(t)$ to be constant equal to $\mathbf{q}_a$ and that each component of w_a is uncorrelated to each other. $\mathbf{q}_a$ can therefore be described as

$$\mathbf{q}_a = \begin{pmatrix}q_{a_x} & 0 & 0\\ 0 & q_{a_y} & 0\\ 0 & 0 & q_{a_z}\end{pmatrix} \tag{1.29}$$

where q_{a_x}, q_{a_y} and q_{a_z} are constant values.

By integrating (1.23) using (1.26) and (1.27), we get:

$$x_{k+1} = \begin{pmatrix}\mathbf{r}_{k+1}\\ \mathbf{v}_{k+1}\\ \beta_{k+1}\end{pmatrix} = \begin{pmatrix}\mathbf{r}_k + \mathbf{v}_k T_s + \mathbf{a}_k\frac{T_s^2}{2}\\ \mathbf{v}_k + \mathbf{a}_k T_s\\ \beta_k\end{pmatrix} + w_k \tag{1.30}$$

w_k is the discrete-time process noise vector modelled as a zero-mean white noise with the covariance matrix [Bar-Shalom et al., 2004]:

$$Q = \begin{pmatrix}\frac{T_s^3}{3}\mathbf{q}_a & \frac{T_s^2}{2}\mathbf{q}_a & \mathbf{0}_{3\times1}\\ \frac{T_s^2}{2}\mathbf{q}_a & T_s\mathbf{q}_a & \mathbf{0}_{3\times1}\\ \mathbf{0}_{1\times3} & \mathbf{0}_{1\times3} & q_\beta T_s\end{pmatrix} \tag{1.31}$$

The derivations of (1.30) and (1.31) are provided in appendix A.1.

Ideal choice of the power spectral density Define $\Delta_{\mathbf{v},noise,k+1}$ the changes in the velocity *not taken into account in the estimation model* over a sampling period T_s, i.e. $\forall t \in [kT_s, (k+1)T_s]$

$$\Delta_{\mathbf{v},noise,k+1} = \mathbf{v}_{k+1} - \mathbf{v}_k - \mathbf{a}_k \cdot T_s \tag{1.32}$$

Denote $\Delta_{v_{x,y,z},noise,k+1}$ the x, y and z component of $\Delta_{\mathbf{v},noise,k+1}$ respectively.

As proposed in [Bar-Shalom et al., 2004], the process noise parameter $\mathbf{q}_{a_{x,y,z}}$ should be chosen such that $\sqrt{q_{a_{x,y,z}}T_s}$ has the same order of magnitude as the changes in the velocity not taken into account in the estimation model over a sampling period $\Delta_{v_{x,y,z},noise,k}$, $\forall k$.

Define $\Delta_{\beta,noise,k+1}$ the changes in the ballistic coefficient not taken into account in the estimation model over a sampling period T_s, $\forall t \in [kT_s, (k+1)T_s]$

$$\Delta_{\beta,noise,k+1} = \beta_{k+1} - \beta_k \tag{1.33}$$

In the same way as for $q_{a_{x,y,z}}$, the process noise parameter q_β should be chosen such that $\sqrt{q_\beta T_s}$ has the same order of magnitude as the changes in the ballistic coefficient not taken into account in the estimation model over the sampling period. Since it is supposed in the model that the ballistic coefficient is constant over the sampling period, this quantity is simply the changes in the real ballistic coefficient over the sampling period $\Delta_{\beta,noise,k}$, $\forall k$.

However, in reality, a good choice of $q_{a_{x,y,z}}$ and q_β cannot be guaranteed since we do not have access to the real state of the debris. Hence, arbitrary values of these parameters must be chosen. These arbitrary values may not be appropriate so an estimator which is robust against a poor choice of these process noise parameters should be implemented.

In this estimation model including β in the state vector, we suppose that during a sampling interval the acceleration $\mathbf{a}(t)$ is a constant plus a noise term as presented in (1.26). Now, we are going to refine the assumption by supposing the derivative of the acceleration $\dot{\mathbf{a}}(t)$ to be a constant plus a noise term. This assumption is used in the estimation model including acceleration in the state vector presented next.

1.3.2.3 Estimation Model with Acceleration as a State Variable

Continuous-time estimation model with acceleration This model includes the position, the velocity and the acceleration of the object in the state vector also in the SEU coordinates. In this model, an expression of the derivative of the acceleration $\dot{\mathbf{a}}(t)$ is derived supposing that $\beta(t)$ is constant over a sampling period.

The state vector at time t, $x(t)$, is defined as

$$x(t) = \begin{pmatrix} \mathbf{r}(t)^T & \mathbf{v}(t)^T & \mathbf{a}(t)^T \end{pmatrix}^T \tag{1.34}$$

Using the flat Earth hypothesis, the acceleration is described as:

$$\mathbf{a}(t) = -\frac{\mathsf{c}_1 e^{-\mathsf{c}_2 r_z(t)} \|\mathbf{v}(t)\|}{2\beta(t)} \mathbf{v}(t) + \begin{pmatrix} 0 \\ 0 \\ -g_E \end{pmatrix} \tag{1.35}$$

Define as previously T_s the sampling period of the estimator. Define the discrete-time state vector $x_k = x(t = kT_s)$. It is assumed that $\forall t \in [kT_s, (k+1)T_s]$:

$$\dot{\mathbf{a}}(t) = \mathbf{f}_k + \boldsymbol{\xi}(t), \text{ where } \mathbf{f}_k \triangleq \dot{\mathbf{a}}(t)|_{\beta=cst, t=kT_s} \tag{1.36}$$

f_k is the derivative of $\mathbf{a}(t)$ in (1.35) supposing that β is constant and computed at $t = kT_s$. Denote $\mathbf{f}_k \triangleq \begin{pmatrix} f_{x_k} & f_{y_k} & f_{z_k} \end{pmatrix}^T$, we have

$$f_{x_k} = -\mathsf{c}_2 a_{x_k} v_{z_k} + a_{x_k} \left[a_{x_k} \left(\frac{1}{v_{x_k}} + \frac{v_{x_k}}{\|\mathbf{v}_k\|^2} \right) + a_{y_k} \frac{v_{y_k}}{\|\mathbf{v}_k^2\|} + a_{z_k} \frac{v_{z_k}}{\|\mathbf{v}_k\|^2} \right] \tag{1.37}$$

$$f_{y_k} = -\mathsf{c}_2 a_{y_k} v_{z_k} + a_{y_k} \left[a_{x_k} \frac{v_{x_k}}{\|\mathbf{v}_k\|^2} + a_{y_k} \left(\frac{1}{v_{y_k}} + \frac{v_{y_k}}{\|\mathbf{v}_k\|^2} \right) + a_{z_k} \frac{v_{z_k}}{\|\mathbf{v}_k\|^2} \right] \tag{1.38}$$

$$f_{z_k} = \left(-\mathsf{c}_2 v_{z_k} + \left[a_{x_k} \frac{v_{x_k}}{\|\mathbf{v}_k\|^2} + a_{y_k} \frac{v_{y_k}}{\|\mathbf{v}_k\|^2} + a_{z_k} \left(\frac{1}{v_{z_k}} + \frac{v_{z_k}}{\|\mathbf{v}_k\|^2} \right) \right] \right) (a_{z_k} + g_E) \tag{1.39}$$

$\boldsymbol{\xi}(t)$ is a continuous zero-mean white noise of spectral density $\tilde{\mathbf{q}}$ representing errors from discretization **and** from the fact that β is actually not constant. In other words,

$$E\{\boldsymbol{\xi}(t)\boldsymbol{\xi}^T(\tau)\} = \tilde{\mathbf{q}}(t)\delta(t-\tau) \tag{1.40}$$

For the sake of simplicity, we assume $\tilde{\mathbf{q}}(t)$ to be constant equal to $\tilde{\mathbf{q}}$ and that each component of $\boldsymbol{\xi}$ is uncorrelated to each other. $\tilde{\mathbf{q}}$ can therefore be described as

$$\tilde{\mathbf{q}} = \begin{pmatrix} \tilde{q}_x & 0 & 0 \\ 0 & \tilde{q}_y & 0 \\ 0 & 0 & \tilde{q}_z \end{pmatrix} \tag{1.41}$$

where $\tilde{q}_x$, $\tilde{q}_y$ and $\tilde{q}_z$ are constant values.

To summarize, the estimation model including acceleration in the state vector in continuous-time $\forall t \in [kT_s, (k+1)T_s]$ is described as

$$\begin{aligned} \dot{\mathbf{r}}(t) &= \mathbf{v}(t) \\ \dot{\mathbf{v}}(t) &= \mathbf{a}(t) = -\frac{\mathsf{c}_1 e^{-\mathsf{c}_2 r_z(t)} \|\mathbf{v}(t)\|}{2\beta(t)}\mathbf{v}(t) + \begin{pmatrix} 0 \\ 0 \\ -g_E \end{pmatrix} \\ \dot{\mathbf{a}}(t) &= \mathbf{f}_k + \boldsymbol{\xi}(t) \end{aligned} \tag{1.42}$$

For the sake of simplicity, seeing that radar measurements are available in discrete-time interval, a discrete-time version of the estimation model will be derived.

Discrete-time estimation model with acceleration Integrating (1.42), the estimation model including acceleration in the state vector in discrete-time can be derived:

$$x_{k+1} = \begin{pmatrix} 1\mathbf{I}_{3\times3} & T_s\mathbf{I}_{3\times3} & \frac{T_s^2}{2}\mathbf{I}_{3\times3} \\ \mathbf{0}_{3\times3} & \mathbf{I}_{3\times3} & T_s\mathbf{I}_{3\times3} \\ \mathbf{0}_{3\times3} & \mathbf{0}_{3\times3} & \mathbf{I}_{3\times3} \end{pmatrix} x_k + \begin{pmatrix} \frac{T_s^3}{6}\mathbf{f}_k \\ \frac{T_s^2}{2}\mathbf{f}_k \\ T_s\mathbf{f}_k \end{pmatrix} + w_k \tag{1.43}$$

where w_k is a discrete-time zero-mean bounded white noise whose covariance matrix is

$$Q = \begin{pmatrix} \frac{1}{20}T_s^5 & \frac{1}{8}T_s^4 & \frac{1}{6}T_s^3 \\ \frac{1}{8}T_s^4 & \frac{1}{3}T_s^3 & \frac{1}{2}T_s^2 \\ \frac{1}{6}T_s^3 & \frac{1}{2}T_s^2 & T_s \end{pmatrix} \otimes \tilde{\mathbf{q}} \tag{1.44}$$

where $\otimes$ is the Kronecker product operator[3]

The derivations of (1.43) and (1.44) are provided in appendix A.2.

[3]If A is an $m \times n$ matrix and B is a $p \times q$ matrix, then the Kronecker product $A \otimes B$ is the $mp \times nq$ block matrix:

$$A \otimes B = \begin{pmatrix} a_{11}B & \cdots & a_{1n}B \\ \vdots & \ddots & \vdots \\ a_{m1}B & \cdots & a_{mn}B \end{pmatrix} \tag{1.45}$$

Ideal Choice of the Power Spectral Density Define $\Delta_{\mathbf{a},noise,k+1}$ the changes in the acceleration not taken into account in the estimation model over a sampling period T_s, i.e. $\forall t \in [kT_s, (k+1)T_s]$:

$$\Delta_{\mathbf{a},noise,k+1} = \mathbf{a}_{k+1} - \mathbf{a}_k - \mathbf{f}_k \cdot T_s \tag{1.46}$$

and denote $\Delta_{a_{x,y,z},noise,k+1}$ the x, y and z component of $\Delta_{\mathbf{a},noise,k+1}$.

As proposed in [Bar-Shalom et al., 2004], $\tilde{q}_{x,y,z}$ should be chosen such that $\sqrt{\tilde{q}_{x,y,z}T_s}$ has the same order of magnitude as the changes in the acceleration not taken into account in the estimation model over a sampling period: $\Delta_{a_{x,y,z},noise,k}$, $\forall k$.

Summary

We precise that for space debris tracking during the re-entries, an estimation model that describes the exact dynamics of the debris is not available. This is due to the unknown variation of $\beta(t)$. Model errors are therefore present and this is one of the reasons that cause the space debris tracking problem difficult. To achieve accurate trajectories of the debris, the chosen estimator must be robust against model errors.

Now, let us take a look at the state of the art of the object tracking problem during atmospheric re-entries. Existing works on the problem are available for military objects only. They will be discussed throughout the next section. We recall that for military objects, the ballistic coefficient β is nearly constant unlike for space debris whose β can have high variations with time. Estimators that are adapted for military object tracking during the re-entries can therefore be not so adequate for space debris. Performances of estimators used for military object tracking during the re-entries in the literature for space debris tracking will be studied in chapter 3.

1.4 State of the Art on Military Object Tracking during the Re-entries

The only available studies on re-entering object tracking concern military objects. The re-entering military object tracking problem when the ballistic coefficient β is a priori known is studied in [Farina et al., 2002], [Austin and Leondes, 1981] and [Liu et al., 2005]. However, in reality the value of β is generally unknown. We focus our interest in the studies of the re-entering object tracking problem when the ballistic coefficient is unknown [Ristic et al., 2003].

The estimators used in [Ristic et al., 2003] are the Extended Kalman Filter, the Unscented Kalman Filter (UKF) and the Regularized Particle Filter (RPF). These estimators will be briefly presented in this section. The performances of these estimators for space debris tracking will be studied in chapter 3.

1.4.1 Extended Kalman Filter (EKF)

The Extended Kalman Filter (EKF) makes use of the formulations of the Kalman Filter (KF) which is the best linear estimator when process noise w_k and measurement noise v_k are uncorrelated and white even though they are non Gaussian [Simon, 2010]. The KF is the best estimator in the sense that it gives the minimum achievable error variance for a

linear system. The proof of the KF is provided in [Kalman, 1960].

The EKF generates estimates for nonlinear systems by linearizing the system at the current estimate and then applies the Kalman Filter equations to the linearized system. Denote $\hat{x}_k^-$ the a priori estimate at instant k, P_k^- the a priori estimation error covariance matrix, $\hat{x}_k$ the a posteriori estimate and P_k the a posteriori error covariance matrix. The algorithm of the EKF can be divided into two stages: prediction and update.

Prediction

$$\hat{x}_k^- = f(\hat{x}_{k-1}) \tag{1.47}$$
$$P_k^- = Q_{k-1} + \hat{F}_{k-1} P_{k-1} \hat{F}_{k-1}^T \tag{1.48}$$

$\hat{F}_{k-1}$ is the Jacobian of f evaluated at $\hat{x}_{k-1}$, i.e.

$$\hat{F}_{k-1} = \left.\frac{\partial f}{\partial x}\right|_{x=\hat{x}_{k-1}} \tag{1.49}$$

Update

$$\hat{x}_k = \hat{x}_k^- + K_k(y_k - h(\hat{x}_k)) \tag{1.50}$$
$$P_k = P_k^- - K_k S_k K_k^T \tag{1.51}$$

where

$$S_k = \hat{H}_k P_k^- \hat{H}_k^T + R_k \tag{1.52}$$
$$K_k = P_k^- \hat{H}_k^T S_k^{-1} \tag{1.53}$$

$\hat{H}_k$ is the Jacobian of h evaluated at $\hat{x}_k^-$, i.e.

$$\hat{H}_k = \left.\frac{\partial h}{\partial x}\right|_{x=\hat{x}_k} \tag{1.54}$$

The EKF is fast and simple to code. However, it is difficult to tune and only reliable for systems that are almost linear over the sampling period [Julier and Uhlmann, 2004].

Now, let us consider another nonlinear estimator based on the Kalman Filter which does not require linearization of the system: the Unscented Kalman Filter (UKF).

1.4.2 Unscented Kalman Filter (UKF)

Rather than linearizing the system as the EKF does to evaluate error covariance matrix, the Unscented Kalman Filter (UKF) first proposed in [Julier and Uhlmann, 2004] propagates the error covariance of the estimate using the Unscented Transform (UT). In the UKF, a set of sample points is deterministically chosen to describe the pdf of the estimate and the nonlinear transformation is applied to each sample point. The UKF therefore avoids system linearization and the calculation of the Jacobian matrices of the state function and of the measurement function is not required. If the density of the estimate is Gaussian, these sample points capture the true mean and the error covariance of the estimate completely [Ristic et al., 2004].

Consider the nonlinear estimation problem defined by (1.18) and (1.19). Denote $p(x_{k-1}|y_0^{k-1})$ the a posteriori pdf of the real state x_{k-1} based on the sequence of measurements y_0^{k-1}. The a posteriori estimate $\hat{x}_{k-1}$ is defined as the expectation of the random variable x_{k-1} whose a posteriori pdf is $p(x_{k-1}|y_0^{k-1})$ and a posteriori error covariance P_{k-1} is defined as the variance of the random variable x_{k-1}.

To have an estimate of the state x_k at instant k, the first step is to calculate a set of $2n_x + 1$ deterministic sample points $\mathcal{X}_{k-1}^i$, for $i = 0, \ldots, 2n_x$, describing the pdf $p(x_{k-1}|y_0^{k-1})$ and the associated weights W_{k-1}^i. Then, we do the prediction step and the update step as in the EKF.

Calculation of sample points and their weights

$$\mathcal{X}_{k-1}^0 = \hat{x}_{k-1}, \quad W_0 = \frac{\kappa}{(n_x + \kappa)} \tag{1.55}$$

$$\text{For } i = 1, \ldots, n_x \quad \mathcal{X}_{k-1}^i = \hat{x}_{k-1} + (\sqrt{(n_x + \kappa)P_{k-1}})_i, \quad W_i = \frac{1}{2(n_x + \kappa)} \tag{1.56}$$

$$\text{For } i = n_x + 1, \ldots, 2n_x \quad \mathcal{X}_{k-1}^i = \hat{x}_{k-1} - (\sqrt{(n_x + \kappa)P_{k-1}})_i, \quad W_i = \frac{1}{2(n_x + \kappa)} \tag{1.57}$$

κ is a scaling parameter such that $\kappa + n_x \neq 0$. $(\sqrt{(n_x + \kappa)P_{k-1}})_i$ is the i^{th} column of the matrix square root of $(n_x + \kappa)P_{k-1}$ denoted by L where $(n_x + \kappa)P_{k-1} = L^T L$.

Prediction Denote $\mathcal{X}_k^{i^-}$ for $i \in [0, 2n_x]$ sample points of the a priori density. They are calculated by applying nonlinear transformation to the sample points of the posterior density $\mathcal{X}_{k-1}^i$ as follows:

$$\mathcal{X}_k^{i^-} = f(\mathcal{X}_{k-1}^i) \tag{1.58}$$

The a priori estimate $\hat{x}_k^-$ and the a priori error covariance P_k^- are defined as

$$\hat{x}_k^- = \sum_{i=0}^{2n_x} W_i f(\mathcal{X}_{k-1}^i) \tag{1.59}$$

$$P_k^- = Q_{k-1} + \sum_{i=0}^{2n_x} W_i [f(\mathcal{X}_{k-1}^i) - \hat{x}_k^-][f(\mathcal{X}_{k-1}^i) - \hat{x}_k^-]^T \tag{1.60}$$

The predicted measurement is:

$$\hat{y}_k = \sum_{i=0}^{2n_x} W_i h(\mathcal{X}_k^{i^-}) \tag{1.61}$$

Update

$$\hat{x}_k = \hat{x}_k^- + K_k(y_k - \hat{y}_k) \tag{1.62}$$

$$P_k = P_k^- - K_k S_k K_k^T \tag{1.63}$$

where

$$K_k = P_{xy} S_k^{-1} \tag{1.64}$$

$$S_k = R_k + P_{yy} \tag{1.65}$$

$$P_{xy} = \sum_{i=0}^{N-1} W_i (\mathcal{X}_k^{i^-} - \hat{x}_k^-)(h(\mathcal{X}_k^{i^-}) - \hat{y}_k)^T \tag{1.66}$$

$$P_{yy} = \sum_{i=0}^{N-1} W_i (h(\mathcal{X}_k^{i^-}) - \hat{y}_k)(h(\mathcal{X}_k^{i^-}) - \hat{y}_k)^T \tag{1.67}$$

The UKF is fast[4] and has been shown to provide smaller estimation errors than the EKF in case of large process noise [Romanenko and Castro, 2004]. However, theoretically, the UT is accurate only if the posterior distribution can be closely approximated by a Gaussian distribution [Julier and Uhlmann, 2004].

Now, the Regularized Particle Filter (RPF) which is also used in [Ristic et al., 2003] for military object tracking during the re-entries will be discussed. Like the UKF, the RPF also uses sample points to represent the distribution of the pdf of the state. However, the sample points of the RPF are chosen randomly and not deterministically.

1.4.3 Regularized Particle Filter (RPF)

The RPF is a variation of Particle Filters whose key idea is to represent the a posteriori pdf of the state $p(x_k|y_0^k)$ by a set of random samples, also called "particles", with associated weights. Then statistical properties of these samples, e.g. the mean and the variance are computed [Ristic et al., 2004]. The PF approaches the optimal Bayesian estimator when the number of samples becomes very large.

The interest of the PF is that it can handle any kind of pdf: either linear or nonlinear and either Gaussian or non Gaussian. An appropriate specification of the state-space model also allows the PF to handle constraints [Cappe et al., 2007]. However, the form of the pdf of the state is supposed to be known and the PF is sensitive to the choice of the chosen form of the pdf. This is the major drawback of the PF.

Sine the a posteriori pdf of the state $p(x_k|y_0^k)$ can be unknown, particles can be generated using another distribution from which we know how to draw samples such as the Gaussian distribution or the uniform distribution. This "another" distribution is called the *importance density*. This sampling method is called "importance sampling". Once we have the particles representing the a posteriori pdf $p(x_k|y_0^k)$, they will be propagated sequentially. This classical version of the PF is called the Sequential Importance Sampling (SIS) algorithm.

However, a common problem of the Importance Sampling Method is the degeneracy phenomenon where after a few iterations, all but one particles will have negligible normalized weights. As a result, a large computational effort is devoted to an update of particles which are barely contributing to the approximation of $p(x_k|y_0^k)$. The particles with low importance weights should be therefore eliminated when a significant degeneracy is observed. Denote N_p the number of the particles. To cope with the degeneracy phenomenon,

[4] In our studies in chapters 3 and 5, the UKF requires the same order of computation time than the EKF.

particles whose weights are lower than a chosen criterion are eliminated and the surviving particles are resampled (with replacement) to have a new set of N_p particles with equal weight.

Although resampling helps us to cope with particle degeneracy, it induces a loss of diversity of particles. In fact, the particles that have high weights are statistically selected many time. This problem, known as *sample impoverishment*, is severe when process noise is very small [Ristic et al., 2004]. In [Musso et al., 2001], a variation of the PF called Regularized Particle Filter (RPF) is proposed to improve the diversity among the particles. In this work, a regularized step where particles are kind of "jittered" during the resampling is added. A very good review on particle filters and the RPF is available in [Ristic et al., 2004]. A summary of the principles of the PF and of the RPF is provided in appendix A.3.

1.4.4 Summary of Military Object Tracking during the Re-entries

In [Ristic et al., 2003], the performances of the EKF, the UKF and the RPF on the trajectory estimation of a military object during atmospheric re-entries are studied. The estimation model used in this study is the one described in (1.30). We recall that the ballistic coefficient β of a military object is nearly constant during the re-entries. Consequently, the hypothesis of a nearly constant β in the estimation model (1.30) does not induce high model errors a priori. It is shown in their work that the EKF and the UKF give high estimation errors while the RPF gives smallest achievable estimation errors[5]. However, the particles filters are known to be sensitive to initialization and model errors [Rawlings and Bakshi, 2006]. The RPF therefore does not seem to be appropriate for space debris tracking during the re-entries where high model errors are present due to unknown dynamics of β. The performances of the EKF, the UKF and the RPF for space debris tracking during the re-entry will therefore be studied in chapter 3.

Knowing that an estimator robust against model errors and against poor initialization should be chosen for our problem, the performances of an optimization based estimator called Moving Horizon Estimator (MHE) which seems to be a good candidate for our problem thanks to its robustness to model errors and poor initialization [Haseltine and Rawlings, 2005][Ungarala, 2009] will also be studied. Another interest of the MHE is that it allows handling nonlinear estimation models and constraints directly during optimization. The state of the art on the MHE will be presented in the next chapter.

[5] by comparison with the Posterior Cramer-Rao bounds which gives the smallest achievable estimation errors for a non-bias filter

1.5 Summary of the Chapter

In this chapter, we have seen that

- Space debris tracking during atmospheric re-entries is necessary for space debris mitigation and for the prediction of the re-entry time and impact point of large objects.
- However, this is a very difficult problem due to unknown precise dynamics of space debris. In fact, the evolution of ballistic coefficient, which characterizes the response of the object to the drag, is unknown. Moreover, an a priori value of the ballistic coefficient given to an estimator may have high errors due to a breakup where the debris disintegrates into small pieces at the beginning of the re-entry.
- Only estimation models that describe the dynamics of the debris approximately can be used. Therefore, high model errors can be present and an estimator robust against model errors should be implemented.
- The classical estimators used in the literature for military object tracking during the re-entries which are the EKF, the UKF and the RPF do not seem to be appropriate for the space debris tracking problem during the re-entries. Another robust estimator should be used instead.
- The Moving Horizon Estimator (MHE) seems to be appropriate for our problem thanks to its robustness against bad initialization and against model errors. The state of the art of the MHE will be briefly discussed in the next chapter.

CHAPTER 2

Reviews on the Moving Horizon Estimator (MHE)

"Study the past, if you would divine the future."

— Confucius

In this chapter, we discuss

- the interests of the MHE for space debris tracking during atmospheric re-entries
- the formulations of the MHE in the literature
- studies on the convergence of the estimation errors of the MHE
- existing works on the computation time reduction of the MHE

2.1 Introduction

The Moving Horizon Estimator (MHE) computes an estimate at the current instant by solving an optimization problem based on information from a fixed-number of latest measurements collected over a finite horizon. The cost function of the MHE is traditionally described by a norm of the difference between real and predicted measurements over the horizon, a norm of the process noise over the horizon and a norm of the difference between an estimate at the beginning of the horizon and an a priori one. The latter term of the cost function is usually referred to as the "arrival cost"[1]. Once a new measurement is available, the oldest measurement is discarded and the horizon is moved forward. This technique keeps the computation time tractable as time goes by. Other advantages of the MHE are its capabilities to handle nonlinear systems without linearization and to incorporate constraints directly since the MHE is optimization-based.

The idea of nonlinear estimation using minimization of a cost function based on measurements dates back to Gauss' least-square method in which the states are derived by

[1] Actually, this term was proposed for the first time as the "approximated arrival cost" in [Rao et al., 2003] where the word "arrival cost" was reserved for the case in which all the measurements since the beginning of the estimation are taken into account. However, for the sake of simplicity the "approximated arrival cost" is referred to as the "arrival cost" in later works instead [Haseltine and Rawlings, 2005][Liu, 2013][Zavala, 2008].

simply fitting them to the measurements in a least-square fashion [Ferreau et al., 2012]. The idea of using a fixed number of most recent measurements for state estimation was proposed for the first time in [Jazwinski, 1968]. This method, called the "limited memory filter", computes the conditional probability density function based on a fixed number of the most recent measurements. It is shown to be more robust against model errors than the Extended Kalman Filter (EKF). In [Moraal and Grizzle, 1995], a method to design an observer[2] for nonlinear system with discrete-time measurements was proposed. The method relies on inverting the state-to-measurement map, which is constructed by relating the system's state at a given time to a fixed number of latest measurements.

In [Michalska and Mayne, 1995], a Moving Horizon Observer for nonlinear continuous-time noise-free systems was proposed. In this work, the states are estimated at discrete-time instants by minimizing an integral error between a fixed number of latest measurements and predicted measurements. The estimation errors of this observer are shown to be globally asymptotically convergent when the system satisfies mild assumptions basically on the smoothness of the system equations and the observability of the system. A Moving Horizon Estimator for nonlinear discrete-time systems under noises was proposed in [Rao et al., 2003] where sufficient conditions for the convergence of the estimation errors were provided. However, the conditions proposed in this work are difficult to be verified in practice. New conditions for the convergence which are possible to be verified in practice were later proposed in [Alessandri et al., 2008][Alessandri et al., 2010]. Their conditions are based on the smoothness of the system equations and the observability of the system. They will be discussed in section 2.2.2.

We have seen in chapter 1 that for space debris tracking during atmospheric re-entries, the ballistic coefficient β can have high unknown variations. This unknown evolution of β induces errors in the estimation model. As a result, a to-be-used estimator for the problem must be robust against model errors. It has been shown that the EKF and the UKF provide high estimation errors in military object tracking during the re-entries even though the ballistic coefficient of a military object is nearly constant [Ristic et al., 2003]. In their work, the Regularized Particle Filter (RPF) is shown to provide small estimation errors by comparison with the Posterior Cramer-Rao bounds. However, the Particle Filters (PF) are known to be sensitive to model errors [Rawlings and Bakshi, 2006]. The RPF therefore does not seem to be appropriate for space debris tracking during the re-entries where high model errors are present due to unknown dynamics of β. An alternative estimator should therefore be chosen for the problem.

The MHE, which is shown to be more robust against poor initialization and model errors than the EKF, the UKF and than the PF [Rawlings and Bakshi, 2006][Haseltine and Rawlings, 2005][Ungarala, 2009], seems to be a good candidate for space debris tracking during the re-entry. In this chapter, we present the formulations of the MHE, followed by a study on the convergence of its estimation errors. After that, we discuss its advantages and drawbacks. The chapter ends with the discussion on existing works on the MHE's computation time reduction.

[2] An estimator providing estimates that converge asymptotically to the real states in a noise-free case, also referred to as a deterministic observer in the literature [Liu, 2013]

System Definition

In the following, we will consider a dynamic system modelled by the following discrete-time equations as described in section 1.3.1:

$$x_k = f(x_{k-1}) + w_{k-1} \tag{2.1a}$$

$$y_k = h(x_k) + v_k \tag{2.1b}$$

where $k \in \mathbb{N}$ is the discrete-time index. $x_k \in \mathbb{R}^{n_x}$ is the state vector and w_k is the process noise representing not only disturbances affecting the system but also model errors [Ristic et al., 2004][Alessandri et al., 2008]. $y_k \in \mathbb{R}^{n_y}$ is the measurement vector which is the output of the system and v_k is the measurement noise. w_k and v_k are assumed to be zero-mean uncorrelated white noises. Denote Q_k and R_k the covariance matrices of w_k and v_k respectively. x_0 is supposed to be unknown.

Constraints on the state or the noises can be imposed and the MHE can take into account constraints directly during the optimization. The constraints can be written as:

$$x_k \in \mathbb{X}_k \subset \mathbb{R}^{n_x}, \;\; w_k \in \mathbb{W}_k \subset \mathbb{R}^{n_x}, \;\; v_k \in \mathbb{V}_k \subset \mathbb{R}^{n_y} \tag{2.2}$$

where $\mathbb{X}_k$ is a convex compact set and $\mathbb{W}_k$ and $\mathbb{V}_k$ are compact sets including 0.

The formulations of the MHE in the literature exist in both deterministic and stochastic frameworks. The deterministic framework refers to the fact that the initial state x_0, the process noise w_k and the measurement noise v_k are considered to be unknown deterministic variables of unknown character that take their values from known compact sets. In the stochastic framework, on the other hand, x_0, w_k and v_k are considered as random variables and assumptions on their statistics are made. Both frameworks can deal with system affected by noises.

Assume that the state vector x_k has to be estimated at each instant $k \geq N$ using the latest $N+1$ measurements collected within a "sliding window" $[k-N, k]$. Denote $\hat{x}_{k-N|k}$ an estimate of x_{k-N} and $\{\hat{w}_{k-N+i|k}\}_{i=0}^{N-1}$ associated process noise estimates, computed at instant k. Define y_{k-N}^{k} the measurement collection over the horizon by

$$y_{k-N}^{k} = \begin{pmatrix} y_{k-N} \\ y_{k-N+1} \\ \vdots \\ y_k \end{pmatrix} \tag{2.3}$$

and w_{k-N}^{k-1} the process noise sequence by

$$w_{k-N}^{k-1} = \begin{pmatrix} w_{k-N} \\ \vdots \\ w_{k-1} \end{pmatrix} \tag{2.4}$$

Denote $\hat{x}_{k-N|k}^{-}$ an a priori value of $\hat{x}_{k-N|k}$. Consider the definition of the norm of the vector as follows.

Definition 1. *(Weighted Norm of a Vector) Recall that for a symmetric positive definite matrix M and a vector $z \in \mathbb{R}^{n_z}$, the weighted norm of z is defined as*

$$\|z\|_M \triangleq (z^T M z)^{1/2} \tag{2.5}$$

Denote $\|z\|$ the vector norm with the weight matrix $M = \mathbf{I}_{n_z \times n_z}$. $\|z\|$ is actually the Euclidean norm of the vector z, also called the 2-norm.

Definition 2. *(Norm of a Matrix) Define $\|\cdot\|_p$ the operator p-norm for any matrix $A \in \mathbb{R}^{m \times n}$ as*

$$\|A\|_p = \max_{z \neq 0} \frac{\|Az\|_p}{\|z\|_p} \tag{2.6}$$

In the case of $p = 2$, we have [Dahleh et al., 2004]

$$\|A\|_2 \quad = \quad \max_{z \neq 0} \frac{\|Az\|_2}{\|z\|_2} = \sigma_{max}(A) \tag{2.7}$$

where $\sigma_{max}(A)$ is the maximum non-zero singular value of A.

Now, let us discuss first the formulation and the stability of the dynamics of the estimation errors of the MHE in the deterministic framework followed by those of the stochastic one.

2.2 MHE in the Deterministic Framework

2.2.1 Formulation

The MHE in the deterministic framework for discrete-time systems can be found in [Alessandri et al., 2003] for linear cases, in [Alessandri et al., 2005] for nonlinear cases with bounded model uncertainties and in [Alessandri et al., 2008] and [Alessandri et al., 2010] for nonlinear cases under bounded noises.

The MHE in this framework is said to be deterministic only in the sense that the initial state x_0, the process noise w_k and the measurement noise v_k are considered as unknown deterministic variables of unknown character taking their values from known compact sets.

The formulation of the MHE in the deterministic framework is to solve:

$$\min_{\hat{x}_{k-N|k}, \{\hat{w}_{k-N+i|k}\}_{i=0}^{N-1}} \mathbf{J}_k(\hat{x}_{k-N|k}, \{\hat{w}_{k-N+i|k}\}_{i=0}^{N-1}, \hat{x}^-_{k-N|k}, y^k_{k-N}) \tag{2.8a}$$

$$\mathbf{J}_k = \left\|\hat{x}_{k-N|k} - \hat{x}^-_{k-N|k}\right\|^2_{\mathcal{P}} + \sum_{i=0}^{N-1} \left\|\hat{w}_{k-N+i|k}\right\|^2_{\mathcal{Q}} + \sum_{i=0}^{N} \left\|y_{k-N+i} - h(\hat{x}_{k-N+i|k})\right\|^2_{\mathcal{R}} \tag{2.8b}$$

subject to

$$\hat{x}_{k-N+i+1|k} = f(\hat{x}_{k-N+i|k}) + \hat{w}_{k-N+i|k}, \ \forall i \in [0, N-1] \tag{2.8c}$$

$$\hat{x}_{k-N|k} \in \mathbb{X}, \ \hat{w}_{k-N+i|k} \in \mathbb{W}, \ y_{k-N+i} - h(\hat{x}_{k-N+i|k}) \in \mathbb{V}, \ \forall i \in [0, N-1] \tag{2.8d}$$

Denote $(\hat{x}^{\circ}_{k-N|k}, \{\hat{w}^{\circ}_{k-N+i|k}\}_{i=0}^{N-1})$ the optimal solution of the problem (2.8) computed at instant k. The a priori estimate at the beginning of the horizon $\hat{x}^{-}_{k-N|k}$ is computed using $(\hat{x}^{\circ}_{k-N-1|k-1}, \hat{w}^{\circ}_{k-N-1|k-1})$ given by the MHE at the previous instant $k-1$ and (2.8c). $\mathcal{P}$, $\mathcal{Q}$ and $\mathcal{R}$ are positive definite weight matrices and are considered as design parameters. The estimate of x_k computed at instant k given by the MHE is denoted by $\hat{x}_{k|k}$ and is computed using $(\hat{x}^{\circ}_{k-N|k}, \{\hat{w}^{\circ}_{k-N+i|k}\}_{i=0}^{N-1})$ propagated through the state equation (2.8c). For $k < N$, the formulation is similar to (2.8) but with the increasing horizon equal to k at each instant k instead. In other words, the formulation in (2.8) is verified for $i \in [\max(0, k-N), \min(k, N-1)]$.

The first term of the cost function can be regarded as the summary of the past measurements y_0^{k-N-1} not taken into account in the cost function. It is described by the distance between an estimate at the beginning of the horizon $\hat{x}_{k-N|k}$ and the a priori value $\hat{x}^{-}_{k-N|k}$ weighted by a positive definite matrix $\mathcal{P} > 0$ representing the confidence in the a priori value. The second term represents the process noise, taking into account system disturbances and model errors, weighted by a positive definite matrix $\mathcal{Q}$. The third term represents the measurement noises. It is described by the distance between the real measurements and the predicted ones weighted by a positive definite matrix $\mathcal{R}$.

The illustration of the MHE is shown in figure 2.1.

2.2.2 Stability of the Dynamics of the Estimation Errors

The stability of the dynamics of the estimation errors of the MHE in the deterministic framework requires some preliminary definitions:

Definition 3. *A function $f(x)$ is said to be locally Lipschitz with respect to its argument x if there exists a positive constant L_f^x such that $\|f(x') - f(x'')\| \leq L_f^x \|x' - x''\|$, for all x' and x'' in a given region of x and L_f^x is the associated Lipschitz constant.*

Definition 4. *(Class K function) A function $\sigma(s) : \mathbb{R}^+ \to \mathbb{R}^+$ is a class K function of s if it is continuous, $\sigma(0) = 0$ and strictly increasing.*

Definition 5. *(Class KL function) A function $\beta_{KL}(s, k) : \mathbb{R}^+ \times \mathbb{N} \to \mathbb{R}^+$ is a class KL function if it is continuous and if for each $k \in \mathbb{N}$, $\beta_{KL}(\cdot, k)$ is a class K function, and if for each $s \geq 0$, $\beta_{KL}(s, \cdot)$ is non-increasing and satisfies $\lim_{k\to\infty} \beta_{KL}(s, k) = 0$.*

Definition 6. *(Robust Global Asymptotic Stability) Denote $\hat{x}_0^-$ an a priori initial estimate. The dynamics of the estimation error $\hat{x}_k - x_k$ of the system (2.1) $\forall k \in \mathbb{N}$ is Robust Global Asymptotic Stable (RGAS) if $\forall x_0 \in \mathbb{X}$, $\forall \hat{x}_0^- \in \mathbb{X}$, $\forall w_0^{k-1} \in \mathbb{W}^k$ and $\forall v_0^k \in \mathbb{V}^{k+1}$, there exist a class KL function α and class K functions δ_w and δ_v such that $\forall k \in \mathbb{N}$*

$$\|\hat{x}_k - x_k\|^2 \leq \alpha(\left\|\hat{x}_0^- - x_0\right\|^2, k) + \delta_w(\left\|w_0^{k-1}\right\|^2) + \delta_v(\left\|v_0^k\right\|^2) \tag{2.9}$$

The RGAS of the dynamics of the estimation errors will be referred to as the convergence of the estimation errors (to a bounded set defined by noises) for the sake of simplicity.

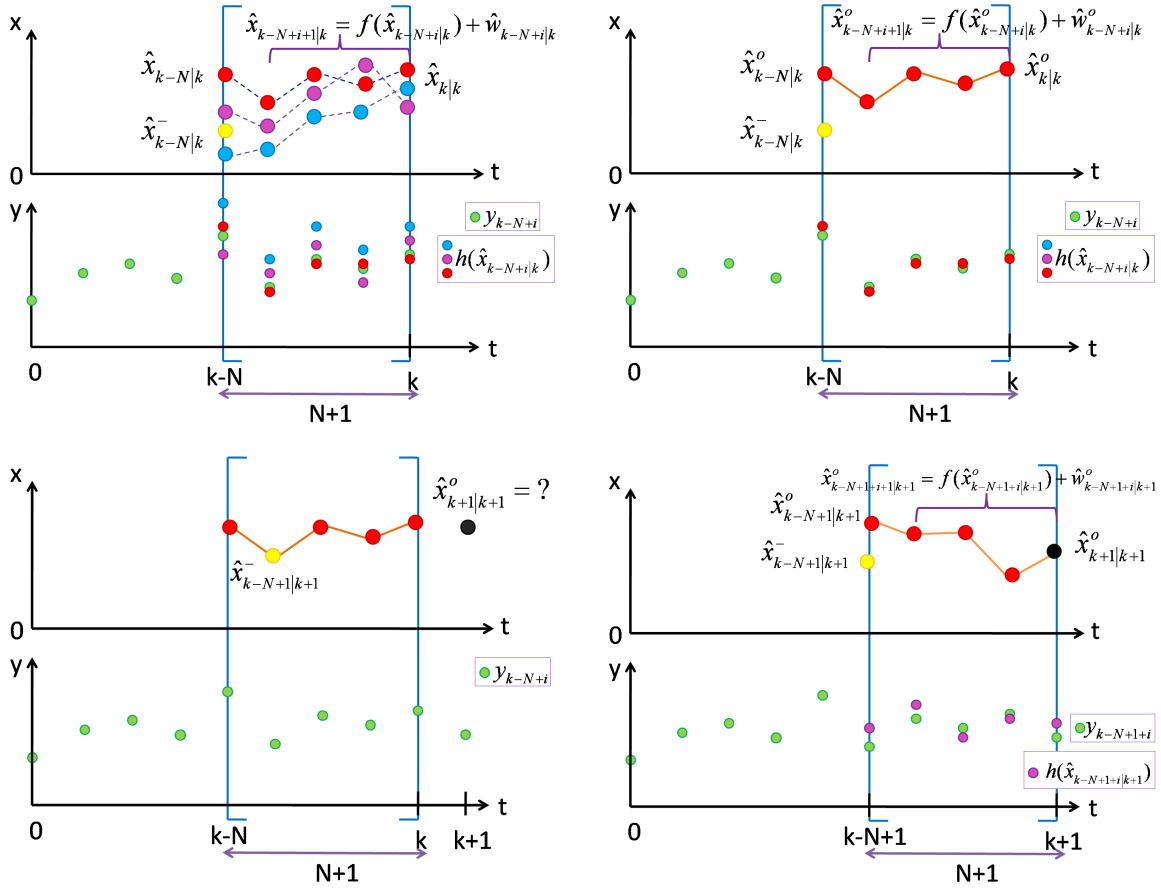

Figure 2.1: Illustration of the MHE: (First row) At instant k, $N+1$ latest measurements from instants $[k-N, k]$ are used to find the optimal estimate at the beginning of the horizon $\hat{x}^{\circ}_{k-N|k}$ and the optimal process noise sequence over the horizon $\{\hat{w}^{\circ}_{k-N+i|k}\}_{i=0}^{N-1}$ minimizing the cost function $\mathbf{J}_k$ in (2.8b). The a priori estimate at the beginning of the horizon $\hat{x}^{-}_{k-N|k}$ is computed using $(\hat{x}^{\circ}_{k-N-1|k-1}, \hat{w}^{\circ}_{k-N-1|k-1})$ given by the MHE at the previous instant $k-1$ and (2.8c). The optimal estimate at instant k, $\hat{x}^{\circ}_{k|k}$, is computed by propagating $\hat{x}^{\circ}_{k-N|k}$ and $\{\hat{w}^{\circ}_{k-N+i|k}\}_{i=0}^{N-1}$ using the state equation (2.8c). (Second row) Once a new measurement arrives at instant $k+1$, the oldest measurement of the last horizon y_{k-N} is discarded and the estimation is done using the new $N+1$ latest measurements from $[k-N+1, k+1]$. This fixed number of measurements taken into account at each iteration allows computation time to be tractable.

Definition 7. *(Observability in $N+1$ steps) Define the observation map of the system* (2.1) *on a window of length $N+1$ by*

$$F(x_{k-N}, w_{k-N}^{k-1}) \triangleq \begin{pmatrix} h(x_{k-N}) \\ h(f^{w_{k-N}}(x_{k-N})) \\ \vdots \\ h \circ f^{w_{k-1}} \circ \cdots \circ f^{w_{k-N}}(x_{k-N}) \end{pmatrix} \tag{2.10}$$

where $\circ$ denotes function composition and $f^{w_i}(x_i) \triangleq f(x_i) + w_i = x_{i+1}$. Denote also

$$f^{w_{k-N}^{k-N+i}}(x_i) = f^{w_{k-N+i}} \circ \cdots \circ f^{w_{k-N}}(x_{k-N}),\ i \in [0, N-1] \tag{2.11}$$

The system (2.1) *is said to be observable in $N+1$ steps if one of these conditions, which are equivalent [Hanba, 2010], is satisfied:*

(a) For a system without process noise, the map $F(x_{k-N}, \mathbf{0}_{n_x N \times 1})$ is injective, i.e. if $F(x'_{k-N}, \mathbf{0}_{n_x N \times 1}) = F(x''_{k-N}, \mathbf{0}_{n_x N \times 1})$ therefore $x'_{k-N} = x''_{k-N}$.

(b) $\forall x_{k-N} \in \mathbb{X}$, $rank\left(\dfrac{\partial F(x_{k-N}, \mathbf{0}_{n_x N \times 1})}{\partial x_{k-N}}\right) = n_x$

(c) $\forall (x', x'') \in \mathbb{X}^2$, there exists a K-function $\phi(\cdot)$ such that

$$\phi(\|x' - x''\|^2) \leq \|F(x', \mathbf{0}_{n_x N \times 1}) - F(x'', \mathbf{0}_{n_x N \times 1})\|^2 \tag{2.12}$$

Let us consider also the triangle inequality [Alessandri et al., 2008] which will be used for the proof of the stability of the dynamics of the estimation errors of the MHE. The triangle inequality states that given l vector $v_1, \ldots, v_l$, we have

$$\left\| \sum_{j=1}^{l} v_j \right\|^2 \leq l \sum_{j=1}^{l} \|v_j\|^2 \tag{2.13}$$

It is shown in [Alessandri et al., 2010] that the dynamics of the estimation errors of the MHE in the deterministic framework is RGAS if the weight matrix $\mathcal{P}$ is adequately chosen.

An adequate $\mathcal{P}$ can be calculated if the system (2.1) satisfies the following assumptions:

(A1) $\mathbb{X}$ is a convex compact set, $\mathbb{W}$ and $\mathbb{V}$ are compact sets with $0 \in \mathbb{W}$ and $0 \in \mathbb{V}$. Define

$$r_w \triangleq \max_{w \in \mathbb{W}} \|w\|,\ \ r_v \triangleq \max_{v \in \mathbb{V}} \|v\| \tag{2.14}$$

(A2) The initial state x_0 is such that, for any possible sequence of process noises $\{w_k\}$, the system trajectory $\{x_k\}$ lies in the convex compact set $\mathbb{X}$, $\forall k$

(A3) f and h are $\mathcal{C}^2$ functions with respect to x on $\mathbb{X}$. f and h are therefore also locally Lipschitz. Define their Lipschitz constants as L_f^x and L_h^x respectively

(A4) The system is observable in $N+1$ steps

(A5) The system (2.1) has finite sensitivity, i.e. the minimum of the class-K function $\phi(\cdot)$ in (2.12) exists. Denote δ the sensitivity parameter of the system (2.1) defined by

$$\delta = \inf_{(x', x'') \in \mathbb{X}^2, x' \neq x''} \frac{\phi(\|x' - x''\|^2)}{\|x' - x''\|^2} > 0 \tag{2.15}$$

Assumption (A5) ensures that a variation of the state vector at the beginning of the horizon x_{k-N} induces a variation in the observation map $F(x_{k-N}, w_{k-N}^{k-1})$ which is in fact the measurement sequence y_{k-N}^{k} in case of zero measurement noise. The larger the δ is, the more observable the system is [Alessandri et al., 2008] (the smaller the number of the measurements needed for constructing the estimate).

The theorem on the convergence of the estimation errors of the MHE is proposed in [Alessandri et al., 2010] for $\mathcal{P} = p\mathbf{I}_{n_x}$ with $p \in \mathbb{R}^+$ as follows:

Theorem 1. *For a discrete-time nonlinear system under bounded additive noises as in* (2.1) *satisfying assumptions (A1)-(A5), the dynamics of the estimation errors of the MHE designed in the deterministic framework defined in* (2.8) *is RGAS if the design parameter* p *where the weight matrix* $\mathcal{P} = p\mathbf{I}_{n_x}$ *is chosen such that*

$$\alpha_{MHE} \triangleq c_1 p + \frac{(L_f^x)^2 c_2 p}{p + c_3 \delta} < 1 \tag{2.16}$$

where c_1*,* c_2 *and* c_3 *are suitable positive constants*

The expression of the constants c_1, c_2 and c_3 were not provided in [Alessandri et al., 2010] nor in any work in the literature. Here are the values of the constants we calculated for the case in which $\mathcal{Q}$ and $\mathcal{R}$ are diagonalizable matrices. The details of the computation are given in appendix B.1.

$$c_1 = \frac{6}{\lambda_{\mathcal{Q},min}},\ c_2 = 12,\ c_3 = \frac{2}{3}\lambda_{\mathcal{R},min} \tag{2.17}$$

where $\lambda_{\mathcal{Q},min}$ and $\lambda_{\mathcal{R},min}$ are the smallest eigenvalues of $\mathcal{Q}$ and $\mathcal{R}$ respectively.

2.3 MHE in the Stochastic Framework

2.3.1 Formulation of the MHE in the Stochastic Framework

The formulation of the MHE in the stochastic framework is derived from the Maximum a Posteriori (MAP) estimator considering a fixed number of latest measurements with the Gaussian hypotheses on the initial state $x_0 \sim \mathcal{N}(\hat{x}_0^-, P_0^-)$ where $\hat{x}_0^-$ denotes the a priori initial estimate and P_0^- denotes the a priori initial error covariance matrix, $w_k \sim \mathcal{N}(0, Q)$ and $v_k \sim \mathcal{N}(0, R)$. The MHE is this framework can be found in [Rao et al., 2003][Rawlings and Bakshi, 2006][Ungarala, 2009] for example.

To proof this, let us consider first the MAP estimator using all the available measurements y_0^k with the above Gaussian hypotheses. This estimator is also referred to as the full information estimator [Rao et al., 2003]. After that, the case in which only a fixed number of the latest measurements are used will be presented. This estimator is referred to as the MHE in the stochastic framework. The use of a fixed number of measurements allows computation time to be tractable.

2.3.1.1 Full Information Estimator

Using the hypotheses: $w_k \sim \mathcal{N}(0, Q)$ and $v_k \sim \mathcal{N}(0, R)$, the estimate $\hat{x}_k$ of the MAP estimator using all the available measurements since the beginning of the estimation y_0^k is obtained by solving [Ungarala, 2009]:

$$\min_{\hat{x}_{0|k},\{\hat{w}_{i|k}\}_{i=0}^{k-1}} \gamma(\hat{x}_{0|k} - \hat{x}_{0|k}^{-}) + \sum_{i=0}^{k-1} \left\|\hat{w}_{i|k}\right\|_{Q^{-1}}^2 + \sum_{i=0}^{k} \|y_i - h(\hat{x}_{i|k})\|_{R^{-1}}^2 \tag{2.18a}$$

$$\hat{x}_{i+1|k} = f(\hat{x}_{i|k}) + \hat{w}_{i|k},\ \forall i \in [0, k-1] \tag{2.18b}$$

$$\hat{x}_{i|k} \in \mathbb{X},\ \ \hat{w}_{i|k} \in \mathbb{W},\ \ y_i - h(\hat{x}_{i|k}) \in \mathbb{V},\ \forall i \in [0, k-1] \tag{2.18c}$$

$\hat{x}_{0|k}^{-}$ is computed using the optimal solution of the full information estimator computed at $k-1$. $\hat{x}_{0|0}^{-} \triangleq \hat{x}_{0}^{-}$. The term γ is called the "initial penalty" [Rao et al., 2003]. It serves as a summary of the prior information at time $k = 0$ and satisfies $\gamma(0) = 0$. It is shown in [Ungarala, 2009] that

$$\gamma(\hat{x}_{0|k} - \hat{x}_{0|k}^{-}) = -\ln p(\hat{x}_{0|k} - \hat{x}_{0|k}^{-}) \tag{2.19}$$

If we assume that $p(\hat{x}_{0|k} - \hat{x}_{0|k}^{-}) \sim \mathcal{N}(0, P_{0|k}^{-})$ like in [Ungarala, 2009][Rao et al., 2003], we have:

$$\gamma(\hat{x}_{0|k} - \hat{x}_{0|k}^{-}) = \|\hat{x}_{0|k} - \hat{x}_{0|k}^{-}\|_{(P_{0|k}^{-})^{-1}}^2 \tag{2.20}$$

Denote $(\hat{x}_{0|k}^{\circ}, \{\hat{w}_{0|k}^{\circ}\}_{i=0}^{k-1})$ the optimal solution of the problem (2.18). The estimate $\hat{x}_k \triangleq \hat{x}_{k|k}^{\circ}$ is computed by propagating the optimal solution $(\hat{x}_{0|k}^{\circ}, \{\hat{w}_{0|k}^{\circ}\}_{i=0}^{k-1})$ using (2.18b).

The computation time of the full information estimator increases with time as more and more measurements are taken into account. To make the computation time tractable, one can use only a fixed number of latest measurements at each instant. This technique is in fact used by the MHE whose formulation is presented next.

2.3.1.2 MHE in the Stochastic Framework

Suppose that the MHE uses $N+1$ latest measurements y_{k-N}^{k} for the estimation. Denote $\hat{x}_{k-N|k}^{-}$ a priori estimate at the beginning of the horizon. Using the hypotheses: $w_k \sim \mathcal{N}(0, Q)$ and $v_k \sim \mathcal{N}(0, R)$ as in the previous section, one can derive the formulation of the MHE as follows [Ungarala, 2009]:

$$\begin{aligned}\min_{\hat{x}_{k-N|k},\{\hat{w}_{k-N+i|k}\}_{i=0}^{N-1}} \quad & \mathcal{Z}_{k-N}(\hat{x}_{k-N|k} - \hat{x}_{k-N|k}^{-}) + \sum_{i=0}^{N-1} \left\|\hat{w}_{k-N+i|k}\right\|_{Q^{-1}}^2 \\ & + \sum_{i=0}^{N} \|y_{k-N+i} - h(\hat{x}_{k-N+i|k})\|_{R^{-1}}^2 \end{aligned} \tag{2.21a}$$

$$\hat{x}_{k-N+i+1|k} = f(\hat{x}_{k-N+i|k}) + \hat{w}_{k-N+i|k},\ \forall i \in [0, N-1] \tag{2.21b}$$

$$\hat{x}_{k-N|k} \in \mathbb{X},\ \ \hat{w}_{k-N+i|k} \in \mathbb{W},\ \ y_{k-N+i} - h(\hat{x}_{k-N+i|k}) \in \mathbb{V} \tag{2.21c}$$

For $i < N$, the full information is implemented, i.e. the horizon at each instant is increasing and equal to k at each instant k. In other words, the formulation in (2.21) is verified for $i \in [\max(0, k-N), \min(k, N-1)]$.

The term $\mathcal{Z}(\hat{x}_{k-N|k} - \hat{x}^-_{k-N|k}) = -\ln p(x_{k-N}|y_0^{k-N-1})$ is called the arrival cost. For a linear unconstrained system, the arrival cost becomes

$$\mathcal{Z}(\hat{x}_{k-N|k} - \hat{x}^-_{k-N|k}) = \|\hat{x}_{k-N|k} - \hat{x}^-_{k-N|k}\|^2_{(P^-_{k-N|k})^{-1}} \tag{2.22}$$

$\hat{x}^-_{k-N|k} \triangleq \hat{x}^\circ_{k-N|k-1}$ is the a priori estimate at the beginning of the horizon at instant k computed from the optimal solution $(\hat{x}^\circ_{k-N-1|k-1}, \{\hat{w}^\circ_{k-N+i|k}\}_{i=0}^{N-1})$ given at instant $k-1$ using (2.21b). $P^-_{k-N|k}$ is the a priori error covariance matrix. It can be computed using the error covariance update equation described in (1.48). The MHE for a linear unconstrained system with $N = 1$ is equivalent to the Kalman Filter. For a nonlinear or constrained system, $p(x_{k-N}|y_0^{k-N-1})$ can be non Gaussian and this density has to be approximated. A common way to approximate this density is to assume that $p(x_{k-N}|y_0^{k-N-1}) \sim \mathcal{N}(\hat{x}^-_{k-N|k}, P^-_{k-N|k})$ [Rao et al., 2003][Qu and Hahn, 2009]. Using this assumption the expression of the "approximated arrival cost"[3] becomes as in (2.22).

The convergence of the estimation errors of the MHE in this framework depends on how well $P^-_{k-N|k}$ describes the density $p(x_{k-N}|y_0^{k-N-1})$. In [Rao et al., 2003], it is proposed to use the a priori error covariance update formulation of the EKF in (1.48) to compute $P^-_{k-N|k}$. Equivalently, this a priori covariance $P^-_{k-N|k}$, can be computed recursively using

$$\begin{aligned} P^-_{k-N|k} &= Q + \hat{F}_{k-N-1} P^-_{k-N-1|k-1} \hat{F}^T_{k-N-1} - \hat{F}_{k-N-1} P^-_{k-N-1|k-1} \hat{H}^T_{k-N-1} \cdots \\ &\quad (R + \hat{H}_{k-N-1} P^-_{k-N-1|k-1} \hat{H}^T_{k-N-1})^{-1} \hat{H}_{k-N-1} P^-_{k-N-1|k-1} \hat{F}^T_{k-N-1} \end{aligned} \tag{2.23a}$$

where

$$\hat{F}_{k-N-1} = \frac{\partial f(x)}{\partial x}|\hat{x}^\circ_{k-N-1|k-1} \tag{2.23b}$$

$$\hat{H}_{k-N-1} = \frac{\partial h(x)}{\partial x}|\hat{x}^\circ_{k-N-1|k-1} \tag{2.23c}$$

One can also update $P^-_{k-N|k}$ using the UKF equations [Qu and Hahn, 2009][Ungarala, 2009] or the PF equations [López-Negrete et al., 2011][Ungarala, 2009]. It has been shown that when the MHE is well initialized, the MHE whose arrival cost is updated by the PF equations provides the smallest errors compared to those updated using EKF and UKF equations. However, when the MHE is badly initialized, the arrival cost updated with UKF equations is shown to be the best choice and that updated with PF the worst[4]. When model mismatch exists, the arrival cost updated with PF equations is shown to be the best choice [Qu and Hahn, 2009].

[3] In [Rao et al., 2003], the term "arrival cost" is reserved to the exact value of

$$\mathcal{Z} = -\ln p(x_{k-N}|y_0^{k-N-1})$$

However, in later works [Haseltine and Rawlings, 2005][Liu, 2013][Zavala, 2008][Qu and Hahn, 2009] the term "arrival cost" refers to the approximated arrival cost instead for the sake of simplicity.

[4] This is not surprising knowing that the PF is well known to be sensitive to poor initialization (see chapter 1).

2.3.2 Stability of the Dynamics of the Estimation Errors of the MHE in Stochastic Framework

It is proven in [Rao et al., 2003] that the dynamics of the estimation errors of the MHE in the stochastic framework defined in (2.21) is RGAS if the system (2.1a) is observable in $N+1$ steps and its "approximated" arrival cost $\mathcal{Z}_{k-N}$ is lower than the "exact" arrival cost representing the case in which every measurement since the beginning of the estimation is taken into account. As stated in [Alessandri et al., 2010], this is difficult to do in practice since the exact arrival cost must be computed at each instant which leads to large computational effort. We, therefore, omit the stability theorem of the MHE in this framework. Although the stability of this MHE is difficult to be guaranteed in practice, it has been studied in many works [Haseltine and Rawlings, 2005][Ungarala, 2009][López-Negrete et al., 2011][Qu and Hahn, 2009] and has been shown to be more robust against poor initialization and model errors compared to the EKF, the UKF and the PF [Rao et al., 2003][Haseltine and Rawlings, 2005][Ungarala, 2009][Suwantong et al., 2012][Suwantong et al., 2013].

Now let us discuss the advantages and the drawbacks of the MHE in both frameworks.

2.4 Advantages and Drawbacks of the MHE

The advantages of the MHE are that

1. It is robust against poor initialization and spurious measurements. This is due to the fact that the estimation is done by optimizing a cost function that takes into account at the same time the initial error, the process noise and the difference between real measurements and predicted ones.

2. It is shown to be more robust against model errors compared to the EKF, the UKF and the PF [Ungarala, 2009].

3. Constraints on the state and on the process and measurement noises can be taken into account directly during the optimization. This can be useful in practice when physical constraints are known, e.g. positive mass or atmospheric density, positive altitude, positive ballistic coefficient.

4. There is no need to linearize the system since the nonlinear model can be handled directly during the optimization.

5. There exist proofs on the stability of the dynamics of the estimation errors of the MHE in the deterministic framework for nonlinear systems, for example in [Alessandri et al., 2008][Alessandri et al., 2010] where the stability can be guaranteed when the weight matrix $\mathcal{P}$ in the arrival cost is adequately chosen. This can be done in practice for a system defined in (2.1a) verifying (A1)-(A5) in section 2.2.2. We note that (A1)-(A5) are assumptions on the smoothness of the state function and the measurement function and the observability of the system.

The drawbacks of the MHE are due to its potentially high number of optimization variables, which is equal to $n_x(N+1)$. This can lead to strong nonconvexities [Zavala, 2008] and the MHE can have difficulties to find the optimal solution. Moreover, large computation time can be induced which would prevent the use of the MHE in real-time applications for systems with fast dynamics.

2.5 Existing Works on MHE's Computation Time Reduction

Several approaches to reduce the computation time of the MHE are proposed in the literature. These approaches consist in using fast optimization techniques adapted to the MHE, finding an approximate solution of the optimization problem in the MHE rather than the exact optimal solution and making use of a "Pre-Estimation" technique. Each approach will be further discussed.

2.5.1 Fast Optimization Methods for the MHE

The optimization problem in the MHE can be efficiently solved by the generalized Gauss-Newton algorithm [Ferreau et al., 2012] which is a variant of a classical Newton method where the minimum of any real-valued function $f(x)$ is derived using the derivative $\dot{f}(x)$. To be precise, starting by a guess value x_0, the derivative at this point $\dot{f}(x)|_{x=x_0}$ is computed and the search direction of the variable depends on the sign of the derivative. The Gauss-Newton method can deal with multivariable functions but can only be used to minimize a sum of squared function values.

This method may need several iterations to find a solution which is locally optimal. High number of iterations increases the computation time and therefore the Guass-Newton based methods are not adapted for online usages of the MHE. To overcome this problem, a real-time iteration (RTI) scheme which performs a single Gauss-Newton iteration per sampling instant to have an approximate solution to the optimization problem quickly is proposed in [Diehl et al., 2002]. The RTI scheme is based on the multiple shooting method [Bock, 1981] which consists in splitting the horizon interval $[k-N, k]$ into N intervals $[i, i+1]$ for $i = k-N, \ldots, k-1$, called multiple shooting intervals, then introducing the initial value of the state at time i as additional optimization parameter and finding an optimized solution for each multiple shooting interval.

A real-time MHE making use of the RTI scheme without taking into account process noise was first developed in [Kraus et al., 2006]. However, in their work, the optimization problem must be initialized around a sufficiently good reference solution which is restrictive and might not hold true in highly nonlinear problems. To tackle this issue, a method called, the advanced-step MH estimation was proposed in [Zavala, 2008]. In this method, approximate estimates are computed nearly instantaneously using reference solutions computed between sampling times. A customized real-time MHE can be generated automatically using an automatic code generation recently proposed in [Ferreau et al., 2012].

2.5.2 Approximate MHE

Another approach to reduce the computation time is to find a suboptimal solution of the optimization problem in the MHE for which a certain error in the minimization of the cost function is allowed. In other words, rather than finding an optimal estimate $\hat{x}^{\circ}_{k-N|k}$ and optimal process noise estimates $\{\hat{w}^{\circ}_{k-N+i|k}\}_{i=0}^{N-1}$ of the optimization problem in (2.8b), we search for an approximate estimate $\hat{x}^{\epsilon}_{k-N|k} \in \mathbb{X}$ and approximate process noise estimates $\{\hat{w}^{\epsilon}_{k-N+i|k}\}_{i=0}^{N-1}$ such that

$$\mathbf{J}_k(\hat{x}^{\epsilon}_{k-N|k}, \{\hat{w}^{\epsilon}_{k-N+i|k}\}_{i=0}^{N-1}, \hat{x}^{-}_{k-N|k}, y_{k-N^k}) - \mathbf{J}_k(\hat{x}^{\circ}_{k-N|k}, \{\hat{w}^{\circ}_{k-N+i|k}\}_{i=0}^{N-1}, \hat{x}^{-}_{k-N|k}, y_{k-N^k}) \leq \epsilon$$

This approach is called the approximate MHE, first proposed in [Alessandri et al., 2008] for an MHE in which process noises are not estimated and for an MHE in which process noises are estimated in [Alessandri et al., 2010]. In these works, the stability of the estimation errors of the approximated MHE has also been proven.

The approximation in this approximate MHE can either be done on-line or off-line. An on-line solution can be obtained using an optimization technique that can ensure a given precision ϵ. An off-line solution can be obtained by approximating the state equation f in (2.8c) using nonlinear approximators. More details on the approximate MHE using nonlinear approximators can be found in [Alessandri et al., 2008] and [Alessandri et al., 2011] where Neural Networks are proposed to be used. Since the Neural Networks are not in the scope of our studies, their principles are omitted here. An insightful description of the Neural Networks is available in [Alessandri et al., 2011]. The approximate MHE was shown in a numerical study to provide the same order of estimation errors as the optimal MHE while using up to 1000 times less computation time.

2.5.3 MHE with Pre-Estimation (MHE-PE)

Another strategy to reduce computation time consists in replacing the state equation, used to compute the state evolution over the horizon, in the MHE by the one of an auxiliary estimator, called pre-estimator. This pre-estimator allows the MHE to "compensate" for model errors without searching for the optimal estimation of the process noise sequence over the horizon via optimization like the MHE.
Such strategy has been proposed in [Sui et al., 2010] for discrete-time linear systems where a deterministic observer is chosen as pre-estimator. A deterministic observer is in fact an estimator dealing with a noise-free system whose dynamics of the estimation errors is RGAS. The definition of the deterministic observer will be provided in (4.8).

In fact, it has been shown that the deterministic observer provides bounded estimation errors for a system under bounded noises [Liu, 2013]. However, the bound can be very high. It is therefore still interesting to combine the MH strategy to the deterministic observer to increase accuracy of the estimates.

In [Sui et al., 2010], it has been shown that for a linear system, the MHE-PE which is a method combining the MH strategy to the deterministic observer provides less estimation errors than the deterministic observer alone. In this paper, it has also been shown to be robust against model errors and require smaller computation time than the classical MHE. This is not surprising since the process noise sequence is no longer included in the optimization parameters for the MHE-PE. The stability of the dynamics of the estimation errors of this MHE for linear systems has been proven to be guaranteed if the weight matrix on the arrival cost is adequately chosen.

2.5.4 Our Approach

We are interested in the MHE-PE approach which deals with a modification in the structure of the MHE to reduce the computation time. The use of this approach can be combined to other time reduction approaches such as fast optimization techniques and approximate schemes. The proof of the convergence of the estimation errors of the MHE with Pre-Estimation (MHE-PE) only exists for the linear system. We therefore propose a proof of this property of the MHE-PE for nonlinear systems under bounded noise in

chapter 4.

The novelties of our work compared to [Sui et al., 2010] are the extension of the method to nonlinear systems and the use of a bounded-error estimator instead of a deterministic observer in the pre-estimation part. Note that fast optimization methods can still be implemented to reduce more computation time. The stability of the proposed MHE-PE will be analyzed and an upper bound on the estimation errors will be derived in chapter 4. Performance of the MHE-PE for space debris trajectory estimation will be studied in chapter 5.

2.6 Summary of the Chapter

In this chapter, we have seen that

- The MHE seems adapted to space debris tracking during the atmospheric re-entry, which generally suffers from model errors and poor initialization, thanks to the MHE's robustness against these factors. Performances of the MHE in this problem will be therefore studied in the next chapter.

- Formulations of the MHE exist in the deterministic framework and the stochastic framework. For the MHE in the stochastic framework, a priori error covariance matrix is chosen as the weight in the arrival cost. This a priori error covariance matrix can be computed using update formula in nonlinear estimators such as those of the EKF, the UKF and the PF. However, the stability of the MHE in this framework is difficult to be guaranteed in practice. On the other hand, the MHE in the deterministic framework is shown to ensure the convergence of the estimation errors when its weight matrix in the arrival cost is adequately chosen. However, to do so parameters on the smoothness of the state function (Lipschitz constant) and the sensitivity parameter of the measurements to the state (δ) must be computed. In this chapter, we also compute the constants in the inequality the MHE in the deterministic framework must satisfy to guarantee the stability.

- MHE uses large computation time due to its high number of optimization parameters. Several works to reduce the MHE's computation time have been proposed including those based on fast optimization algorithms, those based on an approximate scheme of the MHE and those using pre-estimation method which allow the MHE to take into account model errors approximately without considering process noises as optimization parameters.

- Thanks to the robustness of the MHE, it is interesting to study its performance for space debris tracking during atmospheric re-entries. This will be done in the next chapter.

CHAPTER 3

MHE for Space Debris Tracking during Atmospheric Re-Entries

"It is not the strongest of the species that survives, nor the most intelligent, but the one most responsive to change. "

— Charles Darwin

Objectives of this chapter

- To study the performances of the Moving Horizon Estimator (MHE) in the deterministic and the stochastic frameworks for the space debris tracking during atmospheric re-entries. Performances are studied in terms of non-divergence percentage, accuracy of the estimates and computation time compared to those of the classical estimators generally used for ballistic object tracking during the re-entries. These estimators are the Extended Kalman Filter (EKF), the Unscented Kalman Filter (UKF) and the Regularized Particle Filter (RPF). The studies in this chapter will be done for a simplified 1 dimensional cases for the sake of simplicity.
- To compare the performances of the estimators using the estimation model with ballistic coefficient as state variable and those using the estimation model with acceleration as state variable presented in chapter 1.
- To evaluate the robustness of the estimator with respect to bad initialization on the a priori value of the initial ballistic coefficient and bad choice of process noise parameters.

3.1 Introduction

Chapter 1 shows that space debris tracking during atmospheric re-entries generally suffers from model errors. A to-be-used estimator must therefore be robust against these errors. As mentioned in chapter 1, classical nonlinear estimators generally implemented in ballistic object tracking during the re-entries are the Extended Kalman Filter (EKF), the Unscented Kalman Filter (UKF) and the Regularized Particle Filter (RPF). However, the EKF is only reliable for systems that are almost linear over the sampling period [Julier

and Uhlmann, 2004] and is sensitive to bad initialization. The UKF is accurate only when the a posteriori error distribution can be closely approximated by a Gaussian distribution [Ristic et al., 2004][Julier and Uhlmann, 2004]. The RPF is known to be sensitive to poorly chosen process noise parameter and bad initialization [Rawlings and Bakshi, 2006]. An alternative estimator must therefore be chosen for space debris tracking problem during the re-entries.

In this direction, chapter 2 has shown that the Moving Horizon Estimator (MHE) seems to be a good candidate for the space debris tracking problem during the re-entries thanks to its robustness against model errors and against bad initialization. Thus, in this chapter, we study and compare the performances of the MHE, the EKF, the UKF and the RPF for space debris tracking during the re-entries via Monte Carlo simulations of 100 debris trajectories. The studies will be done in a 1 dimensional case since in a 3 dimensional case, the number of optimization parameters of the MHE will be very large and the MHE will require very large computation time. Moreover, in a 3D case, the MHE may have difficulties to find an optimal solution due to this high number of optimization parameters.

This chapter is structured as follows. First, the dynamics of space debris, the measurement equation and the estimation models, previously discussed in chapter 1 in a 3 dimensional case, are presented in a simplified 1 dimensional case. Second, the simulation methods used to simulate the trajectories of spherical space debris during the re-entries will be described. In fact, we are interested in the spherical shape because the expression of the drag coefficient is known and it can represent some types of debris such as upper stages and pressure tanks. Third, we present how to initialize the estimators in terms of position and velocity estimates using the first two radar measurements and how to initialize the estimators in terms of ballistic coefficient and acceleration using an assumption on the diameter of the debris. Thanks to the fact that real trajectories are simulated, we compute a theoretical good choice of process noise parameters that would characterize the model errors adequately. Unfortunately, in reality, since the real dynamics is unknown, a good choice of these process noise parameters cannot be guaranteed. Therefore, the robustness of the estimators when the process noise parameters are not necessarily well chosen will be studied. The performances of the estimators in terms of non-divergence percentage, accuracy of the estimates and computation time will be analyzed. The effect of bad initialization on the performances of the estimators will also be considered. The chapter ends with a discussion about the results and perspectives for a 3 dimensional case which will be proposed in the next two chapters.

3.2 Dynamics of Space Debris and Measurement Equation for a 1D Case

In this section, the dynamics of space debris and the measurement equation described for a 3 dimensional case in section 1.2.1 are formulated for a 1 dimensional case.

Consider that a piece of debris is falling vertically along the observation axis of the radar station (see fig. 3.1), similarly to the problem studied in [Ristic et al., 2003]. Suppose that

- the debris is closed enough to the radar station that the Earth can be considered flat and the acceleration due to the gravity g_E is assumed to be constant

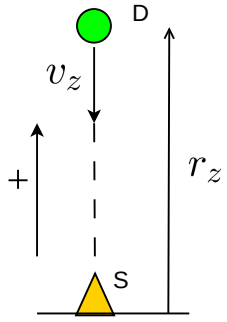

Figure 3.1: Space Debris Trajectory in a 1 dimensional case, D: debris and S: radar station.

- the observation period is short enough that the Earth rotational motion can be neglected
- only the gravitational force and drag force due to the atmosphere are acting on the debris

See section 1.2.1 for all the details on these hypotheses. Let $t \in \mathbb{R}^+$ denote the continuous time index. At time t, let $r_z(t) \in \mathbb{R}^+$ be the position of the object which corresponds to the altitude $r_z(t) = H(t)$ thanks to the flat Earth hypothesis, $v_z(t)$ its velocity, $a_z(t)$ its acceleration, both in the SEU coordinates, and $\beta(t)$ its ballistic coefficient. The dynamics of the debris is described by

$$a_z(t) = \ddot{r}_z(t) = \dot{v}_z(t) = -g_E + \frac{1}{2}\frac{\rho(r_z(t))}{\beta(t)} v_z^2(t) \tag{3.1}$$

The atmosphere density ρ depends on the altitude of the body and is modeled by

$$\rho(r_z(t)) = \mathsf{c}_1 e^{-\mathsf{c}_2 r_z(t)} \tag{3.2}$$

with $\mathsf{c}_1 = 1.227\ kg/m^3$, $\mathsf{c}_2 = 1.093 \cdot 10^{-4}\ m^{-1}$ for $0 \leq r_z < 9144$ m and $\mathsf{c}_1 = 1.754\ kg/m^3$, $\mathsf{c}_2 = 1.490 \cdot 10^{-4}\ m^{-1}$ for $r_z \geq 9144$ m [Ristic et al., 2003]. $\beta \in \mathbb{R}^{+*}$ is the ballistic coefficient of the object defined by

$$\beta(t) = \frac{m(t)}{A(t)C_D(t)} \tag{3.3}$$

where m, A and C_D are the mass, the cross section and the drag coefficient of the object respectively. β represents the body's ability to overcome fluid resistance. For the space debris, β is generally a time varying function. In fact, the debris can be burnt up and its shape can vary with time. The expression of $\beta(t)$ for a spherical ballistic object will be described in appendix C.1. The analytic expression of $\beta(t)$ is very complex for a non-spherical object [Gallais, 2007].

Suppose that the distance measurements are given at regular intervals of T_s seconds and define $r_{z_k} = r_z(t = kT_s)$. Since it is assumed that the radar station is located directly below the falling debris, the measured debris' distance provided by the radar is equivalent to the measured debris' altitude r_z. The measurement equation is

$$y_k = r_{z_k} + v_k \tag{3.4}$$

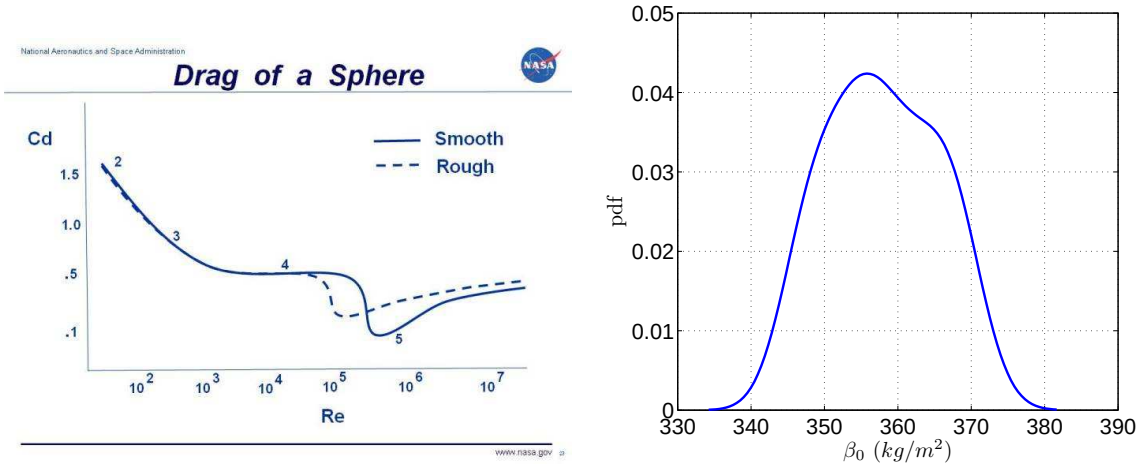

Figure 3.2: Evolution of the drag coefficient of a sphere in function of the Reynolds number, credit: NASA (left). Distribution of the initial ballistic coefficient of the simulated trajectories (right)

where v_k is a discrete-time measurement noise modeled by a zero-mean bounded white noise with variance R_k. For the sake of simplicity, we assume that $R_k = R$, $\forall k$ and

$$R = \sigma_d^2 \tag{3.5}$$

where σ_d is the standard deviation associated to the distance measurement noise.

3.3 Simulations of the Real Trajectories

The trajectories of 100 Aluminium hollow-spherical space debris of width $w = 3$ cm are generated via Monte Carlo simulations. We suppose that each debris has an initial position r_{z_0}, an initial velocity v_{z_0}, and an outer diameter D generated according to the following uniform distributions: $r_{z_0} \sim \mathbf{U}(69, 70)$ km, $v_{z,0} \sim \mathbf{U}(-6500, -5500)$ m/s, $D \sim \mathbf{U}(20, 30)$ cm. Denote ρ_D the density of the debris. The initial mass of the debris is calculated using

$$m = \rho_D \frac{4\pi}{3} \left[\left(\frac{D}{2} \right)^3 - \left(\frac{D}{2} - w \right)^3 \right] \tag{3.6}$$

where $\rho_D = 2700$ kg/m^3 for an Aluminium debris. The used distribution of D give the distribution of the mass $m \in [7.43, 18.63]$ kg.
m and D are supposed to be constant during the re-entry. As a consequence, the ballistic coefficient of the debris depends only on the drag coefficient C_D which depends only on the Reynolds number Re for a sphere. The expression of the drag coefficient of a sphere is given in appendix C.1. The evolution of C_D as a function of Re is presented in fig. 3.2.

Using the values of r_{z_0}, $v_{z,0}$ and D associated values of of β_0 is computed and the distribution of these values of β is presented in figure 3.2. Using equations (3.1), (3.2), (3.3) and the expression of β of a sphere in appendix C.1, the trajectories of 100 spherical space debris during 20 s are calculated. The measurements for each trajectory are simulated using (3.4) by choosing $T_s = 0.1$ s and $\sigma_d = 10$ m. This value of σ_d has the

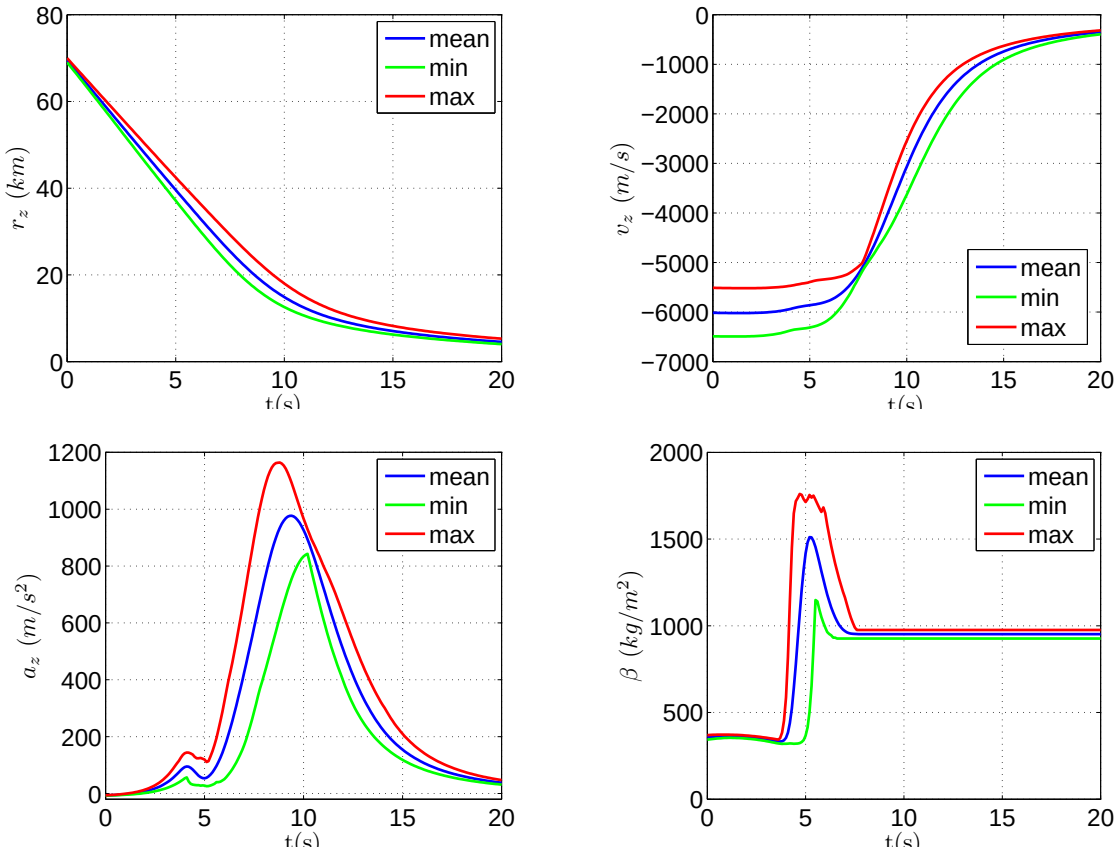

Figure 3.3: Evolutions of the position, velocity, acceleration and ballistic coefficient of one of the simulated trajectories

same order as the resolution of the German Tracking and Imaging Radar (TIRA) and the ESA's ARMOR Radar [Alarcón et al., 2005]. An example of the simulated trajectories is shown in fig.3.3 where we can remark that β has high variation at the beginning and becomes constant during the last 10 s of the trajectories.

Again, we recall that this varying β causes the space debris tracking during the re-entry difficult. Since its variation is a priori unknown, a hypothesis on the dynamics of β must be made in the estimation model. We can, for example, suppose that $\dot{\beta}(t)$ is equal to a continuous zero-mean white noise as in the model with ballistic coefficient described in 1.3.2.2 or that $\dot{a} = \dot{a}|_{\beta=cst}$ is equal to a continuous zero-mean white noise as in the model with acceleration described in 1.3.2.3. These two assumptions will, of course, lead to model errors. These model errors can be taken into account in an estimator through process noises in the estimation model. However, the chosen process noise covariance matrix Q must represent the true model errors. Unfortunately, one cannot guarantee to have a well chosen Q in practice since the dynamics of the system is generally unknown. The to-be-used estimator for space debris tracking during the re-entry should therefore be robust against poor choice of process noise parameters.

3.4 Estimation Models

Our objective is to estimate the position of the debris during the re-entry. To have better accuracy than the one provided by radar measurements, an estimator is implemented. In this section, the estimation models used in the tested estimators (EKF, UKF, RPF and MHEs in the deterministic and the stochastic frameworks) are described for a 1 dimensional case. These estimation models are the one including ballistic coefficient as a state variable and the one including acceleration as a state variable described in section 1.3.2.2 and in section 1.3.2.3 respectively for a 3 dimensional case.

3.4.1 1D Estimation Model with Ballistic Coefficient as a State Variable

The state at time t is defined as

$$x(t) = \begin{pmatrix} r_z(t) & v_z(t) & \beta(t) \end{pmatrix}^T \tag{3.7}$$

The function $\beta(t)$ is a priori unknown and it is assumed in this model that the time derivative of $\beta(t)$: $\dot{\beta}(t)$ is driven by a continuous-time zero-mean white noise $w_\beta(t)$, taking into account the fact that β is not constant over a sampling period. Suppose that $E\{w_\beta(t)w_\beta(\tau)\} = q_\beta(t)\delta(t-\tau)$ with $\delta(\cdot)$ the dirac distribution and q_β the power spectral density of w_β. The estimation model is described by

$$\begin{aligned} \dot{r}_z(t) &= v_z(t) \\ \dot{v}_z(t) &= -g_E + \frac{1}{2}\frac{\rho(r_z(t))}{\beta(t)} v_z^2(t) \\ \dot{\beta}(t) &= w_\beta(t) \end{aligned} \tag{3.8}$$

In order to implement the estimators and since measurements from radar station are available at discrete-time intervals, (3.8) has to be discretized. Denote r_{z_k}, v_{z_k} and β_k the value of $r_z(t)$, $v_z(t)$ and $\beta(t)$ at time $t = kT_s$, for $k \in \mathbb{N}$, where T_s is the sampling period which is chosen equal to the measurement sampling time.

Denote

$$a_{z_k} = -g_E + \frac{1}{2}\frac{\rho(r_{z_k})}{\beta_k} v_{z_k}^2 \tag{3.9}$$

Assume that $\dot{v}_z(t) = a_{z_k} + w_{a_z}(t)$, for $\forall t \in [kT_s, (k+1)T_s]$ with $w_a(t)$ a continuous-time zero-mean white noise, accounting for discretization error. Thus, $E\{w_{a_z}(t)w_{a_z}(\tau)\} = q_{a_z}(t)\delta(t-\tau)$ with q_{a_z} the power spectral density of w_{a_z}. Assume also that the derivative of $\beta(t)$ is driven by a continuous-time zero-mean white noise $w_\beta(t)$ with a power spectral density $q_\beta(t)$. In other words, $E\{w_\beta(t)w_\beta(\tau)\} = q_\beta(t)\delta(t-\tau)$. For the sake of simplicity, $q_{a_z}(t)$ and $q_\beta(t)$ are assumed to be constant.

Using the proof given in appendix A.1, we obtain

$$x_{k+1} = \begin{pmatrix} r_{z_{k+1}} \\ v_{z_{k+1}} \\ \beta_{k+1} \end{pmatrix} = \begin{pmatrix} r_{z_k} + v_{z_k}T_s + a_{z_k}\dfrac{T_s^2}{2} \\ v_{z_k} + a_{z_k}T_s \\ \beta_k \end{pmatrix} + w_k \tag{3.10}$$

w_k is the discrete-time process noise modeled as a zero-mean white noise with the covariance matrix:

$$Q = \begin{pmatrix} q_{a_z}\frac{T_s^3}{3} & q_{a_z}\frac{T_s^2}{2} & 0 \\ q_{a_z}\frac{T_s^2}{2} & q_{a_z}T_s & 0 \\ 0 & 0 & q_\beta T_s \end{pmatrix} \tag{3.11}$$

For the sake of simplicity, q_{a_z} and q_β are assumed to be constant.

3.4.2 1D Estimation Model with Acceleration as a State Variable

Define the state at time t

$$x(t) = \begin{pmatrix} r_z(t) & v_z(t) & a_z(t) \end{pmatrix}^T \tag{3.12}$$

and $x_k = x(t = kT_s)$ where T_s is the estimator's sampling period. Recall that the dynamics of the real β is unknown. It is assumed in this model that $\forall t \in [kT_s, (k+1)T_s]$:

$$\dot{a}_z(t) = f_{z_k} + \xi_z(t) \tag{3.13}$$

$$f_{z_k} \triangleq \dot{a}_z(t)|_{\beta=cst} = (-\mathsf{c}_2 v_{z_k} + \frac{2a_{z_k}}{v_{z_k}})(a_{z_k} + g_E) \tag{3.14}$$

f_{z_k} is derived by deriving the acceleration in continuous-time a_z in (3.1). $\xi_z(t)$ is a continuous zero-mean white noise with spectral density $\tilde{q}_z$ accounting for discretization error **and** model errors from the fact that β is not constant over a sampling period. We have $E\{\xi_z(t)\xi_z(\tau)\} = \tilde{q}_z(t)\delta(t-\tau)$. For the sake of simplicity, $\tilde{q}_z(t)$ is supposed to be constant.

Similarly to the method used in [Bar-Shalom et al., 2004], the following state equation is derived:

$$x_{k+1} = f(x_k) + w_k = \begin{pmatrix} 1 & T_s & \frac{T_s^2}{2} \\ 0 & 1 & T_s \\ 0 & 0 & 1 \end{pmatrix} x_k + \begin{pmatrix} \frac{T_s^3}{6} \\ \frac{T_s^2}{2} \\ T_s \end{pmatrix} f_{z_k} + w_k \tag{3.15}$$

where w_k is a discrete-time zero-mean white noise whose covariance matrix is

$$Q = \begin{pmatrix} \frac{1}{20}T_s^5 & \frac{1}{8}T_s^4 & \frac{1}{6}T_s^3 \\ \frac{1}{8}T_s^4 & \frac{1}{3}T_s^3 & \frac{1}{2}T_s^2 \\ \frac{1}{6}T_s^3 & \frac{1}{2}T_s^2 & T_s \end{pmatrix} \tilde{q}_z \tag{3.16}$$

The proof is given in appendix A.2.

3.5 A Priori Initial Estimates

Let us denote $\hat{r}_{z_k}$ the position estimate, $\hat{v}_{z_k}$ the velocity estimate, $\hat{\beta}_k$ the ballistic coefficient estimate and $\hat{a}_{z_k}$ the acceleration estimate, all at instant k. Denote $\hat{x}_k$ the estimate

and $\hat{x}_k^-$ the a priori estimate of the state x_k at instant k. For the estimation model including ballistic coefficient, we have $\hat{x}_k = \begin{pmatrix} \hat{r}_{z_k} & \hat{v}_{z_k} & \hat{\beta}_k \end{pmatrix}^T$ and for the model including acceleration, we have $\hat{x}_k = \begin{pmatrix} \hat{r}_{z_k} & \hat{v}_{z_k} & \hat{a}_{z_k} \end{pmatrix}^T$. Denote $\hat{x}_0^-$ the a priori *initial* estimates.

The idea is to choose an a priori initial position estimate $\hat{r}_{z_0}^-$, an a priori initial velocity estimate $\hat{v}_{z_0}^-$ using distance measurements and an a priori initial ballistic coefficient estimate $\hat{\beta}_0^-$ using a priori information on the debris (on its mass m, section D or density ρ_D for example). The a priori initial acceleration estimate $\hat{a}_{z_0}^-$ for the model with acceleration is computed using

$$\hat{a}_{z_0}^- = -g_E + \frac{1}{2}\frac{\rho(\hat{r}_{z_0}^-)}{\hat{\beta}_0^-}(\hat{v}_{z_0}^-)^2 \tag{3.17}$$

For each of the 100 generated trajectories, each estimator will be initialized with the **same** a priori initial estimate $\hat{x}_0^-$ for the same estimation model. Let us discuss first the initialization of the a priori initial position $\hat{r}_{z_0}^-$, followed by the a priori initial velocity $\hat{v}_{z_0}^-$ and the a priori ballistic coefficient $\hat{\beta}_0^-$.

3.5.1 A Priori Initial Position and Velocity Estimates

The a priori initial position and velocity estimates $\hat{r}_{z,0}^-$ and $\hat{v}_{z,0}^-$ are initialized by *two-point differencing method* using two measurements [Bar-Shalom et al., 2004]. The two-point differencing method consists in calculating the position of an object using the measurements at the initial instant 0 and the previous one "-1", i.e. at least two measurements have to be collected before starting the estimator. Thanks to this method, we have

$$\hat{r}_{z_0}^- = y_0, \;\; \hat{v}_{z_0}^- = \frac{y_0 - y_{-1}}{T_s} \tag{3.18}$$

Define the a priori initial **error** vector on the position estimate and the velocity estimate as

$$\begin{pmatrix} \tilde{r}_{z_0}^- \\ \tilde{v}_{z_0}^- \end{pmatrix} = \begin{pmatrix} \hat{r}_{z_0}^- \\ \hat{v}_{z_0}^- \end{pmatrix} - \begin{pmatrix} r_{z_0} \\ v_{z_0} \end{pmatrix} \tag{3.19}$$

where r_{z_0} and v_{z_0} are the real initial position and velocity of the debris.

Define $P_{\tilde{r}_{z_0}^-, \tilde{v}_{z_0}^-}$ the covariance matrix of $\begin{pmatrix} \tilde{r}_{z_0}^- & \tilde{v}_{z_0}^- \end{pmatrix}^T$. According to [Bar-Shalom et al., 2004], we have

$$P_{\tilde{r}_{z_0}^-, \tilde{v}_{z_0}^-} = \begin{pmatrix} R & R/T_s \\ R/T_s & 2R/T_s^2 \end{pmatrix} \tag{3.20}$$

where $R = \sigma_d^2$ is the measurement noise covariance matrix.

3.5.2 A Priori Initial Ballistic Coefficient and Accelation Estimates

Recall that a value for the a priori initial ballistic coefficient estimate $\hat{\beta}_0^-$ will be chosen and the a priori initial acceleration estimate $\hat{a}_{z_0}^-$ for the model with acceleration will be computed using (3.17). Denote $\tilde{\beta}_0^- = \hat{\beta}_0^- - \beta_0$ the error on the initial a priori ballistic coefficient estimate and $\sigma_{\tilde{\beta}_0^-}$ the standard deviation of $\tilde{\beta}_0^-$. Denote $\tilde{a}_{z_0}^- = \hat{a}_{z_0}^- - a_{z_0}$ the error on the initial a priori acceleration estimate and $\sigma_{\tilde{a}_{z_0}^-}$ the standard deviation of $\tilde{a}_{z_0}^-$.

$\hat{\beta}_0^-$ and $\hat{a}_{z_0}^-$ are considered uncorrelated to $\hat{r}_{z_0}^-$ and $\hat{v}_{z_0}^-$ since the $\hat{r}_{z_0}^-$ and $\hat{v}_{z_0}^-$ are computed from the measurements alone. As a consequence, we have for the estimation model with ballistic coefficient

$$P_0^- = \begin{pmatrix} R & R/T_s & 0 \\ R/T_s & 2R/T_s^2 & 0 \\ 0 & 0 & \sigma^2_{\tilde{\beta}_0^-} \end{pmatrix} \tag{3.21}$$

and for the estimation model with acceleration

$$P_0^- = \begin{pmatrix} R & R/T_s & 0 \\ R/T_s & 2R/T_s^2 & 0 \\ 0 & 0 & \sigma^2_{\tilde{a}_{z_0}^-} \end{pmatrix} \tag{3.22}$$

Let us discuss how to choose a value for $\hat{\beta}_0^-$, $\sigma_{\tilde{\beta}_0^-}$ and $\sigma_{\tilde{a}_{z_0}^-}$.

3.5.2.1 How to Choose an a Priori Initial Ballistic Coefficient

To have a supposed distribution of possible values of the initial ballistic coefficient β_0, one can make assumptions on the distributions of the mass, the cross section and the drag coefficient of the object. For example, we can suppose that $m \sim \mathbf{U}(m_{min}, m_{max})$, $A \sim \mathbf{U}(A_{min}, A_{max})$ and $C_D \sim \mathbf{U}(C_{D_{min}}, C_{D_{max}})$ and then simulate the distribution of the possible β_0 using (3.3). If the shape and the density of the object are known, we can have a relation between m and A.

For an object whose shape is spherical, its drag coefficient C_D can be computed using the equations in appendix C.1. In this case, we have to suppose a distribution of the altitude and of the velocity of the object. For other types of objects, a table of *average* values of C_D for various shapes resulting from experiments are available in [Moe et al., 1995].

For a cataloged object, a value of the initial ballistic coefficient estimate is given in the Two-Line Element set which is the collection of the orbital elements from which a priori values of the position, the velocity and the ballistic coefficient can be computed. However, the standard deviation of the errors of these a priori values are not available. In [Sang et al., 2013] a method to estimate ballistic coefficients of low altitude debris objects from historical two-line elements are proposed.

In our studies, we suppose that the debris is known to be a hollow sphere with width $w = 3\ cm$ and that the debris is made of Aluminium. Hence, the density of the debris is known and the mass m of the debris can be computed based on an assumption on the debris' outer diameter D using (3.6). The robustness of the estimators against bad initialization will be studied by giving the estimators two different assumptions on the debris' outer diameter D.

3.5.2.2 Test of Robustness against Bad Initialization of the Estimator

The performances of the estimator will be studied for the two following cases of initialization of the a priori initial ballistic coefficient $\hat{\beta}_0^-$:

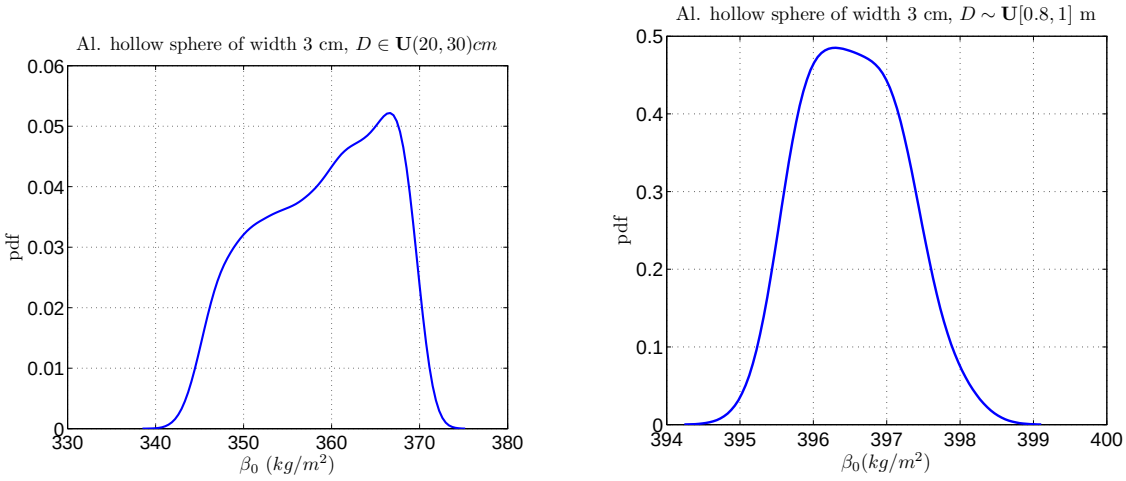

Figure 3.4: *The distribution of the initial ballistic coefficient β_0 of hollow Aluminium spheres generated using initial conditions $r_{z_0} \sim \mathbf{U}(69,70)$ km, $v_{z_0} \sim \mathbf{U}(-6500,-5500)$ km by assuming that the outer diameters D are drawn from $\mathbf{U}(20,30)$ cm which is the distribution of the real diameter (left). The distribution of β_0 of hollow Aluminium spheres generated using the same initial conditions except that the outer diameters are drawn from $\mathbf{U}(80,100)$ cm instead (right). This represents a case where a wrong assumption on the size of the objects is made which can induce a wrong assumption on the distribution of the initial ballistic coefficient.*

Good Initialization Case $\hat{\beta}_0^-$ is derived based on an assumption that the outer diameter $D \sim \mathbf{U}(20,30)$ cm. This is the distribution of the real D. The distribution of β for $r_{z_0} \sim \mathbf{U}(69,70)$ km, $v_{z_0} \sim \mathbf{U}(-6500,-5500)$ m/s and $D \sim \mathbf{U}(20,30)$ cm is presented in figure 3.4 (left). This distribution of D implies that the mass $m \in [7.43, 18.63]$ kg. The value $\hat{\beta}_0^-$ is chosen equal to the mean of the distribution of β_0 with this assumption which is equal to 357.85 kg/m^2. $\sigma_{\tilde{\beta}_0^-}$ is chosen equal to the standard deviation of the distribution which is equal to 7.26 kg/m^2.

Bad Initialization Case We consider a case in which a wrong assumption on the diameters of the debris D is made. Here, it is supposed that $D \sim \mathbf{U}(80,100)$ cm instead of the real distribution $\mathbf{U}(20,30)$ cm. Using this distribution of D, it is supposed that $m \in [150.95, 239.51]$ kg. The "supposed" distribution of β_0 is presented in figure 3.4 (right). In this bad initialization case, $\hat{\beta}_0^-$ is chosen equal to the mean of the distribution of β_0 with this assumption which is equal to 396.48 kg/m^2. The standard deviation of the initial a priori ballistic coefficient estimate error $\sigma_{\tilde{\beta}_0^-}$ is chosen equal to the standard deviation of the distribution which is equal to 0.65 kg/m^2.

Standard Deviation of the A Priori Initial Error of Acceleration Estimate $\sigma_{\tilde{a}_{z_0}^-}$ Using both assumptions on the outer diameter, the distributions of the initial acceleration for each assumption on the diameter D are computed and shown in figure 3.5. We see that the standard deviation of these two distributions are very closed. Using the distributions in figure 3.5, $\sigma_{\tilde{a}_{z_0}^-}$ is chosen equal to 0.3 m/s^2 for both initialization cases.

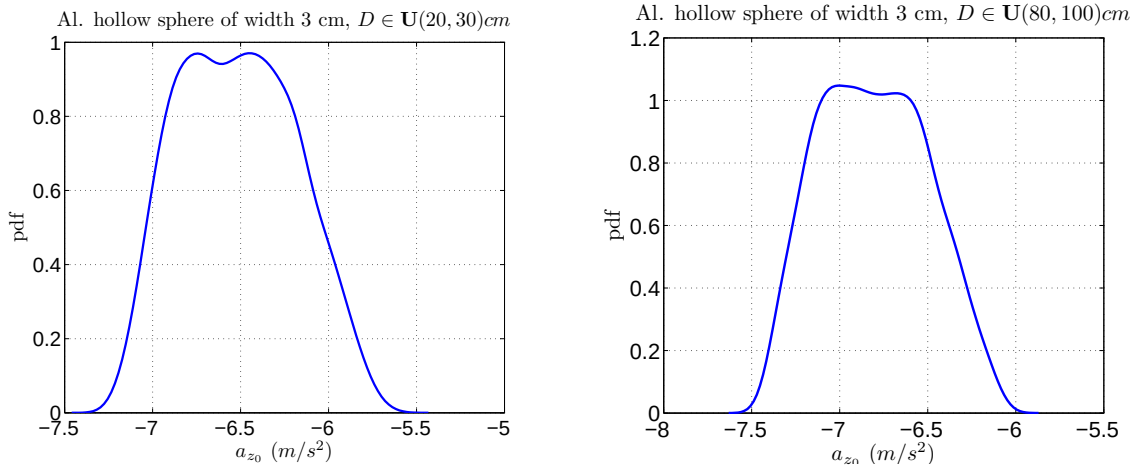

Figure 3.5: *The distribution of the acceleration a_{z_0} of hollow Aluminium spheres generated using initial conditions $r_{z_0} \sim \mathbf{U}(69, 70)$ km, $v_{z_0} \sim \mathbf{U}(-6500, -5500)$ km by assuming that the outer diameters D are drawn from $\mathbf{U}(20, 30)$ cm (left). The distribution of β_0 of hollow Aluminium spheres generated using the same initial conditions except that the outer diameters are drawn from $\mathbf{U}(80, 100)$ cm instead (right). This represents a case where a wrong assumption on the size of the objects is made which can induce a wrong assumption on the distribution of the initial ballistic coefficient and hence on the distribution of the acceleration.*

Now that the initialization of the estimators has been discussed, let us pursue with the tuning of other parameters of the estimators.

3.6 Tunings of the Estimators

3.6.1 Common Tunings for all the Estimators

For each run, the following parameters are given to each estimator:

3.6.1.1 Sampling period

The sampling period of the estimator T_s is chosen equal to the period of measurements for the sake of simplicity. Hence, $T_s = 0.1$ s.

3.6.1.2 Measurement Noise Covariance Matrix

$$R = \sigma_d^2 \tag{3.23}$$

where $\sigma_d = 10$ m. As mentioned before, this value of σ_d has the same order as the resolution of the German Tracking and Imaging Radar (TIRA) and the ESA's ARMOR Radar [Alarcón et al., 2005].

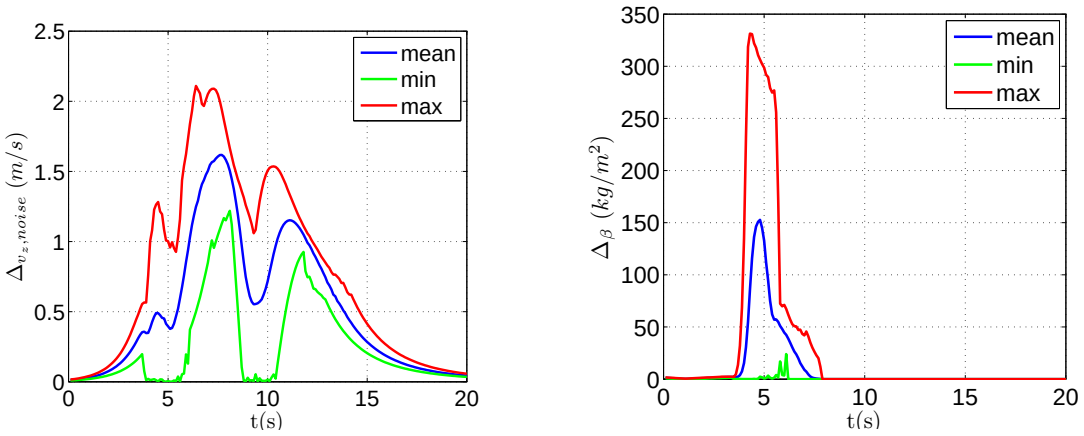

Figure 3.6: The mean, the max and the min of $\Delta_{v_z,noise}$ in time computed using the real trajectories (left) and those of Δ_β (right)

3.6.1.3 Process Noise Covariance Matrix

Estimation Model with Ballistic Coefficient Recall that for the estimation model with ballistic coefficient, the process noise covariance matrix is

$$Q = \begin{pmatrix} q_{a_z}\frac{T_s^3}{3} & q_{a_z}\frac{T_s^2}{2} & 0 \\ q_{a_z}\frac{T_s^2}{2} & q_{a_z}T_s & 0 \\ 0 & 0 & q_\beta T_s \end{pmatrix} \tag{3.24}$$

As discussed in section 1.3.2.2, the process noise parameter q_{a_z}, taking into account the discretization error, should be chosen such that $\sqrt{q_{a_z}T_s}$ has the same order of magnitude as the change in the velocity that is not taken into account in the estimation model and should be represented by process noise over a sampling period defined by

$$\Delta_{v_z,noise,k+1} = v_{z_{k+1}} - v_{z_k} - a_{z_k}T_s,\ \forall k \tag{3.25}$$

And the process noise parameter q_β, taking into account the variation of β, should be chosen such that $\sqrt{q_\beta T_s}$ has the same order of magnitude as the change in the ballistic coefficient over a sampling period defined by

$$\Delta_{\beta,k+1} = \beta_{k+1} - \beta_k,\ \forall k \tag{3.26}$$

According to (3.25) and (3.26), we can see that appropriate values of q_{a_z} and q_β can vary with time. The evolutions of the minimum, the mean and the maximum of $\Delta_{v_z,noise}$ and of Δ_β computed using the generated trajectories are shown in figure 3.6.

Thanks to figure 3.6, we observe that the variation of the change in velocity due to noise $\Delta_{v_z,noise}$ remains in the same order of magnitude in time. However, the change in the ballistic coefficient Δ_β varies much with time during the first 10 s then becomes equal to zero[1]. A single value of q_β cannot, therefore, describe well the value of Δ_β. Figure 3.6

[1]This is not surprising since according to the generated trajectories in figure 3.3 β has high variations at first and then becomes constant afterward.

shows us that a value of $\sqrt{q_\beta T_s} = 100\ kg/m^2$ is adapted for $t \in [0, 10]\ s$ and $\sqrt{q_\beta T_s} = 0\ kg/m^2$ is adapted for $t \in [10, 20]\ s$.

In this study, constant values of q_{a_z} and q_β are chosen for the sake of simplicity. The value $\sqrt{q_{a_z} T_s} = 1\ m/s$ is chosen and the robustness of the estimators to the choice of process noise parameter q_β is studied by comparing the performances of the estimators using two different values of q_β.

Test of robustness of the estimators to the choice of process noise parameter for the estimation model with ballistic coefficient

- The first value of q_β is chosen such that $\sqrt{q_\beta T_s} = 100\ kg/m^2$ which is shown to capture the variation of Δ_β during the first 10 seconds of the trajectories since the maximum of $\Delta_\beta \sim 3\sqrt{q_\beta T_s}$.
- The second value of q_β is chosen such that $\sqrt{q_\beta T_s} = 1\ kg/m^2$. The value $\sqrt{q_\beta T_s} = 0\ kg/m^2$ is not chosen since it is very likely that it will cause the estimators to diverge since β has high variation during the first 10 s. A small value $\sqrt{q_\beta T_s} = 1\ kg/m^2$ is chosen instead.

We note that both values of q_β do not represent the real variations of ballistic coefficient over the whole period of time during the re-entries.

Estimation Model with Acceleration Recall that for the estimation model with acceleration, the process noise covariance matrix is

$$Q = \begin{pmatrix} \frac{1}{20}T_s^5 & \frac{1}{8}T_s^4 & \frac{1}{6}T_s^3 \\ \frac{1}{8}T_s^4 & \frac{1}{3}T_s^3 & \frac{1}{2}T_s^2 \\ \frac{1}{6}T_s^3 & \frac{1}{2}T_s^2 & T_s \end{pmatrix} \tilde{q}_z \tag{3.27}$$

As discussed in section 1.3.2.3, the process noise parameter $\tilde{q}_z$, taking into account the discretization error and the model errors from the fact that β is not constant over a sampling period, should be chosen such that $\sqrt{\tilde{q}_z T_s}$ has the same order of magnitude as the change in the acceleration that is not taken into account in the estimation model over a sampling period defined by

$$\Delta_{a_z,noise,k+1} = a_{z_{k+1}} - a_{z_k} - f_{z_k} T_s,\ \forall k \tag{3.28}$$

According to (3.28), we can see that an appropriate value of $\tilde{q}_z$ should vary with time. The evolutions of the minimum, the mean and the maximum of $\Delta_{a_z,noise}$ are computed using the generated trajectories and are shown in figure 3.7.

Thanks to figure 3.7, we observe that a single value of q_β cannot describe well the value of Δ_β. In fact, the value $\sqrt{\tilde{q}_z T_s} = 10\ m/s$ should describe well the value of $\Delta_{a_z,noise}$ during the first 10 s and the value $\sqrt{\tilde{q}_z T_s} = 1\ m/s$ should describe well the value of $\Delta_{a_z,noise}$ during the last 10 s.

However, since the dynamics of β is generally unknown, $\Delta_{a_z,noise}$ cannot be computed in practice. In this study, a constant value of $\tilde{q}_z$ is chosen for the sake of simplicity. The robustness of the estimators to the choice of process noise parameter $\tilde{q}_z$ are studied by comparing the performances of the estimators using two different values of $\tilde{q}_z$.

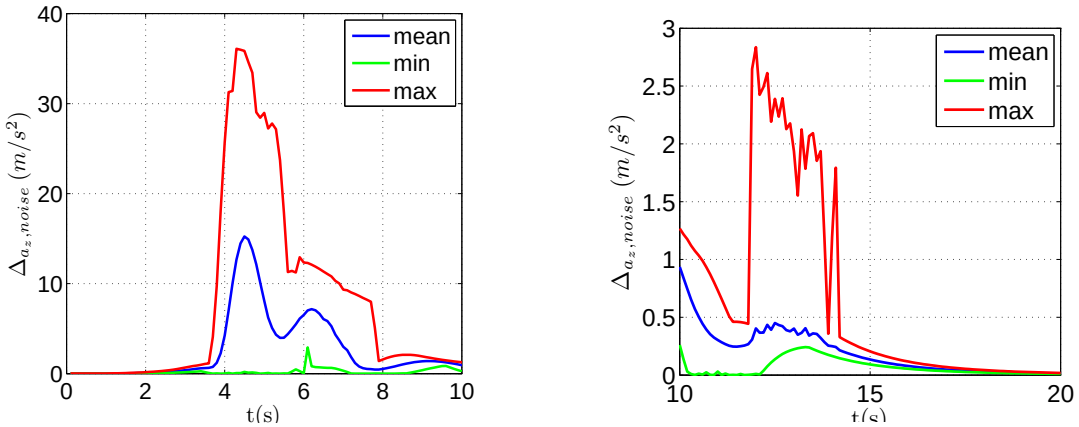

Figure 3.7: The mean, the max and the min of $\Delta_{a_z,noise}$ in time computed using the generated trajectories for $t \in [0, 10]$ s (left) and for $t \in [20, 30]$ s (right)

Test of robustness of the estimators to the choice of process noise parameter for the estimation model with acceleration

The robustness of the estimators to choice of process noise parameter will be studied by comparing the performances of the estimators using two different values of $\tilde{q}_z$:

- The first value of $\tilde{q}_z$ is chosen such that $\sqrt{\tilde{q}_z T_s} = 15\ m/s^2$ which is shown to capture the variation of $\Delta_{a_z,noise}$ during the first 10 seconds of the trajectories.
- The second value of $\tilde{q}_z$ is chosen such that $\sqrt{\tilde{q}_z T_s} = 1.5\ m/s^2$ which is shown to capture the variation of $\Delta_{a_z,noise}$ during the last 10 seconds of the trajectories.

Again, we note that these two values are both not appropriate for the real variation of $\Delta_{a_z,noise}$ over the whole period of time during the re-entry.

Now, let us discuss tuning which are specific for some estimators.

3.6.2 Specific Tuning for the UKF

The tuning parameter κ for the UKF as formulated in section 1.4.2 is chosen equal to $\kappa = 0$. This choice comes from the fact that in [Julier and Uhlmann, 2004], it is recommended to choose $n_x + \kappa = 3$ when the state x_k is assumed to be Gaussian. We recall that n_x is the dimension of the state which is equal to 3 in our case. In our studies, we do not make any assumption on the distribution of x_k. Since a recommended value for κ for other distributions of x_k is not proposed in the literature, we choose the recommended value for the Gaussian case for the sake of simplicity.

3.6.3 Specific Tuning for the RPF

The number of particles N_p for the RPF is chosen equal to 50000. This choice is made to let the RPF uses the same order of computation time as the MHE. Since for the RPF the larger N_p is the higher accuracy of the estimates the RPF provides, we assume that it is not interesting to use the RPF if it requires more computation time than the MHE but gives less accuracy of the estimates. To have an idea on the choice of N_p in the literature,

in the study on the performances of the EKF, the UKF and the RPF for military object tracking during the re-entries in [Ristic et al., 2003], the number of the particle N_p is chosen equal to 8000.

3.6.4 Specific Tunings for the MHE

3.6.4.1 Constraints on the Estimates and on the Process Noise

Since for the MHEs in both frameworks constraints can be imposed during the optimization, it is supposed that their estimate $\hat{x} \in \mathbb{X}$, where for the model with ballistic coefficient,

$$\mathbb{X} \triangleq ([0, 100]\, km \times [-10000, 10]\, m/s \times [200, 2000]\, kg/m^2) \tag{3.29}$$

and for the model with acceleration,

$$\mathbb{X} \triangleq ([0, 100]\, km \times [-10000, 10]\, m/s \times [-20, 2000]\, m/s^2) \tag{3.30}$$

These constraints are chosen by considering the ranges of values of the real positions, velocities, ballistic coefficient and accelerations in figure 3.1.

The constraints on the process noise estimate $\hat{w}$ are different for each estimation model.

Process Noise for the Estimation Model with Ballistic Coefficient Denote

$$\hat{w}_k = \begin{pmatrix} \hat{w}_{r_{z,k}} & \hat{w}_{v_{z,k}} & \hat{w}_{\beta,k} \end{pmatrix}^T$$

the estimated process noise vector and $\hat{w}_{a_{z,k}}$ the estimated process noises on the acceleration. For having less number of optimization parameters, the estimated process noises on the position $\hat{w}_{r_{z,k}}$ and on the velocity $\hat{w}_{v_{z,k}}$ are supposed to be related to $\hat{w}_{a_{z,k}}$:

$$\hat{w}_k = \begin{pmatrix} \frac{T_s^2}{2}\hat{w}_{a_z,k} \\ T_s\hat{w}_{a_z,k} \\ \hat{w}_{\beta,k} \end{pmatrix} \tag{3.31}$$

$\hat{w}_{a_{z,k}}$ and $\hat{w}_{\beta,k}$ are estimated as the result of the optimization problem. $\hat{w}_{a_z,k}$ and $\hat{w}_{\beta,k}$ are imposed to satisfy

$$\hat{w}_{a_z,k} \in [-5, 5]\, m/s^2 \tag{3.32}$$

$$\hat{w}_{\beta,k} \in [-400, 400]\, kg/m^2 \tag{3.33}$$

These choices of constraints are made using the maximum changes in the velocity and in the ballistic coefficient not taken into account in the estimation model in figure 3.6.

Process Noise for the Estimation Model with Acceleration Denote

$$w_k = \begin{pmatrix} \hat{w}_{r_{z,k}} & \hat{w}_{v_{z,k}} & \hat{w}_{a_{z,k}} \end{pmatrix}^T$$

the estimated process noise vector at instant k and $\hat{w}_{a_{z,k}}$ the estimated process noise on the acceleration at instant k. For having less number of optimization parameters, the

estimated process noises on the position $\hat{w}_{r_{z,k}}$ and on the velocity $\hat{w}_{v_{z,k}}$ are supposed to be related to $\hat{w}_{a_{z,k}}$:

$$\hat{w}_k = \begin{pmatrix} \frac{T_s^2}{2} \\ T_s \\ 1 \end{pmatrix} \hat{w}_{a_z,k} \tag{3.34}$$

$\hat{w}_{a_{z,k}}$ is estimated as the result of the optimization problem. The process noise estimate on the acceleration $\hat{w}_{a_z,k}$ is imposed to follow

$$\hat{w}_{a_z,k} \in [-40, 40]\ m/s^2 \tag{3.35}$$

This choices of constraint is made using the maximum changes in the acceleration not taken into account in the estimation model in figure 3.7.

3.6.4.2 Horizon Length

The horizon length N is chosen equal to $2n_x$ where n_x is the state's dimension. This choice is recommended to be good in practice according to [Rao, 2000]. In our case, $N = 6$.

3.6.4.3 Tuning for the Stability of the MHE in the Deterministic Framework

Section 2.2.2 shows that if assumptions (A1)-(A5) are verified, then an appropriate weight matrix $\mathcal{P} = p\mathbf{I}_{n_x \times n_x}$ can be chosen using (2.16) to guarantee the convergence of the estimation errors of the MHE in the deterministic framework described in (2.8). The verification of (A1)-(A5) is shown in appendix C.2. Appendix C.2 shows that the following sensitivity parameters δ can be chosen: for the estimation model with ballistic coefficient $\delta = 1.6 \cdot 10^{-15}$ and for the estimation model with acceleration $\delta = 1.2755 \cdot 10^{-5}$. Using (2.16), the weight parameter p is chosen such that $p = 5 \cdot 10^{-19}$ for the model with ballistic coefficient and $p = 5 \cdot 10^{-9}$ for the model with acceleration to guarantee the convergence of the estimation errors of the MHE.

3.7 Performances of the Estimators

The performances of the following estimators will be studied:

- the EKF
- the UKF
- the RPF
- the MHE in the deterministic framework presented in section 2.2. This MHE will be referred to as the "MHE deter."
- the MHE in the stochastic framework presented in section 2.3 with the covariance error matrix updated using the EKF's update equation. This MHE will be referred to as the "MHE sto."

Recall that in this study, the trajectories of 100 Aluminium hollow-spherical space debris of width $w = 3\ cm$ will be estimated. Each debris has an initial position r_{z_0}, an initial velocity v_{z_0}, and an outer diameter D generated according to the following uniform distributions: $r_{z_0} \sim \mathbf{U}(69, 70)\ km$, $v_{z,0} \sim \mathbf{U}(-6500, -5500)\ m/s$, $D \sim \mathbf{U}(20, 30)\ cm$. The a

priori initial position estimate and velocity estimate $\hat{r}_{z_0}^-$ and $\hat{v}_{z_0}^-$ are computed using the two-point differencing method in (3.18). The a priori initial ballistic coefficient estimate $\hat{\beta}_0^-$ is computed by supposing that it is known that the debris is an Aluminium hollow sphere with width $w = 3\ cm$ but with unknown outer diameter D. An assumption on D is made for the initialization, leading to an assumption on the mass m.

In this study, the performances of the estimators in the good initialization case will be considered first followed by those in the bad initialization case as described in section 3.5.2.2. For each initialization case, the performances of the estimators in these 4 cases will be compared

- Model with ballistic coefficient, $q_\beta = 100^2/T_s\ kg/m^2$
- Model with ballistic coefficient, $q_\beta = 1^2/T_s\ kg/m^2$
- Model with acceleration, $\tilde{q}_z = 15^2/T_s\ m/s^2$
- Model with acceleration, $\tilde{q}_z = 1.5^2/T_s\ m/s^2$

The performances of the estimators will be analyzed in terms of

- non-divergence percentage, i.e. the percentage of the Monte Carlo runs that satisfy the chosen non-divergence criterion described next
- accuracy of the estimates among the non-divergence runs
- mean computation time per iteration

The section ends with the studies of the effect of bad initialization on the performances of the estimators.

3.7.1 Non-Divergence Percentages

We would like to eliminate the cases in which the estimator diverges or gives too high estimation errors. Denote $r_{z_k}^n$ and $\hat{r}_{z_k}^n$ the real position and the position estimate at instant k of the n^{th} Monte Carlo run respectively. We consider that for the n^{th} run, the estimator does not diverge if the estimation error on the position $\hat{r}_{z_k}^n - r_{z_k}^n$ is such that

$$\left|\hat{r}_{z_k}^n - r_{z_k}^n\right| \leq 500\ m,\ \forall k, \tag{3.36}$$

Denote $\mathbb{M}_{nonDV}$ a set containing the indices of the non-divergent runs and $N_{nonDV} = n(\mathbb{M}_{nonDV})$ the number of elements in $\mathbb{M}_{nonDV}$. The bound 500 m of this criterion is arbitrary chosen. It represents the position error of 50 times the standard deviation on the distance measurement noise.

The non-divergence percentages of each estimator for both estimation models and for the different chosen values of the process noise parameter are presented in table 3.1.

Estimator	Model with β		Model with a_z	
	$\sqrt{q_\beta T_s} = 100$	$\sqrt{q_\beta T_s} = 1$	$\sqrt{\tilde{q} T_s} = 15$	$\sqrt{\tilde{q} T_s} = 1.5$
EKF	87	100	100	100
UKF	100	100	100	100
RPF	84	0	100	0
MHE deter.	100	100	100	100
MHE sto.	100	100	100	100

Table 3.1: Non-divergence percentages of each estimator for both estimation models and for the different chosen values of the process noise parameter

We can observe from table 3.1 that the use of estimation model with acceleration provides higher convergence percentages for all estimators compared to the estimation model with ballistic coefficient. It can be observed that the RPF is very sensitive to choice of process noise parameter. It is therefore not reliable for the space debris tracking problems during the re-entry.

It should be noticed that each estimator can be non-divergent but can give high estimation errors. The accuracy of the estimates must be taken into account to judge whether an estimator is better than another one.

3.7.2 Accuracy of the Estimates

For the accuracy studies, define the Root Mean Square Error (RMSE) of the i^{th} component of the estimate $\hat{x}_{i,k}$ *among the non-divergent runs* as

$$RMSE(\hat{x}_{i,k}) = \sqrt{\sum_{n \in \mathbb{M}_{nonDV}} \frac{(\hat{x}_{i,k}^n - x_{i,k}^n)^2}{N_{nonDV}}}, \tag{3.37}$$

Recall that N_{nonDV} is the number of the non-divergent runs.

Define the Average Root Mean Square Error (ARMSE) of the i^{th} component of the estimate $\hat{x}_{i,k}$ *among the non-divergent runs* as the RMSE average over all time instants, i.e.

$$ARMSE(\hat{x}_{i,k}) = \sum_{k=0}^{k_f} \frac{RMSE(\hat{x}_{i,k})}{k_f + 1} \tag{3.38}$$

where k_f is the discrete-time index of the final instant t_f.

The RMSE of the position estimate $\hat{r}_z$ and of the velocity estimate $\hat{v}_z$ are presented in figures 3.8 and 3.9 respectively. The RMSE of the ballistic coefficient estimate $\hat{\beta}$ and of the acceleration estimate $\hat{a}_z$ are presented in figure 3.10. The ARMSE of $\hat{r}_z$ and $\hat{v}_z$ are presented in tables 3.2 and 3.3 respectively. The ARMSE of $\hat{\beta}$ and $\hat{a}_z$ are presented in table 3.4.

The following analyses on the accuracy of the estimates can be made

1. Thanks to tables 3.2 and 3.3, it can be noticed that the EKF, the UKF, the RPF and the MHE in the stochastic framework, when they are non-divergent, provide smaller estimation errors on the position and the velocity estimates when the estimation model with acceleration is used compared to when the estimation model with ballistic coefficient is used.

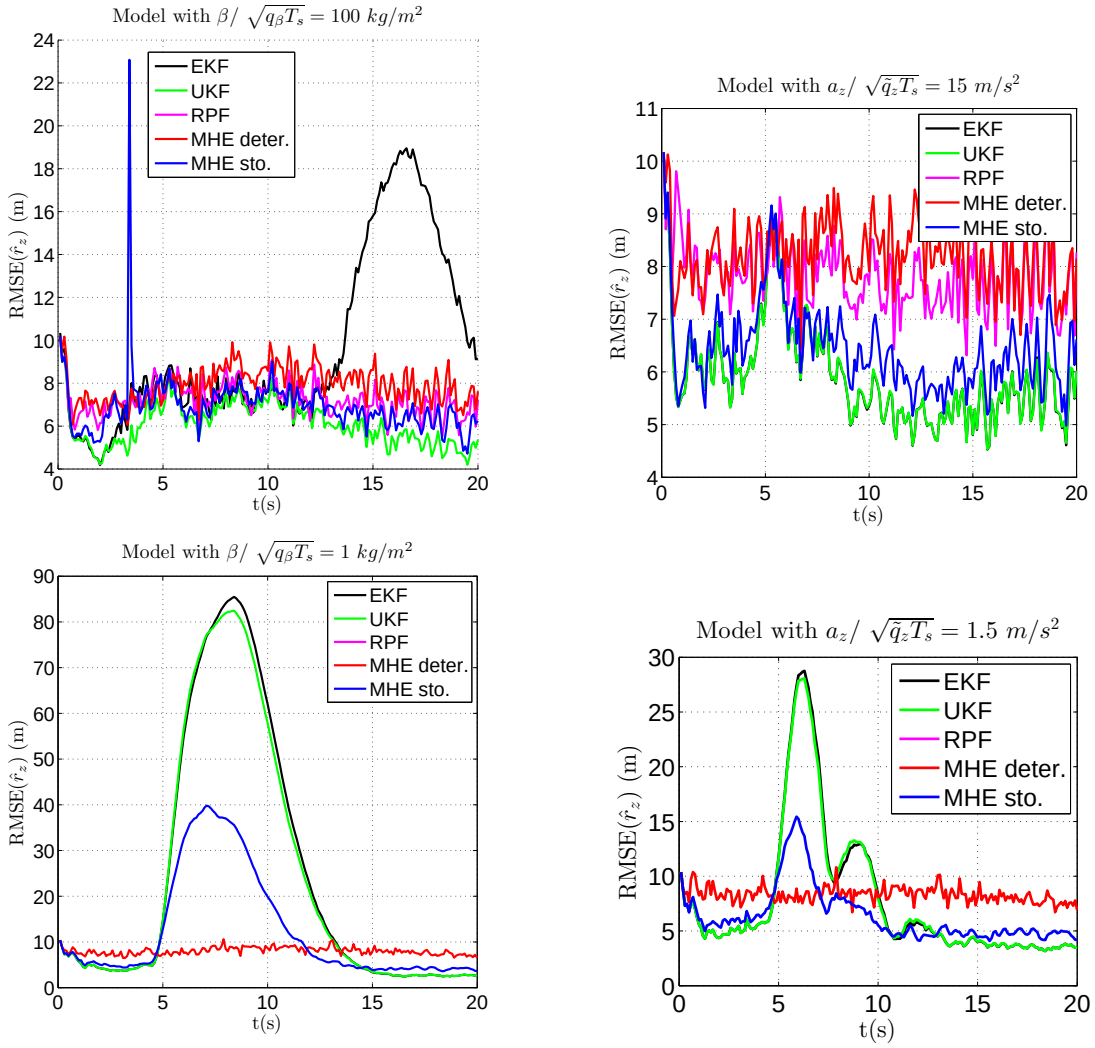

Figure 3.8: RMSE of the position estimates given by each estimator for both estimation models and for all values of process noise parameter

Estimator	$ARMSE(\hat{r}_z)$ (m)			
	Model with β		Model with a_z	
	$\sqrt{q_\beta T_s} = 100$	$\sqrt{q_\beta T_s} = 1$	$\sqrt{\tilde{q}_z T_s} = 15$	$\sqrt{\tilde{q}_z T_s} = 1.5$
EKF	9.63	24.46	5.90	7.73
UKF	6.09	23.81	5.91	7.70
RPF	7.22	×	7.81	×
MHE deter.	7.94	8.00	8.22	8.31
MHE sto.	6.92	12.45	6.45	6.38

Table 3.2: ARMSE of the position estimates given by each estimator for both estimation models and for all values of process noise parameter

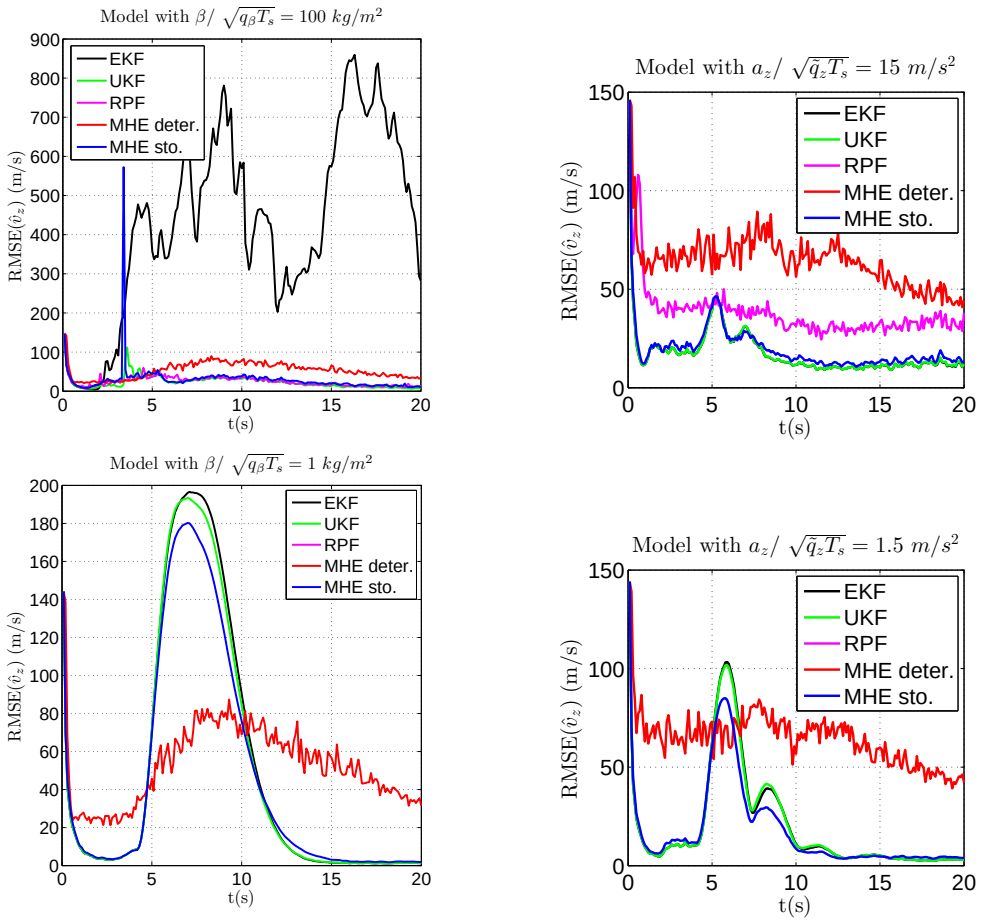

Figure 3.9: RMSE of the velocity estimates given by each estimator for both estimation models and for all values of process noise parameter

Estimator	$ARMSE(\hat{v}_z)\ (m/s)$			
	Model with β		Model with a_z	
	$\sqrt{q_\beta T_s} = 100$	$\sqrt{q_\beta T_s} = 1$	$\sqrt{\tilde{q}_z T_s} = 15$	$\sqrt{\tilde{q}_z T_s} = 1.5$
EKF	432.876	50.21	17.35	19.94
UKF	22.93	48.88	17.40	19.94
RPF	25.06	×	37.79	×
MHE deter.	52.83	52.56	64.17	64.26
MHE sto.	29.58	45.94	19.36	17.59

Table 3.3: ARMSE of the velocity estimates given by each estimator for both estimation models and for all values of process noise parameter

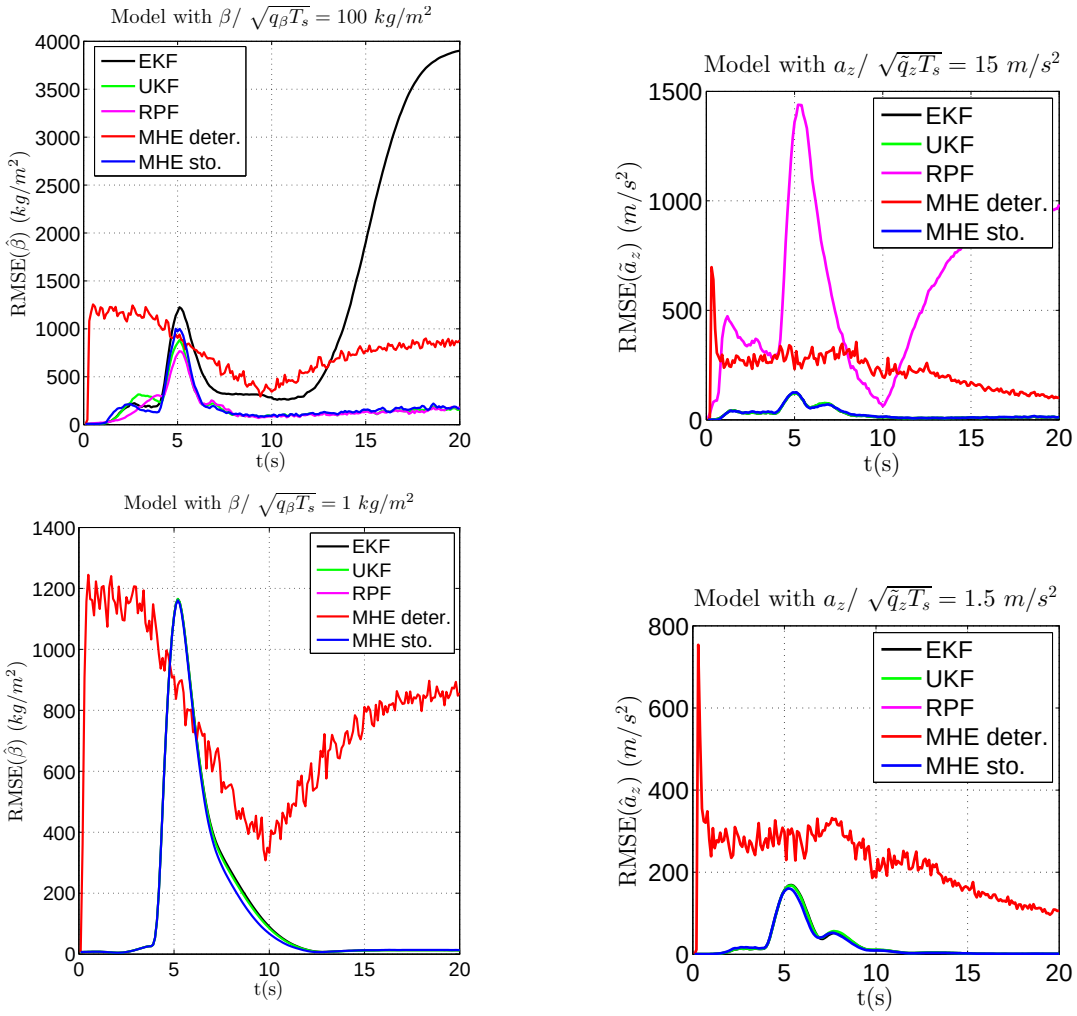

Figure 3.10: RMSE of the ballistic coefficient estimates given by each estimator for the estimation model with ballistic coefficient for all values of process noise parameter (left) and RMSE of the acceleration estimates given by each estimator for the estimation model with acceleration for all values of process noise parameter (right)

Estimator	$ARMSE(\hat{\beta})$ (kg/m^2) Model with β		$ARMSE(\hat{a}_z)$ (m/s^2) Model with a_z	
	$\sqrt{q_\beta T_s} = 100$	$\sqrt{q_\beta T_s} = 1$	$\sqrt{\tilde{q}_z T_s} = 15$	$\sqrt{\tilde{q}_z T_s} = 1.5$
EKF	1183.66	156.22	26.22	23.90
UKF	181.07	154.36	26.45	24.06
RPF	165.43	×	606.27	×
MHE deter.	774.39	771.58	224.29	224.51
MHE sto.	187.28	148.45	27.20	22.74

Table 3.4: ARMSE of the ballistic coefficient estimates given by each estimator for the estimation model with ballistic coefficient for all values of process noise parameter (first two columns) and ARMSE of the acceleration estimates given by each estimator for the estimation model with acceleration for all values of process noise parameter (last two columns)

2. Thanks to figures 3.8 and 3.9 and tables 3.2 and 3.3, it can be noticed that the MHE in the deterministic framework provides the same order of magnitude of estimation errors when it is used with both estimation models.

3. The EKF, the UKF and the RPF are sensitive to the choice of the process noise parameter. They are therefore not adapted to the space debris tracking during the re-entry problems for which a good choice of the process noise parameter cannot be guaranteed.

4. The MHE in the deterministic framework appears to be the most robust against poor choice of the process noise parameter, followed by the MHE in the stochastic framework. In fact, the MHE in the stochastic framework uses the error covariance matrix updated as in the EKF as the weight matrix on the arrival cost. Therefore, it behaves more like the EKF than the MHE in the deterministic framework. The MHE in the stochastic framework is therefore more sensitive to process noise parameter, just like the EKF[2].

5. Although the estimation errors of the MHE in the deterministic framework is a bit higher than those of the EKF and the UKF in average when the estimation model with acceleration is used, it does not produce a spike of high estimation errors like the EKF and the UKF when the process noise parameter is not adequately chosen.

6. For a tracking problem in real-time, the most interesting quantity may be the position estimate. In this case, the MHE in the deterministic framework appears to be the best estimator for the problem thanks to its high robustness against poor choice of process noise parameter.

7. In our studies, a debris in a direct-descent is considered. Hence, the object is supposed to be in the field of view of the radar station and measurements are available along the trajectories with a high enough frequency with respect to the dynamics of the system. As a consequence, there is no need to estimate the ballistic coefficient for any prediction. But if the ballistic coefficient is needed to be estimated, for accurate prediction of the trajectories when the measurements are not available for example, the MHE in the stochastic framework appears to be the best estimator since the MHE in the deterministic framework fails to provide accurate estimates of β[3].

Now that the performances of the estimator in a good initialization case have been studied, let us consider the performances of the estimators in a bad initialization case.

3.7.3 Study Case: Performances of the Estimators in Case of Bad Initialization

Recall that in this study, the a priori initial position estimate and velocity estimate $\hat{r}_{z_0}^-$ and $\hat{v}_{z_0}^-$ are computed using the two-point differencing method in (3.18). The a priori initial

[2]The accuracy of the MHE in the stochastic framework when the error covariance matrix is updated using formulations of another estimator might be able to ameliorate the robustness of the MHE to choice of process noise parameter. As discussed in section 2.3, it is shown in [Qu and Hahn, 2009] and [Ungarala, 2009] that the MHE using the UKF's update formulation provides better accuracy of the estimates compared to the MHE using the EKF's update formulation and to the MHE using the PF's update formulation when the MHEs are badly initialized. When the MHEs are well initialized, however, the PF's update formulation gives the best accuracy.

[3]Recall that when the estimation model with acceleration is used, the ballistic coefficient estimate can be computed using (3.9)

Estimator	Model with β		Model with a_z	
	$\sqrt{q_\beta T_s} = 2$	$\sqrt{q_\beta T_s} = 0.2$	$\sqrt{\tilde{q}_z T_s} = 20$	$\sqrt{\tilde{q}_z T_s} = 2$
EKF	79	100	100	100
UKF	99	100	100	100
RPF	81	0	100	0
MHE deter.	100	100	100	100
MHE sto.	100	100	100	100

Table 3.5: Non-divergence percentage of each estimator for both estimation models and for all values of process noise parameter

Estimator	$ARMSE(\hat{r}_z)$ (m)			
	Model with β		Model with a_z	
	$\sqrt{q_\beta T_s} = 100$	$\sqrt{q_\beta T_s} = 1$	$\sqrt{\tilde{q}_z T_s} = 15$	$\sqrt{\tilde{q}_z T_s} = 1.5$
EKF	6.52	24.72	6.13	7.59
UKF	6.28	24.37	6.13	7.56
RPF	7.48	$\times$	8.03	$\times$
MHE deter.	8.10	8.03	8.38	8.36
MHE sto.	7.00	12.92	6.64	6.28

Table 3.6: ARMSE of the position estimates given by each estimator for both estimation models and for all values of process noise parameter in a bad initialization case

ballistic coefficient estimate $\hat{\beta}_0^-$ is computed by supposing that it is known that the debris is an Aluminium hollow sphere with width $w = 3$ cm but with unknown outer diameter D. An assumption on D is made for the initialization.

In this bad initialization case, a wrong assumption on the outer diameter of the debris D is given to the estimator. In this case, it is supposed that $D \sim \mathbf{U}(80, 100)$ cm which implies $m \in [150.95, 239.51]$ kg. A distribution of β based on this wrong assumption is computed and $\hat{\beta}_0^-$ is chosen as the mean of the distribution. Again, for the estimation model with acceleration, $\hat{a}_{z_0}^-$ is computed from $\hat{\beta}_0^-$ using (3.9).

The non-divergence percentages of the estimators and the ARMSE of the position estimates given by each estimator for both estimation models and for all values of process noise parameter are presented in table 3.5 and 3.6.

By comparing tables 3.5 and 3.6 to tables 3.1 and 3.2, we observe that

1. Bad initialization does not affect the non-divergence percentages of the estimators when the estimation model with acceleration is used. We can conclude that this model is more robust against bad initialization than the one with ballistic coefficient.

2. Bad initialization does not affect the non-divergence percentages of the MHEs. Their non-divergence percentages are 100 % in every case.

3. Bad initialization reduces the non-divergence percentages of the EKF, the UKF and the RPF using the estimation model with ballistic coefficient for $\sqrt{q_\beta T_s} = 100$ kg/m^2.

Estimator	Mean computation time/ iteration (s)			
	Model with β		Model with a_z	
	$\sqrt{q_\beta T_s} = 2$	$\sqrt{q_\beta T_s} = 0.2$	$\sqrt{\tilde{q} T_s} = 20$	$\sqrt{\tilde{q} T_s} = 2$
EKF	$1.4 \cdot 10^{-4}$	$1.4 \cdot 10^{-4}$	$1.4 \cdot 10^{-4}$	$1.4 \cdot 10^{-4}$
UKF	$6.1 \cdot 10^{-4}$	$5.9 \cdot 10^{-4}$	$6.1 \cdot 10^{-4}$	$6.7 \cdot 10^{-4}$
RPF	0.43	0.27	0.43	0.27
MHE deter.	0.29	0.34	0.23	0.34
MHE sto.	0.48	0.20	0.23	0.20

Table 3.7: Mean computation time per iteration used by each estimator for both estimation models and for all values of process noise parameter

4. In the cases in which the non-divergent percentages stay unchanged when the estimators are badly initialized, it can be noticed that the position estimation errors are slightly higher (higher $< 1\ m$) in case of bad initialization.

5. For the EKF, the UKF and the RPF using the estimation model with ballistic for $\sqrt{q_\beta T_s} = 100\ kg/m^2$, since their non-divergent percentages alter, the ARMSE in both initialization cases cannot be compared directly. It is possible that their $ARMSE(\hat{r}_z)$ in the good initialization case be higher than in the bad initialization case since there are less non-divergence runs to be considered in the bad initialization case.

3.7.4 Mean Computation Time

The mean computation time per iteration performed by each estimator for both estimation models and for both values of the process noise parameter using MATLAB on a standard PC are presented in table 3.7. The EKF and the UKF uses small computation times compared to the MHEs and the RPF. However, we recall that they could provide large estimation errors when the process noise parameters are not adequate. The RPF uses large computation like the MHEs while provides larger estimation errors. The MHEs requires large estimation errors. However, in our study, MATLAB functions are used directly for the optimization and there is no particular work to reduce the computation time of the estimators. Recalling that $T_s = 0.1\ s$, it can be noticed that the MHEs in both frameworks require very large computation time. The MHEs are hence not feasible for real-time space debris tracking yet. However, they are the ones who provide the best accuracy of the estimates thanks to their robustness to choice of process noise parameter. It is therefore interesting to work on MHE's computation time reduction.

3.7.5 Conclusions on the Performances of the Estimators

To summarize, concerning the choice of the estimation model, we have seen that the model with acceleration overcomes the model with ballistic coefficient in terms of non-divergence percentages, robustness against a bad choice of process noise parameter and robustness against bad initialization.

Concerning the choice of the estimator, we have seen that the MHEs overcome the EKF, the UKF and the RPF in terms of non-divergence percentages, accuracy of the estimators and robustness against a bad choice of process noise parameter and robustness against bad initialization. Although the MHE in the stochastic framework provides smaller errors

on position estimates than the MHE in the deterministic framework when the process noise parameter is well chosen, the MHE in the deterministic framework is shown to be more robust against a bad choice of process noise parameter. It is therefore the most reliable estimator for the space debris tracking problem during the re-entry since in reality a good choice of this parameter cannot be guaranteed. However, both MHEs require large computation time.

3.8 Toward an MHE with Less Computation Time

In a 3 dimensional case, the MHE will require even more computation time as the number of the optimization parameters will become larger. Not only we will encounter the problem of large computation time, but the MHE will also have more difficulties to numerically find an optimal solution of the optimization problem due to this large number of optimization parameters.

An alternative Moving Horizon strategy using less computation time must therefore be developed to enable the real-time implementation of the MHE to space debris tracking during the re-entry in 3D. We are interested in the MHE with Pre-Estimation approach, discussed in section 2.5.3. This approach concerns a modification of the structure of the MHE and its use can be combined to other time reduction approaches such as fast optimization techniques and approximate schemes to reduce more computation time.

The Moving Horizon with Pre-Estimation (MHE-PE) has been developed for discrete-time linear systems [Sui et al., 2010]. The idea of this strategy is to reduce the number of optimization parameters by propagating the estimate over the horizon using the equation of an auxiliary observer, called pre-estimating observer. Then, the pre-estimating observer inside the MHE-PE is initialized using an optimal solution obtained by minimizing a cost function taking into account the difference between real measurements and predicted measurements over the horizon. This pre-estimating observer allows the MHE-PE to compensate for model errors without searching for the optimal process noise sequence over the horizon via optimization like the classical MHEs.

In the next chapter, we propose an MHE-PE strategy for discrete-time nonlinear systems under bounded noise. The novelty of our work compared to [Sui et al., 2010] is the extension of the method to nonlinear systems. The stability of the dynamics of the estimation errors for the proposed MHE-PE is analyzed and an upper bound on the estimation errors will be derived. Thanks to the reduction of the number of the optimization parameters, the MHE-PE will require less computation time than the classical MHEs. Once the theoretical development has been described in chapter 4, the performances of the MHE-PE for space debris trajectory estimation during the re-entry in a 3D case will be studied in chapter 5.

3.9 Summary of the Chapter

In this chapter, we have seen that

- The estimation model with acceleration overcomes the model with ballistic coefficient in terms of non-divergence percentages, robustness against a bad choice of process noise parameter and robustness against bad initialization.
- The MHEs in the deterministic and in the stochastic frameworks overcome the EKF, the UKF and the RPF for space debris tracking during the re-entries in terms of convergence percentage, robustness against a bad choice of process noise parameter and robustness against bad initialization.
- Although the MHE in the stochastic framework provides smaller estimation errors on position and estimates than the MHE in the deterministic framework when the process noise parameter is well chosen, the MHE in the deterministic framework is shown to be more robust against bad choice of process noise parameters than the MHE in the stochastic framework. Since in reality, a good choice of the process noise parameter cannot be guaranteed, the MHE in the deterministic framework is therefore the most reliable estimator for space debris tracking during the re-entries.
- The MHEs, however, require large computation time. This prevents them from being implemented in real-time for space debris tracking during the re-entries in a 3 dimensional case. An alternative Moving Horizon strategy using less computation time should therefore be developed.

CHAPTER 4

Moving Horizon Estimator with Pre-Estimation (MHE-PE)

"Time is money."

— Benjamin Franklin

Goals of the chapter

- to introduce a fast moving horizon estimation strategy for nonlinear discrete-time systems under bounded noises called the Moving Horizon Estimator with Pre-Estimation (MHE-PE).
- to prove the convergence of the estimation errors of the MHE-PE and to present conditions for the convergence.
- to analyze the performances of the MHE-PE in terms of accuracy of the estimates and computation time compared to those of the classical Moving Horizon Estimator (MHE) via a numerical example of a pressure estimation problem of a gaz-phase reversible reaction

4.1 Introduction

In chapter 3 the performances of the Moving Horizon Estimators (MHEs) in the deterministic and the stochastic frameworks are compared to those of the classical estimators used in object tracking during the re-entries in the literature in a study of 1D space debris tracking during the re-entries. These classical estimators are the the Extended Kalman Filter (EKF), the Unscented Kalman Filter (UKF) and the Regularized Particle Filter (RPF). The performances are studied in terms of non-divergence percentage, accuracy of the estimates and mean computation time. The robustness of the estimators against bad initialization and poor choice of process noise parameters is also studied. The RPF is shown to be very sensitive to poor choice of process noise parameters. It provides 0% of non-divergence percentage if the process noise parameters are not well chosen. The EKF and the UKF are shown to provide high accuracy of the estimates at all instants only when the process noise parameters are adequately chosen. The RPF, the EKF and the UKF are, therefore, not appropriate for space debris tracking during the re-entries since a good

choice of these parameters cannot be guaranteed due to unknown dynamics of space debris as discussed in chapter 1. On the other hand, the classical Moving Horizon Estimators (MHEs) are shown to be robust against poor choice of process noise parameters and bad initialization in every study case in our 1D debris tracking study, i.e. for every tested process noise parameter and for both estimation models. The MHEs are hence the most efficient estimators compared to the others for this tracking problem.

However, it has also been shown that the MHEs require large computation time. This prevents us from implementing them for the 3D space debris tracking during the re-entries. To reduce this computation time, fast optimization techniques for the MHE have been proposed in [Ferreau et al., 2012][Zavala, 2008]. Another strategy to reduce computation time without changing the optimization method consists in propagating the estimate over the horizon using the equation of an auxiliary estimator instead of using the state equation as in the classical MHEs. In this case, model errors are compensated through the structure of the auxiliary estimator without searching for the estimates of process noise sequence over the horizon that minimize a cost function like in the classical MHEs. The initial estimate at the beginning of the horizon hence becomes the only optimization parameter. This strategy, therefore, requires less computation time than the classical one. The strategy will be referred to as the Moving Horizon Estimation with Pre-Estimation (MHE-PE) strategy and the auxiliary estimator will be referred to as the pre-estimator.

The MHE-PE strategy has been proposed in [Sui et al., 2010] for discrete-time linear systems where a deterministic observer, i.e. an estimator of which estimation errors tend to zero in a deterministic (noise-free) case, is chosen as the pre-estimator. In this work, the linear MHE-PE is shown to be robust against model errors and requires smaller computation time than a classical MHE. Thanks to its small computation time and robustness, the MHE-PE strategy suits for the estimation problems for which the computation time of the MHE would be prohibitive such as space debris tracking during the re-entries.

In this chapter, we propose an extension for nonlinear discrete-time systems under bounded noises. The novelties of our work compared to [Sui et al., 2010] are the extension of the method to nonlinear systems and the possibility to use a bounded-error estimator instead of a deterministic observer for the pre-estimation step. The stability of the dynamics of the estimation errors of the proposed MHE-PE is also proven and an upper bound on the estimation errors is derived.

Note that an attempt to incorporate an observer in a MHE strategy for nonlinear systems under bounded noise has been proposed in [Liu, 2013]. However, in their strategy, the observer is only used to impose an additional constraint in the MHE and the process noise estimates are still included in the optimization parameters which induces large computation time.

This chapter is organized as follows. In section 4.2, we recall the notations and definitions that will be used in this chapter. A general definition of an estimator, which is useful for understanding the structure of the pre-estimator in the MHE-PE, will also be given. In section 4.3 the MHE-PE formulation will be defined. In section 4.4 conditions on the estimation model and the pre-estimator to guarantee the convergence of the estimation errors of the MHE-PE will be described. In section 4.5 associated properties of the estimation model and the pre-estimator satisfying conditions in section 4.4 which will be used in the proof of convergence of estimation errors of the MHE-PE will be derived. In section 4.6, we prove the convergence of the estimation errors of the MHE-PE for nonlinear discrete-time estimation model under bounded noises and under conditions introduced in section 4.4. In section 4.7, the performances of the MHE-PE will be compared to those of a classical MHE in terms of accuracy of the estimates and the computation time via a

simulation example of pressure estimation of a gaz-phase reversible reaction.

4.2 Preliminaries

In this section, the notations and the definitions which will be used throughout this chapter are recalled, followed by the definitions of the system in consideration and an estimator in general. The latter will be useful to understand the structure of the pre-estimating estimator in the MHE-PE.

4.2.1 Notations and Definitions

Recall that $\|v\|$ denotes the Euclidean norm of a vector v as defined in definition 1. A function $f(x)$ is said to be locally Lipschitz with respect to its argument x if there exists a positive constant L_f^x such that $\|f(x') - f(x'')\| \leq L_f^x \|x' - x''\|$, for all x' and x'' in a given region of x and L_f^x is the associated Lipschitz constant as defined in definition 3. A continuous function $\phi : [0, a) \to [0, \infty)$ is said to be a class K function if it is strictly increasing and satisfies $\phi(0) = 0$ as defined in definition 4. A function $\beta(r, s)$ is said to be a class KL function if, for each fixed s, $\beta(r, s)$ is a class K function with respect to r and, for each fixed r, $\beta(r, s)$ is decreasing with respect to s and $\beta(r, s) \to 0$ as $s \to \infty$ as defined in definition 5.

4.2.2 Definition of the Estimation Model of the System

As introduced in section 1.3.1, the real system is modelled by the following discrete-time equations:

$$\begin{aligned} x_{k+1} &= f(x_k) + w_k \\ y_k &= h(x_k) + v_k \end{aligned} \tag{4.1}$$

where $x_k \in \mathbb{X} \subset \mathbb{R}^{n_x}$ is the state vector of the model, n_x is the dimension of the state vector and $k \in \mathbb{N}$ is a time index, $y_k \in \mathbb{Y} \subset \mathbb{R}^{n_y}$ is the measurement vector, $w_k \in \mathbb{W} \subset \mathbb{R}^n$ is the process noise, $v_k \in \mathbb{V} \subset \mathbb{R}^m$ is the measurement noise and $k \in \mathbb{N}$ is the time index.

4.2.3 Definition of Estimation Model Associated to the Nominal System

Define the *nominal system* as the “noise-free" part of the system. The estimation model associated to the nominal system is defined as.:

$$\begin{aligned} {}^n x_{k+1} &= f({}^n x_k) \\ {}^n y_k &= h({}^n x_k) \end{aligned} \tag{4.2}$$

where ${}^n x_k \in \mathbb{X}$ is the nominal state and ${}^n y_k \in \mathbb{Y} \subset \mathbb{R}^{n_y}$ is the noise free output. This model will be referred to as “the nominal estimation model”. It will be used in the proof of convergence of the estimation errors of the MHE-PE.

4.2.4 Estimator Definition

Let us define an estimator map $g(\cdot, \cdot)$: $\hat{\mathbb{X}} \times \mathbb{Y} \to \hat{\mathbb{X}}$, with $\hat{\mathbb{X}} \subset \mathbb{R}^{n_x}$ a convex compact set, by:

$$\begin{aligned} \hat{\mathfrak{x}}_{k+1} &= g(\hat{\mathfrak{x}}_k, \gamma_k) \\ \hat{\gamma}_k &= h(\hat{\mathfrak{x}}_k) \end{aligned} \tag{4.3}$$

where $\hat{\mathfrak{x}}_k \in \hat{\mathbb{X}}$ is the estimate given by g, $\gamma_k \in \mathbb{R}^{n_y}$ is the input of g and $\hat{\gamma}_k$ is the predicted measurement given by g. When y_k is used as input ($\gamma_k = y_k$), i.e. when the estimator is applied to the real system, the estimate $\hat{\mathfrak{x}}_k$ will be denoted as $\hat{x}_k$ and the predicted measurement $\hat{\gamma}_k$ will be denoted as $\hat{y}_k$. In the same way, when ${}^n y_k$ is used as input ($\gamma_k = {}^n y_k$), i.e. when the estimator is applied to the nominal system, the estimate $\hat{\mathfrak{x}}_k$ will be denoted as ${}^n\hat{x}_k$ and the predicted measurement $\hat{\gamma}_k$ will be denoted as ${}^n\hat{y}_k$.

Now, let us consider the formulation of the MHE-PE.

4.3 Formulation of the Moving Horizon with Pre-Estimation (MHE-PE)

Assume that the state vector x_k has to be estimated at instant $k \geq N$ using the latest $N+1$ measurements collected within the "sliding horizon" $[k-N, k]$. For $k < N$ the state is estimated using all the available measurements $\{y_j\}_{j=0}^{k}$. Denote $\hat{x}_{k-N|k}$ an estimate of x_{k-N} and $\hat{x}^{\circ}_{k-N|k}$ the optimal estimate of x_{k-N} computed by the MHE-PE at instant k respectively. Recall that $y_{k-N}^{k} = \begin{pmatrix} y_{k-N}^T & y_{k-N+1}^T & \dots & y_k^T \end{pmatrix}^T$ is the measurement collection over the horizon as described in (2.3), $\hat{x}^{-}_{k-N|k}$ is an a priori value of $\hat{x}_{k-N|k}$ computed before the acquisition of y_k and $g(\cdot,\cdot)$ is an estimator defined as in (4.3).

The MHE-PE is formulated as follows:

$$\hat{x}^{o}_{k-N|k} = \arg \min_{\hat{x}_{k-N|k} \in \hat{\mathbb{X}}} \mathbf{J}_k(\hat{x}_{k-N|k}, \hat{x}^{-}_{k-N|k}, y_{k-N}^{k}) \tag{4.4a}$$

$$\mathbf{J}_k = \mu \left\| \hat{x}_{k-N|k} - \hat{x}^{-}_{k-N|k} \right\|^2 + \sum_{i=0}^{N} \left\| y_{k-N+i} - h(\hat{x}_{k-N+i|k}) \right\|^2_{\mathcal{R}} \tag{4.4b}$$

$$\hat{x}_{k-N+i+1|k} = g(\hat{x}_{k-N+i|k}, y_{k-N+i}),\ \forall i \in [0, N-1] \tag{4.4c}$$

where μ is a positive scalar representing confidence in the a priori value $\hat{x}^{-}_{k-N|k}$ and $\mathcal{R}$ is a weight matrix representing confidence in the measurement collection y_{k-N}^{k}. $\mathcal{R}$ can be chosen equal to the inverse of the measurement noise covariance matrix R^{-1} for example. The estimate $\hat{x}^{\circ}_{k|k}$ of x_k at time k provided by the MHE-PE is computed using (4.4c) for $i = 1, \dots, N$ from $\hat{x}^{o}_{k-N|k}$, and $\hat{x}^{-}_{k-N|k}$ is determined from

$$\hat{x}^{-}_{k-N|k} = f(\hat{x}^{\circ}_{k-N-1|k-1}) \tag{4.5}$$

The illustration of the MHE-PE is shown in figure 4.1.

Note that in the MHE-PE the evolution of the state at *each instant* over the horizon is subject to the equation of the estimator g instead of the estimation model as in the classical MHE in (2.8c). To be precise, the MHE-PE locally implements the estimator g which is re-initialized at each instant at the beginning of the horizon by solving the optimization problem (4.4). g is referred to as the "pre-estimator" since it somehow "pre-estimates" the state before the optimization algorithm gives the optimal estimate.

In the MHE-PE, model errors are taken into account "approximately" in the pre-estimation step through the structure of the estimator. This way, the process noise sequence over the horizon does not have to be estimated and the state at the beginning of

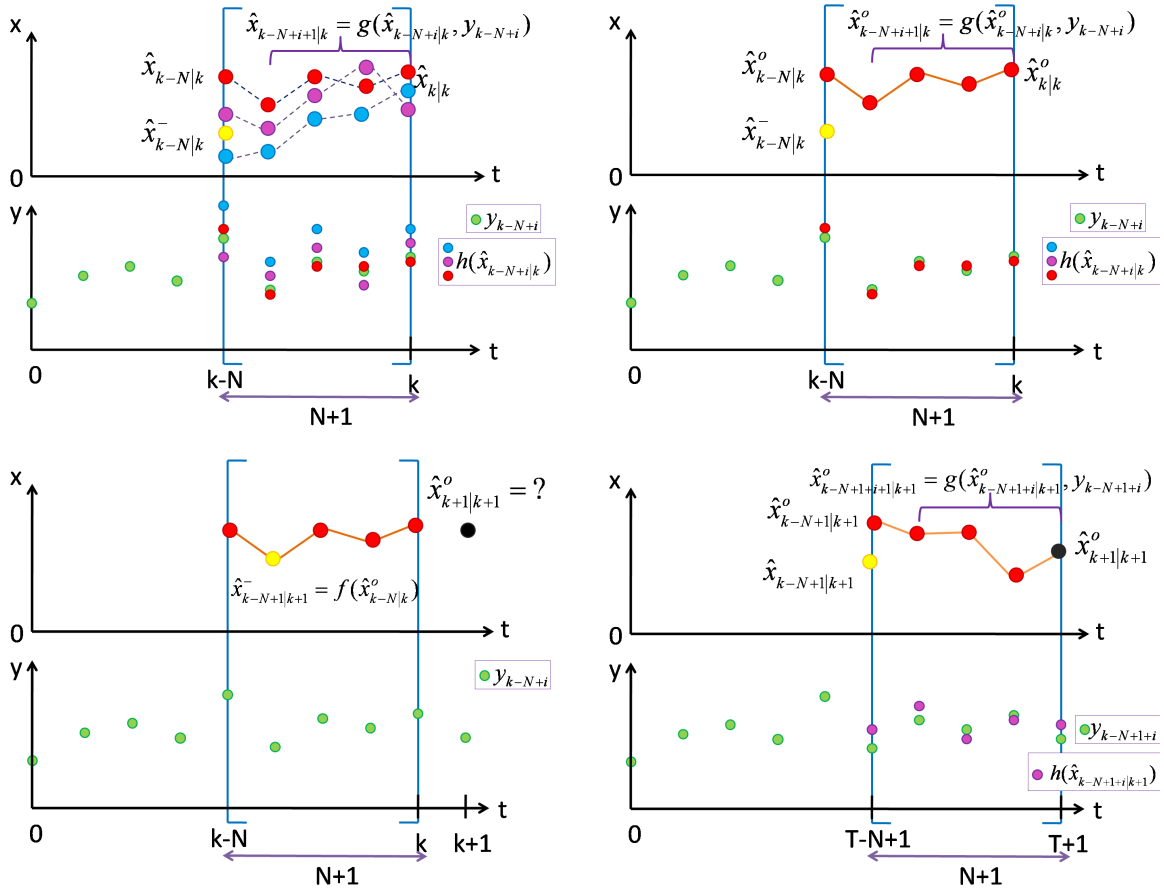

Figure 4.1: Illustration of the MHE-PE: (First row) At instant k, $N+1$ latest measurements from instants $[k-N, k]$ are used to find the optimal estimate at the beginning of the horizon $\hat{x}^{\circ}_{k-N|k}$ minimizing the cost function $\mathbf{J}_k$ in (4.4b). The a priori estimate at the beginning of the horizon $\hat{x}^{-}_{k-N|k}$ is computed using $\hat{x}^{\circ}_{k-N-1|k-1}$ given by the MHE at the previous instant $k-1$ and (4.5). The optimal estimate at instant $\hat{x}^{\circ}_{k|k}$ is computed by propagating $\hat{x}^{\circ}_{k-N|k}$ using the state equation (4.4c) and the measurement collection y^{k}_{k-N}. (Second row) Once a new measurement arrives at instant $k+1$, the oldest measurement of the last horizon y_{k-N} is discarded and the estimation is done using the new $N+1$ latest measurements from $[k-N+1, k+1]$. This fixed number of measurements taken into account at each iteration allows computation time to be tractable.

the horizon $\hat{x}_{k-N|k}$ becomes the only optimization parameter of the problem (4.4). The computation time of the MHE-PE is therefore reduced compared to that of the classical MHE strategies presented in (2.8) and (2.21).

In this chapter, we prove the convergence of the estimation errors of the MHE-PE under some conditions on the estimation model (4.1) and on the pre-estimator g described below.

4.4 Conditions to Guarantee the Stability of the Dynamics of the Estimation Errors of the MHE-PE

The estimation model (4.1) and the pre-estimator are supposed to verify the following conditions:

4.4.1 Conditions on the System

The estimation model (4.1) is supposed to satisfy:

(C1) $\mathbb{X}$ is a convex compact set, $\mathbb{W}$ and $\mathbb{V}$ are compact sets with $0 \in \mathbb{W}$ and $0 \in \mathbb{V}$. Define

$$r_w \triangleq \max_{w \in \mathbb{W}} \|w\|, \;\; r_v \triangleq \max_{v \in \mathbb{V}} \|v\| \tag{4.6}$$

(C2) The initial state x_0 is such that, for any possible sequence of process noise $\{w_k\}$, the system trajectory $\{x_k\}$ lies in the convex compact set $\mathbb{X}$, $\forall k$

(C3) f and h are $\mathcal{C}^2$ functions with respect to x on $\mathbb{X}$. Consequently, f and h are also locally Lipschitz on $\mathbb{X}$. Define their Lipschitz constants as L_f^x and L_h^x respectively.

4.4.2 Conditions on the Pre-Estimator

The pre-estimator g is supposed to satisfy:

(C4) g is locally Lipschitz with respect to its arguments, with the associated Lipschitz constants $L_g^{\hat{x}}$ and L_g^y.

(C5) $\forall {}^n\hat{x}_0 \in \hat{\mathbb{X}}$, $\forall {}^nx_0 \in \mathbb{X}$, there exists a class K function ψ such that $\|{}^n\hat{x}_k - {}^nx_k\|^2 \leq \psi(\|{}^n\hat{x}_0 - {}^nx_0\|^2)$, $\forall k$. This implies that the estimation error of g verifying (C5) in a noise-free case is equal to zero if g is initialized at the real state.

or

(C5a) g provides bounded estimation errors under bounded noise. Let us define c_g an upper bound on the estimation errors of g, i.e. $\forall k$ the estimate provided by g: $\hat{x}_k$ satisfies

$$\|\hat{x}_k - x_k\|^2 \leq c_g^2 \tag{4.7}$$

An example of g that verifies (C5) is a discrete-time deterministic observer defined as follows

Definition 8. *(Discrete-Time Deterministic Observer) Denote ${}^n\hat{x}_k$ the estimate of the nominal state ${}^nx_k$ at instant k provided by the estimator g. g is a discrete-time deterministic observer if $\forall {}^n\hat{x}_0 \in \hat{\mathbb{X}}$. There exists a KL-function β_{KL} such that*

$$\|{}^n\hat{x}_k - {}^nx_k\| \leq \beta_{KL}(\|{}^n\hat{x}_0 - {}^nx_0\|, k) \tag{4.8}$$

(4.8) implies that $\lim_{k\to\infty} {}^n\hat{x}_k = {}^nx_k$, $\forall {}^nx_0 \in \mathbb{X}$ and ${}^n\hat{x}_k = {}^nx_k$, $\forall k$, if ${}^n\hat{x}_0 = {}^nx_0$.

In [Sui et al., 2010], a discrete-time deterministic observer is used as the pre-estimator for a discrete-time linear MHE-PE. Their strategy is shown to provide better accuracy of the estimates compared to the deterministic observer when the latter is implemented only. This improvement is due to the optimization in the MHE-PE which takes into account

the measurement collection over the horizon.

In section 4.5.3, we will show that if the estimator g satisfies (C4) and (C5), then it satisfies (C4) and (C5a). An upper bound on the estimation errors provided by g will also be derived in this case.

Let us define the observation map of the pre-estimator g initialized at $k-N$ by $\hat{x}_{k-N}$ and receiving the real measurements y_{k-N}^{k-1} by

$$G(\hat{x}_{k-N}, y_{k-N}^{k-1}) \triangleq \begin{pmatrix} h(\hat{x}_{k-N}) \\ h \circ g(\hat{x}_{k-N}, y_{k-N}) \\ \vdots \\ h(g^N(\hat{x}_{k-N}, y_{k-N}^{k-1})) \end{pmatrix} = \hat{y}_{k-N}^{k} \tag{4.9}$$

where for $2 \leq i \leq N$

$$g^i(\hat{x}_{k-N}, y_{k-N}^{k-N+i-1}) \triangleq \underbrace{g(g(\ldots g}_{\text{i times}}(\hat{x}_{k-N}, y_{k-N}), \ldots), y_{k-N+i-1})$$

Denote (Σ) the system of the estimator g in (4.3). One of these uniform observability conditions which are equivalent is supposed to be verified:

(C6a) (Σ) is uniformly observable on $\hat{\mathbb{X}}$ with respect to all admissible measurements, i.e. $\exists N > 0$, $\forall y_{k-N}^{k-1} \in \mathbb{Y}^N$, the map $G(\hat{x}_{k-N}, y_{k-N}^{k-1})$ is injective as a function of $\hat{x}_{k-N}$

(C6b) (Σ) satisfies the uniform observability rank condition on $\hat{\mathbb{X}}$ with respect to all admissible measurements, i.e. $\exists N > 0$, $\forall \hat{x}_{k-N} \in \hat{\mathbb{X}}$, $\forall y_{k-N}^{k-1} \in \mathbb{Y}^N$,

$$\operatorname{rank}\left(\frac{\partial G(\hat{x}_{k-N}, y_{k-N}^{k-1})}{\partial \hat{x}_{k-N}}\right) = n_x$$

(C6c) g is K-uniformly observable on $\hat{\mathbb{X}}$ with respect to all admissible measurements, i.e. $\exists N \geq n_x$, $\forall (\hat{x}', \hat{x}'') \in \hat{\mathbb{X}}^2$, $\forall y_{k-N}^{k-1} \in \mathbb{Y}^N$, there exists a K-function $\phi_g(\cdot)$ such that

$$\phi_g(\|\hat{x}' - \hat{x}''\|^2) \leq \|G(\hat{x}', y_{k-N}^{k-1}) - G(\hat{x}'', y_{k-N}^{k-1})\|^2 \tag{4.10}$$

Moreover, g is supposed to satisfy:

(C7) The observation map $G(\cdot, \cdot)$ has a finite sensitivity to the estimate, i.e. the K-function $\phi_g(\cdot)$ in (4.10) satisfies:

$$\delta_g = \inf_{(\hat{x}_1, \hat{x}_2) \in \hat{\mathbb{X}}^2, \hat{x}_1 \neq \hat{x}_2} \frac{\phi_g(\|\hat{x}_1 - \hat{x}_2\|^2)}{\|\hat{x}_1 - \hat{x}_2\|^2} > 0 \tag{4.11}$$

Now propositions derived from the conditions in this section will be described in the next section. These propositions will be useful for the proof of the convergence of the estimation errors of the MHE-PE

4.5 Propositions Derived from the Conditions for the Convergence of the Estimation Errors of the MHE-PE

Before discussing the propositions, let us recall the triangle inequality, which will be used for the proofs of the propositions and of the convergence of the estimation errors of the MHE-PE.

Theorem 2. *(Triangle Inequality) The triangle inequality states that given l vectors $v_1, \dots, v_l$, we have*

$$\left\| \sum_{j=1}^{n} v_j \right\|^2 \leq l \sum_{j=1}^{l} \|v_j\|^2 \tag{4.12}$$

4.5.1 Propositions for the Estimation Model of the Real System

Using (4.1), (4.2), (4.6), condition (C3) and the triangle inequality (4.12), the following propositions are derived by recurrence, $\forall i \in \mathbb{N}^*$.

Proposition 1. *The squared norm of the difference at $k+i$ between the state x_{k+i} of* (4.1) *starting from x_k at k, and the nominal state ${}^n x_{k+i}$ of* (4.2) *starting from ${}^n x_k = x_k$ is bounded as*

$$\|x_{k+i} - {}^n x_{k+i}\|^2 \leq (\sum_{j=0}^{i-1} \{2(L_f^x)^2\}^j) 2r_w^2$$

Proposition 2. *The squared norm of the difference at $k+i$ between the measurement y_{k+i} of* (4.1) *starting from x_k at k and the nominal measurement ${}^n y_{k+i}$ of the nominal state of* (4.2) *starting from ${}^n x_k = x_k$ is bounded as*

$$\|y_{k+i} - {}^n y_{k+i}\|^2 \leq 2(L_h^x)^2 (\sum_{j=0}^{i-1} \{2(L_f^x)^2\}^j) 2r_w^2 + 2r_v^2$$

4.5.2 Propositions for the Pre-Estimator

By using (4.1), (4.2), (4.6), conditions (C3) and (C4) along with the triangle inequality, the following proposition is derived.

Proposition 3. *Consider the model* (4.1) *starting from x_k at k and the nominal model* (4.2) *starting from ${}^n x_k = x_k$. $\forall i \in \mathbb{N}^*$, consider at $k+i$ the estimate $\hat{x}_{k+i}$ of the state x_{k+i} given by g using y_k^{k+i} and initialized at $\hat{x}_k$. $\forall i \in \mathbb{N}^*$, consider at $k+i$ the estimate ${}^n\hat{x}_{k+i}$ of the nominal state ${}^n x_{k+i}$ given by g using ${}^n y_k^{k+i}$ and initialized at ${}^n\hat{x}_k = \hat{x}_k$. We have:*

$$\|\hat{x}_{k+i} - {}^n\hat{x}_{k+i}\|^2 \leq 2(L_g^y)^2 \times \left[4(L_h^x)^2 r_w^2 \sum_{j=0}^{i-1} \left(\{2(L_g^{\hat{x}})^2\}^{i-1-j} \alpha_{k+j} \right) + 2r_v^2 \sum_{j=0}^{i-1} \{2(L_g^{\hat{x}})^2\}^j \right] \tag{4.13}$$

where $\alpha_{k+j} = \sum_{l=0}^{j-1} \{2(L_f^x)^2\}^l$, $\forall j \in \mathbb{N}^+$ and $\alpha_k = 1$

The proofs of these 3 propositions are given in appendix D.1.

4.5.3 Upper Bound on the Estimation Errors of an Estimator verifying Lipschitz property (C4) and K-function property (C5)

In this section, an upper bound on the estimation errors provided by a pre-estimator g verifying Lipschitz property (C4) and K-function property (C5) is derived in case of bounded noise for the model (4.1). The work is inspired by the method proposed in [Liu, 2013] where an upper bound on the estimation errors of a nonlinear continuous-time deterministic observer is derived.

Consider the estimation model starting from the initial state x_k evolving as in (4.1) and the nominal estimation model starting from the same initial condition ${}^n x_k = x_k$ evolving as in (4.2). $\forall i \in \mathbb{N}^*$, denote $\hat{x}_{k+i}$ the estimate provided by the estimator g receiving real (noisy) measurements y_k^{k+i} starting from the initial estimate $\hat{x}_k$. Denote ${}^n\hat{x}_{k+i}$ the estimate provided by g receiving noise-free measurements ${}^n y_k^{k+i}$ and starting from the same initial estimate ${}^n\hat{x}_k = \hat{x}_k$.

We would like to find an upper bound on the squared norm of the estimation error $\|\hat{x}_{k+i} - x_{k+i}\|^2$ at time $k+i$. Remark that

$$\|\hat{x}_{k+i} - x_{k+i}\|^2 \;=\; \|(\hat{x}_{k+i} - {}^n\hat{x}_{k+i}) + ({}^n\hat{x}_{k+i} - {}^n x_{k+i}) + ({}^n x_{k+i} - x_{k+i})\|^2$$

Using the triangle inequality (4.12) for $l = 3$, we have

$$\|\hat{x}_{k+i} - x_{k+i}\|^2 \leq 3\|\hat{x}_{k+i} - {}^n\hat{x}_{k+i}\|^2 + 3\|{}^n\hat{x}_{k+i} - {}^n x_{k+i}\|^2 + 3\|{}^n x_{k+i} - x_{k+i}\|^2 \quad (4.14)$$

Using condition (C5), the second term of the r.h.s. of (4.14) verifies

$$\|{}^n\hat{x}_{k+i} - {}^n x_{k+i}\|^2 \leq \psi(\|{}^n\hat{x}_k - {}^n x_k\|^2) = \psi(\|\hat{x}_k - x_k\|^2) \quad (4.15)$$

Using proposition 1, the third term of the r.h.s. of (4.14) is bounded by

$$\|x_{k+i} - {}^n x_{k+i}\|^2 \leq (\sum_{j=0}^{i-1}\{2(L_f^x)^2\}^j)2r_w^2 \quad (4.16)$$

The first term of the r.h.s. of (4.14) is exactly (4.13) in proposition 3. Hence,

$$\|\hat{x}_{k+i} - {}^n\hat{x}_{k+i}\|^2 \leq 2(L_g^y)^2 \times \left[4(L_h^x)^2 r_w^2 \sum_{j=0}^{i-1}\left(\{2(L_g^{\hat{x}})^2\}^{i-1-j}\alpha_{k+j}\right) + 2r_v^2 \sum_{j=0}^{i-1}\{2(L_g^{\hat{x}})^2\}^j\right] \quad (4.17)$$

where $\alpha_{k+j} = \sum_{l=0}^{j-1}\{2(L_f^x)^2\}^l$, $\forall j \in \mathbb{N}^+$ and $\alpha_k = 1$.

Therefore, the following proposition can be derived:

Proposition 4. *$\forall i \in \mathbb{N}^*$, the squared norm of the difference between the estimate $\hat{x}_{k+1}$ given by an estimator g verifying conditions (C4) and (C5) receiving measurements y_k^{k+i} initialized at time k by $\hat{x}_k$ and the state x_{k+i} of the estimation model 4.1 is bounded as:*

$$\|\hat{x}_{k+i} - x_{k+i}\|^2 \leq 3\psi(\|\hat{x}_k - x_k\|^2) + c_{w,i}r_w^2 + c_{v,i}r_v^2 \quad (4.18)$$

where

$$c_{w,i} = 6\sum_{j=0}^{i-1}\{2(L_f^x)^2\}^j + 24(L_g^y L_h^x)^2 \sum_{j=0}^{i-1}\left(\{2(L_g^{\hat{x}})^2\}^{i-1-j}\alpha_{k+j}\right) \tag{4.19a}$$

$$c_{v,i} = 12(L_g^y)^2 \sum_{j=0}^{i-1}\{2(L_g^{\hat{x}})^2\}^j \tag{4.19b}$$

$$\alpha_{k+j} = \sum_{l=0}^{j-1}\{2(L_f^x)^2\}^l,\ \forall j \in \mathbb{N}^+,\ \alpha_k = 1 \tag{4.19c}$$

Proof. The proof is straightforward by replacing (4.15), (4.16) and (4.17) in (4.14), recalling that ${}^n\hat{x}_k = \hat{x}_k$ and ${}^n x_k = x_k$. □

This result on the existence of an upper bound on the estimation errors provided by an estimator verifying (C4) and (C5) will be used to proof the convergence of the estimation errors of the MHE-PE when such pre-estimating estimator is chosen. The following study is also verified for g verifying (C5a) which provides a bound on the estimation errors as in (4.7).

Now, let us prove the stability of the dynamics of the estimation errors of the MHE-PE with helps from the propositions derived in this section.

4.6 Stability of the Dynamics of the Estimation Errors of the MHE-PE

In this section, we would like to proof the stability of the dynamics of the estimation errors of the MHE-PE satisfying conditions (C1) to (C7). To do so, the following steps will be done:

1. an upper bound on the optimal cost, noted by $\mathbf{J}_k^\circ \triangleq \mathbf{J}_k(\hat{x}_{k-N|k}^\circ, \hat{x}_{k-N|k}^-, y_{k-N}^k)$ where $\hat{x}_{k-N|k}^\circ$ is the optimal solution of the problem (4.4) is calculated.
2. a lower bound on the optimal cost is calculated
3. the upper and the lower bounds are combined to have the dynamics of the estimation errors
4. conditions to guarantee the stability of the dynamics of the estimation errors are determined

This approach is inspired by [Alessandri et al., 2008] where the error dynamics of the MHE (without pre-estimation) as described in section 2.2 is derived.

4.6.1 Upper Bound on the Optimal Cost

Denote x_{k-N}, the state of (4.1) at instant $k-N$. By optimality of $\hat{x}_{k-N|k}^\circ$, we get $\mathbf{J}_k^\circ \leq \mathbf{J}_k(x_{k-N}, \hat{x}_{k-N|k}^-, y_{k-N}^k)$, i.e.

$$\mathbf{J}_k^\circ \leq \mu\|x_{k-N} - \hat{x}_{k-N|k}^-\|^2 + \sum_{i=0}^{N}\|y_{k-N+i} - h(\hat{x}_{k-N+i|k})\|_{\mathcal{R}}^2 \tag{4.20}$$

with

$$\begin{aligned}\hat{x}_{k-N+i+1,k} &= g(\hat{x}_{k-N+i|k}, y_{k-N+i}),\ \forall i \in [0, N-1]\\ \hat{x}_{k-N|k} &= x_{k-N}\end{aligned}$$

Let us find an upper bound on the second term of the r.h.s. of (4.20). Remark that

$$\|y_{k-N+i} - h(\hat{x}_{k-N+i|k})\|^2 = \|y_{k-N+i} - h(x_{k-N+i}) + h(x_{k-N+i}) - h(\hat{x}_{k-N+i|k})\|^2$$

and use the triangle inequality (4.12) to get

$$\|y_{k-N+i} - h(\hat{x}_{k-N+i|k})\|^2 \leq 2\|y_{k-N+i} - h(x_{k-N+i})\|^2 + 2\|h(x_{k-N+i}) - h(\hat{x}_{k-N+i|k})\|^2$$

Then, use (4.1) and condition (C1) to have

$$y_{k-N+i} - h(x_{k-N+i}) = v_{k-N+i} \leq r_v$$

Finally, use the Lipschitz property of h in condition (C3) to get

$$\|y_{k-N+i} - h(\hat{x}_{k-N+i|k})\|^2 \leq 2r_v^2 + 2(L_h^x)^2\|x_{k-N+i} - \hat{x}_{k-N+i|k}\|^2 \tag{4.21}$$

The second term of the r.h.s. of (4.20) therefore becomes

$$\begin{aligned}\sum_{i=0}^{N}\|y_{k-N+i} - h(\hat{x}_{k-N+i|k})\|^2 &\leq 2\sum_{i=0}^{N} r_v^2 + 2(L_h^x)^2\sum_{i=0}^{N}\|x_{k-N+i} - \hat{x}_{k-N+i|k}\|^2 \quad (4.22)\\ &\leq 2(N+1)r_v^2 + 2(L_h^x)^2\sum_{i=0}^{N}\|x_{k-N+i} - \hat{x}_{k-N+i|k}\|^2\end{aligned}$$

To bound the second term of the r.h.s. of (4.22), let us consider two following cases: 1. when the pre-estimator g satisfies condition (C5) and 2. when g satisfies condition (C5a).

In case that g satisfies condition (C5), we can use (4.18) in property 4 for the horizon starting at $k-N$ instead of at k to bound the second term of the r.h.s. of (4.22). Recall that $\psi(\|\hat{x}_{k-N|k} - x_{k-N}\|^2) = 0$ since $\hat{x}_{k-N|k} = x_{k-N}$. As a result,

$$\|x_{k-N+i} - \hat{x}_{k-N+i|k}\|^2 \leq c_{w,i}r_w^2 + c_{v,i}r_v^2 \tag{4.23}$$

In case that g satisfies condition (C5a), we have

$$\|x_{k-N+i} - \hat{x}_{k-N+i|k}\|^2 \leq c_g^2 \tag{4.24}$$

Replace (4.23) in (4.22) for g satisfying (C5) to get

$$\sum_{i=0}^{N}\|y_{k-N+i} - h(\hat{x}_{k-N+i|k})\|^2 \leq 2(N+1)r_v^2 + 2(L_h^x)^2\sum_{i=0}^{N}(c_{w,i}r_w^2 + c_{v,i}r_v^2) \tag{4.25}$$

where $c_{w,i}$, $c_{v,i}$ are defined in (4.19).

Replace (4.24) in (4.22) for g satisfying (C5a) to get

$$\sum_{i=0}^{N}\|y_{k-N+i} - h(\hat{x}_{k-N+i|k})\|^2 \leq 2(N+1)r_v^2 + 2(L_h^x)^2(N+1)c_g^2 \tag{4.26}$$

Denote $\lambda_{\mathcal{R},max}$ the largest eigenvalue of the weight matrix $\mathcal{R}$, we have

$$\sum_{i=0}^{N} \|y_{k-N+i} - h(\hat{x}_{k-N+i|k})\|_{\mathcal{R}}^2 \leq \lambda_{\mathcal{R},max} \sum_{i=0}^{N} \|y_{k-N+i} - h(\hat{x}_{k-N+i|k})\|^2 \tag{4.27}$$

As a consequence, for g satisfying (C5)

$$\sum_{i=0}^{N} \|y_{k-N+i} - h(\hat{x}_{k-N+i|k})\|_{\mathcal{R}}^2 \leq \lambda_{\mathcal{R},max} \left(2(N+1)r_v^2 + 2(L_h^x)^2 \sum_{i=0}^{N} (c_{w,i} r_w^2 + c_{v,i} r_v^2) \right) \tag{4.28}$$

Or equivalently,

$$\sum_{i=0}^{N} \|y_{k-N+i} - h(\hat{x}_{k-N+i|k})\|_{\mathcal{R}}^2 \leq \lambda_{\mathcal{R},max} \left(l_{w,N} r_w^2 + l_{v,N} r_v^2 \right) \tag{4.29a}$$

$$l_{w,N} = 2(L_h^x)^2 \sum_{i=1}^{N} c_{w,i} \tag{4.29b}$$

$$l_{v,N} = 2(L_h^x)^2 \sum_{i=1}^{N} c_{v,i} + 2(N+1) \tag{4.29c}$$

where $c_{w,i}$ and $c_{v,i}$ are defined in (4.19).

Replace (4.26) in (4.27) for g satisfying (C5a) to get

$$\sum_{i=0}^{N} \|y_{k-N+i} - h(\hat{x}_{k-N+i|k})\|_{\mathcal{R}}^2 \leq 2(N+1)\lambda_{\mathcal{R},max} \left(r_v^2 + (L_h^x)^2 c_g^2 \right) \tag{4.30}$$

To summarize, an upper bound on the optimal cost $\mathbf{J}_k^\circ$ is given by

$$\mathbf{J}_k^o \leq \mu \|x_{k-N} - \hat{x}_{k-N|k}^-\|^2 + c_N^2 \tag{4.31}$$

For g satisfying (C5)

$$c_N^2 = \lambda_{\mathcal{R},max} \left(l_{w,N} r_w^2 + l_{v,N} r_v^2 \right) \tag{4.32}$$

where $l_{w,N}$ and $l_{v,N}$ are defined in (4.29).

For g satisfying (C5a)

$$c_N^2 = 2(N+1)\lambda_{\mathcal{R},max} \left(r_v^2 + (L_h^x)^2 c_g^2 \right) \tag{4.33}$$

where c_g is defined in (4.7).

Now that we have an upper bound on the optimal cost, let us pursue with the computation of a lower bound.

4.6.2 Lower Bound on the Optimal Cost

We start by determining a lower bound on any common cost $\mathbf{J}_k$ in (4.4), so $\hat{x}_{k-N|k}$ will be replaced by $\hat{x}_{k-N}$ to refer to any value of the estimate at the beginning of the horizon in general. After that, a lower bound on the optimal cost $\mathbf{J}_k^\circ$ will be derived by replacing

$\hat{x}_{k-N}$ by $\hat{x}^{\circ}_{k-N|k}$.

Recall that the observation map of the nominal estimation model (4.2) defined in (2.10) starting from ${}^{n}x_{k-N} = x_{k-N}$ at $k-N$ is

$$F(x_{k-N}, \mathbf{0}_{n_x N\times 1}) \triangleq \begin{pmatrix} h(x_{k-N}) \\ h(f(x_{k-N})) \\ \vdots \\ h\circ f\circ\cdots\circ f(x_{k-N}) \end{pmatrix} = {}^{n}y^{k}_{k-N} \tag{4.34}$$

where ${}^{n}y^{k-1}_{k-N}$ is the vector of the noise free measurements in (4.2) initialized at time $k-N$ with ${}^{n}x_{k-N} = x_{k-N}$.

The observation map of the pre-estimator g initialized at $k-N$ by $\hat{x}_{k-N}$ and receiving the real measurements y^{k}_{k-N} defined in (4.9) is

$$G(\hat{x}_{k-N}, y^{k-1}_{k-N}) \triangleq \begin{pmatrix} h(\hat{x}_{k-N}) \\ h\circ g(\hat{x}_{k-N}, y_{k-N}) \\ \vdots \\ h(g^{N}(\hat{x}_{k-N}, y^{k-1}_{k-N})) \end{pmatrix} = \hat{y}^{k}_{k-N} \tag{4.35}$$

where for $2 \leq i \leq N$

$$g^{i}(\hat{x}_{k-N}, y^{k-N+i-1}_{k-N}) \triangleq \underbrace{g(g(\ldots g}_{\text{i times}}(\hat{x}_{k-N}, y_{k-N}), \ldots), y_{k-N+i-1}) \tag{4.36}$$

Using the definition of the Euclidean norm, the second term of the r.h.s. of the cost function (4.4b) becomes

$$\sum_{i=0}^{N} \|y_{k-N+i} - h(\hat{x}_{k-N+i})\|^2_{\mathcal{R}} = \|y^{k}_{k-N} - G(\hat{x}_{k-N}, y^{k-1}_{k-N})\|^2_{\mathcal{R}}$$

.

Remark that

$$\begin{aligned} G(\hat{x}_{k-N}, {}^{n}y^{k-1}_{k-N}) - G(x_{k-N}, {}^{n}y^{k-1}_{k-N}) \;=\; & (G(\hat{x}_{k-N}, {}^{n}y^{k-1}_{k-N}) - G(\hat{x}_{k-N}, y^{k-1}_{k-N})) \\ & +(G(\hat{x}_{k-N}, y^{k-1}_{k-N}) - y^{k}_{k-N}) \\ & +(y^{k}_{k-N} - F(x_{k-N}, \mathbf{0}_{n_x N\times 1})) \\ & +(F(x_{k-N}, \mathbf{0}_{n_x N\times 1}) - G(x_{k-N}, {}^{n}y^{k-1}_{k-N})) \end{aligned} \tag{4.37}$$

Thanks to the triangle inequality (4.12), we deduce:

$$\begin{aligned} \|G(\hat{x}_{k-N}, {}^{n}y^{k-1}_{k-N}) - G(x_{k-N}, {}^{n}y^{k-1}_{k-N})\|^2 \;\leq\; & 4\left\|y^{k}_{k-N} - G(\hat{x}_{k-N}, y^{k-1}_{k-N})\right\|^2 \\ & +4\left\|y^{k}_{k-N} - F(x_{k-N}, \mathbf{0}_{n_x N\times 1})\right\|^2 \\ & +4\left\|F(x_{k-N}, \mathbf{0}_{n_x N\times 1}) - G(x_{k-N}, {}^{n}y^{k-1}_{k-N})\right\|^2 \\ & +4\left\|G(\hat{x}_{k-N}, y^{k-1}_{k-N}) - G(\hat{x}_{k-N}, {}^{n}y^{k-1}_{k-N})\right\|^2 \end{aligned} \tag{4.38}$$

Denote $\lambda_{\mathcal{R},min}$ the smallest eigenvalue of $\mathcal{R}$ and rearrange (4.38) to get a lower bound of the second term of the r.h.s. of the cost function (4.4b) as follows:

$$\begin{aligned}\|y_{k-N}^{k} - G(\hat{x}_{k-N}, y_{k-N}^{k-1})\|_{\mathcal{R}}^2 \quad \geq \quad & \frac{1}{4}\lambda_{\mathcal{R},min}\|G(\hat{x}_{k-N}, {}^{n}y_{k-N}^{k-1}) - G(x_{k-N}, {}^{n}y_{k-N}^{k-1})\|^2 \\ & -\lambda_{\mathcal{R},min}\|y_{k-N}^{k} - F(x_{k-N})\|^2 \\ & -\lambda_{\mathcal{R},min}\left\|F(x_{k-N}) - G(x_{k-N}, {}^{n}y_{k-N}^{k-1})\right\|^2 \\ & -\lambda_{\mathcal{R},min}\left\|G(\hat{x}_{k-N}, y_{k-N}^{k-1}) - G(\hat{x}_{k-N}, {}^{n}y_{k-N}^{k-1})\right\|^2 \end{aligned} \quad (4.39)$$

Consider the system of the pre-estimator g in (4.3) for which the input is the measurement y. Since (C6) (a, b or c which are equivalent) and (C7) are supposed to be verified. Use (4.10) and (4.11) to obtain a lower bound on the first term of the r.h.s. of (4.39) as follows:

$$\|G(x_{k-N}, {}^{n}y_{k-N}^{k-1}) - G(\hat{x}_{k-N}, {}^{n}y_{k-N}^{k-1})\|^2 \geq \delta_g\|\hat{x}_{k-N} - x_{k-N}\|^2 \quad (4.40)$$

Consider now the second term of the r.h.s. of (4.39). Similarly to [Alessandri et al., 2008], we have

$$\|y_{k-N}^{k} - F(x_{k-N})\|^2 \leq c_{Ale,N}^2 \quad (4.41)$$

$$c_{Ale,N} \triangleq \Delta_w\sqrt{N}r_w + \sqrt{N+1}r_v + \frac{\bar{k}}{2}\sqrt{\frac{N(N+1)(2N+1)}{6}}r_w^2$$

where Δ_w and $\bar{k}$ characterize the model sensitivity to state noise, see the details in appendix B.1.

Consider now the third term of the r.h.s. of (4.39). For a pre-estimator g satisfying (C5), this term is equal to zero since the estimate in a noise-free case is equal to the state at all instant if g is initialized at the real state. For a pre-estimator g satisfying (C5a), we have

$$\left\|F(x_{k-N}, \mathbf{0}_{n_xN\times 1}) - G(x_{k-N}, {}^{n}y_{k-N}^{k-1})\right\|^2 = \left\|\begin{pmatrix} h(x_{k-N}) - h(x_{k-N}) \\ h({}^{n}x_{k-N+1}) - h({}^{n}\hat{x}_{k-N+1})) \\ \vdots \\ h({}^{n}x_k) - h({}^{n}\hat{x}_k) \end{pmatrix}\right\|^2 \quad (4.42)$$

Use the Lipschitz property of h to get

$$\left\|F(x_{k-N}, \mathbf{0}_{n_xN\times 1}) - G(x_{k-N}, {}^{n}y_{k-N}^{k-1})\right\|^2 \leq (L_h^x)^2\sum_{i=0}^{N}\underbrace{\|x_{k-N+i} - {}^{n}\hat{x}_{k-N+i}\|^2}_{\leq c_g^2 \text{thanks to (4.7)}} \quad (4.43)$$

Hence, for g satisfying (C5a)

$$\left\|F(x_{k-N}, \mathbf{0}_{n_xN\times 1}) - G(x_{k-N}, {}^{n}y_{k-N}^{k-1})\right\|^2 \leq (L_h^x)^2(N+1)c_g^2 \quad (4.44)$$

Use the Lipschitz property of h and the definition of the Euclidean norm, the forth term of the r.h.s of (4.39) can finally be bounded as

$$\left\|G(\hat{x}_{k-N}, y_{k-N}^{k-1}) - G(\hat{x}_{k-N}, {}^{n}y_{k-N}^{k-1})\right\|^2 \leq (L_h^x)^2\sum_{i=1}^{N}\mathcal{G}_i \quad (4.45)$$

where $\mathcal{G}_i \triangleq \left\| g^i(\hat{x}_{k-N}, y_{k-N}^{k-N+i-1}) - g^i(\hat{x}_{k-N}, {}^n y_{k-N}^{k-N+i-1}) \right\|^2$.

Recall that (4.36) gives

$$g^i(\hat{x}_{k-N}, y_{k-N}^{k-N+i-1}) \triangleq \underbrace{g(g(\ldots g}_{\text{i times}}(\hat{x}_{k-N}, y_{k-N}), \ldots), y_{k-N+i-1}) \tag{4.46}$$

Using the Lipschitz property of g, we have

$$\mathcal{G}_i \leq \left\| L_g^{\hat{x}}(g^{i-1}(\hat{x}_{k-N}, y_{k-N}^{k-N+i-1})) - g^{i-2}(\hat{x}_{k-N}, {}^n y_{k-N}^{k-N+i-2}) + L_g^y(y_{k-N+i-1} - {}^n y_{k-N+i-1}) \right\|^2$$

Use the triangle inequality (4.12) to get

$$\mathcal{G}_i \leq \underbrace{2(L_g^{\hat{x}})^2 \mathcal{G}_{i-1}}_{\text{for } i \geq 1} + 2(L_g^y)^2 \| y_{k-N+i-1} - {}^n y_{k-N+i-1} \|^2 \tag{4.47}$$

To calculate an upper bound on $\mathcal{G}_i$, consider the following proposition:

Proposition 5.

$$\mathcal{G}_i \leq 2\left(L_g^y\right)^2 \left(\underbrace{2r_v^2 \sum_{j=0}^{i-1} \left(2\left(L_g^{\hat{x}}\right)^2\right)^j}_{for\ i \geq 1} + \underbrace{2\left(L_h^x\right)^2 2r_w^2 \sum_{j=0}^{i-2} \left(2(L_f^x)^2 + 2(L_g^{\hat{x}})^2\right)^j}_{for\ i \geq 2} \right) \tag{4.48}$$

The proof of proposition (5) is provided in appendix D.1.4.

Replace (4.48) in (4.45) to get an upper bound of the forth term of the r.h.s of (4.39)

$$\left\| G(\hat{x}_{k-N}, y_{k-N}^{k-1}) - G(x_{t-N}, {}^n y_{k-N}^{k-1}) \right\|^2 \leq (L_h^x)^2 \lambda_N^2 \tag{4.49}$$

where

$$\lambda_N^2 = 2(L_g^y)^2 \left(2{r_v}^2 \sum_{i=1}^{N} \sum_{j=0}^{i-1} \left(2(L_g^{\hat{x}})^2\right)^j + 2(L_h^x)^2 2r_w^2 \sum_{i=2}^{N} \sum_{j=0}^{i-2} \left(2(L_f^x)^2 + 2(L_g^{\hat{x}})^2\right)^j \right) \tag{4.50}$$

So now we have lower bounds for each term on the r.h.s of (4.39). Replace (4.40), (B.11), and (4.49) in (4.39) to obtain a lower bound on the second term of the r.h.s. of the cost function (4.4b) for a pre-estimator satisfying (C5):

$$\begin{aligned} \left\| y_{k-N}^k - G(\hat{x}_{k-N}, y_{k-N}^k) \right\|_{\mathcal{R}}^2 \geq\ & \frac{1}{4}\lambda_{\mathcal{R},min}\delta_g \left\| \hat{x}_{k-N} - x_{k-N} \right\|^2 \\ & -\lambda_{\mathcal{R},min}\left((L_h^x)^2 \lambda_N^2 + c_{Ale,N}^2 \right) \end{aligned} \tag{4.51}$$

For a pre-estimator g satisfying (C5a), we have

$$\begin{aligned} \left\| y_{k-N}^k - G(\hat{x}_{k-N}, y_{k-N}^k) \right\|_{\mathcal{R}}^2 \geq\ & \frac{1}{4}\lambda_{\mathcal{R},min}\delta_g \left\| \hat{x}_{k-N} - x_{k-N} \right\|^2 \\ & -\lambda_{\mathcal{R},min}\left((L_h^x)^2 \lambda_N^2 + c_{Ale,N}^2 + (L_h^x)^2 (N+1) c_g^2 \right) \end{aligned} \tag{4.52}$$

Now that we have a lower bound for the second term of the cost function $\mathbf{J}_k$, let us continue with a lower bound on its first term: $\mu\|\hat{x}_{k-N} - \hat{x}^-_{k-N|k}\|^2$. First of all, use the triangle inequality (4.12) to have

$$\begin{aligned} \|x_{k-N} - \hat{x}_{k-N}\|^2 &= \left\|(x_{k-N} - \hat{x}^-_{k-N|k}) + (\hat{x}^-_{k-N|k} - \hat{x}_{k-N})\right\|^2 \\ &\leq 2\left\|x_{k-N} - \hat{x}^-_{k-N|k}\right\|^2 + 2\left\|\hat{x}_{k-N} - \hat{x}^-_{k-N|k}\right\|^2 \end{aligned} \tag{4.53}$$

Rearrange (4.53) to have

$$\left\|\hat{x}_{k-N} - \hat{x}^-_{k-N|k}\right\|^2 \geq \frac{1}{2}\|x_{k-N} - \hat{x}_{k-N}\|^2 - \left\|x_{k-N} - \hat{x}^-_{k-N|k}\right\|^2 \tag{4.54}$$

Combine the lower bound on the first term of $\mathbf{J}_k$ (4.54) and that on the second term (4.51) to get for g satisfying (C5)

$$\begin{aligned} \mathbf{J}_k \leq\ & \left(\frac{1}{2}\mu + \frac{1}{4}\lambda_{\mathcal{R},min}\cdot\delta_g\right)\left\|\hat{x}_{k-N|k} - x_{k-N}\right\|^2 - \mu\left\|x_{k-N} - \hat{x}^-_{k-N|k}\right\|^2 \\ & -\lambda_{\mathcal{R},min}\left((L^x_h)^2\lambda^2_N + c^2_{Ale,N}\right) \end{aligned} \tag{4.55}$$

and for g satisfying (C5a)

$$\begin{aligned} \mathbf{J}_k \leq\ & \left(\frac{1}{2}\mu + \frac{1}{4}\lambda_{\mathcal{R},min}\cdot\delta_g\right)\left\|\hat{x}_{k-N|k} - x_{k-N}\right\|^2 - \mu\left\|x_{k-N} - \hat{x}^-_{k-N|k}\right\|^2 \\ & -\lambda_{\mathcal{R},min}\left((L^x_h)^2\lambda^2_N + c^2_{Ale,N} + (L^x_h)^2(N+1)c^2_g\right) \end{aligned} \tag{4.56}$$

Replace the general notation $\hat{x}_{k-N}$ by the solution $\hat{x}^\circ_{k-N|k}$. By defining

$$e^\circ_{k-N} \triangleq \hat{x}^\circ_{k-N|k} - x_{k-N} \tag{4.57}$$

a lower bound on the optimal cost $\mathbf{J}^\circ_k$ is

$$\mathbf{J}^\circ_k \leq \left(\frac{1}{2}\mu + \frac{1}{4}\lambda_{\mathcal{R},min}\cdot\delta_g\right)\|e^\circ_{k-N}\|^2 - \mu\left\|x_{k-N} - \hat{x}^-_{k-N|k}\right\|^2 - \mathcal{C}^2_N \tag{4.58}$$

where for g satisfying (C5)

$$\mathcal{C}^2_N = \lambda_{\mathcal{R},min}\left((L^x_h)^2\lambda^2_N + c^2_{Ale,N}\right) \tag{4.59}$$

and for g satisfying (C5a)

$$\mathcal{C}^2_N = \lambda_{\mathcal{R},min}\left((L^x_h)^2\lambda^2_N + c^2_{Ale,N} + (L^x_h)^2(N+1)c^2_g\right) \tag{4.60}$$

Now that a lower bound on the optimal cost $\mathbf{J}^\circ_k$ has been calculated, it will be combined with the upper bound on $\mathbf{J}^\circ_k$ computed in the previous section to analyze the dynamics of the estimation error of the MHE-PE to show its convergence.

4.6.3 Stability of the Dynamics of the Estimation Errors of the MHE-PE

Combine the upper bound on the optimal cost $\mathbf{J}^\circ_k$ in (4.31) with its lower bound in (4.58) to get:

$$\frac{1}{2}\left(\mu + \frac{1}{2}\lambda_{\mathcal{R},min}\delta_g\right)\|e^\circ_{k-N}\|^2 \leq 2\mu\left\|x_{k-N} - \hat{x}^-_{k-N|k}\right\|^2 + \mathcal{C}^2_N \tag{4.61}$$

Since $\hat{x}^-_{k-N|k} \triangleq f(\hat{x}^\circ_{k-N-1|k-1})$,

$$\left\|x_{k-N} - \hat{x}^-_{k-N|k}\right\|^2 = \left\|f(x_{k-N-1}) + w_{k-N-1} - f(\hat{x}^\circ_{k-N-1|k-1})\right\|^2 \tag{4.62}$$

Use the triangle inequality (4.12) and the Lipschitz property of f to have

$$\left\|x_{k-N} - \hat{x}^-_{k-N|k}\right\|^2 \leq 2(L^x_f)^2 \left\|e^\circ_{k-N-1}\right\|^2 + 2r^2_w \tag{4.63}$$

Define $d_x \triangleq \max_{(x,x')\in\mathbb{X}^2} \|x - x'\|$, we have for $k - N = 0$

$$\left\|x_0 - \hat{x}^-_0\right\|^2 \leq d^2_x \tag{4.64}$$

Replace (4.63) in (4.61) to have

$$\frac{1}{2}\left(\mu + \frac{1}{2}\lambda_{\mathcal{R},min}\delta_g\right)\left\|e^\circ_{k-N}\right\|^2 \leq 4\mu(L^x_f)^2\left\|e^\circ_{k-N-1}\right\|^2 + 4\mu r^2_w + \mathcal{C}^2_N \tag{4.65}$$

Rearrange (4.65) to have

$$\left\|e^\circ_{k-N}\right\|^2 \leq \frac{8\mu(L^x_f)^2}{\mu + \frac{1}{2}\lambda_{\mathcal{R},min}\delta_g}\left\|e^\circ_{k-N-1}\right\|^2 + \frac{2}{\mu + \frac{1}{2}\lambda_{\mathcal{R},min}\delta_g}\left(4\mu r^2_w + \mathcal{C}^2_N\right) \tag{4.66}$$

The following theorem is therefore derived:

Theorem 3 (Convergence of the Estimation Errors of the MHE-PE)**.** *Consider a discrete-time nonlinear estimation model verifying assumptions (C1)-(C3). If the pre-estimator of the MHE-PE verifies (C4)-(C7), then the squared norm of the estimation error of the MHE-PE is bounded as* $\left\|e^\circ_{k-N}\right\|^2 \leq \zeta_{k-N}$ *where* $\{\zeta_k\}$ *is a sequence generated by*

$$\begin{aligned} \zeta_0 &= \beta_0 \\ \zeta_k &= \alpha_{MHE-PE}\zeta_{k-1} + \beta_{MHE-PE},\ \forall k \in \mathbb{N}^* \end{aligned} \tag{4.67}$$

with

$$\alpha_{MHE-PE} = \frac{8\mu(L^x_f)^2}{\mu + \frac{\lambda_{\mathcal{R},min}\delta_g}{2}} \qquad \beta_{MHE-PE} = \frac{2}{\mu + \frac{\lambda_{\mathcal{R},min}\delta_g}{2}}(4\mu r^2_w + \mathcal{C}^2_N)$$
$$\beta_0 = \frac{2}{\mu + \frac{\lambda_{\mathcal{R},min}\delta_g}{2}}(2\mu d^2_x + \mathcal{C}^2_N)$$

where $\mathcal{C}^2_N$ *is defined in* (4.59) *for* g *satisfying (C5) and in* (4.60) *for* g *satisfying (C5a).* $d_x \triangleq \max_{(x,x')\in\mathbb{X}^2} \|x - x'\|$*. Moreover, if* μ *is selected such that*

$$\alpha_{MHE-PE} \triangleq \frac{8\mu(L^x_f)^2}{(\mu + \frac{\lambda_{\mathcal{R},min}\delta_g}{2})} < 1 \tag{4.68}$$

The sequence $\{\zeta_k\}$ *has the following properties:*

(a) $\{\zeta_k\}$ *converges exponentially to the asymptotic value*

$$e^{\circ}_{\infty}(\mu) \triangleq \frac{\beta_{MHE-PE}}{(1-\alpha_{MHE-PE})} \tag{4.69}$$

(b) if $\zeta_k > e^{\circ}_{\infty}(\mu)$*, then* $\zeta_k < \zeta_{k-1}$

Thanks to theorem 3, the convergence of the estimation errors of the MHE-PE can be guaranteed by choosing an appropriate μ satisfying condition (4.68). This is easy to do for any value of L^x_f, once δ_g is calculated using (4.11).

In the case of a noise-free system ($r_w = r_v = 0$), the asymptotic convergence to zero of the estimation errors of the MHE-PE is guaranteed by the following corollary:

Corollary 1. *Suppose that conditions (C1)-(C7) hold. If* $r_w = r_v = 0$, $\left\|e^{\circ}_{k-N}\right\|^2 \leq \alpha^{k-N}_{MHE-PE}\beta_0$, $\forall k \geq N$. *Moreover, if* μ *satisfies* (4.68), $\lim_{k\to\infty}\left\|e^{\circ}_{k-N}\right\|^2 = 0$.

Remarks

1. From (4.69), we can see that the smaller α_{MHE-PE} is and the smaller β_{MHE-PE} is the smaller e°_{∞} becomes.
2. Theoretically, the smaller α_{MHE-PE}, the faster the convergence.
3. $\dfrac{\partial \alpha_{MHE-PE}}{\partial \mu} = \dfrac{4\lambda_{\mathcal{R},min}\delta_g (L^x_f)^2}{(\mu + \frac{\lambda_{\mathcal{R},min}\delta_g}{2})^2} > 0$. Hence, the larger μ, the larger α_{MHE-PE} and the slower the convergence.
4. The larger the horizon N is, the larger $\mathcal{C}_N$ is. This large $\mathcal{C}_N$ induces a large value of the asymptotic bound on the estimation errors e°_{∞}. This theoretical bound is however usually very large because it is computed using upper bounds of many variables. In practice, the estimation errors are much smaller than the value of this theoretical bound.
5. If $8(L^x_f)^2 \leq 1$, $\alpha_{MHE-PE} < \dfrac{1}{1 + \frac{\lambda_{\mathcal{R},min}\delta_g/2}{\mu}}$ and one can choose any $\mu \geq 0$.
6. If $8(L^x_f)^2 > 1$, μ must be chosen such that $\dfrac{\mu}{(\mu + \frac{\lambda_{\mathcal{R},min}\delta_g}{2})} < \dfrac{8\mu(L^x_f)^2}{(\mu + \frac{\lambda_{\mathcal{R},min}\delta_g}{2})} < 1$.

   Hence,

   $$\mu < 8\mu(L^x_f)^2 < \mu + \frac{\lambda_{\mathcal{R},min}\delta_g}{2}$$

   which implies that

   $$0 \leq \mu \leq \frac{\lambda_{\mathcal{R},min}\delta_g/2}{(8(L^x_f)^2) - 1}$$

   In the same way as explained in [Alessandri et al., 2008], this means that the smaller the L^x_f (i.e. the more contractive the estimation model) and the larger the δ_g (i.e. the more observable the pre-estimator) the wider range of values of μ that satisfies condition (4.68).

7. Knowing that the estimates at the end of the horizon $\hat{x}_{k|k}$ is computed using

$$\hat{x}_{k-N+i+1|k} = g(\hat{x}_{k-N+i|k}, y_{k-N+i}),\ \forall i \in [0, N-1] \tag{4.70}$$

Thanks to the locally Lipschitz property of g, we can see that the convergence of the squared norm of the estimation errors $\left\|\hat{x}_{k-N+i+1|k} - x_k\right\|^2$ is also guaranteed.

8. the value of β_{MHE-PE} (hence the asymptotic value e°_{∞}) can be computed. In this case, $c_{Ale,N}$ which depends on Δ_w and $\bar{k}$ must be computed. Recall that Δ_w defined in (B.6) is a norm of the Jacobian matrix of the observation map $F(x_{k-1}, w_{k-N}^{k-1})$ with respect to the process noise sequence w_{k-N}^{k-1}. The analytic expression of the Jacobian matrix $\dfrac{\partial F(x_{k-1}, w_{k-N}^{k-1})}{\partial w_{k-N}^{k-1}}$ can be computed using symbolic calculation in MATLAB. Then, the norm of this Jacobian matrix can be computed using hypothesis on the definition domain of the state and the process noise.

Now that the convergence of the estimation errors of the MHE-PE satisfying (C1)-(C7) has been proven, let us illustrate its performance compared to the classical MHE presented in chapter 2 for the study case of a pressure estimation problem of a gas-phase, reversible reaction will be chosen.

4.7 Simulation Example

The performances of

- the MHE-PE whose pre-estimator is a deterministic observer
- the MHE in the stochastic framework as described in section 2.3
- the EKF
- the deterministic observer used as the pre-estimator in the MHE-PE

are compared through a pressure estimation problem of a gas-phase, reversible reaction as defined in [Haseltine and Rawlings, 2005] in terms of accuracy of the estimates and computation time. The MHE in the stochastic framework is chosen rather than that of the deterministic framework for the sake of simplicity since in the stochastic framework the weight matrices can be chosen as the inverse matrices of the process noise covariance matrix, the measurement noise covariance matrix and the covariance error matrix directly. The performances of the deterministic observer are studied to verify whether the use of the MHE-PE is interesting when a deterministic observer exists for the estimation model knowing that the stability of the estimation errors of the deterministic observer is already guaranteed.

4.7.1 Physical System

Consider the following gas-phase, reversible reaction of two gases: A and B [Haseltine and Rawlings, 2005]

$$2A \xrightarrow{\bar{k}_g} B, \qquad \bar{k}_g = 0.16\,(atm \cdot s)^{-1} \tag{4.71}$$

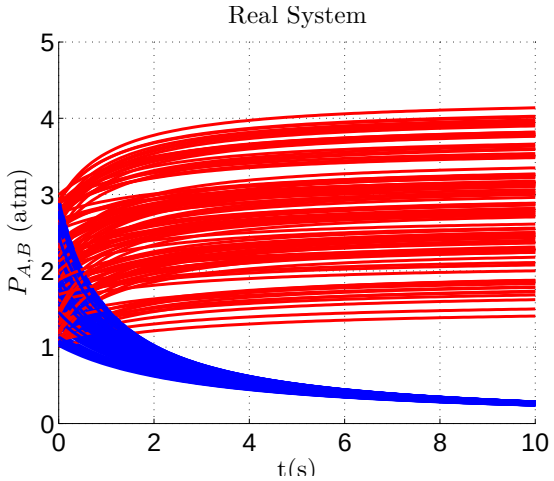

Figure 4.2: Partial pressures of the 100 simulated reactions

with stoichiometric matrix

$$\nu = \begin{pmatrix} -2 & 1 \end{pmatrix}^T$$

and reaction rate

$$r = \bar{k}_g P_A^2$$

where P_A and P_B denote the partial pressures of gas A and gas B respectively.

Define the state to be

$$x = \begin{pmatrix} P_A \\ P_B \end{pmatrix} \tag{4.72}$$

The measurement of the system is the total pressure of the system. Suppose that it is available every T_s s. Define $x_k = x(t = kT_s)$. The measurement equation of the system is therefore

$$y_k = \begin{pmatrix} 1 & 1 \end{pmatrix} x_k + v_k \tag{4.73}$$

where v_k is the measurement noise. In our study, $T_s = 0.1$ s and $v_k \sim \mathbf{U}(-0.3, 0.3)$ atm. This choice of measurement noise is inspired by the chosen value in [Haseltine and Rawlings, 2005] where $v_k \sim \mathcal{N}(0, 0.1^2)$. In our study, the uniform distribution for the noise is chosen to have bounded measurement noises.

We assume that the ideal gas law holds (high temperature, low pressure) and that the reaction occurs in a well-mixed isothermal batch reactor. According to [Martínez-Forero et al., 2010], the ODE system for this chemical reaction is of the form

$$\dot{x} = \nu r \tag{4.74}$$

In this study, 100 reactions are simulated using Monte Carlo method. The initial pressures P_{A_0} and P_{B_0} of each reaction is drawn from the Uniform distribution $\mathbf{U}(1, 3)$ atm[1]. The simulated partial pressures are shown in figure 4.2.

[1]In [Haseltine and Rawlings, 2005] the study is done for a single reaction started from $P_{A_0} = 3$ atm and $P_{B_0} = 1$ atm. Here, we would like to study also the robustness of the estimators to the initial condtion. Hence, P_{A_0} and P_{B_0} are drawn from the proposed distribution.

4.7.2 Estimation Model

The estimators are implemented in discrete-time. According to [Haseltine and Rawlings, 2005], the following discretized version of the nonlinear model (4.74) is used as the estimation model

$$x_{k+1} = f(x_k) + w_k = \begin{pmatrix} \dfrac{x_{1,k}}{2\bar{k}_g T_s x_{1,k} + 1} \\ x_{2,k} + \dfrac{\bar{k}_g T_s x_{1,k}^2}{2\bar{k}_g T_s x_{1,k} + 1} \end{pmatrix} + w_k \tag{4.75}$$

4.7.3 Tuning of the Estimators

The same tuning as in [Haseltine and Rawlings, 2005] is used: the a priori initial error covariance matrix $P_0 = \text{diag}\begin{pmatrix} 6^2 & 6^2 \end{pmatrix}$, the process noise covariance matrix $Q = \text{diag}\begin{pmatrix} 0.001^2 & 0.001^2 \end{pmatrix}$, the measurement noise covariance $R = 0.1^2$ and the a priori initial estimate $\hat{x}_0^- = \begin{pmatrix} 0.1 & 4.5 \end{pmatrix}^T$.

The constraint $\hat{\mathbb{X}} = [0.1, 15]^2$ is imposed to every MHE and MHE-PE for every run. The process noise estimates given by the MHE are imposed to be in the interval $[-0.005, 0.005]^2$.

Concerning the pre-estimator of the MHE-PE, recalling that a deterministic observer satisfies (C5), it is chosen as the pre-estimation estimator g for the MHE-PE. A deterministic observer associated to the system can be computed by solving an LMI problem as proposed in [Zhang et al., 2012]. This LMI problem will be recalled in appendix .By solving the LMI using MATLAB, we find a deterministic observer for the noise-free system associated to system (4.75) as follows:

$$\hat{x}_{k+1} = g(\hat{x}_k, y_k) = f(\hat{x}_k) + L(y_k - \begin{pmatrix} 1 & 1 \end{pmatrix} \hat{x}_k) \tag{4.76}$$

where $L = \begin{pmatrix} 0.0026 & 0.7046 \end{pmatrix}^T$.

The system (4.75) and the pre-estimation estimator g in (4.76) are proven to satisfy conditions (C1)-(C7). The details are given in appendix D.3. Appendix D.3 also shows that the values of $L_f^x = 1.2$, $\delta_g = 2.5 \cdot 10^{-5}$ can be chosen. Using these values and the condition to guarantee the stability of the estimation errors of the MHE-PE in (4.68), we find that $\mu = 10^{-4}$ which gives $\alpha_{MHE-PE} = 0.8533$ can be chosen. Three sizes of horizon: $N = 4$, $N = 20$ and $N = 50$ are chosen for the MHE-PE and the MHE.

Consider a more practical way to choose the weight parameter μ without computing the sensibility parameter δ_g, recall that

$$\mathbf{J}_k = \mu \left\| \hat{x}_{k-N|k} - \hat{x}_{k-N|k}^- \right\|^2 + \sum_{i=0}^{N} \left\| y_{k-N+i} - h(\hat{x}_{k-N+i|k}) \right\|^2 \tag{4.77}$$

Equivalent to the MHE in the stochastic framework in 2.3, the order of μ could be chosen such that

$$\mu \sim \frac{\left\| P^{-1} \right\|_p}{N \cdot R^{-1}} \tag{4.78}$$

In this study,

$$\mu \sim \frac{6^{-2}}{0.1^{-2} N} = \frac{2.8 \cdot 10^{-4}}{N}$$

For $N = 4$, $\mu = 6.9 \cdot 10^{-5}$, for $N = 20$, $\mu = 1.4 \cdot 10^{-5}$ and for $N = 40$, $\mu = 6.9 \cdot 10^{-6}$. This value of μ gives $\alpha_{MHE-PE} = 1.98$, $\alpha_{MHE-PE} = 0.13$ and $\alpha_{MHE-PE} = 0.06$.

Recall that this method (4.78) may not guarantee the stability of the estimation error of the MHE-PE theoretically. However, during the study we observe that even when $\alpha_{MHE-PE} > 1$, the MHE-PE still provides small estimation errors. This is in fact because of the value of theoretical μ that verifies the stability condition (4.68) is computed using bounds on many variables. Hence, it represents a pessimistic case where the value of μ tends to be very small, i.e. the pre-estimator is "not much observable".

4.7.4 Performances of the Estimators

The accuracy of the estimates are studied in terms of Root Mean Square Error (RMSE) and the Asymptotic Root Mean Square Error (ARMSE) defined in (3.37) and (3.38) respectively. In this study, the non-divergence percentage is equal to 100% for every estimator. Therefore the number of the non-divergence runs is equal to the number of the Monte Carlo runs which is equal to 100. Recall that $x_{i,k}$ is the state and $\hat{x}_{i,k}$ is the estimate, both of the i^th component of the state at instant k. We have

$$RMSE(\hat{x}_{i,k}) = \sqrt{\sum_{n=1}^{100} \frac{(\hat{x}_{i,k}^n - x_k^n)^2}{100}} \tag{4.79}$$

Recall that the ARMSE of the estimate is

$$ARMSE(\hat{x}_{i,k}) = \sum_{k=0}^{k_f} \frac{RMSE(\hat{x}_{i,k})}{k_f + 1} \tag{4.80}$$

where k_f is the discrete-time index of the final instant t_f.

Define $\|RMSE(\hat{x})\| = \left\| \begin{pmatrix} RMSE(\hat{x}_{1,k}) & \dots & RMSE(\hat{x}_{n_x,k}) \end{pmatrix}^T \right\|$ the norm of the RMSE of the estimate and $\|ARMSE(\hat{x})\| = \left\| \begin{pmatrix} ARMSE(\hat{x}_{1,k}) & \dots & ARMSE(\hat{x}_{n_x,k}) \end{pmatrix}^T \right\|$ the norm of the RMSE of the estimate.

The values of $\|RMSE(\hat{x})\|$ of the RMSE provided by each estimator are shown in figure 4.3. In this study, the theoretical upper bound on the estimation errors is found to be much larger than the real estimation errors so it is not given in figure 4.3. The values of $\|ARMSE(\hat{x})\|$ and the computation times per iteration (min, mean and max) are presented in table 4.1.

Thanks to figure 4.3 and table 4.1, we can remark that

1. the EKF gives high RMSE
2. the deterministic observer gives small RMSE at the end but it converges slowly. The MHE-PEs with $N = 20$ and provide less estimation errors than the deterministic observer and can be implemented in real-time since its computation time is smaller than the sampling period $T_s = 0.1\ s$. It is therefore interesting to implement the MHE-PE with a sufficiently high horizon rather than the deterministic observer.

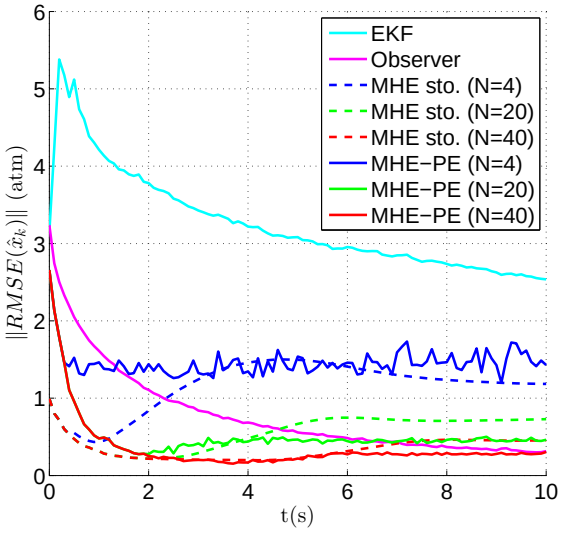

Figure 4.3: RMSE given by each tested estimator

Estimator	$\|ARMSE(\hat{x})\|$ (atm)	min time/ite. (s)	mean time/ite. (s)	max time/ite. (s)
EKF	3.26	$3.06 \cdot 10^{-5}$	$3.42 \cdot 10^{-5}$	$1.61 \cdot 10^{-4}$
Deter. Observer	0.80	$2.31 \cdot 10^{-6}$	$5.13 \cdot 10^{-6}$	$2.28 \cdot 10^{-5}$
MHE sto. (N=4)	1.16	0.08	0.12	0.14
MHE sto. (N=20)	0.56	1.30	2.50	3.82
MHE sto. (N=40)	0.34	4.26	6.24	7.65
MHE-PE (N=4)	1.46	0.05	0.06	0.37
MHE-PE (N=20)	0.51	0.07	0.09	0.39
MHE-PE (N=40)	0.36	0.09	0.11	0.42

Table 4.1: Norm of the ARMSE of the estimate and min, max and mean computation times per iteration of each estimator

3. from figure 4.3, we observe that for $N = 20$ and $N = 40$, the MHE-PE provides less RMSE of the estimate than the MHE. This may be due to the fact that the MHE has a large number of optimization parameters and the optimization algorithm find a local optimum instead of the global one.

4. the MHE-PE requires much less computation time than the MHE and provides better accuracy of the estimates for $N = 20$ and $N = 40$.

5. we can observe that the accuracy of the estimates of the MHE-PE and the MHE becomes better when the horizon length N is larger. However, the larger horizon induces large computation time, too. A compromise must therefore be made.

To conclude, the MHE-PE leads to a good trade-off between accuracy and small computation time making it an interesting alternative to MHE strategy for discrete-time nonlinear systems under bounded noise, for which a pre-estimator verifying (C4)-(C7) can be designed. Therefore, the MHE-PE can be considered as an alternative estimator to save computation time which opens the possibilities of real-time applications of Moving

Horizon strategies. In the next chapter, we will implement the MHE-PE to the 3D space debris tracking problem during atmospheric re-entries.

4.8 Conclusions

In this chapter,

- we develop a new Moving Horizon strategy to reduce the computation time of the "classical" MH strategies. This strategy is called "the Moving Horizon Estimator with Pre-Estimation" (MHE-PE). The MHE-PE uses an auxiliary estimator, called the pre-estimator, to propagate the estimate over the horizon. The pre-estimator in the MHE-PE is initialized at the beginning of the horizon by minimizing a cost function 4.4b. This pre-estimator helps to compensate for model errors without having to estimate the optimal process noise sequence over the horizon. Hence, the number of parameters to be optimized is reduced and the MHE-PE requires smaller computation time compared to the classical MHEs

- we prove the stability of the dynamics of the estimation errors of the MHE-PE when the conditions described in section 4.4 are verified and the weight matrix satisfies an inequality (4.68).

- the performance of the proposed MHE-PE offers a good trade-off between accuracy of the estimates and small computation time compared to the classical MHE. The MHE-PE can be considered as an alternative estimator to save computation time which opens the possibilities of real-time applications of Moving Horizon strategies.

CHAPTER 5

MHE-PE for 3D Space Debris Tracking during Atmospheric Re-Entries

"When it is obvious that the goals cannot be reached, don't adjust the goals, adjust the action steps."

— Confucius

Objective of this Chapter

- To analyze the performances of the Moving Horizon Estimator with Pre-Estimation (MHE-PE) developed in chapter 4 for space debris tracking during the re-entries in 3 dimensional cases compared to classical estimators such as the Extended Kalman Filter (EKF), the Unscented Kalman Filter (UKF), the Regularized Particle Filter (RPF) and the Moving Horizon Estimator (MHE). The performances will be compared in terms of non-divergence percentage, accuracy of the estimates and computation time.

5.1 Introduction

In this chapter we study the performances of the MHE-PE for space debris tracking during the re-entry in 3 dimensional cases compared to the EKF, the UKF, the RPF and the MHE. Only the MHE in the deterministic framework will be tested thanks to its higher robustness with respect to model errors compared to the MHE in the stochastic framework as seen in section 3.7. In addition, only the estimation model including acceleration will be used since it overcomes the model with ballistic coefficient in terms of non-divergence percentages, robustness against a bad choice of process noise parameter and robustness against bad initialization.

The chapter is organized as follows. First, we recall briefly the dynamics of the space debris during the re-entries and the equation of the radar measurements in function of the position of the debris in 3D cases. Second, we describe how we simulate the trajectories of the debris. They will be considered as the "real trajectories" for the study. Third, we recall briefly the estimation model that will be used in the estimators. Fourth, we show how to initialize and tune the estimators. Finally, we study the performances of the estimators in terms of non-divergence percentage, accuracy of the estimates and computation time.

5.2 Dynamics of 3D Space Debris during the Re-entries and Measurement Equation

5.2.1 Dynamics of 3D Space Debris during the Re-entries

The lectures are invited to review the hypotheses on the dynamics of space debris during the re-entry as well as the derivation of the dynamic equation in section 1.2.1.

As defined in section 1.2.1, $\mathbf{r}_{EF}$, $\mathbf{v}_{EF}$ and $\mathbf{a}_{EF}$ are the position, the velocity and the acceleration of the debris in the ECEF coordinates respectively. H is the altitude of the object defined as

$$H(\mathbf{r}_{EF}(t)) = \|\mathbf{r}_{EF}(t)\| - R_E \tag{5.1}$$

where R_E is the mean Earth radius.

The ballistic coefficient β of the object is defined as

$$\beta(t) = \frac{m(t)}{C_D(t)A(t)} \tag{5.2}$$

where m is the mass of the object, A is the cross section and C_D is the drag coefficient of the object.

The dynamics of the object is described by

$$\mathbf{a}_{EF}(t) = -\frac{G_E M}{\|\mathbf{r}_{EF}(t)\|^3}\mathbf{r}_{EF}(t) - \frac{\rho(H(\mathbf{r}_{EF}(t)))}{2\beta(t)}\|\mathbf{v}_{EF}(t)\|\mathbf{v}_{EF}(t) \tag{5.3}$$

The first term on the r.h.s. represents the gravity and the second term represents the acceleration due to the drag. G_E is the Earth's gravitational constant, M is the mass of the Earth. The atmosphere density ρ depends on the altitude of the object H, modeled by

$$\rho(H(t)) = \mathsf{c}_1 e^{-\mathsf{c}_2 H(t)} \tag{5.4}$$

$\mathsf{c}_1 = 1.227\ kg/m^3$, $\mathsf{c}_2 = 1.093 \cdot 10^{-4}\ m^{-1}$ for $H < 9144\ m$ and $\mathsf{c}_1 = 1.754\ kg/m^3$, $\mathsf{c}_2 = 1.490 \cdot 10^{-4}\ m^{-1}$ for $H \geq 9144\ m$ [Farina et al., 2002].

We recall that the evolution of $\beta(t)$ is generally unknown. This will prevent us from having an estimation model that describes the real dynamics of the debris. Estimation problem in space debris during the re-entry therefore suffers from model errors. The trajectory estimation of the debris will be done using radar measurements. Let us discuss the measurement equation of the problem.

5.2.2 Measurement Equation for 3D Space Debris Tracking during the Re-entries

Recall that $\mathbf{r}$, $\mathbf{v}$ and $\mathbf{a}$ are the position, the velocity and the acceleration of the debris in the SEU coordinates respectively. Recall that the SEU coordinates are centered at the radar station S with axes along the south, east and up directions. The radar measurements are supposed to be available every T_s second. Define $\mathbf{r}_k = \mathbf{r}(t = kT_s)$, $k \in \mathbb{N}$. As described in

section 1.2.2, the discrete-time measurement vector at instant k is defined as

$$y_k = h(x_k) + v_k = \begin{pmatrix} d_k^m \\ el_k^m \\ az_k^m \end{pmatrix} = \begin{pmatrix} d_k \\ el_k \\ az_k \end{pmatrix} + v_k = \begin{pmatrix} \sqrt{r_{x_k}^2 + r_{y_k}^2 + r_{z_k}^2} \\ \arcsin(\frac{r_{z_k}}{d_k}) \\ \arctan(\frac{r_{y_k}}{-r_{x_k}}) \end{pmatrix} + v_k \tag{5.5}$$

where

$$d_k = \sqrt{r_{x_k}^2 + r_{y_k}^2 + r_{z_k}^2} \tag{5.6}$$

$$el_k = \begin{cases} \arcsin(\frac{r_{z_k}}{d_k}) & \text{if } r_{z_k} \neq d_k \\ \frac{\pi}{2} & \text{otherwise} \end{cases} \tag{5.7}$$

$$az_k = \arctan(\frac{r_{y_k}}{-r_{x_k}}) \tag{5.8}$$

d is the distance, el is the elevation angle and az is the azimuth angle, all between the debris and the radar station. The superscribe m stands for "measured". v_k is a discrete-time measurement noise modeled by a zero-mean bounded white noise with covariance matrix.

$$R = \begin{pmatrix} \sigma_d^2 & 0 & 0 \\ 0 & \sigma_{el}^2 & 0 \\ 0 & 0 & \sigma_{az}^2 \end{pmatrix} \tag{5.9}$$

where σ_d, σ_{el} and σ_{az} are the standard deviations associated to the measurement errors.

Now that the dynamic of space debris and the measurement equation for the 3D re-entry cases have been discussed, let us discuss how we simulate the trajectories of the debris. These simulated trajectories will be considered as the "real trajectories". Then, we simulate associated radar measurements from the simulated trajectories and give them to the estimators to study their performances. The position, the velocity and the acceleration of the debris in the SEU coordinates will be estimated. Remark that the measurements are actually the position vector in the spherical coordinates (with measurement noises).

5.3 Simulation of the Trajectories of 3D Space Debris during the Re-entries

Since we do not have access to real debris re-entry data, we will use the dynamic equation in (5.3) to simulate the "considered to be real" trajectories of 100 spherical objects during the re-entries using Monte Carlo simulations by integrating the dynamic equation of the debris (5.3) using an ordinary differential equation initial value problem solver in MATLAB with an interval of integration of 10^{-3} s. The spherical shape is chosen because the evolution of the drag coefficient C_D is known. We suppose that the density of the object is known. We also suppose that the mass m and the cross section A of the debris are constant during the re-entry. After that, the radar measurements in discrete-time will be simulated using (5.5). The trajectory estimation problem will be done by giving these discrete-time radar measurements to the tested estimators which are also in discrete-time.

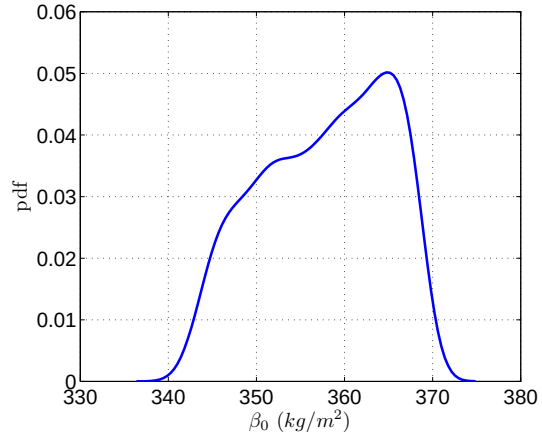

Figure 5.1: *Distribution of the initial ballistic coefficient of hollow Aluminium spheres of width 3 cm whose initial altitudes are drawn from* $H \sim \mathbf{U}(69, 70)$ *km, whose speeds are drawn from* $\|\mathbf{v}_{EF_0}\| \sim \mathbf{U}(5000, 10000)$ *m/s and whose outer diameters are drawn from* $D \sim \mathbf{U}(20, 30)$ *cm. The mass of the debris* $m \in [7.43, 18.63]$ *kg.*

5.3.1 Initial Conditions of the Objects

The trajectories of 100 Aluminium hollow-spherical objects of width $w = 3$ *cm* are simulated via Monte Carlo simulations. Each object has different initial altitude H_0, initial longitude λ_{D_0}, initial latitude ϕ_{D_0}, initial flight path angle γ_0: angle between the local horizontal plane and the velocity of the object (see figure 5.2), initial heading angle θ_0: angle between the north direction and the projection of the velocity vector on the horizontal plane, initial speed $\|\mathbf{v}_{EF_0}\|$, which is equal to $\|\mathbf{v}_0\|$ thanks to (1.11), and outer diameter D. The initial mass of the debris is calculated using (3.6). Recall that m and D are supposed to be constant during the re-entry.

The quantities H_0, λ_{D_0}, ϕ_{D_0}, γ_0, θ_0, $\|\mathbf{v}_{EF_0}\|$, D are generated according to the following uniform distributions: $H_0 \sim \mathbf{U}(69, 70)$ *km*, $\lambda_{D_0} \sim \mathbf{U}(2.284443°, 2.407881°)$, $\phi_{D_0} \sim \mathbf{U}(48.820315°, 48.897227°)$, $\gamma_0 \sim \mathbf{U}(-30°, -80°)$, $\theta_0 \sim \mathbf{U}(20°, 40°)$, $\|\mathbf{v}_{EF_0}\| \sim \mathbf{U}(5000, 10000)$ *m/s* and $D \sim \mathbf{U}(0.2, 0.3)$ *m*. These ranges of λ_{D_0} and ϕ_{D_0} represent in fact the ranges of latitude and longitude covering Paris. It will be assumed that the radar station is located at the center of Paris afterwards. The used distribution of D gives the distribution of the mass $m \sim \mathbf{U}(7.43, 18.63)$ *kg*. The initial ballistic coefficients β_0 of the debris are computed using equations in appendix C.1. The distribution of the generated β_0 is shown in figure 5.1. The mean of the distribution is equal to 357.7257 kg/m^2 and the standard deviation of the distribution is equal to 7.1936 kg/m^2.

The initial position of the debris in the ECEF coordinates $\mathbf{r}_{EF_0}$ can be computed from (see figure 5.2 (left)):

$$\mathbf{r}_{EF_0} = (H_0 + R_E) \begin{pmatrix} \cos\phi_{D_0} \cos\lambda_{D_0} \\ \cos\phi_{D_0} \sin\lambda_{D_0} \\ \sin\phi_{D_0} \end{pmatrix} \tag{5.10}$$

Consider the SEU_D coordinates centered at the center of mass of the debris D with unit vectors along the south, the east and the up directions (see figures 5.2 (right)). Denote $\vec{e}_{south_D}$, $\vec{e}_{east_D}$ and $\vec{e}_{up_D}$ the unit vectors of the SEU_D coordinates. They are related to the unit vectors of the ECEF coordinates as

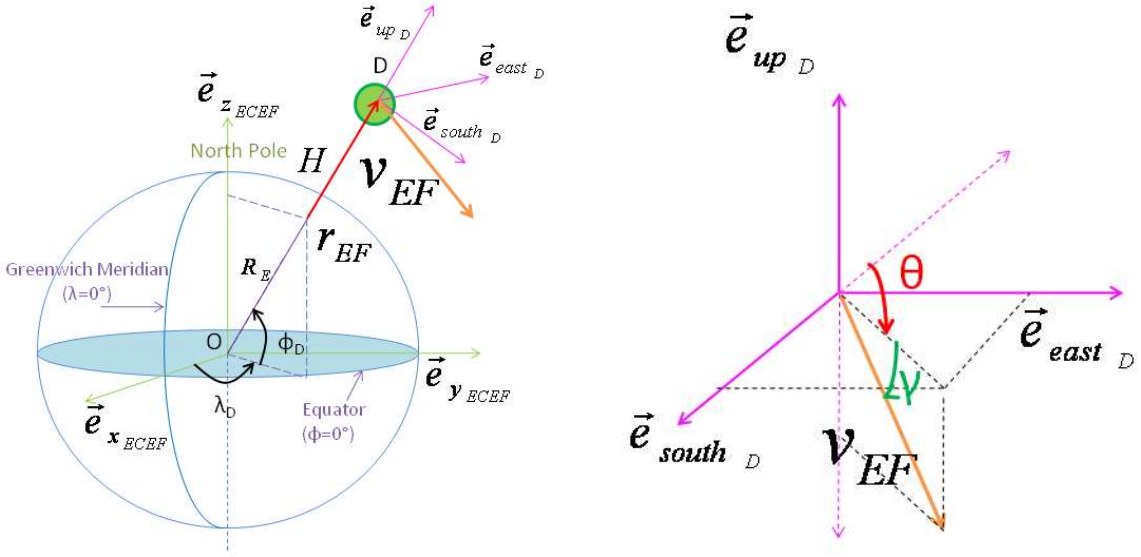

Figure 5.2: *Given the altitude H, the speed $\|\mathbf{v}_{EF}\|$, the longitude λ_D, the latitude ϕ_D, the flight path angle γ and the heading angle θ of the object D, the position $\mathbf{r}_{EF}$ and the velocity $\mathbf{v}_{EF}$ in the ECEF coordinates can be calculated using* (5.10) *and* (5.13)

$$\begin{pmatrix} \vec{e}_{south_D} \\ \vec{e}_{east_D} \\ \vec{e}_{up_D} \end{pmatrix} = \begin{pmatrix} sin\phi_D cos\lambda_D & sin\phi_D sin\lambda_D & -cos\phi_D \\ -sin\lambda_D & cos\lambda_D & 0 \\ cos\phi_D cos\lambda_D & cos\phi_D sin\lambda_D & sin\phi_D \end{pmatrix} \begin{pmatrix} \vec{e}_{x_{ECEF}} \\ \vec{e}_{y_{ECEF}} \\ \vec{e}_{z_{ECEF}} \end{pmatrix} \tag{5.11}$$

Remark that the velocity in the ECEF coordinates $\mathbf{v}_{EF}$ can be described in the SEU_D coordinates as (see fig.5.2)

$$\mathbf{v}_{EF} = -\|\mathbf{v}_{EF}\| cos\gamma cos\theta \vec{e}_{south_D} + \|\mathbf{v}_{EF}\| cos\gamma sin\theta \vec{e}_{east_D} + \|\mathbf{v}_{EF}\| sin\gamma \vec{e}_{up_D} \tag{5.12}$$

Replace (5.11) in (5.12), we get $\mathbf{v}_{EF}$ in the ECEF coordinates as

$$\mathbf{v}_{EF} = \begin{pmatrix} -\|\mathbf{v}_{EF}\| cos\gamma cos\theta sin\phi_D cos\lambda_D - \|\mathbf{v}_{EF}\| cos\gamma sin\theta sin\lambda_D + \|\mathbf{v}_{EF}\| sin\gamma cos\phi_D cos\lambda_D \\ \|\mathbf{v}_{EF}\| cos\gamma sin\theta sin\phi_D sin\lambda_D + \|\mathbf{v}_{EF}\| cos\gamma sin\theta cos\lambda_D + \|\mathbf{v}_{EF}\| sin\gamma cos\phi_D sin\lambda_D \\ -\|\mathbf{v}_{EF}\| cos\gamma cos\theta - cos\phi_D + \|\mathbf{v}_{EF}\| sin\gamma sin\phi_D \end{pmatrix} \tag{5.13}$$

5.3.2 Simulated Trajectories and Measurements

Using all the initial conditions, the trajectories of the 100 objects are simulated by integrating the dynamic equation of the debris in the ECEF coordinates (5.3) using an ordinary differential equation initial value problem solver in MATLAB with an interval of integration of 10^{-3} s for 20 seconds of the re-entry. Recall that the position $\mathbf{r}$, the velocity $\mathbf{v}$ and the acceleration $\mathbf{a}$ in the SEU coordinates can be computed from the values in the ECEF coordinates using the coordinate transformation equation (1.10). The evolutions of $\mathbf{r}$, $\mathbf{v}$ and $\mathbf{a}$ as well as the ballistic coefficient β with time are shown in fig.5.3. In this figure, the minimum, the mean and the maximum of the variables among the 100 simulated trajectories at each instant are plotted.

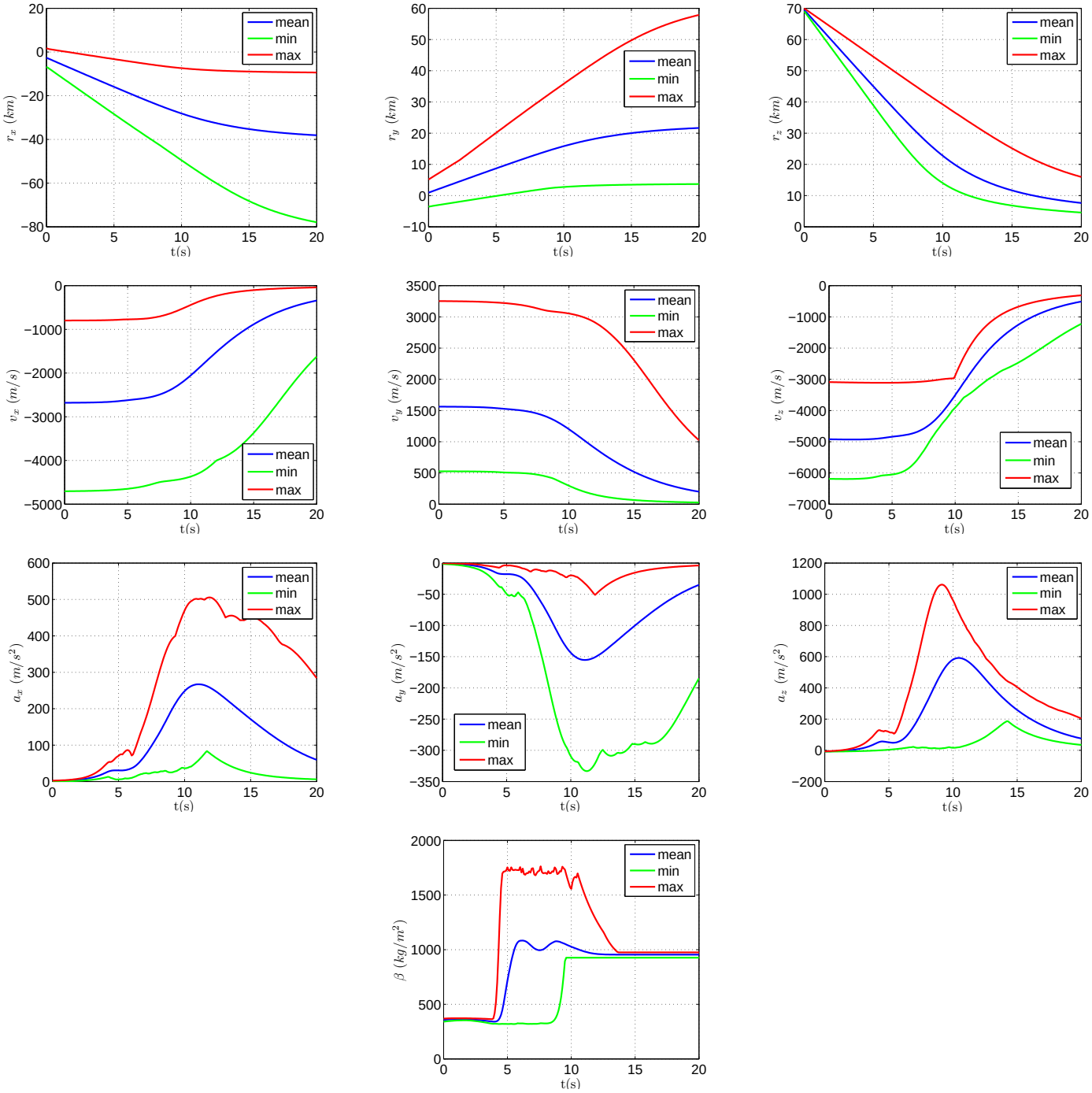

Figure 5.3: *The minimum, the mean and the maximum among the* 100 *simulated trajectories at each instant of the time evolution of the components of the position* $\mathbf{r}$*, the velocity* $\mathbf{v}$*, the acceleration* $\mathbf{a}$ *in the SEU coordinates and the ballistic coefficient* β

These generated trajectories are considered as the real trajectories of the space debris. Associated radar measurements are simulated using (5.5). The standard deviation associated to the distance measurement noise σ_d is chosen equal to 10 m. Those associated to the angle measurement noise σ_{el} and σ_{az} are chosen equal to 0.005°. The measurements are available every $T_s = 0.1$ s. These values of σ_d, σ_{el} and σ_{az} have the same order as the resolution of the German Tracking and Imaging Radar (TIRA) and the ESA's ARMOR Radar [Alarcón et al., 2005].

5.4 Estimation Model with Acceleration for 3D Space Debris Tracking during the Re-entries

Recall that the position, the velocity and the acceleration of the debris will be estimated in the SEU coordinates. The state vector in discrete-time is defined as

$$x_k = \begin{pmatrix} \mathbf{r}_k^T & \mathbf{v}_k^T & \mathbf{a}_k^T \end{pmatrix}^T \tag{5.14}$$

It is assumed that $\forall \tau \in [kT_s, (k+1)T_s]$:

$$\dot{\mathbf{a}}(t) = \mathbf{f}_k + \boldsymbol{\xi}(t), \tag{5.15}$$

where denote $\mathbf{f}_k \triangleq \begin{pmatrix} f_{x_k} & f_{y_k} & f_{z_k} \end{pmatrix}^T$, we have

$$f_{x_k} = -\mathsf{c}_2 a_{x_k} v_{z_k} + a_{x_k}\left[a_{x_k}\left(\frac{1}{v_{x_k}} + \frac{v_{x_k}}{\|\mathbf{v}_k\|^2}\right) + a_{y_k}\frac{v_{y_k}}{\|\mathbf{v}_k^2\|} + a_{z_k}\frac{v_{z_k}}{\|\mathbf{v}_k\|^2}\right] \tag{5.16}$$

$$f_{y_k} = -\mathsf{c}_2 a_{y_k} v_{z_k} + a_{y_k}\left[a_{x_k}\frac{v_{x_k}}{\|\mathbf{v}_k\|^2} + a_{y_k}\left(\frac{1}{v_{y_k}} + \frac{v_{y_k}}{\|\mathbf{v}_k\|^2}\right) + a_{z_k}\frac{v_{z_k}}{\|\mathbf{v}_k\|^2}\right] \tag{5.17}$$

$$f_{z_k} = \left(-\mathsf{c}_2 v_{z_k} + \left[a_{x_k}\frac{v_{x_k}}{\|\mathbf{v}_k\|^2} + a_{y_k}\frac{v_{y_k}}{\|\mathbf{v}_k\|^2} + a_{z_k}\left(\frac{1}{v_{z_k}} + \frac{v_{z_k}}{\|\mathbf{v}_k\|^2}\right)\right]\right)(a_{z_k} + g) \tag{5.18}$$

$\boldsymbol{\xi}(t)$ is a continuous zero-mean white noise of spectral density $\tilde{\mathbf{q}}$ representing errors from discretization **and** from the fact that β is actually not constant. In other words,

$$E\{\boldsymbol{\xi}(t)\boldsymbol{\xi}^T(\tau)\} = \tilde{\mathbf{q}}(t)\delta(t-\tau) \tag{5.19}$$

For the sake of simplicity, we assume $\tilde{\mathbf{q}}(t)$ to be constant equal to $\tilde{\mathbf{q}}$ and that each component of $\boldsymbol{\xi}$ is uncorrelated to each other. $\tilde{\mathbf{q}}$ can therefore be described as

$$\tilde{\mathbf{q}} = \begin{pmatrix} \tilde{q}_x & 0 & 0 \\ 0 & \tilde{q}_y & 0 \\ 0 & 0 & \tilde{q}_z \end{pmatrix} \tag{5.20}$$

where $\tilde{q}_x$, $\tilde{q}_y$ and $\tilde{q}_z$ are constant values.

$$x_{k+1} = \begin{pmatrix} \mathbf{I}_{3\times3} & T_s\mathbf{I}_{3\times3} & \frac{T_s^2}{2}\mathbf{I}_{3\times3} \\ \mathbf{0}_{3\times3} & \mathbf{I}_{3\times3} & T_s\mathbf{I}_{3\times3} \\ \mathbf{0}_{3\times3} & \mathbf{0}_{3\times3} & \mathbf{I}_{3\times3} \end{pmatrix} x_k + \begin{pmatrix} \frac{T_s^3}{6}\mathbf{f}_k \\ \frac{T_s^2}{2}\mathbf{f}_k \\ T_s\mathbf{f}_k \end{pmatrix} + w_k \tag{5.21}$$

where w_k is a discrete-time zero-mean bounded white noise whose covariance matrix is

$$Q = \begin{pmatrix} \frac{1}{20}T_s^5 & \frac{1}{8}T_s^4 & \frac{1}{6}T_s^3 \\ \frac{1}{8}T_s^4 & \frac{1}{3}T_s^3 & \frac{1}{2}T_s^2 \\ \frac{1}{6}T_s^3 & \frac{1}{2}T_s^2 & T_s \end{pmatrix} \otimes \tilde{\mathbf{q}} \tag{5.22}$$

The derivations of (5.21) and (5.22) are provided in appendix A.2.

The readers are invited to review section 1.3.2.3 for further details. Now, let us discussed how to compute the a priori initial estimates.

5.5 A Priori Initial Estimates

Let us denote the estimate of the state vector given by an estimator at each instant k as

$$\hat{x}_k = \begin{pmatrix} \hat{\mathbf{r}}_k \\ \hat{\mathbf{v}}_k \\ \hat{\mathbf{a}}_k \end{pmatrix} \tag{5.23}$$

and the a priori estimate at instant k as

$$\hat{x}_k^- = \begin{pmatrix} \hat{\mathbf{r}}_k^- \\ \hat{\mathbf{v}}_k^- \\ \hat{\mathbf{a}}_k^- \end{pmatrix} \tag{5.24}$$

In the same way, the a priori *initial* estimate will be denoted by

$$\hat{x}_0^- = \begin{pmatrix} \hat{\mathbf{r}}_0^- \\ \hat{\mathbf{v}}_0^- \\ \hat{\mathbf{a}}_0^- \end{pmatrix}$$

For each of the 100 generated trajectories, each estimator will be initialized with the **same** a priori initial estimate $\hat{x}_0^-$. First the initialization of the a priori initial position $\hat{\mathbf{r}}_0^-$ will be discussed, followed by those of the a priori initial velocity $\hat{\mathbf{v}}_0^-$ and of the a priori initial acceleration $\hat{\mathbf{a}}_0^-$

5.5.1 A Priori Initial Position and Velocity

Denote $\mathbf{r}_k^m$ the position of the debris calculated using the measurement

$$y_k = \begin{pmatrix} d_k^m & el_k^m & az_k^m \end{pmatrix}^T$$

where d_k^m is the distance measurement, el_k^m is the elevation angle measurement and az_k^m is the azimuth angle measurement, all at instant k.

$\mathbf{r}_k^m$ is related to the measurement y_k by

$$\mathbf{r}_k^m = \begin{pmatrix} r_{x_k}^m \\ r_{y_k}^m \\ r_{z_k}^m \end{pmatrix} = \begin{pmatrix} -d_k^m \cos el_k^m \cos az_k^m \\ d_k^m \cos el_k^m \sin az_k^m \\ d_k^m \sin el_k^m \end{pmatrix} \tag{5.25}$$

As proposed in [Park and Lee, 2001], the a priori initial position estimate $\hat{\mathbf{r}}_0^-$ is defined as

$$\hat{\mathbf{r}}_0^- = \begin{pmatrix} r_{x_0}^m & r_{y_0}^m & r_{z_0}^m \end{pmatrix}^T = \mathbf{r}_0^m \tag{5.26}$$

$\hat{\mathbf{v}}_0^-$ is initialized by *two-point differencing method* [Bar-Shalom et al., 2004]. The two-point differencing method consists in calculating the position of the object using the measurements at the initial instant 0 and at an instant before the initial instant denoted by[1] -1: y_0 and y_{-1}. The a priori initial velocity estimate $\hat{\mathbf{v}}_0^-$ is defined as

$$\hat{\mathbf{v}}_0^- = \begin{pmatrix} \frac{r_{x_0}^m - r_{x_{-1}}^m}{T_s} & \frac{r_{y_0}^m - r_{y_{-1}}^m}{T_s} & \frac{r_{z_0}^m - r_{z_{-1}}^m}{T_s} \end{pmatrix}^T \tag{5.27}$$

Define the a priori initial **error** vector on the position estimate and the velocity estimate as

$$\begin{pmatrix} \tilde{\mathbf{r}}_0^- \\ \tilde{\mathbf{v}}_0^- \end{pmatrix} = \begin{pmatrix} \hat{\mathbf{r}}_0^- \\ \hat{\mathbf{v}}_0^- \end{pmatrix} - \begin{pmatrix} \mathbf{r}_0 \\ \mathbf{v}_0 \end{pmatrix} \tag{5.28}$$

where $\mathbf{r}_0$ and $\mathbf{v}_0$ are the real initial position and velocity of the object.

Define $P_{\tilde{\mathbf{r}}_0^-, \tilde{\mathbf{v}}_0^-}$ the a priori initial error covariance matrix as the covariance matrix of $\begin{pmatrix} \tilde{\mathbf{r}}_0^- & \tilde{\mathbf{v}}_0^- \end{pmatrix}^T$. According to [Park and Lee, 2001], we have

$$P_{\tilde{\mathbf{r}}_0^-, \tilde{\mathbf{v}}_0^-} = \begin{pmatrix} \bar{R}_0^c & \bar{R}_0^c/T_s \\ \bar{R}_0^c/T_s & 2\bar{R}_0^c/T_s^2 \end{pmatrix} \tag{5.29}$$

where $\bar{R}_0^c$ is the variance of the noise on the "measured" initial position $\mathbf{r}_0^m$, or equivalently the a priori initial position estimate $\hat{\mathbf{r}}_0^-$. For $\sigma_d \ll d_k$ and $\sigma_{el}, \sigma_{az} \ll 1$, $\bar{R}_0^c$ is computed from

$$\bar{R}_0^c = J_0 \begin{pmatrix} \sigma_d^2 + (d_0^m)^2 \frac{(\sigma_{el}^4 + \sigma_{az}^4)}{2} & 0 & 0 \\ 0 & \sigma_{el}^2 & 0 \\ 0 & 0 & \sigma_{az}^2 \end{pmatrix} J_0^T \tag{5.30}$$

J_0 is computed from

$$J_0 = \begin{pmatrix} \partial r_x/\partial d & \partial r_x/\partial el & \partial r_x/\partial az \\ \partial r_y/\partial d & \partial r_y/\partial el & \partial r_y/\partial az \\ \partial r_z/\partial d & \partial r_z/\partial el & \partial r_z/\partial az \end{pmatrix} \tag{5.31}$$

computed at $\begin{pmatrix} d & el & az \end{pmatrix}^T = y_0$ The distances of the simulated trajectories are plotted in figure 5.4 where we can observe that $d_k > 10^4\ m$. Recall that $\sigma_d = 10\ m$ and $\sigma_{el} = \sigma_{az} = 0.005° = 8.7266 \cdot 10^{-5}$, $\sigma_d \ll d_k$ and $\sigma_{el}, \sigma_{az} \ll 1$ in our study.

To summarize, we use (5.26) and (5.27) to initialize the a priori initial position estimate $\hat{\mathbf{r}}_0^-$ and the a priori initial velocity estimate $\hat{\mathbf{v}}_0^-$ respectively.

The covariance matrix of the errors $\begin{pmatrix} \tilde{\mathbf{r}}_0^{-T} & \tilde{\mathbf{v}}_0^{-T} \end{pmatrix}^T$ is defined as in (5.29). Now, let us discuss the a priori initial estimate on the acceleration.

[1] In other words, the estimation can begin after the acquisition of at least two measurements. In this study, the first instant of the estimation is defined as the initial instant or instant 0.

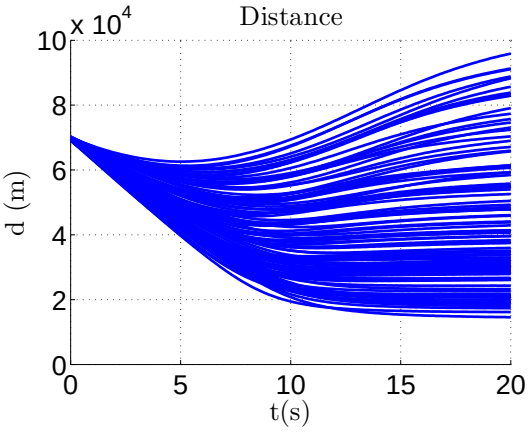

Figure 5.4: Evolution of distance in time for the simulated trajectories.

5.5.2 A Priori Initial Acceleration

5.5.2.1 Main idea

The idea is to specify a distribution of possible values of the initial ballistic coefficient β_0, then choose a value of an a priori initial ballistic coefficient estimate $\hat{\beta}_0^-$ from this supposed distribution, for example the mean of the distribution. Finally, we compute the a priori initial acceleration estimate $\hat{\mathbf{a}}_0^-$ using

$$\hat{\mathbf{a}}_0^- = -\frac{c_1 e^{-c_2 \hat{r}_{z_0}^-} \left\| \hat{\mathbf{v}}_0^- \right\|}{2\hat{\beta}_0^-} \hat{\mathbf{v}}_0^- + \begin{pmatrix} 0 \\ 0 \\ -g \end{pmatrix} \tag{5.32}$$

the standard deviation of the error of the a priori initial acceleration $\hat{\mathbf{a}}_0^-$ will be chosen from a given distribution of a_0 which is computed by using the supposed distribution of β_0 using

$$a_0 = -\frac{c_1 e^{-c_2 r_{z_0}} \left\| \mathbf{v}_0 \right\|}{2\beta_0} \mathbf{v}_0 + \begin{pmatrix} 0 \\ 0 \\ -g \end{pmatrix} \tag{5.33}$$

5.5.2.2 Choice of the a priori initial ballistic coefficient estimate $\hat{\beta}_0^-$

To derive a distribution of possible values of the initial ballistic coefficient β_0, one can make assumptions that the distributions of the mass, the cross section and the drag coefficient of the object are known. For example, we can suppose that $m \sim \mathbf{U}(m_{min}, m_{max})$, $A \sim \mathbf{U}(A_{min}, A_{max})$ and $C_D \sim \mathbf{U}(C_{D_{min}}, C_{D_{max}})$ and then simulate the distribution of the possible β_0 using (5.2).

If the shape and the density of the object are known, we can have the relation between m and A. For an object whose shape is nearly spherical, we can compute its C_D using (C.2). In this case we have to suppose a distribution on the altitude and the velocity of the object. For other types of objects, a table of *average* values of C_D for various shapes resulting from experiments is available in [Moe et al., 1995].

For a catalogued object, a value of the initial ballistic coefficient estimate is given in the Two-Line Element set which is the collection of estimates on the orbital elements giving a priori values of the position, the velocity and the ballistic coefficient. However,

the standard deviations of the errors of these a priori values are not available. In [Sang et al., 2013] a method to estimate ballistic coefficients of low altitude debris from historical two-line elements is proposed. Note that in case of an object created from a breakup, TLE data are not available.

5.5.2.3 Error Covariance of the a Priori Initial Acceleration Estimate

The errors on the a priori initial acceleration estimate $\hat{\mathbf{a}}_0^-$ depend on the errors on the a priori initial ballistic coefficient estimate $\hat{\beta}_0^-$. Define $\tilde{\mathbf{a}}_0^- = \hat{\mathbf{a}}_0^- - \mathbf{a}_0$ the error on the a priori initial acceleration estimate and $\sigma_{\tilde{a}_{0_{x,y,z}}^-}$ the standard deviation of each component of $\tilde{\mathbf{a}}_0^-$. Denote $P_{\tilde{\mathbf{a}}_0^-}$ the error covariance matrix of the a priori initial acceleration estimation error. By supposing that each component of the errors is non-correlated, we have

$$P_{\tilde{\mathbf{a}}_0^-} = \begin{pmatrix} \sigma_{\tilde{a}_{0_x}^-} & 0 & 0 \\ 0 & \sigma_{\tilde{a}_{0_y}^-} & 0 \\ 0 & 0 & \sigma_{\tilde{a}_{0_z}^-} \end{pmatrix} \tag{5.34}$$

$\sigma_{\tilde{a}_{0_{x,y,z}}^-}$ is chosen from a supposed distribution of a_0 which is computed using the supposed distribution β_0 chosen as discussed in the previous section.

5.5.3 A Priori Initial Error Covariance Matrix

Denote P_0^- the a priori initial error covariance matrix of the a priori initial estimate $\hat{x}_0^-$. the a priori initial position and velocity estimates $\hat{\mathbf{r}}_0^-$, $\hat{\mathbf{v}}_0^-$ are computed from the measurements alone so they do not depend on the a priori initial acceleration $\hat{\mathbf{a}}_0^-$, we have

$$P_0^- = \begin{pmatrix} \bar{R}_0^c & \bar{R}_0^c/T_s & 0_{3\times3} \\ \bar{R}_0^c/T_s & 2\bar{R}_0^c/T_s^2 & 0_{3\times3} \\ 0_{3\times3} & 0_{3\times3} & P_{\tilde{\mathbf{a}}_0^-} \end{pmatrix} \tag{5.35}$$

where $\bar{R}_0^c$ is computed from (5.30) and $P_{\tilde{\mathbf{a}}_0^-}$ is computed from (5.34).

5.5.4 Test of Robustness against Bad Initialization of the Estimators

In the same way as in section 3.5.2.2 to study the robustness of the estimators against bad initialization, it is supposed that the debris is known to be a hollow spherical debris of width 3 cm, starting at the altitude of $H \sim \mathbf{U}(69, 70)$ km and having the speed of $\|\mathbf{v}\|_0 \sim \mathbf{U}(5000, 10000)$ m/s. Two cases of initialization of the a priori initial ballistic coefficient $\hat{\beta}_0^-$ will be studied:

- Good initialization case: in this case $\hat{\beta}_0^-$ is chosen equal to the mean of the distribution of the ballistic coefficients of the real trajectories presented in figure 5.5 (left). In this good initialization case, $\hat{\beta}_0^-$ is chosen equal to 357 kg/m^2. Recall that the real distribution of $D \sim \mathbf{U}(20, 30)$ cm gives the distribution of the mass $m \in [7.43, 18.63]$ kg.

- Bad initialization case: in this case, we imitate a case in which a wrong assumption on the diameters of the debris D is made, which is possible in reality. In this study, it is supposed that $D \sim \mathbf{U}(80, 100)$ cm instead of the real distribution $\mathbf{U}(20, 30)$ cm. The "supposed" distribution of β_0 with this wrong assumption on D is presented in figure 5.5 (right). In this bad initialization case, $\hat{\beta}_0^-$ is chosen equal to 396.5 kg/m^2.

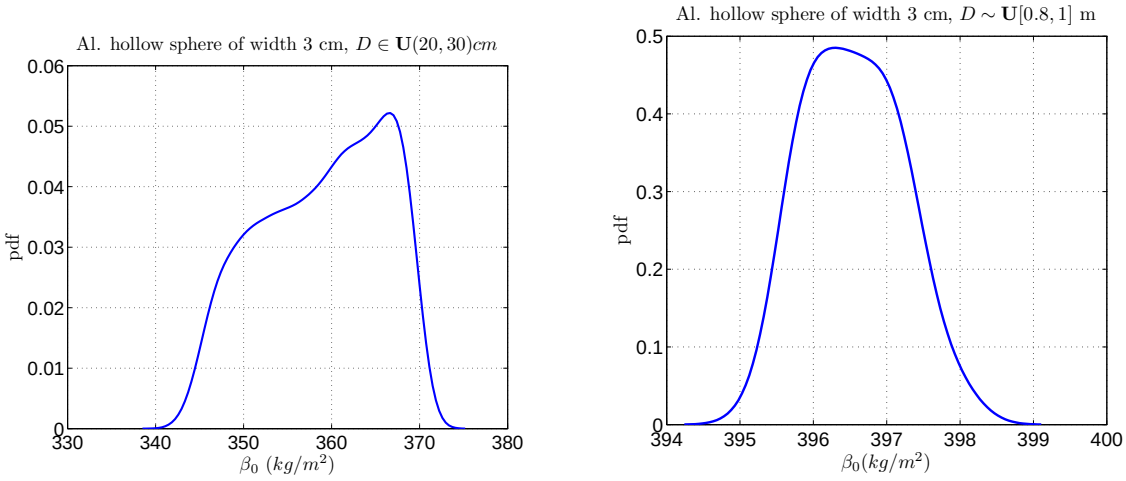

Figure 5.5: *The distribution of the real initial ballistic coefficient β_0 of hollow Aluminium spheres generated using initial conditions in section 5.3.1 with the real distribution of the outer diameter $\mathbf{U}(20,30)$ cm (left) and with the "wrong" distribution $D \sim \mathbf{U}(80,100)$ cm instead (right).*

With this wrong assumption on D, the mass is supposed to be $m \in [150.95, 239.51]$ kg instead of the real distribution $m \in [7.43, 18.63]$ kg.

5.6 Tunings of the Estimators

5.6.1 Common Tunings for All the Estimators

For each run, the following noise covariance matrices are given to each estimator:

5.6.1.1 Sampling period

The sampling period of the estimator T_s is chosen equal to the period of measurements. In our studies, $T_s = 0.1$ s.

5.6.1.2 Measurement noise covariance matrix

$$R = \begin{pmatrix} \sigma_d^2 & 0 & 0 \\ 0 & \sigma_{el}^2 & 0 \\ 0 & 0 & \sigma_{az}^2 \end{pmatrix} \tag{5.36}$$

where $\sigma_d = 10\ m$ and $\sigma_{el} = \sigma_{az} = 0.005^\circ$ are chosen.

5.6.1.3 Process noise covariance matrix

$$Q = \begin{pmatrix} \frac{1}{20}T_s^5 & \frac{1}{8}T_s^4 & \frac{1}{6}T_s^3 \\ \frac{1}{8}T_s^4 & \frac{1}{3}T_s^3 & \frac{1}{2}T_s^2 \\ \frac{1}{6}T_s^3 & \frac{1}{2}T_s^2 & T_s \end{pmatrix} \otimes \begin{pmatrix} \tilde{q}_x & 0 & 0 \\ 0 & \tilde{q}_y & 0 \\ 0 & 0 & \tilde{q}_z \end{pmatrix} \tag{5.37}$$

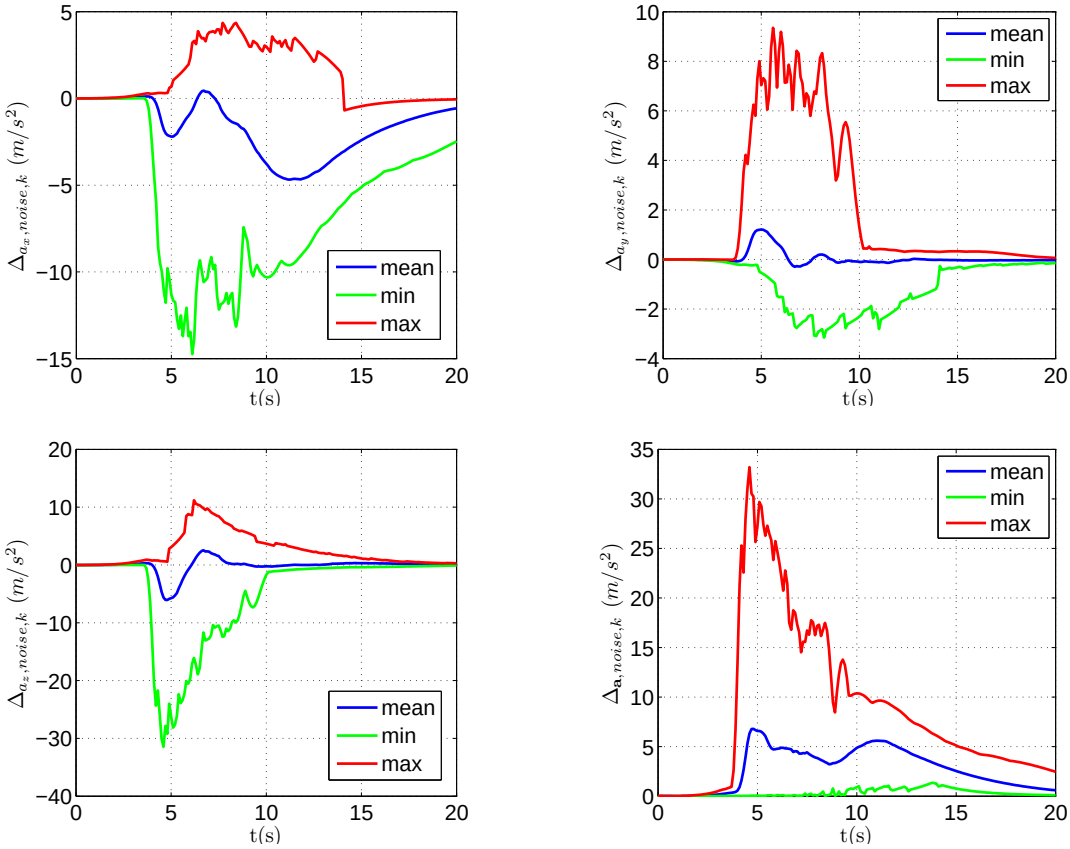

Figure 5.6: *Evolution of the mean, the minimum and the maximum of the acceleration variation due to process noise* $\Delta_{a_{x,y,z},noise,k}$ *and of* $\|\Delta_{\mathbf{a},noise,k}\|$ *for the 100 generated "considered to be real" trajectories at each instant* k

As discussed in 1.3.2.3, $\tilde{q}_{x,y,z}$ should be chosen such that $\sqrt{\tilde{q}_{x,y,z}T_s}$ has the same order of magnitude as the changes in the components of the acceleration not taken into account in the estimation model over a sampling period: $\Delta_{a_{x,y,z},noise,k}$ as defined in (1.46), $\forall k$. However, in reality, the quantity $\Delta_{a_{x,y,z},noise,k}$ is unknown for space debris and an arbitrary value of $\tilde{q}_{x,y,z}$ must be chosen. As a consequence, a to-be-used estimator for space debris tracking durign the re-entries must be robust againt a bad choice of process noise parameter.

Fig. 5.6 shows the evolution of the mean, the minimum and the maximum of the acceleration variation not taken into account in the estimation model $\Delta_{a_{x,y,z},noise,k}$ and of the norm of $\Delta_{\mathbf{a},noise,k}$ among the 100 generated "considered-to-be" real trajectories at each instant k. However, in reality, these values are not available due to the unknown dynamics of $\beta(t)$. Therefore, an arbitrary value for $\tilde{\mathbf{q}}$ has to be chosen. Moreover, as we can see in fig. 5.6, the values of $\Delta_{a_{x,y,z},noise,k}$ can vary in time so a single value of $\tilde{\mathbf{q}}$ will not be appropriate during the whole re-entries phase. An estimator which is robust against a poor choice of $\tilde{\mathbf{q}}$ should therefore be implemented.

In this study, since $\Delta_{a_x,noise}$, $\Delta_{a_y,noise}$ and $\Delta_{a_z,noise}$ have the same order of magnitude, for the sake of simplicity, we choose $\tilde{q}_x = \tilde{q}_y = \tilde{q}_z \triangleq \tilde{q}$.

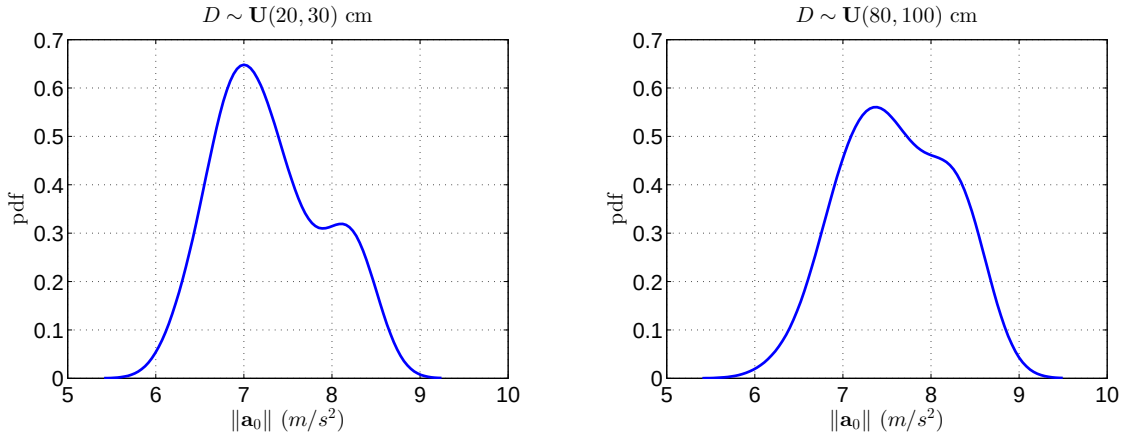

Figure 5.7: *The distribution of the norm of the acceleration* $\|\mathbf{a}_0\|$ *for the good initialization case where the diameter* D *is supposed to follow the real distribution* $D \in \mathbf{U}(20, 30)$ *cm (left) and that for the bad initialization case where it is supposed that* $D \in \mathbf{U}(80, 100)$ *cm instead (right).*

5.6.1.4 Test of robustness of the estimators to the choice of process noise parameter

The robustness of the estimators against choice of process noise parameter will be studied by comparing the performances of the estimators using two different values of $\tilde{q}$:

- The first value of $\tilde{q}$ is chosen such that $\sqrt{\tilde{q}T_s} = 15\ m/s^2$ which is shown to capture the variation of $\|\Delta_{\mathbf{a},noise,k}\|$ during the first 10 seconds of the trajectories (see figure 5.6 downright).
- The second value of $\tilde{q}$ is chosen such that $\sqrt{\tilde{q}T_s} = 1.5\ m/s^2$ which is shown to capture the variation of $\|\Delta_{\mathbf{a},noise,k}\|$ during the last 10 seconds of the trajectories.

We note that these two values are both not appropriate to cover all the real variations of acceleration not taken into account in the estimation model.

5.6.1.5 A Priori Initial Error Covariance Matrix

The a priori initial error covariance matrix P_0^- is computed using (5.35). Concerning the standard deviation of the error of the a priori initial acceleration estimate, for the sake of simplicity we choose $\sigma_{\tilde{a}_{0_x}^-} = \sigma_{\tilde{a}_{0_y}^-} = \sigma_{\tilde{a}_{0_z}^-} \triangleq \sigma_{\tilde{a}_0^-}$. We generate supposed distributions of the norm of the acceleration $\|\mathbf{a}_0\|$ for two cases of the initialization on $\hat{\beta}_0^-$ as discussed in section 5.5.4 and show them in figure 5.7. Since the standard deviation of both distributions are closed, we choose therefore for both cases of initialization $\sigma_{\tilde{a}_0^-} = 2\ m/s^2$.

Now, let us discuss tunings which are specific to each estimator.

5.6.2 Specific Tuning for the UKF

The tuning parameter κ for the UKF as formulated in section 1.4.2 is chosen equal to $\kappa = -6$. This choice comes from the fact that in [Julier and Uhlmann, 2004], it is recommended to choose $n_x + \kappa = 3$ when the state x_k is assumed to be Gaussian. We

recall that n_x is the dimension of the state which is equal to 9 in our case. In our studies, we do not make any assumption on the distribution of x_k. The recommended value for the Gaussian case is chosen for the sake of simplicity.

5.6.3 Specific Tuning for the RPF

For the RPF the larger N_p is, the higher accuracy of the estimates the RPF provides. Indeed, we assume that it is not interesting to use the RPF if it requires more computation time than the MHE-PE but gives less accuracy of the estimates. As a consequence, the RPF with the number of particles $R_p = 20000$, which is verified to require the same order of computation time as the MHE-PE, is chosen.

5.6.4 Specific Tunings for the MHE and the MHE-PE

5.6.4.1 Constraints on the estimates and on the process noise

Since for the MHE and the MHE-PE constraints can be imposed during the optimization, it is supposed for that their estimate $\hat{x}_k$ over the horizon satisfies

$$\begin{aligned} \hat{\mathbf{r}}_k &\in [-100, 100] \times [-100, 100] \times]0, 100]\, km \\ \hat{\mathbf{v}}_k &\in [-10000, 0[\times]0, 10000] \times [-10000, 0[\, m/s \\ \hat{\mathbf{a}}_k &\in [-2500, 2500]^3\, m/s^2 \end{aligned} \tag{5.38}$$

These choices of constraints are made by considering the ranges of values of the real positions, velocities and accelerations in figure 5.3.

For the MHE, the process noises are also supposed to be bounded. For the sake of simplification, it is supposed that the estimated process noises on the position estimate and on the velocity estimate can be computed from the estimated process noises on the acceleration. Denote the process noise estimate

$$\hat{w}_k = \begin{pmatrix} \hat{w}_{r_x,k} & \hat{w}_{r_y,k} & \hat{w}_{r_z,k} & \hat{w}_{v_x,k} & \hat{w}_{v_y,k} & \hat{w}_{v_z,k} & \hat{w}_{a_x,k} & \hat{w}_{a_y,k} & \hat{w}_{a_z,k} \end{pmatrix}^T$$

To reduce the number of optimization parameters, it is supposed that the process noises on the position and on the velocity are related to the process noise on the acceleration component by component. In this case,

$$\hat{w}_k = \begin{pmatrix} \frac{T_s^2}{2} \\ T_s \\ 1 \end{pmatrix} \otimes \begin{pmatrix} \hat{w}_{a_x,k} \\ \hat{w}_{a_y,k} \\ \hat{w}_{a_z,k} \end{pmatrix} \tag{5.39}$$

The estimated process noise $\hat{w}_k$ is imposed to be restricted to

$$\hat{w}_{a_{x,y,z},k} \in ([-100, 100])\, m/s^2 \tag{5.40}$$

This choice is made based on the values of $\Delta_{\mathbf{a},noise,k}$ in figure 5.6.

5.6.4.2 Horizon length

The horizon length N is chosen equal to $2 \cdot n_x$ where n_x is the state's dimension. This choice is recommended to be good in practice according to [Rao, 2000]. In our case, $N = 18$.

5.6.4.3 Tunings for the Stability of the Estimation Error of the MHE

It is shown in section 2.2.2 that if (A1)-(A5) are verified and the weight matrix $\mathcal{P}$ defined in (2.8b) is chosen equal to $p\mathbf{I}_{n_x}$, then to guarantee the convergence of the estimation error of the MHE, the weight parameter p must be chosen such that

$$\alpha_{MHE} \triangleq c_1 p + \frac{(L_f^x)^2 c_2 p}{p + c_3 \delta} < 1 \tag{5.41}$$

where

$$c_1 = \frac{6}{\lambda_{\mathcal{Q},min}},\ c_2 = 12,\ c_3 = \frac{2}{3}\lambda_{\mathcal{R},min} \tag{5.42}$$

$\lambda_{\mathcal{Q},min}$ and $\lambda_{\mathcal{R},min}$ are the smallest eigenvalues of $\mathcal{Q}$ and $\mathcal{R}$ respectively.

Recall that in our studies, $\mathcal{Q} = Q^{-1}$ and $\mathcal{R} = R^{-1}$. The verification of assumptions (A1)-(A5) for the MHE is provided in appendix E.1 where the sensitivity parameter δ is shown to be equal to $1.6 \cdot 10^{-15}$. In this study, the value of p such that $p = 5 \cdot 10^{-19}$ is chosen for both values of $\tilde{q}$ chosen in section 5.6.1.4. This value of p gives $\alpha_{MHE} \approx 0.77$. This small value of p results from the small value of δ. This small value of δ must be chosen to verify the condition (A7) for the stability. The performances of the MHE with larger values of p have also been studied even though the stability condition (A7) is not verified where we observe that the MHE still provides the same accuracy of the estimates.

5.6.4.4 Tunings for the Stability of the Estimation Error of the MHE-PE

We have seen in section 4.4 that conditions (C1)-(C7) must at least be satisfied to guarantee the convergence of the estimation errors of the MHE-PE. The verification of conditions (C1)-(C7) is provided in appendix E.2 where it is shown that the sensitivity parameter of the pre-estimator can be chosen equal to $\delta_g = 1.6 \cdot 10^{-15}$.

As stated in theorem 3, once (C1)-(C7) are verified, the convergence of the estimation errors of the MHE-PE can be guaranteed if the weight parameter μ is selected such that

$$\alpha_{MHE-PE} \triangleq \frac{8\mu(L_f^x)^2}{(\mu + \frac{\lambda_{\mathcal{R},min}\delta_g}{2})} < 1 \tag{5.43}$$

In this study, the value of μ such that $\mu = 5 \cdot 10^{-19}$ is chosen for both values of $\tilde{q}$ chosen in section 5.6.1.4. This value of μ gives $\alpha_{MHE-PE} \approx 0.68$. This small value of μ results from the small value of δ_g. This small value of δ_g must be chosen to verify the condition (C7) for the stability. The performances of the MHE-PE with larger values of p have also been studied even though the stability condition (C7) is not verified where we observe that the MHE-PE still provides the same accuracy of the estimates.

5.7 Performances of the Estimators

To summarize, the performances of the estimators in these 4 cases will be compared

- Good initialization of $\hat{\beta}_0^-$ with $\tilde{q} = 15^2/T_s$ (adapted for $t \in [0, 10]$ s)
- Good initialization of $\hat{\beta}_0^-$ with $\tilde{q} = 1.5^2/T_s$ (adapted for $t \in [10, 20]$ s)
- Bad initialization of $\hat{\beta}_0^-$ with $\tilde{q} = 15^2/T_s$ (adapted for $t \in [0, 10]$ s)

- Bad initialization of $\hat{\beta}_0^-$ with $\tilde{q} = 1.5^2/T_s$ (adapted for $t \in [10, 20]$ s)

We recall that the good initialization of $\hat{\beta}_0^-$ is due to the right assumption on the range of the diameter of the debris D. To precise, $D \in \mathbf{U}(20, 30)$ cm which is the real range of the diameter of the generated debris is imposed to the estimator. The bad initialization case represents the wrong assumption on the range of D where we give $D \in \mathbf{U}(80, 100)$ cm to the estimator instead of the real range $D \in \mathbf{U}(20, 30)$.

The performances of the estimators will be analysed in terms of non-divergence percentage, accuracy of the estimates and computation time.

5.7.1 Non-divergence Percentages

In the same way as in section 3.7.1, we would like to eliminate the cases in which the estimator diverges or gives too high estimation errors. Denote $\mathbf{r}_k^n$ and $\hat{\mathbf{r}}_k^n$ the real position and the position estimate at instant k for the n^{th} Monte Carlo run respectively.

We consider that for the n^{th} run, the estimator does not diverge if for each component i of the estimation error on the position $\hat{\mathbf{r}}_k^n - \mathbf{r}_k^n$ is such that

$$\left|\hat{r}_{i,k}^n - r_{i,k}^n\right| \leq 500\ m,\ \forall k,\ \forall i \in \{x, y, z\} \tag{5.44}$$

Denote $\mathbb{M}_{nonDV}$ a set containing the indices of the non-divergent run and $N_{nonDV} = n(\mathbb{M}_{nonDV})$ the number of elements in $\mathbb{M}_{nonDV}$.

The non-divergence percentages of each estimator for both initializations of $\hat{\beta}_0^-$ and for both process noise parameter values are presented in Table 5.1. Thanks to this table, we can conclude that all estimators except the RPF provides 100% of non-divergence percentage for both cases of initialization and for both values of process noise parameter $\tilde{q}$. The RPF provides a non-zero non-divergence percentage only when it is well initialized and the process noise parameter is well chosen.

We must keep in mind that these non-divergence percentages only show the percentages of the runs in which the position estimation errors do not exceed 500 m. The accuracy of the estimates given by each estimator of the non-divergence runs will be compared in the next section.

Estimator	Good init.		Bad initi	
	$\sqrt{\tilde{q}T_s} = 15$	$\sqrt{\tilde{q}T_s} = 1.5$	$\sqrt{\tilde{q}T_s} = 15$	$\sqrt{\tilde{q}T_s} = 1.5$
EKF	100	100	100	100
UKF	100	100	100	100
RPF	67	0	0	0
MHE-PE	100	100	100	100
MHE	100	100	100	100

Table 5.1: Non-divergence percentage of each estimator for good and bad initialization of a priori initial ballistic coefficient estimate and for the process noise parameter adapted for the first half and for the second half of the trajectory

5.7.2 Accuracy of the Estimates

The RMSE of the estimate $\hat{x}$ defined in (3.37) and the ARMSE of $\hat{x}$ defined in (3.38) for the non-divergence runs are presented in this section. Denote

$$\|RMSE(\hat{\mathbf{r}})\| = \left\| \begin{pmatrix} RMSE(\hat{r}_x) & RMSE(\hat{r}_y) & RMSE(\hat{r}_z) \end{pmatrix}^T \right\|$$

$$\|RMSE(\hat{\mathbf{v}})\| = \left\| \begin{pmatrix} RMSE(\hat{v}_x) & RMSE(\hat{v}_y) & RMSE(\hat{v}_z) \end{pmatrix}^T \right\|$$

and

$$\|RMSE(\hat{\mathbf{a}})\| = \left\| \begin{pmatrix} RMSE(\hat{a}_x) & RMSE(\hat{a}_y) & RMSE(\hat{a}_z) \end{pmatrix}^T \right\|$$

the norm of the RMSE on the position estimates, the norm of the RMSE on the velocity estimates and the norm of the RMSE on the acceleration estimates respectively.

Denote

$$\|ARMSE(\hat{\mathbf{r}})\| = \left\| \begin{pmatrix} ARMSE(\hat{r}_x) & ARMSE(\hat{r}_y) & ARMSE(\hat{r}_z) \end{pmatrix}^T \right\|$$

$$\|ARMSE(\hat{\mathbf{v}})\| = \left\| \begin{pmatrix} ARMSE(\hat{v}_x) & ARMSE(\hat{v}_y) & ARMSE(\hat{v}_z) \end{pmatrix}^T \right\|$$

and

$$\|ARMSE(\hat{\mathbf{a}})\| = \left\| \begin{pmatrix} ARMSE(\hat{a}_x) & ARMSE(\hat{a}_y) & ARMSE(\hat{a}_z) \end{pmatrix}^T \right\|$$

the norm of the ARMSE on the position estimates, the norm of the ARMSE on the velocity estimates and the norm of the ARMSE on the acceleration estimates respectively.

$\|RMSE(\hat{\mathbf{r}})\|$, $\|RMSE(\hat{\mathbf{v}})\|$ and $\|RMSE(\hat{\mathbf{a}})\|$ are plotted in figures 5.8, 5.9 and 5.10 respectively. The $\|ARMSE(\hat{\mathbf{r}})\|$, $\|ARMSE(\hat{\mathbf{v}})\|$ and $\|ARMSE(\hat{\mathbf{a}})\|$ are presented in tables 5.2, 5.3 and 5.4 respectively.

Thanks to the RMSE and the ARMSE of the estimates, we can remark that

1. The RPF is very sensitive to bad initialization and to bad choice of process noise parameter. To provide small estimation errors, it must be well initialized and the process noise parameter must be adequately chosen at the same time. The RPF is therefore **not at all** adapted for space debris tracking during the re-entries in which bad initialization and bad choice of process noise parameter are possible.

2. The EKF, the UKF, the MHE-PE and the MHE are not sensitive to the bad initialization of $\hat{\beta}_0^-$. They provide the same order of magnitude of the errors of the estimates whether they are well initialized on $\hat{\beta}_0^-$ or not for the same process noise parameter.

3. However, the EKF and the UKF are sensitive to the value of the process noise parameter $\tilde{q}$. Therefore, they are also not adapted for space debris tracking during the re-entries since the dynamics of the debris is not fully known and a good choice of process noise parameter is unknown. When $\sqrt{\tilde{q}T_s} = 15\ m/s^2$ the norm of the ARMSE on the position estimates $\|RMSE(\hat{\mathbf{r}})\|$ provided by the EKF and the UKF are around 7 m but when $\sqrt{\tilde{q}T_s} = 1.5\ m/s^2$ their $\|RMSE(\hat{\mathbf{r}})\|$ are around $15-19$ m. The same trend is shown for the velocity estimates and the acceleration estimates.

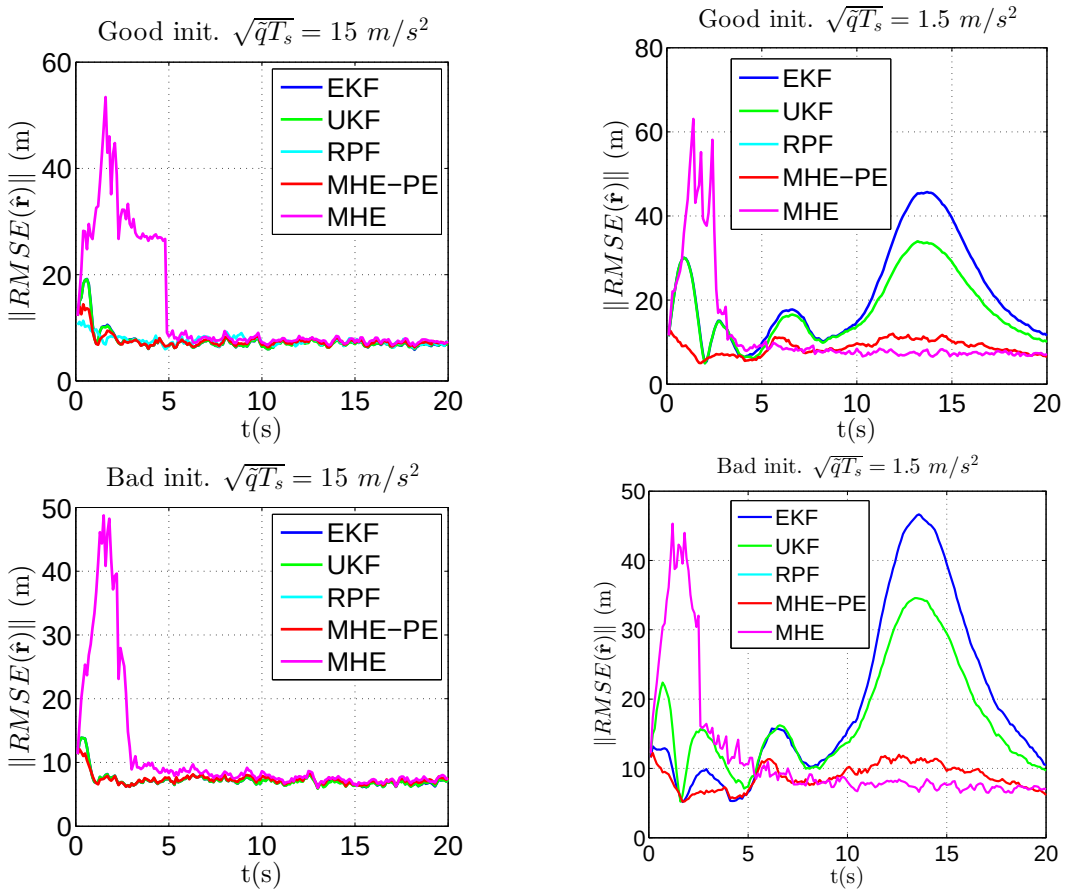

Figure 5.8: $\|RMSE(\hat{\mathbf{r}})\|$ given by each estimator for good and bad initialization of a priori initial ballistic coefficient estimate $\hat{\beta}_0^-$ and for both values of process noise parameter $\tilde{q}$.

4. The MHE-PE is not sensitive to the choice of $\tilde{q}$. It provides the same order of magnitude of ARMSE for both values of $\tilde{q}$. Its norm of the ARMSE on the position estimates $\|ARMSE(\hat{\mathbf{r}})\|$ is around $7 - 8.5$ m. The same trend is shown for the velocity estimates and the acceleration estimates.

5. The MHE is also not sensitive to the choice of $\tilde{q}$. However, it provides larger estimation errors at the beginning of the estimation compared to the other estimators. This may be due to local minima since the number of optimization parameter of the MHE is very large. Still, the MHE provides smaller estimation errors compared to other estimators from $t = 5$ s.

5.7.3 Computation Time

The minimum, mean and the maximum computation times per iteration used by each estimator implemented with MATLAB on a standard PC for every study case are presented in table 5.5. We can see that the EKF and the UKF requires very small computation time. However, we recall that they can provide high estimation errors when the process noise parameter is not adequately chosen. Hence, they are still not adapted for space debris tracking during the re-entries where a good choice of process noise parameter could not be guaranteed. The RPF not only requires large computation time but also is very sensitive

Estimator	$\|ARMSE(\hat{\mathbf{r}})\|$ (m)			
	Good init.		Bad initi	
	$\sqrt{q_\beta T_s} = 15$	$\sqrt{q_\beta T_s} = 1.5$	$\sqrt{\tilde{q} T_s} = 15$	$\sqrt{\tilde{q} T_s} = 1.5$
EKF	7.24	19.25	6.98	18.25
UKF	7.21	15.97	6.96	15.77
RPF	7.30	×	×	×
MHE-PE	7.23	8.23	7.01	8.29
MHE	12.43	11.40	10.98	11.10

Table 5.2: $\|ARMSE(\hat{\mathbf{r}})\|$ given by each estimator for good and bad initialization of a priori initial ballistic coefficient estimate $\hat{\beta}_0^-$ and for both values of process noise parameter $\tilde{q}$.

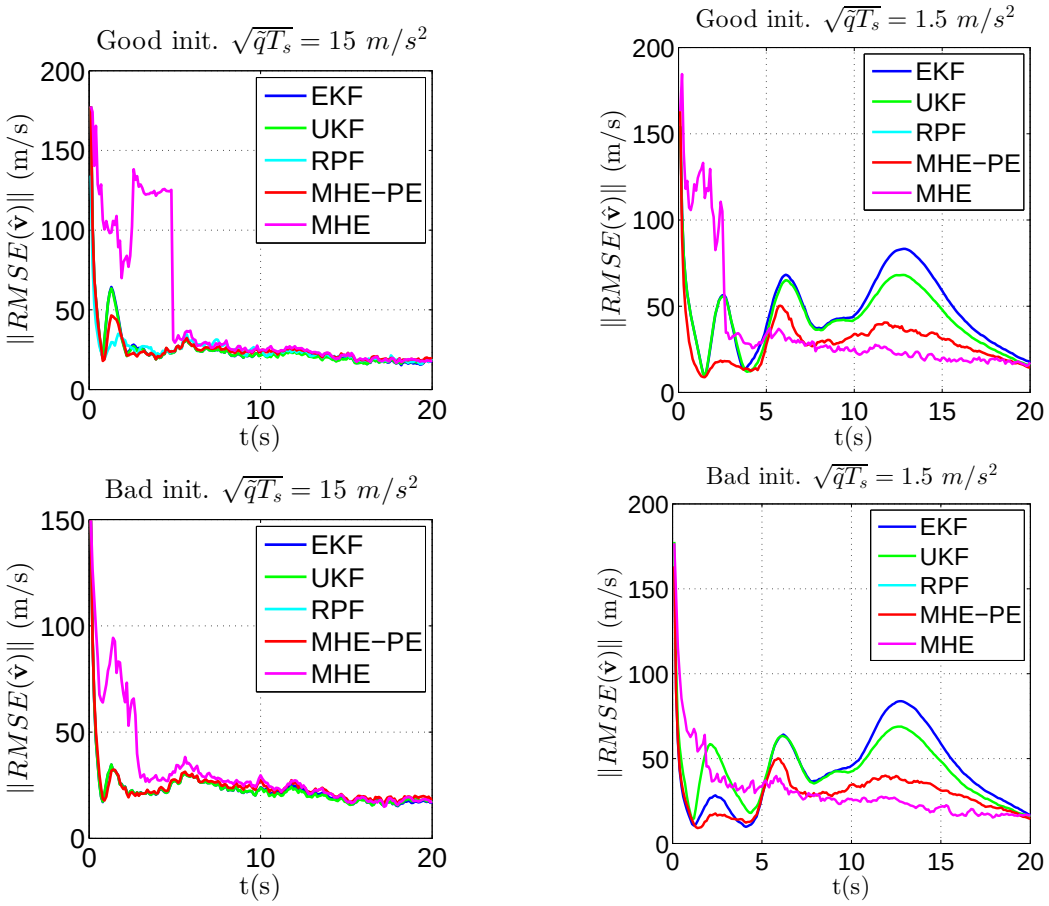

Figure 5.9: $\|RMSE(\hat{\mathbf{v}})\|$ given by each estimator for good and bad initialization of a priori initial ballistic coefficient estimate $\hat{\beta}_0^-$ and for both values of process noise parameter $\tilde{q}$.

Estimator	$\|ARMSE(\hat{\mathbf{v}})\|$ (m/s)			
	Good init.		Bad initi	
	$\sqrt{q_\beta T_s} = 15$	$\sqrt{q_\beta T_s} = 1.5$	$\sqrt{\tilde{q} T_s} = 15$	$\sqrt{\tilde{q} T_s} = 1.5$
EKF	23.91	42.00	22.42	39.68
UKF	23.70	37.54	22.28	36.50
RPF	23.81	×	×	×
MHE-PE	24.30	26.27	23.53	26.60
MHE	43.12	34.47	30.25	29.06

Table 5.3: $\|ARMSE(\hat{\mathbf{v}})\|$ given by each estimator for good and bad initialization of a priori initial ballistic coefficient estimate $\hat{\beta}_0^-$ and for both values of process noise parameter $\tilde{q}$.

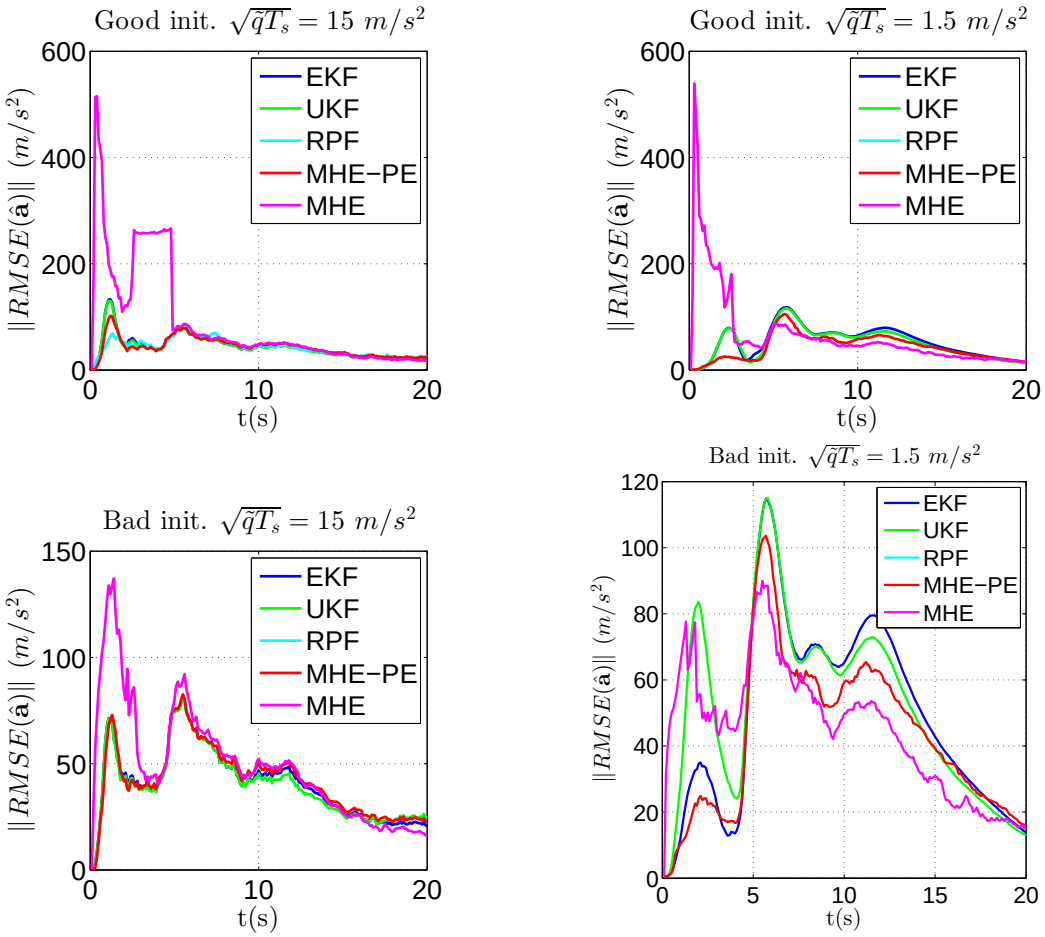

Figure 5.10: $\|RMSE(\hat{\mathbf{a}})\|$ given by each estimator for good and bad initialization of a priori initial ballistic coefficient estimate $\hat{\beta}_0^-$ and for both values of process noise parameter $\tilde{q}$.

Estimator	$\|ARMSE(\hat{\mathbf{a}}\|)$ (m/s^2)			
	Good init.		Bad initi	
	$\sqrt{q_\beta T_s} = 15$	$\sqrt{q_\beta T_s} = 1.5$	$\sqrt{\tilde{q} T_s} = 15$	$\sqrt{\tilde{q} T_s} = 1.5$
EKF	41.84	46.47	39.09	44.02
UKF	41.15	44.08	38.61	46.15
RPF	41.46	×	×	×
MHE-PE	41.39	38.52	40.35	38.82
MHE	82.89	61.54	46.38	41.56

Table 5.4: $\|ARMSE(\hat{\mathbf{a}})\|$ given by each estimator for good and bad initialization of a priori initial ballistic coefficient estimate $\hat{\beta}_0^-$ and for both values of process noise parameter $\tilde{q}$.

Estimator	Computation time/ite (s)		
	Min	Mean	Max
EKF	$3 \cdot 10^{-4}$	$3 \cdot 10^{-4}$	$5 \cdot 10^{-5}$
UKF	0.002	0.002	0.011
RPF	0.045	1.578	2.195
MHE-PE	0.482	0.865	1.588
MHE	2.638	5.330	7.438

Table 5.5: Minimum, mean and maximum computation times per iteration used by each estimator

to the choice of process noise parameter. Hence, it is not adapted for the problem at all. We can observe that the MHE-PE is around 6 times faster than the MHE.

5.7.4 Result Analyses

Thanks to the results of the performances of each estimator, we can conclude that

1. The RPF is not adapted when a good initialization and a good choice of process noise parameter cannot be guaranteed. Unfortunately, this is generally the case for space debris tracking during the re-entries. Hence, the RPF is not appropriate for the problem.

2. Thanks to its small computation time, the EKF is the most interesting estimator when a good choice of process noise parameter can be guaranteed. However, since the dynamics of the ballistic coefficient β of space debris during the re-entries is not fully known, unlike military objects whose β can be considered constant, a good choice of process noise parameter for space debris tracking cannot be guaranteed in general. The MHE-PE and the MHE, which show to be robust against bad choice of process noise parameter, should therefore be chosen for space debris tracking during the re-entries.

3. The MHE-PE uses less computation time than the MHE while providing the same accuracy of the estimate. The MHE-PE is therefore the most interesting estimator for space debris tracking during the re-entries. Even though its computation time in this study is not small enough for a real-time tracking application, the computation time can still be reduced using a faster programming language, a faster computer and a faster optimization algorithm as discussed in section 2.5.1 for example.

5.8 Conclusions

In this chapter, we have seen that

- In this chapter the Moving Horizon with Pre-Estimation (MHE-PE) developed in the previous chapter is implemented to solve the 3D space debris tracking problem during atmospheric re-entry. Trajectories of 100 hollow Aluminium spheres of width $w = 3\ cm$ with a diameter $D \sim \mathbf{U}(20, 30)\ cm$ starting at altitude between $69 - 70\ km$ with speed of $5 - 10\ km/s$ are simulated via Monte Carlo method. Noisy radar measurements are simulated and given to the EKF, the UKF, the RPF, the MHE-PE and the MHE to determine the trajectory estimates.

- The robustness against bad initialization of the estimators is studied by supposing a wrong assumption on the diameter of the debris to the estimators. The real distribution of the diameter is $D \sim \mathbf{U}(20, 30)\ cm$ which implies $m \in [7.43, 18.63]\ kg$. The wrong assumption on D is $D \sim \mathbf{U}(80, 100)\ cm$ which implies $m \in [150.95, 239.51]\ kg$. The study shows that the EKF, the UKF, the MHE-PE and the MHE are robust against bad initialization. To precise, the order of magnitude of their accuracy of the estimates is the same whether when they are well initialized or badly initialized. The RPF, however, is sensitive to a bad choice of process noise parameter.

- The MHE-PE and the MHE are shown to be robust against poor choice of process noise parameter while the EKF, the UKF and the RPF are not. This robustness is important for space debris tracking during the re-entries since the dynamics of the debris is generally not fully known and the a priori initial estimate of the ballistic coefficient may have high errors.

- The EKF and the UKF are shown to be robust against bad initialization but not against bad choice of process noise parameter. They are adapted for the systems whose dynamics is fully known such as military object tracking where the ballistic coefficient of the object can be considered constant but not for space debris tracking during the re-entries in which a good choice of process noise parameter cannot be guaranteed.

- The MHE exhibits high errors at the beginning of the estimation which may due to presence of local minima.

- The MHE-PE uses approximately 6 times less computation time than the MHE in this application while providing small estimation errors for every tested initialization cases and tested process noise parameter values. As a result, the MHE-PE is the most efficient estimator compared to the EKF, the UKF, the RPF and the MHE-PE for space debris tracking during the re-entries.

- The computation time of the MHE-PE in this study is not sufficiently small for a real-time space debris tracking yet. However, it could still be reduced when the MHE-PE is combined to fast optimization techniques or programmed in a faster language.

CHAPTER 6

Conclusions and Perspectives

"What gets us into trouble is not what we don't know. It's what we know for sure that just ain't so."

— Mark Twain

Motivation for Space Debris Tracking during Atmospheric Re-Entries

Space debris tracking during atmospheric re-entries is now an important issue since there will be more and more re-entries due to debris mitigation policy and possible debris removal projects. In fact, Space Agencies worldwide have established debris mitigation guidelines requesting satellites in LEOs to de-orbit at their end of operational life and re-enter the atmosphere. NASA is working on a space debris removal project aiming to use laser to de-orbit defunct satellites in LEOs to make them re-enter. Switzerland and Japan are working on projects using robots and electrical nets to capture pieces of space debris and throw them back to the Earth's atmosphere. To prevent dangers from these re-entering objects, they must be tracked during the re-entries.

Challenge in Space Debris Tracking during the Re-Entries

Available studies on re-entry object tracking at the beginning of this work concerned only military objects [Farina et al., 2002][Austin and Leondes, 1981][Liu et al., 2005][Ristic et al., 2003]. Military object tracking during the re-entries is less complex than the case of space debris. In fact, the ballistic coefficient (β), a parameter characterizing the object's ability to resist the drag which is the aerodynamic force opposite to the direction of the velocity which depends on the mass, the cross section and the form of the object, of a military object is nearly constant during the re-entries. On the other hand the evolution of the ballistic coefficient β of the debris is generally unknown. As a consequence, one can only use an estimation model that describes the real dynamics of the debris during the re-entries approximately in an estimator. The space debris tracking problem during the re-entries suffers therefore from model errors. Moreover, re-entering debris can break up and disintegrate in many pieces. In this case, an a priori value of the ballistic coefficient will not be available which may lead to bad initialization of the used estimators. The to-be-used estimator for space debris tracking during the re-entries must therefore be robust

against model errors, large measurement noise and bad initialization. According to the literature, the Moving Horizon Estimator (MHE) seemed to be a good candidate for the problem.

Interests and Limitation of the Moving Horizon Estimator

In fact, the MHE provides a lot of advantages. First, it is robust against poor initialization, model errors and bad choice of process noise parameter. This is due to the fact that the estimation takes into account several measurements and that it is done by optimizing a cost function taking into account at the same time the initial error, the process noise and the difference between real measurements and predicted ones. Second, there is no need for system linearization since the nonlinear model can be handled directly during the optimization. Third, constraints on the state and on the process and measurement noises can be taken into account directly during the optimization. This can be useful in practice when physical constraints are known, e.g. positive mass or atmospheric density, positive altitude, positive ballistic coefficient. Lastly, the stability of the dynamics of the estimation errors of the MHE can be guaranteed if the weight parameter is adequately chosen. The MHE is therefore an efficient estimator especially when model errors are present or when bad initialization can occur like for space debris tracking during atmospheric re-entries. However, the classical MHE may have a large number of optimization variables which induces large computation time.

Objectives of this Work

This work was therefore set out to develop a new Moving Horizon (MH) strategy that keeps the accuracy of the estimates and the robustness against bad initialization and model errors as the classical MHE but requires less computation time compared to the classical MHE and to implement the developed moving horizon strategy for space debris tracking during the re-entries.

What We Did

First step: Studying the Performances of the MHE for 1D Space Debris Tracking during the Re-entres

To verify that the classical MHE is adapted to the space debris tracking problem during the re-entries, we started by evaluating the performances of the classical MHE for the problem in 1 dimensional cases in terms of non-divergence percentage, accuracy of the estimate and computation time compared to those of the Extended Kalman Filter (EKF), the Unscented Kalman Filter (UKF), the Regularized Particle Filter (RPF) which are classical estimators used in existing works in military object tracking during the re-entries.

Two types of MHE were used: the one in the deterministic framework where the initial state, the process and the measurement noises are considered as unknown deterministic variables and the one in the stochastic framework where these variables are considered as random variables. Two estimation models were proposed. The first model includes the ballistic coefficient as a state variable, assuming that the ballistic coefficient is constant over a sampling period. The second model includes the acceleration as a state variable,

assuming that the ballistic coefficient is constant over a sampling period during the computation of the derivative of the acceleration.

To overcome model errors, the process noise covariance matrix, i.e. the process noise parameter, must be adequately chosen to represent the variation of the state not taken into account in the estimation models. Unfortunately, for space debris, an appropriate choice of process noise parameter could not be guaranteed because of unknown dynamics of the debris. Moreover, we showed that the variation of the state not taken into account in the estimation models in our study, which could be computed since we have access to the generated considered-to-be real trajectories, has high variation with time. As a result, a constant value of process noise parameters cannot cover all the unmodelled state variation of the entire re-entry. A to-be-used estimator for the debris tracking problem during the re-entries must therefore be robust against a bad choice of process noise parameter, too. In this study, the robustness of the estimators against bad initialization was also studied by giving a wrong assumption on the size of the debris to the estimators.

The results showed that

- the model with acceleration overcomes the model with ballistic coefficient in terms of non-divergence percentages, robustness against a bad choice of process noise parameter and robustness against bad initialization
- every tested estimator except the RPF is robust against bad initialization
- the MHEs are the only estimator among the tested ones which are robust against a bad choice of process noise parameter. They are therefore the only estimator adapted for the space debris tracking problem during the re-entries in which a good choice of process noise parameter cannot be guaranteed

However, the MHEs require very large computation times (around 1000 times larger than those of the EKF and the UKF). This disabled the MHEs to be used in real-time space debris application especially in 3 dimensional cases where the number of optimization variables will be even larger.

Second Step: Developing an Moving Horizon Estimation Strategy Requiring Less Computation Time than the Classical MHE

Hence, we developed a new Moving Horizon Estimation strategy to reduce the computation time of the "classical" strategies for nonlinear system. This strategy was referred to as, the Moving Horizon Estimator with Pre-Estimation (MHE-PE). While the classical MHE uses the state equation to propagate the estimate over the horizon, the MHE-PE uses an auxiliary estimator, called the pre-estimator, to do so instead. The pre-estimator in the MHE-PE is initialized at the beginning of the horizon by minimizing a cost function representing the difference between the real measurements and the predicted ones over the horizon and the difference between the searching initial estimate at the beginning of the horizon and a priori value one. This auxiliary estimator helps to compensate for model errors without having to estimate the optimal process noise sequence over the horizon. Hence, the number of parameters to be optimized is reduced to the initial state at the beginning of the horizon.

In this study, we established conditions on the stability of the dynamics of the estimation errors of the MHE-PE. To precise, we demonstrated that in case that some conditions on the continuity, on the observability and on the finite sensitivity of the system are verified, if the weight on the term of the initial estimate at the beginning of the horizon respect an inequality then the stability of the dynamics of the estimation errors of the MHE-PE is guaranteed. In the tested numerical example on the pressure estimation problems of reversible gas-phase system, the MHE-PE showed to require smaller computation time compared to the MHE, while keeping its robustness and accuracy advantages. The MHE-PE therefore seemed to suit for the estimation problems for which the computation time of the MHE would have been prohibitive such as space debris tracking during the re-entries in 3 dimensional cases.

Third Step: Implementing of the Developed MH strategy (MHE-PE) for 3D Space Debris Tracking during the Re-Entries

Finally, the performances of the developed MHE-PE for 3D space debris tracking problem during atmospheric re-entries compared to the EKF, the UKF, the RPF and the MHE were studied. The same robustness tests against bad choice of process noise parameter and bad initialization as for the study in 1D cases were done. For this study in 3D cases, only the estimation model with acceleration was used since it had been shown to overcome the estimation model with ballistic coefficient previously and only the MHE in the deterministic framework was tested thanks to its higher robustness to bad choice of process noise parameters compared to the MHE in the stochastic framework.

The results showed that the MHE-PE and the MHE are the only ones among every tested estimator that is robust against poor choice of process noise parameter. They are therefore the only ones in the study which are adapted for space debris tracking problem during the re-entries. Moreover, the MHE-PE was shown to use around 6 times less computation time than the MHE while providing the same order of magnitude of the estimation errors. As a result, the MHE-PE is the most efficient estimator among the tested ones for space debris tracking problem during the re-entries.

Conclusions

In this work, we proved the stability of the dynamics of the estimation errors of the MHE-PE for nonlinear discrete-time system and verified that the developed MHE-PE is the most efficient estimator compared to the EKF, the UKF, the RPF and the MHE for 3D space debris tracking during the re-entries. Not only it provides good accuracy of the estimates and shows robustness against bad initialization and poor choice of process noise parameter, but it also requires less computation time than the MHE while keeping the same order of accuracy of the estimates. We note that this computation time reduction is achieved by changing only the structure of the estimator without having to change an optimization method. The study was done with MATLAB on a standard PC and we saw that the computation time of the MHE-PE was not small enough for real a real-time space debris tracking yet. However, the computation time of the MHE-PE can still be reduced by programming the MHE-PE in a faster language or by combining the MHE-PE with fast optimization techniques as proposed in [Ferreau et al., 2012][Zavala, 2008], for example.

Perspectives

For further development of this work, we propose to

- Study the effect of the horizon length on the performances of the MHE-PE. The larger the horizon length is, the smaller the estimation errors of the MHE-PE are. However, a larger horizon length also induces larger computation time. A compromise should therefore be made.

- Develop a method to compute the maximum horizon length that should not be exceeded for the MHE-PE. This could be inspired by the work on the Finite Memory Observer (FMO) which is a recursive estimator using a collection of some latest measurements to compute the estimate at each instant. In [Kratz et al., 1997][Graton et al., 2014], a method to determine the maximum horizon length from which the accuracy of the estimates of the FMO will not be improved for linear time-invariant and linear time-varying systems.

- Develop a strategy for having adaptive process noise parameters which could represent model errors at each instant. This can be done for the estimation model with acceleration by estimate the change in acceleration not taking into account in the estimation model $\Delta_{a_{x,y,z},noise,k}$ using state estimates from two consecutive instants.

- Develop a strategy for having adaptive estimation model parameters and adaptive tuning parameters for the MHE and the MHE-PE. These tuning parameters could be the horizon length or the weight matrix. This can be inspired by the work for the Model Predictive Control (MPC), which is a dual of the MHE strategy, in [Mamboundou and Langlois, 2011]. In this work, a Model Predictive Control strategy with adaptive model parameter and adaptive tuning parameters is proposed for linear systems with time-varying parameters. This strategy is called "Indirect adaptive model predictive control supervised by fuzzy logic". In this strategy, when the difference between the predicted measurement of the model and the real measurement reaches a chosen threshold, a new set of the parameters of the model is recomputed based on the recursive least-squares method. In addition, if the difference between the predicted measurement of the model and the real measurement reaches another chosen threshold which is set to be higher than the first one, a new set of the tunings parameters of predictive controller (horizons of prediction, control, and weighting of the control signal) is computed using the fuzzy logic supervisor. The stability of this Model Prediction Controller has also been proven and the control robustness regarding model switching has also been studied in a control problem of a diesel generator [Mamboundou and Langlois, 2012].

- Study the performances of the MHE-PE for a nonlinear system with multiplicative noises. Recently, a method to design an observer for a nonlinear system with multiplicative noises has been proposed [Barbata et al., 2014a] and [Barbata et al., 2014b]. A combination of the MHE-PE and the observer in [Barbata et al., 2014a] and [Barbata et al., 2014b] may provide better accuracy of the estimates compared to when the observer is implemented alone.

- Compare the performances of the MHE-PE with the Receding-Horizon Nonlinear Kalman (RNK) Filter recently proposed in [Rengaswamy et al., 2013] even though the proof of the stability of the RNK Filter does not yet exist.

- Study the performances of the tested estimators for slow re-entries of space debris where the debris orbits around the Earth many times before entering the fast re-entries phase. In this case, measurements are available only for certain periods of the trajectories since the field of view of the radar stations generally do not cover all the globe. As a consequence, predictions of the state should be computed for a long time when measurements are not available which may induce bad initialization of the estimator when the estimation restarts again after an acquisition of new measurements.

- Study the effect of the size of the weight parameter μ of the MHE-PE on its performances. In fact, performances of the MHE-PE have been studied for many values of μ and we found out that the MHE-PE always showed to provide high accuracy of the estimate even when the tested value of μ is higher than the theoretical value satisfying the stability condition. This is possible because the condition on the value of μ is a sufficient condition for the stability of the dynamics of the estimation errors of the MHE-PE. This condition is in practice conservative because the calculation of a μ satisfying the stability condition uses upper bounds of many parameters successively. The value of μ is therefore usually very pessimistic. The value of μ tends to be very small which represents the case where the system of the pre-estimator is "not much observable", i.e. we need a lot of measurements to be able to construct the estimate at the beginning of the horizon.

- Implement the MHE-PE with fast optimization techniques such as the ones proposed in [Ferreau et al., 2012][Zavala, 2008] using a faster programming language to see if the computation time is small enough for a real-time application.

APPENDIX A

Appendices for Chapter 1

A.1 Derivation of the Estimation Model with Ballistic Coefficient in the State Vector in Discrete-Time Version

Using (1.26), equation (1.23) can be written as:

$$\begin{pmatrix} \dot{\mathbf{r}} \\ \dot{\mathbf{v}} \\ \dot{\beta} \end{pmatrix} = \begin{pmatrix} \mathbf{0}_{3\times3} & \mathbf{I}_{3\times3} & \mathbf{0}_{3\times1} \\ \mathbf{0}_{3\times3} & \mathbf{0}_{3\times3} & \mathbf{0}_{3\times1} \\ \mathbf{0}_{1\times3} & \mathbf{0}_{1\times3} & 0 \end{pmatrix} \begin{pmatrix} \mathbf{r} \\ \mathbf{v} \\ \beta \end{pmatrix} + \begin{pmatrix} \mathbf{0}_{3\times1} \\ \mathbf{a}_k \\ 0 \end{pmatrix} + \begin{pmatrix} \mathbf{0}_{3\times1} \\ \mathbf{w}_a(t) \\ w_\beta(t) \end{pmatrix} \tag{A.1}$$

Denote

$$A_1 = \begin{pmatrix} \mathbf{0}_{3\times3} & \mathbf{I}_{3\times3} & \mathbf{0}_{3\times1} \\ \mathbf{0}_{3\times3} & \mathbf{0}_{3\times3} & \mathbf{0}_{3\times1} \\ \mathbf{0}_{1\times3} & \mathbf{0}_{1\times3} & 0 \end{pmatrix}$$

Integrating (A.1) to have

$$x_{k+1} = e^{A_1 T_s} x_k + \int_0^{T_s} e^{A_1(T_s-\tau)} \begin{pmatrix} \mathbf{0}_{3\times1} \\ \mathbf{a}_k \\ 0 \end{pmatrix} d\tau + \int_0^{T_s} e^{A_1(T_s-\tau)} \begin{pmatrix} \mathbf{0}_{3\times1} \\ \mathbf{w}_a(kT_s+\tau) \\ w_\beta(kT_s+\tau) \end{pmatrix} d\tau \tag{A.2}$$

Denote

$$w_k = \int_0^{T_s} e^{A_1(T_s-\tau)} \begin{pmatrix} \mathbf{0}_{3\times1} \\ \mathbf{w}_a(kT_s+\tau) \\ w_\beta(kT_s+\tau) \end{pmatrix} d\tau \tag{A.3}$$

Since $A_1^2 = \mathbf{0}_{7\times7}$, we have

$$e^{A_1\tau} = \begin{pmatrix} \mathbf{I}_{3\times3} & \tau\mathbf{I}_{3\times3} & \mathbf{0}_{3\times1} \\ \mathbf{0}_{3\times3} & \mathbf{I}_{3\times3} & \mathbf{0}_{3\times1} \\ \mathbf{0}_{1\times3} & \mathbf{0}_{1\times3} & 1 \end{pmatrix} \tag{A.4}$$

(A.2) becomes

$$x_{k+1} = \begin{pmatrix} \mathbf{r}_k + \mathbf{v}_k T_s + \mathbf{a}_k \dfrac{T_s^2}{2} \\ \mathbf{v}_k + \mathbf{a}_k T_s \\ \beta_k \end{pmatrix} + w_k \tag{A.5}$$

which equivalent to (1.30) where w_k is equal to

$$w_k = \int_0^{T_s} \begin{pmatrix} (T_s - \tau)\mathbf{w}_a(kT_s + \tau) \\ w_\beta(kT_s + \tau) \end{pmatrix} d\tau \tag{A.6}$$

The covariance of the discrete-time process noise w_k denoted by Q can be written as

$$Q = E\{w_k w_k^T\} = \int_0^{T_s} \begin{pmatrix} (T_s - \tau)\mathbf{w}_a(kT_s + \tau) \\ \mathbf{w}_a(kT_s + \tau) \\ w_\beta(kT_s + \tau) \end{pmatrix} \begin{pmatrix} (T_s - \tau)\mathbf{w}_a(kT_s + \tau) \\ \mathbf{w}_a(kT_s + \tau) \\ w_\beta(kT_s + \tau) \end{pmatrix}^T d\tau \tag{A.7}$$

Using (1.22) and (1.28), Q becomes

$$Q = \int_0^{T_s} \begin{pmatrix} (T_s - \tau)^2\mathbf{q}_a & (T_s - \tau)\mathbf{q}_a & \mathbf{0}_{3\times1} \\ (T_s - \tau)\mathbf{q}_a & \mathbf{q}_a & \mathbf{0}_{3\times1} \\ \mathbf{0}_{1\times3} & \mathbf{0}_{1\times3} & q_\beta \end{pmatrix} d\tau \tag{A.8}$$

Integrate (A.8) to have (1.31). ■

A.2 Derivation of the Estimation Model with Acceleration in the State Vector in Discrete-Time Version

(1.42) can be written as

$$\dot{x}(t) = \begin{pmatrix} \mathbf{0}_{3\times3} & \mathbf{I}_{3\times3} & \mathbf{0}_{3\times3} \\ \mathbf{0}_{3\times3} & \mathbf{0}_{3\times3} & \mathbf{I}_{3\times3} \\ \mathbf{0}_{3\times3} & \mathbf{0}_{3\times3} & \mathbf{0}_{3\times3} \end{pmatrix} x(t) + \begin{pmatrix} \mathbf{0}_{3\times1} \\ \mathbf{0}_{3\times1} \\ \mathbf{f}_k \end{pmatrix} + \begin{pmatrix} \mathbf{0}_{3\times1} \\ \mathbf{0}_{3\times1} \\ \boldsymbol{\xi}(t) \end{pmatrix} \tag{A.9}$$

Denote

$$A_2 = \begin{pmatrix} \mathbf{0}_{3\times3} & \mathbf{I}_{3\times3} & \mathbf{0}_{3\times3} \\ \mathbf{0}_{3\times3} & \mathbf{0}_{3\times3} & \mathbf{I}_{3\times3} \\ \mathbf{0}_{3\times3} & \mathbf{0}_{3\times3} & \mathbf{0}_{3\times3} \end{pmatrix} \tag{A.10}$$

Integrate (A.9) to have

$$x_{k+1} = e^{A_2 T_s} x_k + \int_0^{T_s} e^{A_2(T_s-\tau)} \begin{pmatrix} \mathbf{0}_{3\times1} \\ \mathbf{0}_{3\times1} \\ \mathbf{f}_k \end{pmatrix} d\tau + \int_0^{T_s} e^{A_2(T_s-\tau)} \begin{pmatrix} \mathbf{0}_{3\times1} \\ \mathbf{0}_{3\times1} \\ \boldsymbol{\xi}(kT_s + \tau) \end{pmatrix} d\tau \tag{A.11}$$

Denote

$$w_k = \int_0^{T_s} e^{A_2(T_s-\tau)} \begin{pmatrix} \mathbf{0}_{3\times1} \\ \mathbf{0}_{3\times1} \\ \boldsymbol{\xi}(kT_s + \tau) \end{pmatrix} d\tau \tag{A.12}$$

Since, $(A_2\tau)^3 = \mathbf{0}_{9\times9}$, we have

$$e^{A_2\tau} = \begin{pmatrix} \mathbf{I}_{3\times3} & \tau\mathbf{I}_{3\times3} & \tau^2/2\mathbf{I}_{3\times3} \\ \mathbf{0}_{3\times3} & \mathbf{I}_{3\times3} & \tau\mathbf{I}_{3\times3} \\ \mathbf{0}_{3\times3} & \mathbf{0}_{3\times3} & \mathbf{I}_{3\times3} \end{pmatrix} \tag{A.13}$$

(A.11) becomes

$$x_{k+1} = \begin{pmatrix} \mathbf{I}_{3\times3} & T_s\mathbf{I}_{3\times3} & \frac{T_s^2}{2}\mathbf{I}_{3\times3} \\ \mathbf{0}_{3\times3} & \mathbf{I}_{3\times3} & T_s\mathbf{I}_{3\times3} \\ \mathbf{0}_{3\times3} & \mathbf{0}_{3\times3} & \mathbf{I}_{3\times3} \end{pmatrix} x_k + \begin{pmatrix} \frac{T_s^3}{6}\mathbf{f}_k \\ \frac{T_s^2}{2}\mathbf{f}_k \\ T_s\mathbf{f}_k \end{pmatrix} + w_k \tag{A.14}$$

which is equivalent to (1.43) where w_k is equal to

$$w_k = \int_0^{T_s} \begin{pmatrix} \frac{(T_s-\tau)^2}{2}\mathbf{I}_3 \\ (T_s-\tau)\mathbf{I}_3 \\ \mathbf{I}_3 \end{pmatrix} \boldsymbol{\xi}(kT_s+\tau)d\tau \tag{A.15}$$

Using (1.40), the covariance of the discrete-time process noise w_k denoted by Q can be written as

$$Q = E\{w_k w_k^T\} = \int_0^{T_s} \begin{pmatrix} \frac{(T_s-\tau)^2}{2}\mathbf{I}_3 \\ (T_s-\tau)\mathbf{I}_3 \\ \mathbf{I}_3 \end{pmatrix} \begin{pmatrix} \frac{(T_s-\tau)^2}{2}\mathbf{I}_3 & (T_s-\tau)\mathbf{I}_3 & \mathbf{I}_3 \end{pmatrix} \tilde{\mathbf{q}}d\tau \tag{A.16}$$

Do the matrix multiplication to get

$$Q = \int_0^{T_s} \begin{pmatrix} \frac{(T_s-\tau)^4}{4}\mathbf{I}_3 & \frac{(T_s-\tau)^3}{2}\mathbf{I}_3 & \frac{(T_s-\tau)^2}{2}\mathbf{I}_3 \\ \frac{(T_s-\tau)^3}{2}\mathbf{I}_3 & (T_s-\tau)^2\mathbf{I}_3 & (T_s-\tau)\mathbf{I}_3 \\ \frac{(T_s-\tau)^2}{2}\mathbf{I}_3 & (T_s-\tau)\mathbf{I}_3 & \mathbf{I}_3 \end{pmatrix} \tilde{\mathbf{q}}d\tau \tag{A.17}$$

Integrate (A.17) to have

$$Q = \begin{pmatrix} \frac{1}{20}T_s^5\mathbf{I}_{3\times3} & \frac{1}{8}T_s^4\mathbf{I}_{3\times3} & \frac{1}{6}T_s^3\mathbf{I}_{3\times3} \\ \frac{1}{8}T_s^4\mathbf{I}_{3\times3} & \frac{1}{3}T_s^3\mathbf{I}_{3\times3} & \frac{1}{2}T_s^2\mathbf{I}_{3\times3} \\ \frac{1}{6}T_s^3\mathbf{I}_{3\times3} & \frac{1}{2}T_s^2\mathbf{I}_{3\times3} & T_s\mathbf{I}_{3\times3} \end{pmatrix} \otimes \tilde{\mathbf{q}} \tag{A.18}$$

which is equivalent to (1.44). ■

A.3 Particle Filters and Regularized Particle Filters

An estimation problem for particle filters is described in a stochastic framework where the initial state and the process and measurement noises are assumed to be random variables. The a posteriori density $p(x_k|y_0^k)$ is computed first. Then, the a posteriori estimate $\hat{x}_k$ is defined as the expectation of the real state x_k whose density is equal to $p(x_k|y_0^k)$. To summarize, the goal of the estimation problem in the stochastic framework is to derive:

$$E[x_k|y_0^k] \triangleq \int x_k \cdot p(x_k|y_0^k)dx_k \tag{A.19}$$

An approximate solution of the integral in (A.19) is obtained by generating N_p random samples, also called *particles* and approximating $p(x_k|y_0^k)$ by point masses:

$$p(x_k|y_0^k) \approx \sum_{i=1}^{N_p} w_{k,p}^i \delta(x_k - x_{k,p}^{(i)}) \tag{A.20}$$

where δ is the Dirac distribution.

Denoted $\{x_{k,p}^{(i)}\}_{1\leq i\leq N_p}$ random samples drawn from the posterior density $p(x_k|y_0^k)$. Thanks to (A.20), (A.19) becomes

$$E[x_k|y_0^k] \approx \sum_{i=1}^{N_p} w_{k,p}^i x_{k,p}^{(i)} \tag{A.21}$$

This approximation method is called Monte Carlo Integration. Particle filters use Monte Carlo Integration to approximate the a posteriori density of the state $p(x_k|y_0^k)$ and then compute the expectation of the state to have an a posteriori estimate $\hat{x}_k$ defined by

$$\hat{x}_k \triangleq \sum_{i=1}^{N_p} w_{k,p}^i x_{k,p}^{(i)} \tag{A.22}$$

Importance Sampling

When the distribution $p(x_k|y_0^k)$ is unknown or when it is difficult to draw particles from $p(x_k|y_0^k)$ directly, the sampling can be done using another distribution $q(x_k|y_0^k)$, called the *importance distribution*. A very common importance distribution is the Gaussian distribution. The condition is that the importance distribution $q(x_k|y_0^k)$ must have larger support than $p(x_k|y_0^k)$.

Denote $x_{k,q}^{(i)}$ for $i = 1, \ldots, N_p$ particles drawn from the importance distribution $q(x_k|y_0^k)$ and $w_{k,q}^i$ associated importance weights. In this case, we have

$$p(x_k|y_0^k) \approx \sum_{i=0}^{N_p} w_{k,q}^{(i)} \delta(x_k - x_{k,q}^{(i)}) \tag{A.23}$$

$$E[x_k|y_0^k] \approx \sum_{i=1}^{N_p} w_{k,q}^i x_{k,q}^{(i)} \tag{A.24}$$

Remark that the integral in (A.19) can be written as

$$E[x_k|y_0^k] = \int x_k \cdot \frac{p(x_k|y_0^k)}{q(x_k|y_0^k)} q(x_k|y_0^k) dx_k \approx \sum_{i=1}^{N_p} w_{k,q}^i x_{k,q}^{(i)} \tag{A.25}$$

Therefore,

$$w_{k,q}^{(i)} = \frac{\tilde{w}_k^{(i)}}{\sum_{i=1}^{N_p} \tilde{w}_k^{(i)}} \tag{A.26}$$

where

$$\tilde{w}_k^{(i)} \triangleq p(x_k|y_0^k)/q(x_k|y_0^k) \tag{A.27}$$

$\tilde{w}_k^{(i)}$ is called the unnormalized importance weight. In the next section, a method to compute the unnormalized importance weight recursively, known as Sequential Importance Sampling (SIS), is presented.

Sequential Importance Sampling

Sequential Importance Sampling (SIS) method consists in recursively propagating importance weights $w_{k,q}^{(i)}$ and particles $x_{k,q}^{(i)}$ as each measurement is received sequentially. Using Bayes' rule [1], it can be shown that if the chosen importance density can be factorized as

$$q(x_k|y_0^k) = q(x_k|x_{k-1}, y_0^k)q(x_{k-1}|y_0^{k-1}) \tag{A.30}$$

therefore the unnormalized weight $\tilde{w}_k^{(i)}$ can be derived sequentially

$$\tilde{w}_k^{(i)} \propto \tilde{w}_{k-1}^{(i)} \frac{p(y_k|x_{k,q}^{(i)})p(x_{k,q}^{(i)}|x_{k-1,q}^{(i)})}{q(x_{k,q}^{(i)}|x_{k-1,q}^{(i)}, y_0^k)} \tag{A.31}$$

In practice, the importance density is chosen equal to the a priori density, i.e. the samples will be drawn from

$$q(x_{k,q}^{(i)}|x_{k-1,q}^{(i)}, y_0^k) := p(x_{k,q}^{(i)}|x_{k-1,q}^{(i)}) \tag{A.32}$$

In this case, the unnormalized importance weights can be computed recursively using

$$\tilde{w}_k^{(i)} = \tilde{w}_{k-1}^{(i)} p(y_k|x_{k,q}^{(i)}) \tag{A.33}$$

After that, the normalized importance weights is computed using (A.26).

Remark: Computing $p(y_k|x_{k,q}^{(i)})$ in Gaussian cases

When the estimation model and the measurement model are driven by zero-mean white Gaussian process noises $w_k \sim \mathcal{N}(0, Q)$ and $v_k \sim \mathcal{N}(0, R)$ respectively, we have

$$p(x_{k,q}^{(i)}|x_{k-1,q}^{(i)}) \propto \exp\left(-\frac{1}{2}(x_{k,q}^{(i)} - f(x_{k-1,q}^{(i)}))^T Q^{-1}(x_{k,q}^{(i)} - f(x_{k-1,q}^{(i)}))\right) \tag{A.34}$$

$$p(y_k|x_{k,q}^{(i)}) \propto \exp\left(-\frac{1}{2}(y_k - h(x_{k,q}^{(i)}))^T R^{-1}(y_k - h(x_{k,q}^{(i)}))\right) \tag{A.35}$$

Degeneracy and Resampling

A common problem when an importance density is used is the degeneracy phenomenon, where after a few iterations, all but one particles will have negligible normalized weights. As a result, a large computational effort is devoted to updating particles barely contributing to the approximation of $p(x_k|y_0^k)$. The particles with low importance weights should be therefore eliminated when a significant degeneracy is observed. The level of degeneracy can be measured by calculating the approximated effective sample size $\hat{N}_{eff}$ [Ristic et al., 2004] defined as

$$\hat{N}_{eff} = \frac{1}{\sum_{i=1}^{N_p} (w_{k,q}^{(i)})^2} \tag{A.36}$$

[1] Using Bayes' rule, we have

$$p(x_k|y_0^k) = \frac{p(y_k|x_k)p(x_k|x_{k-1})}{p(y_k|y_0^{k-1})} p(x_{k-1}|y_0^{k-1}) \tag{A.28}$$

$$\propto p(y_k|x_k)p(x_k|x_{k-1})p(x_{k-1}|y_0^{k-1}) \tag{A.29}$$

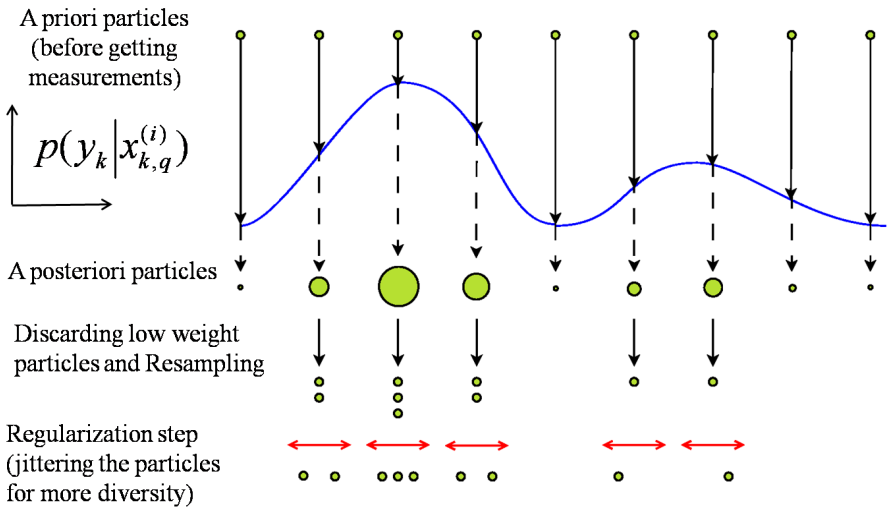

Figure A.1: *A single cycle of the Regularized Particle Filter (RPF). The red arrows represent the action of "jittering" the particles.*

It is easy to verify that $1 \leq \hat{N}_{eff} \leq N_p$. In fact, if we consider two extreme cases: (1) when the weights are equal to each other, in that case $\hat{N}_{eff} = N_p$ and (2) when the weight of one particle is equal to 1 (so the weights of the other particles are equal to 0), in that case $\hat{N}_{eff} = 1$ [Ristic et al., 2004], small $\hat{N}_{eff}$ therefore indicates a severe degeneracy.

One strategy to eliminate particles with low importance weights and to concentrate on particles with high importance weights is to resample the particles whenever $\hat{N}_{eff}$ is lower than a threshold N_{thr}. This involves generating a new set of particles and weights $\{x_{k,q}^{*(i)}, w_{k,q}^{*(i)}\}$ by resampling *with replacement* N_p times from an approximate discrete representation of $p(x_k|y_0^k)$ in (A.23). The new importance weights $w_{k,q}^{*(i)}$ are set to N_p^{-1} for each particle.

Regularized Particle Filter

Although resampling helps us cope with particle degeneracy, it induces a loss of diversity of particles. In fact, the particles that have high weights are statistically selected many times. This problem, known as *sample impoverishment*, is severe when process noise is very small [Ristic et al., 2004]. A method to improve the diversity among the particles called the Regularized Particle Filter (RPF) is proposed in [Musso et al., 2001]. The main idea of the RPF is to do the resampling step using an approximate continuous representation of $p(x_k|y_0^k)$ rather than a discrete-one like in (A.23). This way, particles are kind of "jittered" during the resampling.

The algorithm of the RPF [Ristic et al., 2004] with N_p number of particles and the degeneracy threshold set to N_{thr} is shown in algorithm A.1 where $p(x_0)$ denotes the initial a priori density of the estimate. The estimation is supposed to be done from time index $k = 0$ to $k = k_f$. An illustration of a single cycle of the RPF with resampling step is also given in Fig.A.1.

Algorithm A.1: Regularization Particle Filter (RPF) Algorithm whose importance sampling is chosen equal to the a priori density as in (A.32).

for $k = 0$ **do**
  for $i = 1, \ldots, N_p$ **do**
    Sample independently $x_{0,q}^{(i)}$ from the initial prior density $p(x_0)$.
    Update
    Compute the unnormalized weights $\tilde{w}_{0,q}^{(i)} = p(y_0|x_{0,q}^{(i)})$.
    For $k = 0$, compute the normalized weights $w_{k,q}^{(i)}$ using

$$w_k^{(i)} = \frac{\tilde{w}_k^{(i)}}{\sum_{i=1}^{N_p} \tilde{w}_k^{(i)}} \tag{A.37}$$

  This gives a set of N_p particles and weights $\{x_{0,q}^{(i)}, w_{0,q}^{(i)}\}_{i=1}^{N_p}$.
  The estimate $\hat{x}_0$ is computed using

$$\hat{x}_k = \sum_{i=1}^{N_p} w_{k,q}^{(i)} x_{k,q}^{(i)} \tag{A.38}$$

for $k = 1, \ldots, k_f$ **do**
  Prediction
    for $i = 1, \ldots, N_p$ **do**
      Draw $x_{k,q}^{(i)} \sim p(x_k|x_{k-1,q}^{(i)})$.
  Update
    for $i = 1, \ldots, N_p$ **do**
      Compute the unnormalized weights $\tilde{w}_k^{(i)} = \tilde{w}_{k-1}^{(i)} p(y_k|x_{k,q}^{(i)})$.
      Compute the normalized weights $w_{k,q}^{(i)}$ using (A.37).
  if $\hat{N}_{eff} < N_{thr}$ **then**
    Resampling
      for $i = 1, \ldots, N_p$ **do**
        Calculate the empirical covariance matrix S_k of $\{x_{k,q}^{(i)}, w_{k,q}^{(i)}\}_{i=1}^{N_p}$.
        Compute D_k such that $D_k D_k^T = S_k$.
        Resample the particles with replacement and assign the new associated importance weights to $1/N_p$ for every particles.
        This give a new set of particles $\{x_{k,q}^{*(i)}, N_p^{-1}\}_{i=1}^{N_p}$.
        Draw $\epsilon^{(i)} \sim K$ from the Epanechnikov kernel or the Gaussian kernel (see [Musso et al., 2001] for details).
        Define $x_{k,q}^{*(i)} \leftarrow x_{k,q}^{*(i)} + h_{opt} D_k \epsilon_k$
        where $h_{opt} = A \cdot N^{-\frac{1}{n_x+4}}$ and $A = [4/(n_x+2)]^{\frac{1}{n_x+4}}$.
        Assign $\{x_{k,q}^{(i)}, w_{k,q}^{(i)}\}_{i=1}^{N_p} \leftarrow \{x_{k,q}^{*(i)}, N_p^{-1}\}_{i=1}^{N_p}$
  Computation of the estimate $\hat{x}_k$ is computed using (A.38)

APPENDIX B

Appendices for Chapter 2

B.1 Calculation of the Constants in the MHE's Stability Theorem

We would like to have expressions of the constants c_1, c_2 and c_3 in theorem 1 for the convergence of the estimation errors of the MHE defined in (2.8) when the weight matrix on the arrival cost $\mathcal{P} = p\mathbf{I}_{n_x}$ and $\mathcal{Q}$ and $\mathcal{R}$ are diagonalizable matrices[1]. To do so, inspired by the work in [Alessandri et al., 2008], we calculate an upper bound and a lower bound on the optimal cost $\mathbf{J}_k^\circ$ defined as the cost corresponding to the optimal estimate $\hat{x}_{k-N|k}^\circ$, i.e. $\mathbf{J}_k^\circ \triangleq \mathbf{J}(\hat{x}_{k-N|k}^\circ, \hat{x}_{k-N|k}^-, y_{k-N}^k)$. Then, combining the upper bound to the lower bound gives the dynamics of the estimation errors and of the estimated process noise sequence.

Denote $\lambda_{\mathcal{Q},max}$ and $\lambda_{\mathcal{Q},min}$ the maximum and the minimum eigenvalues of $\mathcal{Q}$ respectively. In the same way, denote $\lambda_{\mathcal{R},max}$ and $\lambda_{\mathcal{R},min}$ the maximum and the minimum eigenvalues of $\mathcal{R}$ respectively.

Using the definition of the observation map in (2.10), the third term in the cost function $\mathbf{J}_k$ in (2.8b) becomes

$$\sum_{i=0}^{N} \|y_{k-N+i} - h(\hat{x}_{k-N+i|k})\|_{\mathcal{R}}^2 = \left\|y_{k-N}^k - F(\hat{x}_{k-N|k}, \hat{w}_{k-N}^{k-1})\right\|_{\mathcal{R}}^2 \tag{B.1}$$

Therefore, the cost function can be written as

$$\mathbf{J}_k = \left\|\hat{x}_{k-N|k} - \hat{x}_{k-N|k}^-\right\|_{\mathcal{P}}^2 + \sum_{i=0}^{N-1} \left\|\hat{w}_{k-N+i|k}\right\|_{\mathcal{Q}}^2 + \left\|y_{k-N}^k - F(\hat{x}_{k-N|k}, \hat{w}_{k-N|k}^{k-1})\right\|_{\mathcal{R}}^2 \tag{B.2}$$

With the assumption $\mathcal{P} = p\mathbf{I}_{n_x}$, (B.2) becomes

$$\mathbf{J}_k = p\left\|\hat{x}_{k-N|k} - \hat{x}_{k-N|k}^-\right\|^2 + \sum_{i=0}^{N-1} \left\|\hat{w}_{k-N+i|k}\right\|_{\mathcal{Q}}^2 + \left\|y_{k-N}^k - F(\hat{x}_{k-N|k}, \hat{w}_{k-N|k}^{k-1})\right\|_{\mathcal{R}}^2 \tag{B.3}$$

[1] A symmetric positive definite matrix is diagonalizable.

Notations and Definitions for Stability Studies

Let us define as in [Alessandri et al., 2008] $\forall x'_{k-N} \in \mathbb{X}$, $\forall w_{k-N+i} \in \mathbb{W}$, $i = 0, 1, \ldots, N-1$

$$D_w(x'_{k-N}) \triangleq \begin{pmatrix} \frac{\partial y_{k-N}}{\partial w_{k-N}} & \frac{\partial y_{k-N}}{\partial w_{k-N+1}} & \cdots & \frac{\partial y_{k-N}}{\partial w_{k-1}} \\ \vdots & \vdots & \ddots & \vdots \\ \frac{\partial y_k}{\partial w_{k-N}} & \frac{\partial y_k}{\partial w_{k-N+1}} & \cdots & \frac{\partial y_k}{\partial w_{k-1}} \end{pmatrix} \tag{B.4}$$

Using (2.11), we have

$$D_w(x'_{k-N}) = \begin{pmatrix} 0 & 0 & \cdots & 0 \\ \frac{\partial (h \circ f_{(1)}^{w_{k-N}})}{\partial w_{k-N}} & 0 & \cdots & 0 \\ \frac{\partial (h \circ f_{(2)}^{w_{k-N}^{k-N+1}})}{\partial w_{k-N}} & \frac{\partial (h \circ f_{(2)}^{w_{k-N}^{k-N+1}})}{\partial w_{k-N+1}} & \cdots & 0 \\ \vdots & \vdots & \ddots & \vdots \\ \frac{\partial (h \circ f_{(N)}^{w_{k-N}^{k-1}})}{\partial w_{k-N}} & \frac{\partial (h \circ f_{(N)}^{w_{k-N}^{k-1}})}{\partial w_{k-N+1}} & \cdots & \frac{\partial (h \circ f_{(N)}^{w_{k-N}^{k-1}})}{\partial w_{k-1}} \end{pmatrix} \tag{B.5}$$

$$\Delta_w \triangleq \max_{x'_{k-N} \in \mathbb{X}} \left\| D_w(x'_{k-N}) \right\|_p |_{w_{k-N}^{k-1} = \mathbf{0}_{n_x N \times 1}} \tag{B.6}$$

Recall that $\| \cdot \|_p$ is the operator p-norm defined as in (2.6). Any matrix norm can be chosen. In this study, the 2-norm as defined in (2.7) is chosen.

$$\bar{k} \triangleq \max_{i=1,\ldots,N} \bar{k}_i \tag{B.7}$$

where $\bar{k}_i > 0$ are suitable scalars such that

$$\begin{aligned} \left\| \frac{\partial (h \circ f_{(1)}^{w_{k-N}})}{\partial w_{k-N}} |_{w_{k-N} = w'_{k-N}} - \frac{\partial (h \circ f_{(1)}^{w_{k-N}})}{\partial w_{k-N}} |_{w_{k-N}=0} \right\|_p &\leq \bar{k}_1 \left\| w'_{k-N} \right\|_p \\ &\vdots \\ \left\| \frac{\partial (h \circ f_{(N)}^{w_{k-N}^{k-1}})}{\partial w_{k-N}^{k-1}} |_{w_{k-N}^{k-1} = w'^{k-1}_{k-N}} - \frac{\partial (h \circ f_{(N)}^{w_{k-N}^{k-1}})}{\partial w_{k-N}^{k-1}} |_{w_{k-N}^{k-1} = \mathbf{0}_{n_x N \times 1}} \right\|_p &\leq \bar{k}_N \left\| w'^{k-1}_{k-N} \right\|_p \end{aligned} \tag{B.8}$$

The constant $\bar{k}_i$ exists as we are dealing with compositions of $\mathcal{C}^2$ functions. Equation (B.8) is obtained using mean-value theorem [Alessandri et al., 2008]. The mean-value theorem is recalled here [Burke, 2014]: if a function $\varkappa : \mathbb{R}^n \to \mathbb{R}$ is differentiable, then for every $x', x'' \in \mathbb{R}^n$, there exists $x''' \in [x', x'']$ such that

$$\varkappa(x') - \varkappa(x'') = \left(\frac{\partial \varkappa}{\partial x} \right) |_{x = x'''} (x' - x'') \tag{B.9}$$

The constant $\bar{k}_i$ may not be easy to computed. However, we will see later on that the values of $\bar{k}_i$ are not needed to guarantee the stability of the estimation errors of the MHE. They only affect the asymptotic bound of the estimation errors.

Upper Bound on the Optimal Cost $\mathbf{J}_k^\circ$

Recall that the notation x_{k-N} is used for the *real* state of the system (2.1a) at $k-N$. Since $\mathbf{J}_k^\circ$ is the optimal solution of (2.8), it is smaller than the cost calculated at the real state x_{k-N} with zero process noise $\mathbf{0}_{n_x N\times 1}$. In other words,

$$\begin{aligned}\mathbf{J}_k^\circ &\leq p\left\|x_{k-N}-\hat{x}_{k-N|k}^-\right\|^2+\left\|y_k^{k-N}-F(x_{k-N},\mathbf{0}_{n_xN\times1})\right\|_{\mathcal{R}}^2\\ &\leq p\left\|x_{k-N}-\hat{x}_{k-N|k}^-\right\|^2+\lambda_{\mathcal{R},max}\left\|y_k^{k-N}-F(x_{k-N},\mathbf{0}_{n_xN\times1})\right\|^2 \end{aligned}\tag{B.10}$$

According to [Alessandri et al., 2008], the last term on the r.h.s of (B.10) follows

$$\left\|y_k^{k-N}-F(x_{k-N},\mathbf{0}_{n_xN\times1})\right\|^2\leq c_{Ale,N}^2 \tag{B.11}$$

where

$$c_{Ale,N}\triangleq\Delta_w\sqrt{N}r_w+\sqrt{N+1}r_v+\frac{\bar{k}}{2}\sqrt{\frac{N(N+1)(2N+1)}{6}}r_w^2 \tag{B.12}$$

Therefore, we have an upper bound on the optimal cost $\mathbf{J}_k^\circ$ as follows

$$\mathbf{J}_k^\circ\leq p\left\|x_{k-N}-\hat{x}_{k-N|k-1}\right\|^2+\lambda_{\mathcal{R},max}c_{Ale,N}^2 \tag{B.13}$$

Now, let us pursue with the calculation of a lower bound of the optimal cost.

Lower Bound on the Optimal Cost $\mathbf{J}_k^\circ$

Denote, for $i=0,\ldots,N$, $\hat{x}_{k-N}$ any estimate of x_{k-N} and $\hat{w}_{k-N}^{k-1}$ any sequence of estimated process noises from $k-N$ to $k-1$. We would like to compute the cost in (B.3) for any solution $(\hat{x}_{k-N},\hat{w}_{k-N}^{k-1})$, not necessarily computed at k. Thanks to the triangle inequality (2.13), we obtain

$$\begin{aligned}\|F(x_{k-N},\mathbf{0}_{n_xN\times1})-F(\hat{x}_{k-N},\mathbf{0}_{n_xN\times1})\|^2 &\leq 3\left\|F(x_{k-N},\mathbf{0}_{n_xN\times1})-y_{k-N}^k\right\|^2\\ &\quad+3\left\|y_{k-N}^k-F(\hat{x}_{k-N},\hat{w}_{k-N}^{k-1})\right\|^2\\ &\quad+3\left\|F(\hat{x}_{k-N},\hat{w}_{k-N}^{k-1})-F(\hat{x}_{k-N},\mathbf{0}_{n_xN\times1})\right\|^2\end{aligned}$$

Using (2.12) and (B.11) and the fact that $\mathcal{R}$ is diagonalizable, the third term of the cost function (B.3) becomes

$$\begin{aligned}\left\|y_k^{k-N}-F(x_{k-N},\mathbf{0}_{n_xN\times1})\right\|_{\mathcal{R}}^2 &\geq \lambda_{\mathcal{R},min}(\frac{1}{3}\phi(\|x_{k-N}-\hat{x}_{k-N}\|^2)-c_{Ale,N}^2\\ &\quad-\left\|F(\hat{x}_{k-N},\hat{w}_{k-N}^{k-1})-F(\hat{x}_{k-N},\mathbf{0}_{n_xN\times1})\right\|^2)\end{aligned}\tag{B.14}$$

According to [Alessandri et al., 2008], we have

$$\left\|F(\hat{x}_{k-N},\hat{w}_{k-N}^{k-1})-F(\hat{x}_{k-N},\mathbf{0}_{n_xN\times1})\right\|^2\leq(\Delta_w\sqrt{N}r_w+\frac{\bar{k}}{2}\sqrt{\frac{N(N+1)(2N+1)}{6}}r_w^2)^2 \tag{B.15}$$

Hence, (B.14) becomes

$$\begin{aligned}\left\|y_k^{k-N}-F(x_{k-N},\mathbf{0}_{n_xN\times1})\right\|_{\mathcal{R}}^2 &\geq \lambda_{\mathcal{R},min}[\frac{1}{3}\phi(\|x_{k-N}-\hat{x}_{k-N}\|^2)-c_{Ale,N}^2\\ &\quad-(\Delta_w\sqrt{N}r_w+\frac{\bar{k}}{2}\sqrt{\frac{N(N+1)(2N+1)}{6}}r_w^2)^2]\end{aligned}\tag{B.16}$$

Using the triangle inequality, we obtain

$$p\left\|\hat{x}_{k-N}-\hat{x}_{k-N|k-1}\right\|^2 \geq \frac{1}{2}p\left\|x_{k-N}-\hat{x}_{k-N}\right\|^2 - p\left\|x_{k-N}-\hat{x}_{k-N|k-1}\right\|^2 \tag{B.17}$$

Again, since $\mathcal{Q}$ is diagonalizable we can write

$$\sum_{i=0}^{N-1}\left\|\hat{w}_{k-N+i|k}\right\|_{\mathcal{Q}}^2 \geq \lambda_{\mathcal{Q},min}\sum_{i=0}^{N-1}\left\|\hat{w}_{k-N+i}\right\|^2 \tag{B.18}$$

Define by $e^{\circ}_{k-N|k} \triangleq x_{k-N}-\hat{x}^{\circ}_{k-N|k}$ the estimation error of the optimal estimate of x_{k-N} given by the MHE computed at instant k and the associated optimal process noise sequence $\{\hat{w}^{\circ}{}^{k-1}_{k-N|k}\}$. Remark that $\sum_{i=0}^{N-1}\left\|\hat{w}^{\circ}_{k-N+i|k}\right\|^2 = \left\|\hat{w}^{\circ}{}^{k-1}_{k-N|k}\right\|^2$. Combine (B.16)-(B.18) to have the lower bound:

$$\mathbf{J}^{\circ}_k \geq \frac{1}{2}p\left\|e^{\circ}_{k-N|k}\right\|^2 - p\left\|x_{k-N}-\hat{x}^{-}_{k-N|k}\right\|^2 + \frac{1}{3}\lambda_{\mathcal{R},min}\phi(\left\|e^{\circ}_{k-N|k}\right\|^2) - \lambda_{\mathcal{R},min}c'^2 + \lambda_{\mathcal{Q},min}\left\|\hat{w}^{\circ}{}^{k-1}_{k-N|k}\right\|^2 \tag{B.19}$$

where

$$c'^2 = c^2_{Ale,N} + (\Delta_w\sqrt{N}r_w + \frac{\bar{k}}{2}\sqrt{\frac{N(N+1)(2N+1)}{6}}r_w^2)^2 \tag{B.20}$$

Now, let us combine the upper and the lower bounds on the optimal cost to have the dynamics of the estimation errors e°_{k-N} and the associated estimated process noise $\hat{w}^{\circ}{}^{k-1}_{k-N}$.

Dynamics of the Estimation Errors of the MHE

Combining the upper bound in (B.13) to the lower bound in (B.19), we obtain

$$\begin{aligned} p\left\|x_{k-N}-\hat{x}^{-}_{k-N|k}\right\|^2 + \lambda_{\mathcal{R},max}c^2_{Ale,N} \;\geq\; & \frac{1}{2}p\left\|e^{\circ}_{k-N|k}\right\|^2 - p\left\|x_{k-N}-\hat{x}^{-}_{k-N|k}\right\|^2 \\ & + \frac{1}{3}\lambda_{\mathcal{R},min}\phi(\left\|e^{\circ}_{k-N|k}\right\|^2) - \lambda_{\mathcal{R},min}c'^2 + \lambda_{\mathcal{Q},min}\left\|\hat{w}^{\circ}{}^{k-1}_{k-N|k}\right\|^2 \end{aligned} \tag{B.21}$$

Rearrange (B.21) and use (2.15) to have

$$\left(\frac{p}{2}+\frac{\lambda_{\mathcal{R},min}}{3}\delta\right)\left\|e^{\circ}_{k-N|k}\right\|^2 + \lambda_{\mathcal{Q},min}\left\|\hat{w}^{\circ}{}^{k-1}_{k-N|k}\right\|^2 \leq 2p\left\|x_{k-N}-\hat{x}_{k-N|k-1}\right\|^2 + \mathbf{c}^2$$

where

$$\mathbf{c}^2 = \lambda_{\mathcal{R},max}c^2_{Ale,N} + \lambda_{\mathcal{R},min}c'^2 \tag{B.22}$$

Now, using the fact that $\hat{x}^{-}_{k-N|k} = f(\hat{x}^{\circ}_{k-N-1|k-1}) + \hat{w}^{\circ}_{k-N-1|k-1}$, $x_{k-N} = f(x_{k-N-1}) + w_{k-N-1}$ and the Lipschitz continuity of f, we have

$$\begin{aligned} \left\|x_{k-N}-\hat{x}^{-}_{k-N|k}\right\|^2 &= \left\|f(x_{k-N-1}) - f(\hat{x}^{\circ}_{k-N-1|k-1}) - \hat{w}^{\circ}_{k-N-1|k-1} + w_{k-N-1}\right\|^2 \\ &\leq 3(L^x_f)^2\left\|e^{\circ}_{k-N-1|k-1}\right\|^2 + 3\left\|\hat{w}^{\circ}_{k-N-1|k-1}\right\|^2 + 3r_w^2 \end{aligned} \tag{B.23}$$

Replace (B.23) into (B.22) to get

$$\begin{aligned} \left(\frac{p}{2}+\frac{\lambda_{\mathcal{R},min}}{3}\delta\right)\left\|e^{\circ}_{k-N|k}\right\|^2 \;+\; & \lambda_{\mathcal{Q},min}\sum_{i=0}^{N-1}\left\|\hat{w}^{\circ}_{k-N+i|k}\right\|^2 \\ & \leq 2p\left(3(L^x_f)^2\left\|e^{\circ}_{k-N-1|k-1}\right\|^2 + 3\left\|\hat{w}^{\circ}_{k-N-1|k-1}\right\|^2 + 3r_w^2\right) + \mathbf{c}^2 \end{aligned} \tag{B.24}$$

Using the fact that $\left\|\hat{w}^{\circ}_{k-N-1|k-1}\right\|^2 \leq \left\|\hat{w^{\circ}}^{k-2}_{k-N-1|k-1}\right\|^2$, we obtain

$$\begin{aligned}
\left\|e^{\circ}_{k-N|k}\right\|^2 &\leq \frac{1}{p+\frac{2\lambda_{\mathcal{R},min}}{3}\delta}\left(12p(L_f^x)^2\left\|e^{\circ}_{k-N-1|k-1}\right\|^2 + 12p\left\|\hat{w^{\circ}}^{k-2}_{k-N-1|k-1}\right\|^2 + 12pr_w^2 + 2\mathbf{c}^2\right)\\
\left\|\hat{w^{\circ}}^{k-1}_{k-N|k}\right\|^2 &\leq \frac{1}{\lambda_{\mathcal{Q},min}}\left(6p(L_f^x)^2\left\|e^{\circ}_{k-N-1|k-1}\right\|^2 + 6p\left\|\hat{w^{\circ}}^{k-2}_{k-N-1|k-1}\right\|^2 + 6pr_w^2 + \mathbf{c}^2\right) \qquad \text{(B.25)}
\end{aligned}$$

In other words, we find the stability theorem 1 proposed in [Alessandri et al., 2010]

$$\left\|e^{\circ}_{k-N|k}\right\|^2 \leq \xi_{k-N} \qquad \text{(B.26)}$$

$$\left\|\hat{w^{\circ}}^{k-1}_{k-N|k}\right\|^2 \leq \omega_{k-N} \qquad \text{(B.27)}$$

where the sequences $\{\xi_k\}$ and $\{\omega_k\}$ are generated by the linear system

$$\begin{pmatrix}\omega_{k+1}\\ \xi_{k+1}\end{pmatrix} = A(p,\delta)\begin{pmatrix}\omega_k\\ \xi_k\end{pmatrix} + B(p,\delta)\begin{pmatrix}r_w^2\\ r_v^2\end{pmatrix} \qquad \text{(B.28)}$$

with

$$\begin{aligned}
A(p,\delta) &\triangleq \begin{pmatrix} c_1 p & c_1(L_f^x)^2 p\\ c_2 p/(p+c_3\delta) & c_2(L_f^x)^2 p/(p+c_3\delta)\end{pmatrix}\\
B(p,\delta) &\triangleq \begin{pmatrix} c_4 p + c_5 & c_6\\ (c_7 p + c_8)/(p+c_3\delta) & c_9/(p+c_3\delta)\end{pmatrix}
\end{aligned}$$

where thanks to our calculation in this section, we find

$$c_1 = \frac{6}{\lambda_{\mathcal{Q},min}},\ c_2 = 12,\ c_3 = \frac{2}{3}\lambda_{\mathcal{R},min} \qquad \text{(B.29)}$$

The expressions of $c_4, \ldots, c_9$ can be computed using the expression of $\mathbf{c}^2$. To compute $\mathbf{c}$, one has to compute the values of Δ_w in (B.6) and $\bar{k}_i$ in (B.8). One way to compute Δ_w is to use the symbolic calculation in MATLAB to have an analytical expression of D_w then make hypotheses on the ranges of possible values of the state and the process noise to compute Δ_w. To compute $\bar{k}_i$, remark that $\bar{k}_i$ is in fact a Lipschitz constant of the function $\frac{\partial(h\circ f_i^{w_{k-N}^{k-i}})}{\partial w_{k-N}^{k-1}}$. The Lipschitz constant can be computed using the symbolic calculation in MATLAB to have an analytical expression of the Jacobian matrix of $\frac{\partial(h\circ f_i^{w_{k-N}^{k-i}})}{\partial w_{k-N}^{k-1}}$ then make hypotheses on the ranges of possible values of the state and the process noise to compute the norm of the Jacobian matrix, or equivalently the Lipschitz constant. Remark that the computed value of $\mathbf{c}$ tends to be very large since it is computed using upper bounds of many variables. However, in practice, we see that the estimation errors provided by the MHE are small even though the computed theoretical bound is very high.

The convergence of the estimation errors or the stability of the dynamics of the estimation errors can be guaranteed if the eigenvalue of the matrix $A(p,\delta) < 1$, hence the stability result in theorem 1.

We note that an upper bound on the estimation error $e^{\circ}_{k|k} = \|x_k - \hat{x}^{\circ}_k\|^2$ can be easily derived by simple Lipschitz arguments.

The dynamics of the system (B.28) is asymptotically stable and the upper bounding sequences $\{\xi_k\}$ and $\{\omega_k\}$ converge exponentially to the asymptotic values $\xi_\infty(p,\delta)$ and $\omega_\infty(p,\delta)$ where

$$\begin{pmatrix} \omega_\infty \\ \xi_\infty \end{pmatrix} \triangleq (\mathbf{I}_2 - A(p,\delta)))^{-1} B(p,\delta) \begin{pmatrix} r_w \\ r_v \end{pmatrix} \tag{B.30}$$

if (2.16) is satisfied [Alessandri et al., 2010].

APPENDIX C

Appendices for Chapter 3

C.1 Evolution of the Ballistic Coefficient of a Sphere

The evolution of the ballistic coefficient can be calculated from

$$\beta = \frac{m}{C_D A} \tag{C.1}$$

Recall that m and the cross section $A = \pi \left(\frac{D}{2}\right)^2$ are supposed to be constant during the re-entry. For a spherical object, the drag coefficient C_D depends only on the Reynolds number Re. The expression of $C_D(\cdot)$ for a sphere derived from experimental data is [Morrison, 2010][Collins, 2012]:

$$\begin{aligned}
C_D &= \frac{24}{Re} + \frac{2.6\left(\frac{Re}{5.0}\right)}{1+\left(\frac{Re}{5.0}\right)^{1.52}} + \frac{0.411\left(\frac{Re}{2.63\cdot 10^5}\right)^{-7.94}}{1+\left(\frac{Re}{2.63\cdot 10^5}\right)^{-8.00}} \\
&\quad + \frac{Re^{0.80}}{4.61\cdot 10^5}, \text{ if } Re \leq 4.77\cdot 10^5 \\
C_D &= -0.485 + 0.1\log Re, \text{ if } 4.77\cdot 10^5 < Re \leq 1.2\cdot 10^6 \\
C_D &= 0.19 - \frac{8\cdot 10^4}{Re}, \text{ if } 1.2\cdot 10^6 < Re \leq 2\cdot 10^6 \\
C_D &= 0.15, \text{ if } Re \geq 2\cdot 10^6
\end{aligned} \tag{C.2}$$

Recall that the norm of the velocity in the ECEF coordinates $\|\mathbf{v}_{EF}\|$ is equal to the norm of the velocity in the SEU coordinates $\|\mathbf{v}\|$ (1.11). In chapter 3 the simulation of the 1D trajectories is done by integrating the acceleration in the SEU coordinates. In chapter 5 the simulation of the 3D trajectories is done by integrating the acceleration in the ECEF coordinates. To generalize, denote $\|\vec{v}\| = \|\mathbf{v}_{EF}\| = \|\mathbf{v}\|$.

The Reynolds number $Re(H(t), \|\vec{v}(t)\|)$ is calculated from

$$Re = \frac{\rho(H)\,\|\vec{v}\|\,D}{\mu_{atm}(H)} \tag{C.3}$$

D is the diameter of the sphere, $\mu_{atm}(H)$ is the atmospheric dynamic viscosity which is strongly influenced by the temperature $T_{atm}(H)$. $\mu_{atm}(H)$ is obtained from the Sutherland's formula [Smits and Dussauge, 2006]:

$$\mu(H) = \mu_0 \frac{T_{atm,0} + C}{T_{atm}(H) + C} \left(\frac{T_{atm}(H)}{T_{atm,0}} \right)^{\frac{3}{2}} \tag{C.4}$$

with the air's reference temperature $T_{atm,0} = 291.15$ K, the air's reference viscosity at the reference temperature $\mu_0 = 18.27 \cdot 10^{-6}$ Pa·s and the Sutherland's constant for air $C_s = 120$ K. The temperature T depends on the altitude of the object and is given by the atmospheric model US76. The model US76 is a table that gives values for atmospheric temperature, density and pressure in given ranges of altitude published by the U.S. Committee on Extension to the standard atmosphere in 1976.

C.2 Verification of the Assumptions on the Stability of the Estimation Errors of the MHE in the Deterministic Framework

Let us consider first (A1):

(A1) $\mathbb{X}$ is a convex compact set, $\mathbb{W}$ and $\mathbb{V}$ are compact sets with $0 \in \mathbb{W}$ and $0 \in \mathbb{V}$.

Assumption (A1) is verified since $\mathbb{X}$ defined in section 3.6.4.1 is a convex compact set, $\mathbb{W}$ defined in the same section is a compact set and the measurement noise v_k in (3.4) is modeled by a zero-mean bounded white noise.

Let us pursue with assumption (A2):

(A2) The initial state x_0 is such that, for any possible sequence of process noises $\{w_k\}$, the system trajectory $\{x_k\}$ lies in the convex compact set $\mathbb{X}$, $\forall k$

The convex compact set $\mathbb{X}$ is defined in section 3.6.4.1 using the real evolution of the position, the velocity, the ballistic coefficient and the acceleration of the generated trajectories shown in figure 3.3. Hence, (A2) is verified. Now, consider assumption (A3):

(A3) f and h are $\mathcal{C}^2$ functions with respect to x on $\mathbb{X}$. f and h are therefore also locally Lipschitz. Define their Lipschitz constants as L_f^x and L_h^x respectively

It is easy to see that the state function f defined in (3.10) for the estimation model with ballistic coefficient is $\mathcal{C}^2$. The state function f defined in (3.15) for the estimation model with acceleration is $\mathcal{C}^2$ if $v_z \neq 0$ m/s. The case of zero velocity is out of interest since it means that the debris has reached the ground. Concerning the measurement function h, recall that $y_k = h(x_k) = r_{z_k}$, it is immediate that h is $\mathcal{C}^2$.

Now, let us choose Lipschitz constants L_f^x. The constant Lipschitz for the measurement function h: L_h^x is not needed for the stability of the estimation errors of the MHE. However, it is immediate to see that $L_h^x = 1$ can be chosen since

$$\|r'_z - r''_z\| \leq \|x' - x''\| \tag{C.5}$$

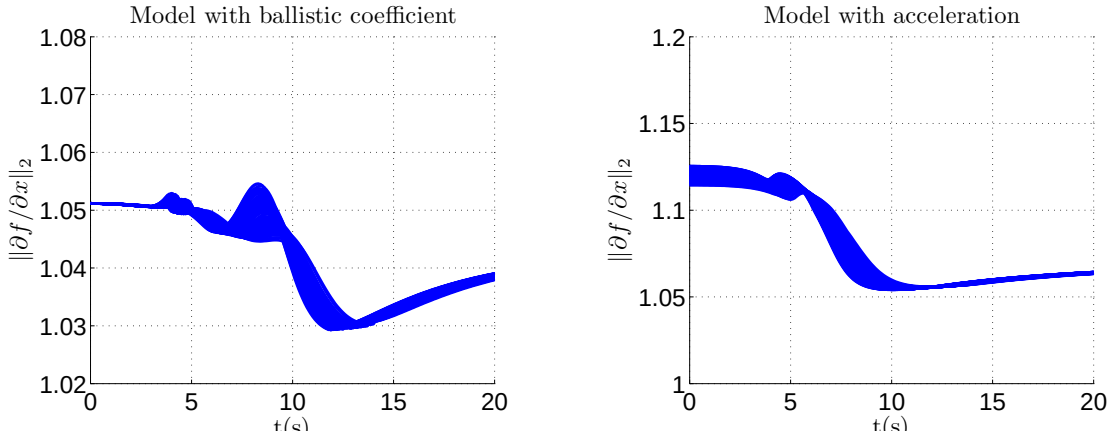

Figure C.1: Norm of the Jacobian of the state function $\left\|\frac{\partial f}{\partial x}\right\|_2$ of each trajectory in time: for the estimation model with ballistic coefficient (left) and for that with acceleration (right)

Denote x_k^n the state at instant k of the n^{th} Monte Carlo run. According to [Khalil and Grizzle, 2002] the Lipschitz constant can be chosen such that

$$L_f^x > \max_{\forall k,\forall n} \left\| \left.\frac{\partial f}{\partial x}\right|_{x=x_k^n} \right\|_p \tag{C.6}$$

$$L_h^x > \max_{\forall k,\forall n} \left\| \left.\frac{\partial h}{\partial x}\right|_{x=x_k^n} \right\|_p \tag{C.7}$$

where $\|\cdot\|_p$ is the operator p-norm defined in (2.6). Any norm can be chosen for determining L_f^x. In our study, the 2-norm as defined in (2.7) is chosen.

The evolutions of $\left\| \left.\frac{\partial f}{\partial x}\right|_{x=x_k^n} \right\|_2$ for each n^{th} run are computed and shown in figure C.1 for the estimation model with ballistic coefficient (left) and for that with acceleration (right). Thanks to this figure, a Lipschitz constant $L_f^x = 1.2$ is chosen for both models.

Now, let us consider assumption (A4):

(A4) The system is observable in $N+1$ steps

This assumption is verified using symbolic calculation in MATLAB by computing the rank of the derivative of the observation map $F(x_{k-N}, \mathbf{0}_{n_x N\times 1})$ as function of x_{k-N} which turns out to be equal to $n_x = 3$. This implies that $\forall (x', x'') \in \mathbb{X}^2$, there exists a class K function $\phi(\cdot)$ such that

$$\phi(\|x' - x''\|^2) \leq \|F(x', \mathbf{0}_{n_x N\times 1}) - F(x'', \mathbf{0}_{n_x N\times 1})\|^2 \tag{C.8}$$

Consider now (A5):

(A5) The system has finite sensitivity, i.e. the minimum of the class-K function $\phi(\cdot)$ in (C.8) exists. Denote δ the sensitivity parameter of the system. It is defined as

$$\delta = \inf_{(x',x'')\in\mathbb{X}^2, x'\neq x''} \frac{\phi(\|x' - x''\|^2)}{\|x' - x''\|^2} > 0 \tag{C.9}$$

Denote $F_{1:n_x}(x, \mathbf{0}_{n_x N\times 1})$ the first n_x components of $F(x, \mathbf{0}_{n_x N\times 1})$. Recall that we have $n_x = 3$ and remark that ϕ can be chosen such that

$$\phi(\|x' - x''\|^2) \leq \|F_{1:3}(x', \mathbf{0}_{n_x N\times 1}) - F_{1:3}(x'', \mathbf{0}_{n_x N\times 1})\|^2 \tag{C.10}$$

It is verified using symbolic calculation in MATLAB that the rank of the derivative of the observation map $F_{1:3}(x_{k-N}, \mathbf{0}_{n_x N\times 1})$ as function of x_{k-N} is equal to 3. Hence, $F_{1:3}(x_{k-N}, \mathbf{0}_{n_x N\times 1})$ is invertible.

According to [Von Neumann and Goldstine, 1947], a matrix lower bound $\|A\|_{l,p}$ is such that

$$\|A\|_{l,p} = \min_{x\neq 0} \frac{\|Ax\|_p}{\|x\|_p} \tag{C.11}$$

Moreover, if A is an invertible matrix therefore,

$$\left\|A^{-1}\right\|_p = \|A\|_{l,p}^{-1} \tag{C.12}$$

Denote $\dfrac{\partial F_{1:3}(x_{k-N}, \mathbf{0}_{n_x N\times 1})}{\partial x_{k-N}}$ the Jacobian matrix of the map $F_{1:3}(x_{k-N}, \mathbf{0}_{n_x N\times 1})$ and $\left\|\dfrac{\partial F_{1:3}(x_{k-N}, \mathbf{0}_{n_x N\times 1})}{\partial x_{k-N}}\right\|_{l,2}$ its lower norm. Using the mean-value inequality for multivariable function in [Kuttler, 2009], we get

$$\left\|\frac{\partial F_{1:3}(x_{k-N}, \mathbf{0}_{n_x N\times 1})}{\partial x_{k-N}}\right\|_{l,2}^2 \|x' - x''\|^2 \leq \|F_{1:3}(x', \mathbf{0}_{n_x N\times 1}) - F_{1:3}(x'', \mathbf{0}_{n_x N\times 1})\|^2 \tag{C.13}$$

Hence, ϕ can be chosen such that

$$\phi(\|x' - x''\|^2) = \left\|\frac{\partial F_{1:3}(x_{k-N}, \mathbf{0}_{n_x N\times 1})}{\partial x_{k-N}}\right\|_{l,2}^2 \|x' - x''\|^2 \tag{C.14}$$

Then, the sensitivity parameter δ in (C.9) can be chosen such that

$$\delta = \left\|\frac{\partial F_{1:3}(x_{k-N}, \mathbf{0}_{n_x N\times 1})}{\partial x_{k-N}}\right\|_{l,2}^2 \tag{C.15}$$

The values of $\left\|\left(\dfrac{\partial F_{1:3}(x_{k-N}, \mathbf{0}_{n_x N\times 1})}{\partial x_{k-N}}\right)^{-1}\right\|_2$ of each simulated trajectory are computed using MATLAB and its lower norm is obtained using (C.12). We find that for the estimation model with ballistic coefficient $\delta = 1.6 \cdot 10^{-15}$ and for the estimation model with acceleration $\delta = 1.2755 \cdot 10^{-5}$ can be chosen. Assumption (A5) is hence verified if these values of δ are chosen.

Remark that the value of δ is very small. This may be due to the fact that δ is computed using bounds on many variables which results in a pessimistic value of δ, i.e. a very small value of δ which represents a situation in which the system is not much observable.

APPENDIX D

Appendices for Chapter 4

D.1 Proof of the Propositions in Chapter 4

D.1.1 Proof of Proposition 1

Proposition 1 states that:

The squared norm of the difference at $k+i$ between the real state x_{k+i} of (4.1) starting from x_k at k, and the nominal state ${}^n x_{k+i}$ of (4.2) starting from ${}^n x_k = x_k$ is bounded as

$$\|x_{k+i} - {}^n x_{k+i}\|^2 \leq (\sum_{j=0}^{i-1} \{2(L_f^x)^2\}^j) 2r_w^2 \tag{D.1}$$

Proof. For $i = 1$: since ${}^n x_k = x_k$, $\|x_{k+1} - {}^n x_{k+1}\|^2 = \|f(x_k) + w_k - f({}^n x_k)\|^2 \leq r_w^2$. Now suppose that it holds for i. At $i+1$, we have:

$$\|x_{k+i+1} - {}^n x_{k+i+1}\|^2 \quad = \quad \|f(x_{k+i}) + w_{k+i} - f({}^n x_{k+i})\|^2$$

Using the triangle inequality (4.12), we get

$$\|x_{k+i+1} - {}^n x_{k+i+1}\|^2 \leq 2\|f(x_k) - f({}^n x_k)\|^2 + 2\|w_k\|^2$$

Using the Lipschitz property of f, we have

$$\|f(x_k) - f({}^n x_k)\|^2 \leq (L_f^x)^2 \|x_k - {}^n x_k\|^2$$

Using the bound on the process noise (4.6) in condition (C1) to have $\|w_k\|^2 \leq r_w^2$. Hence,

$$\begin{aligned}
\|x_{k+i+1} - {}^n x_{k+i+1}\|^2 &\leq 2(L_f^x)^2 \|x_{k+i} - {}^n x_{k+i}\|^2 + 2r_w^2 \\
&\leq 2(L_f^x)^2 \left(\sum_{j=0}^{i-1} \{2(L_f^x)^2\}^j \right) 2r_w^2 + 2r_w^2 = \left(\sum_{j=1}^{i} \{2(L_f^x)^2\}^j + 1 \right) 2r_w^2 \\
&\leq (\sum_{j=0}^{i} \{2(L_f^x)^2\}^j) 2r_w^2
\end{aligned}$$

which completes the proof by recurrence. □

D.1.2 Proof of Proposition 2

Proposition 2 states that:
The squared norm of the difference at $k+i$ between the real measurement y_{k+i} of (4.1) starting from x_k at k and the nominal measurement ${}^n y_{k+i}$ of the nominal state of (4.2) starting from ${}^n x_k = x_k$ is bounded as

$$\|y_{k+i} - {}^n y_{k+i}\|^2 \leq 2(L_h^x)^2 (\sum_{j=0}^{i-1} \{2(L_f^x)^2\}^j) 2r_w^2 + 2r_v^2 \tag{D.2}$$

Proof. For $i = 1$

$$\|y_{k+1} - {}^n y_{k+1}\|^2 = \|h(f(x_k) + w_k) + v_k - h(f({}^n x_k))\|^2$$

Using the triangle inequality (4.12), the Lipschitz property of h and the bound on the measurement noise (4.6) in condition (C1), we get

$$\|y_{k+1} - {}^n y_{k+1}\|^2 \leq 2(L_h^x)^2 2r_w^2 + 2r_v^2$$

Suppose that the proposition holds for i. At $i+1$, we have:

$$\begin{aligned} \|y_{k+i+1} - {}^n y_{k+i+1}\|^2 &= \|h(f(x_{k+i}) + w_{k+i}) + v_{k+i} - h(f({}^n x_{k+i}))\|^2 \\ &\leq 2(L_h^x)^2 \left(2\|f(x_{k+i}) - f({}^n x_{k+i})\|^2 + 2r_w^2\right) + 2r_v^2 \\ &\leq 2(L_h^x)^2 \left(2(L_f^x)^2 \|x_{k+i} - {}^n x_{k+i}\|^2 + 2r_w^2\right) + 2r_v^2 \end{aligned}$$

Using (D.1) to have

$$\begin{aligned} \|y_{k+i+1} - {}^n y_{k+i+1}\|^2 &\leq 2(L_h^x)^2 \left(2(L_f^x)^2 (\sum_{j=0}^{i-1} \{2(L_f^x)^2\}^j) 2r_w^2 + 2r_w^2\right) + 2r_v^2 \\ &\leq 2(L_h^x)^2 (\sum_{j=0}^{i} \{2(L_f^x)^2\}^j) 2r_w^2 + 2r_v^2 \end{aligned}$$

which completes the proof by recurrence. □

D.1.3 Proof of Proposition 3

Proposition 3 states that:
Consider the estimation model (4.1) starting from x_k at k and the nominal estimation model (4.2) starting from ${}^n x_k = x_k$. $\forall i \in \mathbb{N}^*$, consider at $k+i$ the estimate $\hat{x}_{k+i}$ of the state x_{k+i} given by g using y_k^{k+i} and initialized at $\hat{x}_k$. $\forall i \in \mathbb{N}^*$, consider at $k+i$ the estimate ${}^n\hat{x}_{k+i}$ of the nominal state ${}^n x_{k+i}$ given by g using ${}^n y_k^{k+i}$ and initialized at ${}^n\hat{x}_k = \hat{x}_k$. We have:

$$\|\hat{x}_{k+i} - {}^n\hat{x}_{k+i}\|^2 \leq 2(L_g^y)^2 \times \left[4(L_h^x)^2 r_w^2 \sum_{j=0}^{i-1} \left(\{2(L_g^{\hat{x}})^2\}^{i-1-j} \alpha_{k+j}\right) + 2r_v^2 \sum_{j=0}^{i-1} \{2(L_g^{\hat{x}})^2\}^j\right] \tag{D.3}$$

where $\alpha_{k+j} = \sum_{l=0}^{j-1} \{2(L_f^x)^2\}^l$, $\forall j \in \mathbb{N}^+$ and $\alpha_k = 1$

Proof. Let us start by considering when $i = 1$. Using the Lipschitz property of the pre-estimator g and the triangle inequality (4.12) to get

$$\begin{aligned}\|\hat{x}_{k+1} - {}^n\hat{x}_{k+1}\|^2 &= \|g(\hat{x}_k, y_k) - g({}^n\hat{x}_k, {}^n y_k)\|^2 \\ &\leq 2L_g^{\hat{x}} \|\hat{x}_k - {}^n\hat{x}_k\|^2 + 2L_g^y \|y_k - {}^n y_k\|^2\end{aligned}$$

Since ${}^n\hat{x}_k = \hat{x}_k$, we get

$$\|\hat{x}_{k+1} - {}^n\hat{x}_{k+1}\|^2 \leq 2(L_g^y)^2 \|y_k - {}^n y_k\|^2$$

Using (D.2) for $i = 0$, we have

$$\|\hat{x}_{k+1} - {}^n\hat{x}_{k+1}\|^2 \leq 2(L_g^y)^2 \left(2(L_h^x)^2 2r_w^2 + 2r_v^2\right)$$

Hence proposition 3 in (D.3) holds for $i = 1$.

Now suppose that the proposition holds for $i \in \mathbb{N}^*$, i.e. suppose that (D.3) is verified. Let us prove that it is also the case for $i+1$. Use the Lipschitz property of the pre-estimator g and the triangle inequality (4.12) to get

$$\begin{aligned}\|\hat{x}_{k+i+1} - {}^n\hat{x}_{k+i+1}\|^2 &= \|g(\hat{x}_{k+i}, y_{k+i}) - g({}^n\hat{x}_{k+i}, {}^n y_{k+i})\|^2 \\ &\leq 2(L_g^{\hat{x}})^2 \|\hat{x}_{k+i} - {}^n\hat{x}_{k+i}\|^2 + 2(L_g^y)^2 \|y_{k+i} - {}^n y_{k+i}\|^2 \quad \text{(D.4)}\end{aligned}$$

Replace (D.3) and (D.2) in (D.4) to have

$$\begin{aligned}\|\hat{x}_{k+i+1} - {}^n\hat{x}_{k+i+1}\|^2 &\leq 2(L_g^{\hat{x}})^2 2(L_g^y)^2 \left[4(L_h^x)^2 r_w^2 \sum_{j=0}^{i-1} \{2(L_g^{\hat{x}})^2\}^{i-1-j} \alpha_{k+j} + 2r_v^2 \sum_{j=0}^{i-1} \{2(L_g^{\hat{x}})^2\}^j\right] \\ &\quad + 2(L_g^y)^2 \left(2(L_h^x)^2 (\sum_{j=0}^{i-1} \{2(L_f^x)^2\}^j) 2r_w^2 + 2r_v^2\right) \\ &\leq 2(L_g^y)^2 2r_v^2 \sum_{j=0}^{i} \{2(L_g^{\hat{x}})^2\}^j \\ &\quad + 2(L_g^y)^2 2(L_h^x)^2 2r_w^2 \left(2(L_g^{\hat{x}})^2 \sum_{j=0}^{i-1} \{2(L_g^{\hat{x}})^2\}^{i-1-j} \alpha_{k+j} + \sum_{j=0}^{i-1} \{2(L_f^x)^2\}^j\right) \quad \text{(D.5)}\end{aligned}$$

Remark that

$$\begin{aligned}2(L_g^{\hat{x}})^2 \sum_{j=0}^{i-1} \{2(L_g^{\hat{x}})^2\}^{i-1-j} \alpha_{k+j} + \sum_{j=0}^{i-1} \{2(L_f^x)^2\}^j &= 2(L_g^x)^2 \left(\sum_{j=1}^{i-1} \{2(L_g^{\hat{x}})^2\}^{i-1-j} \alpha_{k+j} + \{2(L_g^{\hat{x}})\}^{i-1}\right) \\ &\quad + \sum_{j=0}^{i-1} \{2(L_f^x)^2\}^j \\ &= \sum_{j=1}^{i-1} \{2(L_g^{\hat{x}})^2\}^{i-j} \alpha_{k+j} + \{2(L_g^{\hat{x}})^2\}^i + \sum_{j=0}^{i-1} \{2(L_f^x)^2\}^j \quad \text{(D.6)}\end{aligned}$$

Remark that $\sum_{j=0}^{i-1}\{2(L_f^x)^2\}^j = \alpha_{k+i}$ and $\{2(L_g^{\hat{x}})^2\}^i = \{2(L_g^{\hat{x}})^2\}^{i-j}\alpha_{k+j}|_{j=0}$. Therefore,

$$2(L_g^{\hat{x}})^2\sum_{j=0}^{i-1}\{2(L_g^{\hat{x}})^2\}^{i-1-j}\alpha_{k+j} + \sum_{j=0}^{i-1}\{2(L_f^x)^2\}^j \quad = \quad \sum_{j=0}^{i}\{2(L_g^{\hat{x}})^2\}^{i-j}\alpha_{k+j} \qquad \text{(D.7)}$$

Replace (D.7) in (D.5) to have

$$\|\hat{x}_{k+i+1} - {}^n\hat{x}_{k+i+1}\|^2 \quad \leq \quad 2(L_g^y)^2 2r_v^2\sum_{j=0}^{i}\{2(L_g^{\hat{x}})^2\}^j + 2(L_g^y)^2 2(L_h^x)^2 2r_w^2\sum_{j=0}^{i}\{2(L_g^{\hat{x}})^2\}^{i-j}\alpha_{k+j}$$

Hence, proposition 3 is verified for $i+1$ which completes the proof by recurrence. Rearrange (D.8) to have

$$\|\hat{x}_{k+i+1} - {}^n\hat{x}_{k+i+1}\|^2 \quad \leq \quad 2(L_g^y)^2 \times \left[4(L_h^x)^2 r_w^2\sum_{j=0}^{i}\left(\{2(L_g^{\hat{x}})^2\}^{i-j}\alpha_{k+j}\right) + 2r_v^2\sum_{j=0}^{i}\{2(L_g^{\hat{x}})^2\}^j\right] \qquad \text{(D.8)}$$

□

D.1.4 Proof of Proposition 5

Recall that the proposition 5 states that

$$\mathcal{G}_i \leq 2\left(L_g^y\right)^2\left(\underbrace{2r_v^2\sum_{j=0}^{i-1}\left(2\left(L_g^{\hat{x}}\right)^2\right)^j}_{\text{for } i\geq 1} + \underbrace{2\left(L_h^x\right)^2 2r_w^2\sum_{j=0}^{i-2}\left(2(L_f^x)^2 + 2(L_g^{\hat{x}})^2\right)^j}_{\text{for } i\geq 2}\right) \qquad \text{(D.9)}$$

Proof. It is easy to verify that the proposition 5 holds for $i = 1$ and $i = 2$ using (4.47) and proposition 2, where $k - N$ is considered as the first instant of the window. Now suppose that the proposition 5 holds for i and prove that it is also the case for $i + 1$. Equations (4.47) and (D.9) give

$$\begin{aligned}\mathcal{G}_{i+1} \quad \leq \quad & 2(L_g^y)^2\left[2r_v^2\sum_{j=1}^{i}\left(2(L_g^{\hat{x}})^2\right)^j + 4(L_h^x L_g^{\hat{x}})^2 2r_w^2\sum_{j=0}^{i-2}\left(2(L_f^x)^2 + 2(L_g^{\hat{x}})^2\right)^j\right] \\ & +2(L_g^y)^2\left\|y_{k-N+i} - {}^n y_{k-N+i}\right\|^2 \end{aligned} \qquad \text{(D.10)}$$

Use proposition 2 to get

$$\begin{aligned}\mathcal{G}_{i+1} \quad \leq \quad & 2(L_g^y)^2\left[2r_v^2\sum_{j=1}^{i}\left(2(L_g^{\hat{x}})^2\right)^j + 4(L_h^x L_g^{\hat{x}})^2 2r_w^2\sum_{j=0}^{i-2}\left(2(L_f^x)^2 + 2(L_g^{\hat{x}})^2\right)^j\right] \\ & +2(L_g^y)^2 2(L_h^x)^2\left(\sum_{j=0}^{i-1}\left(2(L_f^x)^2\right)^j\right)2r_w^2 + 2(L_g^y)^2 2r_v^2 \end{aligned} \qquad \text{(D.11)}$$

Rearrange (D.11) to get

$$\begin{aligned}\mathcal{G}_{i+1} &\leq 2(L_g^y)^2 2r_v^2 \sum_{j=0}^{i}\left(2(L_g^{\hat{x}})^2\right)^j \\ &+2(L_g^y)^2 2(L_h^x)^2 2r_w^2\left(2(L_g^{\hat{x}})^2\sum_{j=0}^{i-2}\left(2(L_f^x)^2+2(L_g^{\hat{x}})^2\right)^j+\sum_{j=0}^{i-1}\left(2(L_f^x)^2\right)^j\right)\end{aligned} \tag{D.12}$$

To finish the proof, consider the following lemma:

Lemma 1. *If $a>0$ and $b>0$, for $i\geq 2$ we have*

$$a\sum_{j=0}^{i-2}(a+b)^j+\sum_{j=0}^{i-1}b^j\leq\sum_{j=0}^{i-1}(a+b)^j \tag{D.13}$$

Proof. It is evident that the lemma holds for $i=2$. Now suppose that it holds for i. It holds for $i+1$ if and only if

$$a\sum_{j=0}^{i-2}(a+b)^j+a(a+b)^{i-1}+\sum_{j=0}^{i-1}b^j+b^i\leq\sum_{j=0}^{i-1}(a+b)^j+(a+b)^i \tag{D.14}$$

Thanks to (D.13), there is only $a(a+b)^{i-1}+b^i\leq(a+b)^i$ left to be verified. Since $a>0$ and $b>0$, we have

$$\left(\frac{b}{a+b}\right)^i\leq\frac{b}{a+b}\Rightarrow\frac{b^i}{(a+b)^{i-1}}\leq b\Rightarrow a+\frac{b^i}{(a+b)^{i-1}}\leq a+b\Rightarrow a(a+b)^{i-1}+b^i\leq(a+b)^i$$

As a consequence, (D.14) is verified. Thus, the proposition holds for $i+1$ if it holds for i which completes the proof by recurrence. □

Using lemma 1, proposition 5 holds for $i+1$, which completes the proof by recurrence. □

D.2 LMI Problem for Designing an Observer

Consider the following discrete-time nonlinear system described by

$$x_{k+1}=Ax_k+f_{nl}(x_k,y_k) \tag{D.15}$$

$$y_k=Cx_k \tag{D.16}$$

where $x_k\in\mathbb{R}^{n_x}$ is the state vector and $y_k\in\mathbb{R}^{n_y}$ is the measurement of the system. A and C are the constant matrix of appropriate dimensions. The continuous function $f_{nl}:\mathbb{R}^{n_x}\times\mathbb{R}^{n_y}\to\mathbb{R}^{n_x}$ is a nonlinear map. It is supposed to be Lipschitz with respect to x_k. Denote $L_{f_{nl}}^x$ the associated Lipschitz constant.

To design an observer for system (D.15), [Zhang et al., 2012] proposed to design an observer of the form

$$\hat{x}_{k+1}=A\hat{x}_k+f(\hat{x}_k,y_k)+L(y_k-C\hat{x}_k) \tag{D.17}$$

where L is the gain matrix of the observer computed using the following proposition

Proposition 6. *Assume that the system* (D.15) *has a Lipschitz property. Then, the dynamics of the estimation errors of the observer* (D.17) *is asymptotically stable if there exist scalars* $\alpha > 0$ *and* $\beta > 0$ *and matrices*[1] $P > \alpha \mathbf{I}_{n_x \times n_x}$, $Q > 0$ *and* R *of appropriate dimensions such that the following LMI is feasible*

$$\begin{pmatrix} -P + \beta (L^x_{f_{nl}})^2 \mathbf{I}_{n_x \times n_x} & \eta \tilde{R} & 0 & \eta \tilde{R} \\ * & \eta P - Q - \beta \mathbf{I}_{n_x \times n_x} & 0 & 0 \\ * & * & Q - \alpha \mathbf{I}_{n_x \times n_x} & 0 \\ * & * & * & -\eta P \end{pmatrix} < 0 \tag{D.18}$$

where $\eta = 1 + (L^x_{f_{nl}})^2$ *and* $\tilde{R} = A^T P - C^T R$. *When* (D.18) *is feasible, the gain matrix* L *is given by* $L = P^{-1} R^T$.

D.3 Verifications of the Conditions for the Convergence the Estimation Errors of the MHE-PE in the Numerical Example

(C1)-(C2) are immediate. Let us consider (C3).

(C3) f and h are $\mathcal{C}^2$ functions with respect to x on $\mathbb{X}$. Consequently, f and h are also locally Lipschitz on $\mathbb{X}$. Define their Lipschitz constants as L^x_f and L^x_h respectively.

Recall that

$$x_{k+1} = f(x_k) + w_k = \begin{pmatrix} \dfrac{x_{1,k}}{2\bar{k}_g T_s x_{1,k} + 1} \\ x_{2,k} + \dfrac{\bar{k}_g T_s x^2_{1,k}}{2\bar{k}_g T_s x_{1,k} + 1} \end{pmatrix} + w_k \tag{D.19}$$

and $y_k = h(x_k) = \begin{pmatrix} 1 & 1 \end{pmatrix} x_k$. We can see that f and h are compositions of $\mathcal{C}^2$ functions. Hence, they are $\mathcal{C}^2$ functions. Let us use the same method as in appendix C.2. Denote x^n_k the state at instant k of the n^{th} run. According to [Khalil and Grizzle, 2002] the Lipschitz constant can be chosen such that

$$L^x_f > \max_{\forall k, \forall n} \left\| \frac{\partial f}{\partial x} |_{x = x^n_k} \right\|_p \tag{D.20}$$

where $\|A\|_p$ is a p-norm of the matrix A.
Here, the infinity-norm is chosen. In this case,

$$\left\| \frac{\partial f}{\partial x} \right\|_\infty = \max\{ | \frac{1}{(2\bar{k}_g T_s x_{1,k} + 1)^2} |, \ | \frac{2\bar{k}_g T_s x_{1,k} (2\bar{k}_g T_s x_{1,k} + 1 - k_g T_s x^2_{1,k})}{(2\bar{k}_g T_s x_{1,k} + 1)^2} | + 1 \}$$

Knowing that $x_k \in [0, 5]^2$, $\max(\dfrac{1}{(2\bar{k}_g T_s x_{1,k} + 1)^2}) = 1$. Moreover,

$$\frac{2\bar{k}_g T_s x_{1,k} (2\bar{k}_g T_s x_{1,k} + 1 - k_g T_s x^2_{1,k})}{(2\bar{k}_g T_s x_{1,k} + 1)^2} < \frac{2\bar{k}_g T_s x_{1,k} (2\bar{k}_g T_s x_{1,k} + 1)}{(2\bar{k}_g T_s x_{1,k} + 1)^2} < 2\bar{k}_g T_s x_{1,k} < 0.192$$

We can choose $L^x_f > 1 + 0.192$. In this study, $L^x_f = 1.2$ is chosen.

Now, let us consider (C4)-(C7).

[1] A matrix $A > 0$ is positive-definite matrix. In other words, all the eigenvalues of A is positive

(C4) g is locally Lipschitz with respect to its arguments. Indeed, recalling that

$$\hat{x}_{k+1} = g(\hat{x}_k, y_k) = f(\hat{x}_k) + L(y_k - \begin{pmatrix} 1 & 1 \end{pmatrix} \hat{x}_k)$$

where $L \triangleq \begin{pmatrix} l_1 & l_2 \end{pmatrix}^T$ is the observer gain $l_{1,2} \in \mathbb{R}$. We can see that g is a $\mathcal{C}^2$ function since it is a composition of $\mathcal{C}^2$ functions. As a consequence, g is locally Lipschitz with respect to its arguments. To precise,

$$\hat{x}'_{k+1} - \hat{x}''_{k+1} = f(\hat{x}'_k) - f(\hat{x}''_k) + \begin{pmatrix} l_1(y'_k - y''_k) \\ l_2(y'_k - y''_k) \end{pmatrix} - \begin{pmatrix} l_1 & l_1 \\ l_2 & l_2 \end{pmatrix} (\hat{x}'_k - \hat{x}''_k)$$

Using symbolic calculation in MATLAB, we find that the eigenvalues of $\begin{pmatrix} l_1 & l_1 \\ l_2 & l_2 \end{pmatrix}$ are 0 and $l_1 + l_2$. Hence,

$$\begin{aligned} \|\hat{x}'_{k+1} - \hat{x}''_{k+1}\| &\leq L_f^x \|\hat{x}'_k - \hat{x}''_k\| + \max(l_1, l_2) \|y'_k - y''_k\| + (l_1 + l_2) \|\hat{x}'_k - \hat{x}''_k\| \\ &\leq (L_f^x + l_1 + l_2) \|\hat{x}'_k - \hat{x}''_k\| + \max(l_1, l_2) \|y'_k - y''_k\| \end{aligned}$$

Therefore, the Lipschitz constants $L_g^{\hat{x}} = L_f^x + l_1 + l_2$ and $L_g^y = \max(l_1, l_2)$.

(C5) $\forall {}^n\hat{x}_0 \in \hat{\mathbb{X}}$, $\forall {}^n x_0 \in \mathbb{X}$, there exists a class K function ψ such that $\|{}^n\hat{x}_k - {}^n x_k\|^2 \leq \psi(\|{}^n\hat{x}_0 - {}^n x_0\|^2)$, $\forall k$. This condition is verified since g is a deterministic observer, see the definition of the deterministic observer in (4.8).

(C6) $\forall \hat{x}_{k-N} \in \mathbb{X}$, $\forall y_{k-N}^{k-1}$, $\text{rank}(\dfrac{\partial G(\hat{x}_{k-N}, y_{k-N}^{k-1})}{\partial \hat{x}_{k-N}}) = n_x$: verified using symbolic calculation in MATLAB.

(C7) $\exists \delta_g > 0$ s.t. $\left\| G(\hat{x}'_{k-N}, y_{k-N}^{k-1}) - G(\hat{x}''_{k-N}, y_{k-N}^{k-1}) \right\|^2 \geq \delta_g \left\| \hat{x}'_{k-N} - \hat{x}''_{k-N} \right\|^2$. Using the same reasoning as in appendix C.2, δ_g can be chosen such that

$$\delta_g = \left\| \frac{\partial G_{1:2}(\hat{x}_{k-N}, y_{k-N}^{k-1})}{\partial \hat{x}_{k-N}} \right\|_{l,2}^2 \tag{D.21}$$

where $\|A\|_{l,2}$ is a matrix lower bound of the matrix A which can be computed using (C.12) when A is invertible. The value of $\left\| \dfrac{\partial G_{1:2}(\hat{x}_{k-N}, y_{k-N}^{k-1})}{\partial \hat{x}_{k-N}} \right\|_{l,2}$ associated to the simulated system is computed in MATLAB where the value 0.0050 is found. As a consequence, $\delta_g = 0.005^2 = 2.5 \cdot 10^{-5}$ is chosen.

APPENDIX E

Appendices for Chapter 5

E.1 Verification of the Assumptions on the Stability of the Estimation Errors of the MHE for Chapter 5

Recall that for our problem, the state function f is defined as

$$f(x_k) = \begin{pmatrix} \mathbf{I}_{3\times3} & T_s\mathbf{I}_{3\times3} & \frac{T_s^2}{2}\mathbf{I}_{3\times3} \\ \mathbf{0}_{3\times3} & \mathbf{I}_{3\times3} & T_s\mathbf{I}_{3\times3} \\ \mathbf{0}_{3\times3} & \mathbf{0}_{3\times3} & \mathbf{I}_{3\times3} \end{pmatrix} x_k + \begin{pmatrix} \mathbf{0}_{3\times1} \\ \mathbf{0}_{3\times1} \\ \mathbf{f}_k T_s \end{pmatrix} \tag{E.1}$$

where $\mathbf{f}_k \triangleq \begin{pmatrix} f_{x_k} & f_{y_k} & f_{z_k} \end{pmatrix}^T$ and

$$f_{x_k} = -c_2 a_{x_k} v_{z_k} + a_{x_k}\left[a_{x_k}\left(\frac{1}{v_{x_k}} + \frac{v_{x_k}}{\|\mathbf{v}_k\|^2}\right) + a_{y_k}\frac{v_{y_k}}{\|\mathbf{v}_k^2\|} + a_{z_k}\frac{v_{z_k}}{\|\mathbf{v}_k\|^2}\right] \tag{E.2a}$$

$$f_{y_k} = -c_2 a_{y_k} v_{z_k} + a_{y_k}\left[a_{x_k}\frac{v_{x_k}}{\|\mathbf{v}_k\|^2} + a_{y_k}\left(\frac{1}{v_{y_k}} + \frac{v_{y_k}}{\|\mathbf{v}_k\|^2}\right) + a_{z_k}\frac{v_{z_k}}{\|\mathbf{v}_k\|^2}\right] \tag{E.2b}$$

$$f_{z_k} = \left(-c_2 v_{z_k} + \left[a_{x_k}\frac{v_{x_k}}{\|\mathbf{v}_k\|^2} + a_{y_k}\frac{v_{y_k}}{\|\mathbf{v}_k\|^2} + a_{z_k}\left(\frac{1}{v_{z_k}} + \frac{v_{z_k}}{\|\mathbf{v}_k\|^2}\right)\right]\right)(a_{z_k} + g) \tag{E.2c}$$

and the measurement function h is defined for $r_{z_k} \neq d_k$ as

$$h(x_k) = \begin{pmatrix} d_k \\ el_k \\ az_k \end{pmatrix} = \begin{pmatrix} \sqrt{r_{x_k}^2 + r_{y_k}^2 + r_{z_k}^2} \\ \arcsin(\frac{r_{z_k}}{d_k}) \\ \arctan(\frac{r_{y_k}}{-r_{x_k}}) \end{pmatrix} \tag{E.3}$$

otherwise, $el_k \triangleq \pi/2$.

- Let us start by considering assumptions (A1)-(A2):

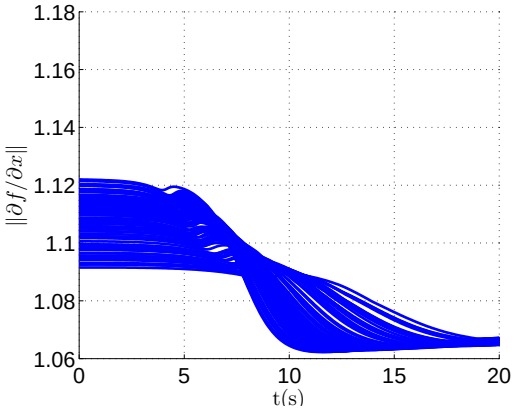

Figure E.1: *Values of* $\|\mathbf{J}_f\|_2$ *at each instant for each of the* 100 *real trajectories*

(A1) $\mathbb{X}$ is a convex compact set, $\mathbb{W}$ and $\mathbb{V}$ are compact sets with $0 \in \mathbb{W}$ and $0 \in \mathbb{V}$

(A2) The initial state x_0 is such that, for any possible sequence of process noises $\{w_k\}$, the system trajectory $\{x_k\}$ lies in the convex compact set $\mathbb{X}$, $\forall k$

Using the constraints on the estimates defined in (5.38), those on the process noise in (5.39) and (5.40) and the fact that the measurement noises are assumed to belong to a compact set containing 0, we can conclude that (A1) is verified. Concerning (A2), the constraint set $\mathbb{X}$ defined in (5.38) is chosen to cover the real state, see figure 5.3. Hence, (A2) is verified in this study.

- Now, let us consider (A3):

(A3) f and h are $\mathcal{C}^2$ functions with respect to x on $\mathbb{X}$. f and h are therefore also locally Lipschitz. Define their Lipschitz constants as L_f^x and L_h^x respectively

The values of $\|\mathbf{J}_f\|_2$ at each instant of the simulated 100 trajectories are plotted in figure E.1. We choose the constant Lipschitz of the state function $L_f^x = 1.2$.

Let us consider now $\mathbf{J}_h$. Since the measurements only depend on the position $\mathbf{r}$, we have

$$\mathbf{J}_h = \begin{pmatrix} \frac{r_x}{\|\mathbf{r}\|} & \frac{r_y}{\|\mathbf{r}\|} & \frac{r_z}{\|\mathbf{r}\|} & \mathbf{0}_{1\times 6} \\ -\frac{r_x r_z}{\sqrt{1-\frac{r_z^2}{\|\mathbf{r}\|}}\,\|\mathbf{r}\|^3} & -\frac{r_y r_z}{\sqrt{1-\frac{r_z^2}{\|\mathbf{r}\|}}\,\|\mathbf{r}\|^3} & \frac{r_x^2+r_y^2}{\sqrt{1-\frac{r_z^2}{\|\mathbf{r}\|}}\,\|\mathbf{r}\|^3} & \mathbf{0}_{1\times 6} \\ \frac{r_y}{r_x^2+r_y^2} & \frac{-r_x}{r_x^2+r_y^2} & 0 & \mathbf{0}_{1\times 6} \end{pmatrix} \tag{E.4}$$

Using symbolic calculation in MATLAB, we can show that the singular values of $\mathbf{J}_h$ are 1, $\frac{1}{\|\mathbf{r}\|}$ and $\frac{1}{\sqrt{r_x^2+r_y^2}}$. Since $\|\mathbf{r}\| > 1$ and $\sqrt{r_x^2+r_y^2} > 1$ at each instant for all the considered trajectories as can be seen in figure 5.3, we choose the Lipschitz constant of the state function $L_h^x = 1$.

- Let us consider now assumption (A4):

(A4) The system is observable in $N+1$ steps

Recall that the observation map of the system on a window of length $N+1$ as defined in (2.10) is

$$F(x_{k-N}, w_{k-N}^{k-1}) \triangleq \begin{pmatrix} h(x_{k-N}) \\ h(f^{w_{k-N}}(x_{k-N})) \\ \vdots \\ h \circ f^{w_{k-1}} \circ \cdots \circ f^{w_{k-N}}(x_{k-N}) \end{pmatrix} = y_{k-N}^{k} \tag{E.5}$$

where $\circ$ denotes function composition and $f^{w_i}(x_i) \triangleq f(x_i) + w_i = x_{i+1}$. Denote also

$$f^{w_{k-N}^{k-N+i}}(x_i) = f^{w_{k-N+i}} \circ \cdots \circ f^{w_{k-N}}(x_{k-N}),\ i \in [0, N-1] \tag{E.6}$$

The system is said to be observable in $N+1$ steps if one of these conditions, which are equivalent [Hanba, 2010], is satisfied:

(a) For a system without process noise, the map $F(x_{k-N}, \mathbf{0}_{n_x N \times 1})$ is injective, i.e. if $F(x'_{k-N}, \mathbf{0}_{n_x N \times 1}) = F(x''_{k-N}, \mathbf{0}_{n_x N \times 1})$ therefore $x'_{k-N} = x''_{k-N}$.

(b) $\forall x_{k-N} \in \mathbb{X}$, $\operatorname{rank}\left(\dfrac{\partial F(x_{k-N}, \mathbf{0}_{n_x N \times 1})}{\partial x_{k-N}}\right) = n_x$

(c) $\forall (x', x'') \in \mathbb{X}^2$, there exists a K-function $\phi(\cdot)$ such that

$$\phi(\|x' - x''\|^2) \leq \|F(x', \mathbf{0}_{n_x N \times 1}) - F(x'', \mathbf{0}_{n_x N \times 1})\|^2 \tag{E.7}$$

Here, we would like to show that F is injective, or equivalently

$$\operatorname{rank}\left(\frac{\partial F(x_{k-N}, \mathbf{0}_{n_x N \times 1}}{\partial x_{k-N}}\right) = n_x$$

We started by using symbolic calculation in MATLAB to compute the rank of the above Jacobian. However, the derivation of the observation map defined in the local coordinates is too complex that the computer does not have enough memory to compute the rank. To overcome this, we remark that the measurements are in fact the position of the debris in the spherical coordinates (distance, elevation and azimuth angles) Denote the measurement function in the Cartesian coordinates as

$$h_{cart}(x_k) \triangleq \begin{pmatrix} r_{x_k} & r_{y_k} & r_{z_k} \end{pmatrix}^T \tag{E.8}$$

Remark that there is a bijection between the position of the debris in the spherical coordinates and that in the SEU coordinates which is a Cartesian coordinates. As a consequence, if the observation map for the measurement function in the Cartesian coordinates $F_{cart}(x_{k-N}, \mathbf{0}_{n_x N \times 1})$:

$$F_{cart}(x_{k-N}, \mathbf{0}_{n_x N \times 1}) = \begin{pmatrix} h_{cart}(x_{k-N}) \\ h_{cart}(f(x_{k-N})) \\ \vdots \\ h_{cart} \circ f^0 \circ \cdots \circ f^0(x_{k-N}) \end{pmatrix} \tag{E.9}$$

is injective, therefore $F(x_{k-N}, \mathbf{0}_{n_x N \times 1})$ is also injective.

Using symbolic calculation in MATLAB, we can show that for $N = 2$

$$\text{rank}\left(\frac{\partial F_{cart}(x_{k-N}, \mathbf{0}_{n_x N\times 1})}{\partial x_{k-N}}\right) = 9$$

Since a rank of a function cannot exceed the dimension of the state n_x, we can conclude that rank $\left(\frac{\partial F_{cart}(x_{k-N}, \mathbf{0}_{n_x N\times 1})}{\partial x_{k-N}}\right) = 9$ for $N \geq 2$. In other words, since the initial state at the beginning of the horizon x_{k-N} can be constructed using 3 measurements y_{k-N}^{k-N+2}, it will still be constructed when more measurements are used.

Hence, since $F_{cart}(x_{k-N}, \mathbf{0}_{n_x N\times 1})$ is injective, $F(x_{k-N}, \mathbf{0}_{n_x N\times 1})$ is also injective. Assumption (A4) is therefore verified.

- Now, let us consider (A5):

(A5) The system has a finite sensitivity, i.e. the K-function $\phi(\cdot)$ in (E.7) satisfies:

$$\delta = \inf_{(x',x'')\in\mathbb{X}^2, x'\neq x''} \frac{\phi(\|x' - x''\|^2)}{\|x' - x''\|^2} > 0 \tag{E.10}$$

In the same way as in appendix C.2, if the sensitivity parameter δ in (E.10) is chosen such that

$$\delta = \left\| \frac{\partial F_{1:n_x}(x_{k-N}, \mathbf{0}_{n_x N\times 1})}{\partial x_{k-N}} \right\|_{l,2}^2 \tag{E.11}$$

then (A5) is verified.

The values of $\left\| \left(\frac{\partial F_{1:9}(x_{k-N}, \mathbf{0}_{n_x N\times 1})}{\partial x_{k-N}} \right) \right\|_{l,2}$ of each simulated trajectories are computed using MATLAB where we find that $\delta = 1.6 \cdot 10^{-15}$. Assumption (A5) is hence verified.

E.2 Verification of the Assumptions on the Stability of the Estimation Errors of the MHE-PE for Chapter 5

Conditions (C1)-(C3) are identical to (A1)-(A3) so they have been verified in the previous section. Let us consider now conditions (C4)-(C7) which are conditions on the pre-estimating estimator g.

Concerning the choice of the pre-estimator g, our first attempt is to find a deterministic observer for the system of space debris tracking during the re-entries in 3D since we know that a deterministic observer verifies (C5). However, a deterministic observer does not exist for every system. In [Benallouch et al., 2012][Zhang et al., 2012], a method to design a deterministic observer for a Lipschitz discrete-time nonlinear system whose measurement function is linear is proposed. However, in our study, the measurement function is not linear, we have to find therefore an alternative pre-estimator.

We start by choosing for the pre-estimator g an Extended Kalman Filter (EKF) as presented in section 1.4.1. In this case, the pre-estimating estimator g is of the form

$$\hat{x}_{k+1} = g(\hat{x}_k, y_k) = f(\hat{x}_k) + K_k(y_k - h(\hat{x}_k)) \tag{E.12}$$

Using the formulation of the EKF in section 1.4.1, we can deduce the expression of the gain K_k as follows:

$$K_k = (Q + \hat{F}_{k-1} P_{k-1} \hat{F}_{k-1}^T)\hat{H}_k^T \left(\hat{H}_k(Q + \hat{F}_{k-1} P_{k-1} \hat{F}_{k-1}^T)\hat{H}_k^T + R_k\right)^{-1} \tag{E.13}$$

Recall that $\hat{F}_{k-1} = \dfrac{\partial f}{\partial x}|_{x=\hat{x}_{k-1}}$ and $\hat{H}_k = \dfrac{\partial h}{\partial x}|_{x=\hat{x}_k}$.

Using the fact that P_0, Q, R are bounded and that the estimate $\hat{x}_k$ of the pre-estimator g in the MHE-PE is bounded $\forall k$ thanks to (5.38), it can be concluded that the Kalman gain K_k of the EKF used as the pre-estimator in the MHE-PE is bounded $\forall k$ as well.

Equivalently, $\exists c_{K,k} \in \mathbb{R}^+$ such that

$$\|K_k x\|_p \leq c_{K,k} \|x\|_p \tag{E.14}$$

Since f and h are locally Lipschitz, it is immediate to see that g is also locally Lipschitz with respect to its argument $\hat{x}$ and y. Hence, condition

(C4) g is locally Lipschitz with respect to its arguments

is verified.

- Consider now condition (C5):

(C5) $\forall \hat{x}_0 \in \hat{\mathbb{X}}$, $\forall x_0 \in \mathbb{X}$, there exists a class K function ψ such that $\|{}^n\hat{x}_k - {}^n x_k\|^2 \leq \psi(\|{}^n\hat{x}_0 - {}^n x_0\|^2)$, $\forall k$

Recall that for the noise-free version of the system is written as

$$\begin{aligned} {}^n x_{k+1} &= f({}^n x_k) && \text{(E.15)} \\ {}^n y_k &= h({}^n x_k) && \text{(E.16)} \end{aligned}$$

and an EKF for this system is

$${}^n\hat{x}_{k+1} = f({}^n\hat{x}_k) + K_k({}^n y_k - h({}^n\hat{x}_k)) \tag{E.17}$$

Therefore,

$${}^n\hat{x}_{k+1} - {}^n x_{k+1} = f({}^n\hat{x}_k) - f({}^n x_k) + K_k(h({}^n x_k) - h({}^n\hat{x}_k)) \tag{E.18}$$

Using the triangle inequalities, we obtain

$$\|{}^n\hat{x}_{k+1} - {}^n x_{k+1}\|^2 \leq 2\|f({}^n\hat{x}_k) - f({}^n x_k)\|^2 + 2K_k \|(h({}^n x_k) - h({}^n\hat{x}_k))\|^2 \tag{E.19}$$

Using (E.14), we deduce

$$\|{}^n\hat{x}_{k+1} - {}^n x_{k+1}\|^2 \leq 2\|f({}^n\hat{x}_k) - f({}^n x_k)\|^2 + 2c_{K,k}^2 \|(h({}^n x_k) - h({}^n\hat{x}_k))\|^2 \tag{E.20}$$

Finally, using the Lipschitz properties of f and h, we have

$$\|{}^n\hat{x}_{k+1} - {}^n x_{k+1}\|^2 \leq \left(2(L_f^x)^2 + 2c_{K,k}^2 (L_h^x)^2\right) \|{}^n\hat{x}_k - {}^n x_k\|^2 \tag{E.21}$$

It is easy to derive by recurrence that

$$\|{}^n\hat{x}_k - {}^n x_k\|^2 \leq \left(\prod_{j=0}^{k} \left(2(L_f^x)^2 + 2c_{K,j}^2 (L_h^x)^2\right)\right) \|{}^n\hat{x}_0 - {}^n x_0\|^2 \tag{E.22}$$

Hence, the EKF verifies (C5) provided that the Kalman gain is bounded bounded.

- Now, let us consider (C6). Consider the system (Σ) of the observer g in (4.3). Condition (C6b) states that

(C6b) (Σ) must satisfy the uniform observability rank condition on $\hat{\mathbb{X}}$ with respect to all admissible measurements, i.e. $\exists N > 0$, $\forall \hat{x}_{k-N} \in \hat{\mathbb{X}}$, $\forall y_{k-N}^{k-1} \in \mathbb{Y}^N$,

$$\operatorname{rank}\left(\frac{\partial G(\hat{x}_{k-N}, y_{k-n}^{k-1})}{\partial \hat{x}_{k-N}}\right) = n_x$$

where G is the observation maps of the pre-estimating estimator g initialized at $k-N$ by $\hat{x}_{k-N}$ receiving the real measurements y_{k-N}^{k} is defined as

$$G(\hat{x}_{k-N}, y_{k-N}^{k-1}) \triangleq \begin{pmatrix} h(\hat{x}_{k-N}) \\ h \circ g(\hat{x}_{k-N}, y_{k-N}) \\ \vdots \\ h(g^N(\hat{x}_{k-N}, y_{k-N}^{k-1})) \end{pmatrix} \tag{E.23}$$

where for $i \geq 1$

$$g^i(\hat{x}_{k-N}, y_{k-N}^{k-N+i-1}) \triangleq \underbrace{g(g \ldots g}_{\text{i times}}(\hat{x}_{k-N}, y_{k-N}), \ldots, y_{k-N+i-1})$$

Use the same reasoning as for the observability of the observation map $F(x_{k-N}, \mathbf{0}_{n_x(N-1)})$. Consider first the observation map of the estimator g defined by the position measurement in Cartesian coordinates:

$$G_{cart}(\hat{x}_{k-N}, y_{k-n}^{k-1}) \triangleq \begin{pmatrix} h_{cart}(\hat{x}_{k-N}) \\ h_{cart} \circ g(\hat{x}_{k-N}, y_{k-N}) \\ \vdots \\ h_{cart}(g^N(\hat{x}_{k-N}, y_{k-N}^{k-1})) \end{pmatrix} \tag{E.24}$$

where for $i \geq 1$

$$g^i(\hat{x}_{k-N}, y_{k-N}^{k-N+i-1}) \triangleq \underbrace{g(g \ldots g}_{\text{i times}}(\hat{x}_{k-N}, y_{k-N}), \ldots, y_{k-N+i-1})$$

where h_{cart} is defined in (E.8).

We verify using MATLAB that for $N = 2$,

$$\operatorname{rank}\left(\frac{\partial G_{cart}}{\partial \hat{x}_{k-N}}\right) = 9$$

when an EKF is chosen as pre-estimating estimator g. Using the fact that for any two functions f and g, if $g \circ f$ is injective, then f is injective (g does not need to be so). We can conclude that $G(\hat{x}_{k-N}, y_{k-n}^{k-1})$ is injective. Hence, condition (C6b) is verified.

Recall that (C6a), (C6b) and (C6c) are equivalent. As a result, we have

(C6c) g is K-uniformly observable on $\hat{\mathbb{X}}$ with respect to all admissible measurements, i.e. $\exists N > 0$, $\forall (\hat{x}', \hat{x}'') \in \hat{\mathbb{X}}^2$, $\forall y \in \mathbb{Y}$, there exists a class K function $\phi_g(\cdot)$ such that

$$\phi_g(\|\hat{x}' - \hat{x}''\|^2) \leq \|G(\hat{x}', y_{k-N}^{k-1}) - G(\hat{x}'', y_{k-N}^{k-1})\|^2$$

- The condition (C7) states that

(C7) The observation map $G(\cdot,\cdot)$ must have a finite sensitivity to the estimate, i.e. the K-function $\phi_g(\cdot)$ in (E.2) satisfies:

$$\delta_g = \inf_{(\hat{x}_1,\hat{x}_2)\in\hat{\mathbb{X}}^2,\hat{x}_1\neq\hat{x}_2} \frac{\phi_g(\|\hat{x}_1-\hat{x}_2\|^2)}{\|\hat{x}_1-\hat{x}_2\|^2} > 0$$

By remarking that the first n_x components of $G(\hat{x}, y_{k-N}^{k-1})$ are identical to that of $F(x,\mathbf{0})$, we can conclude that $\delta_g = \delta$ in (E.11). Hence, if $\delta_g = 1.6\cdot 10^{-15}$, (C7) is verified.

Bibliography

[Aerospace.org, 2013] Aerospace.org (2013). Available at `http://www.aerospace.org/cords/reentry-predictions/`.

[Ailor, 2012] Ailor, W. (2012). Space debris reentry hazards. Technical report, Scientific & Technical Subcommittee of the United Nations Committee on the Peaceful Uses of Outer Space.

[Alarcón et al., 2005] Alarcón, J., Klinkrad, H., Cuesta, J., and Martinez, F. (2005). Independent orbit determination for collision avoidance. In *4th European Conference on Space Debris*, volume 587, page 331.

[Alessandri et al., 2003] Alessandri, A., Baglietto, M., and Battistelli, G. (2003). Receding-horizon estimation for discrete-time linear systems. *IEEE Transactions on Automatic Control*, 48(3):473–478.

[Alessandri et al., 2005] Alessandri, A., Baglietto, M., and Battistelli, G. (2005). Robust receding-horizon estimation for discrete-time linear systems in the presence of bounded uncertainties. In *44th IEEE Conference on Decision and Control, 2005 and 2005 European Control Conference. CDC-ECC '05*, pages 4269–4274.

[Alessandri et al., 2008] Alessandri, A., Baglietto, M., and Battistelli, G. (2008). Moving horizon state estimation for nonlinear discrete-time systems: New stability results and approximation schemes. *Automatica*, 44(7).

[Alessandri et al., 2011] Alessandri, A., Baglietto, M., Battistelli, G., and Gaggero, M. (2011). Moving-horizon state estimation for nonlinear systems using neural networks. *IEEE Transactions on Neural Networks*, 22(5).

[Alessandri et al., 2010] Alessandri, A., Baglietto, M., Battistelli, G., and Zavala, V. (2010). Advances in moving horizon estimation for nonlinear systems. *49th IEEE Conference on Decision and Control*.

[Austin and Leondes, 1981] Austin, J. and Leondes, C. (1981). Statistically linearized estimation of reentry trajectories. *IEEE Transactions on Aerospace and Electronic Systems*, AES-17(1):54–61.

[Bar-Shalom et al., 2004] Bar-Shalom, Y., Li, X. R., and Kirubarajan, T. (2004). *Estimation with applications to tracking and navigation: theory algorithms and software*. John Wiley & Sons.

[Barbata et al., 2014a] Barbata, A., Zasadzinski, M., Ali, H., and Messaoud, H. (2014a). Observer design for a class of singular stochastic nonlinear systems. In *2014 European Control Conference (ECC)*, pages 294–299.

[Barbata et al., 2014b] Barbata, A., Zasadzinski, M., Souley Ali, H., and Messaoud, H. (2014b). Exponential observer for a class of one-sided lipschitz stochastic nonlinear systems. *IEEE Transactions on Automatic Control*.

[Battie et al., 2012] Battie, F., Fossati, T., Gallucci, S., and Volpi, M. (2012). Vega launch vehicle upper stage re-entry survivability analysis. In *Satellite Telecommunications (ESTEL), 2012 IEEE First AESS European Conference on*, pages 1–7. IEEE.

[Benallouch et al., 2012] Benallouch, M., Boutayeb, M., and Zasadzinski, M. (2012). Observer design for one-sided lipschitz discrete-time systems. *Systems & Control Letters*, 61(9):879–886.

[Bock, 1981] Bock, H. G. (1981). *Numerical treatment of inverse problems in chemical reaction kinetics*. Springer.

[Brooks, 2010] Brooks, E. M. (2010). Estimating characteristics of a maneuvering reentry vehicle observed by multiple sensors. Technical report, DTIC Document.

[Brown, 2008] Brown, J. L. (2008). The effect of forebody geometry on turbulent heating and thermal protection system sizing for future mars mission concepts. *NASA Ames Research Center*, 2.

[Burke, 2014] Burke, J. (2014). Multivariable calculus review. Technical report, University of Washington.

[Burns, 2013] Burns, C. (2013). Space junk apocalypse: just like Gravity-.

[Cappe et al., 2007] Cappe, O., Godsill, S., and Moulines, E. (2007). An overview of existing methods and recent advances in sequential monte carlo. *Proceedings of the IEEE*, 95(5).

[Cardillo et al., 1999] Cardillo, G., Mrstik, A., and Plambeck, T. (1999). A track filter for reentry objects with uncertain drag. *Aerospace and Electronic Systems, IEEE Transactions on*, 35(2):394–409.

[Collins, 2012] Collins, A. (2012). Available at `http://arc.id.au/CannonballDrag.html`.

[Dahleh et al., 2004] Dahleh, M., Dahleh, M. A., and Verghese, G. (2004). Lectures on dynamic systems and control. *Department of Electrical Engineering and Computer Science, Massachuasetts Institute of Technology*, 4(100):1–100.

[Diehl et al., 2002] Diehl, M., Bock, H., Schloder, J. P., Findeisen, R., Nagy, Z., and Frank (2002). Real-time optimization and nonlinear model predictive control of processes governed by differential-algebraic equations. *Journal of Process Control*, 12(4):577 – 585.

[Farina et al., 2002] Farina, A., Ristic, B., and Benvenuti, D. (2002). Tracking a ballistic target: comparison of several nonlinear filters. *IEEE Transactions on Aerospace and Electronic Systems*, 38(3).

[Ferreau et al., 2012] Ferreau, H., Kraus, T., Vukov, M., Saeys, W., and Diehl, M. (2012). High-speed moving horizon estimation based on automatic code generation. In *2012 IEEE 51st Annual Conference on Decision and Control (CDC)*, pages 687–692.

[Gallais, 2007] Gallais, P. (2007). *Atmospheric Re-Entry Vehicle Mechanics*. Springer, Berlin Heidelberg.

[Graton et al., 2014] Graton, G., Kratz, F., and Fantini, J. (2014). Finite memory observers for linear time-varying systems: Theory and diagnosis applications. *Journal of the Franklin Institute*, 351(2):785 – 810.

[Hanba, 2010] Hanba, S. (2010). Further results on the uniform observability of discrete-time nonlinear systems. *IEEE Transactions on Automatic Control*, 55(4).

[Haseltine and Rawlings, 2005] Haseltine, E. L. and Rawlings, J. B. (2005). Critical evaluation of Extended Kalman Filtering and Moving Horizon Estimation. *Industrial & engineering chemistry research*, 44(8).

[Imburgia, 2011] Imburgia, J. S. (2011). Space debris and its threat to national security: A proposal for a binding international agreement to clean up junk. *Vanderbilt Journal of Transnational Law*, 44.

[Jazwinski, 1968] Jazwinski, A. (1968). Limited memory optimal filtering. *IEEE Transactions on Automatic Control*, 13(5):558–563.

[Julier and Uhlmann, 2004] Julier, S. and Uhlmann, J. (2004). Unscented filtering and nonlinear estimation. *Proceedings of the IEEE*, 92(3).

[Kalman, 1960] Kalman, R. E. (1960). A new approach to linear filtering and prediction problems. *Journal of basic Engineering*, 82(1).

[Kessler et al., 2010] Kessler, D. J., Johnson, N. L., Liou, J., and Matney, M. (2010). The kessler syndrome: implications to future space operations. *Advances in the Astronautical Sciences*, 137(8).

[Khalil and Grizzle, 2002] Khalil, H. K. and Grizzle, J. (2002). *Nonlinear systems*, volume 3. Prentice hall Upper Saddle River.

[Klinkrad, 2005] Klinkrad, H. (2005). Re-entry prediction and on-ground risk assessment. *SIXTH US/RUSSIAN SPACE SURVEILLANCE WORKSHOP*.

[Klinkrad, 2006] Klinkrad, H. (2006). *Space debris: models and risk analysis*. Springer.

[Kratz et al., 1997] Kratz, F., Nuninger, J., and J., R. (1997). Finite memory observer based method for failure detection in dynamic system. In *11th Symposium on System Identification*, pages 1189–1194.

[Kraus et al., 2006] Kraus, T., Kuhl, P., Wirsching, L., Bock, H., and Diehl, M. (2006). A moving horizon state estimation algorithm applied to the tennessee eastman benchmark process. In *2006 IEEE International Conference on Multisensor Fusion and Integration for Intelligent Systems*, pages 377–382.

[Kuttler, 2009] Kuttler, K. (2009). Multivariable advanced calculus. *preprint ed.*

[Liu et al., 2005] Liu, C.-Y., Wang, H.-M., and Tuan, P.-C. (2005). Input estimation algorithms for reentry vehicle trajectory estimation. *Defence Science Journal*, 55(4).

[Liu, 2013] Liu, J. (2013). Moving horizon state estimation for nonlinear systems with bounded uncertainties. *Chemical Engineering Science*, 93.

[López-Negrete et al., 2011] López-Negrete, R., Patwardhan, S. C., and Biegler, L. T. (2011). Constrained particle filter approach to approximate the arrival cost in moving horizon estimation. *Journal of Process Control*, 21(6):909–919.

[Mamboundou and Langlois, 2011] Mamboundou, J. and Langlois, N. (2011). Indirect adaptive model predictive control supervised by fuzzy logic. In *2011 IEEE International Conference on Fuzzy Systems (FUZZ)*, pages 2979–2986.

[Mamboundou and Langlois, 2012] Mamboundou, J. and Langlois, N. (2012). Robustness analysis of indirect adaptive model predictive control supervised by fuzzy logic. In *2012 IEEE International Conference on Industrial Technology (ICIT)*, pages 284–291.

[Martínez-Forero et al., 2010] Martínez-Forero, I., Peláez-López, A., and Villoslada, P. (2010). Steady state detection of chemical reaction networks using a simplified analytical method. *PloS one*, 5(6).

[Mason et al., 2011] Mason, J., Stupl, J., Marshall, W., and Levit, C. (2011). Orbital debris–debris collision avoidance. *Advances in Space Research*, 48(10):1643–1655.

[Mechtly, 1964] Mechtly, E. (1964). *The International System of Units: Physical Constants and Conversion Factors*, volume 7012. Scientific and Technical Information Division, National Aeronautics and Space Administration.

[Mehrholz et al., 2002] Mehrholz, D., Leushacke, L., Flury, W., Jehn, R., Klinkrad, H., and Landgraf, M. (2002). Detecting, tracking and imaging space debris. *ESA bulletin*, 109.

[Michalska and Mayne, 1995] Michalska, H. and Mayne, D. Q. (1995). Moving horizon observers and observer-based control. *IEEE Transactions on Automatic Control*, 40(6):995–1006.

[Minvielle, 2002] Minvielle, P. (2002). Tracking a ballistic re-entry vehicle with a sequential monte-carlo filter. In *IEEE Aerospace Conference Proceedings*, volume 4.

[Moe et al., 1995] Moe, M. M., Wallace, S. D., and Moe, K. (1995). Recommended drag coefficients for aeronomic satellites. *The Upper Mesosphere and Lower Thermosphere: A Review of Experiment and Theory*, pages 349–356.

[Moraal and Grizzle, 1995] Moraal, P. and Grizzle, J. (1995). Observer design for nonlinear systems with discrete-time measurements. *IEEE Transactions on Automatic Control*, 40(3):395–404.

[Morrison, 2010] Morrison, F. A. (2010). Data correlation for drag coefficient for sphere. *Michigan Technology University, Houghton, MI.*

[Morrison, 2012] Morrison, F. A. (2012). Space debris reentry hazards. *Scientific & Technical Subcommittee of the United Nations Committee on the Peaceful Uses of Outer Space.*

[Musso et al., 2001] Musso, C., Oudjane, N., and Le Gland, F. (2001). Improving regularised particle filters. In *Sequential Monte Carlo methods in practice*, pages 247–271. Springer.

[Nachbar, 2013] Nachbar, J. (2013). The inverse function theorem in $\mathbb{R}^n$. Technical report, Washington University in St. Louis.

[NASA, 2012] NASA (2012). Orbital debris frequently asked questions. Available at `http://orbitaldebris.jsc.nasa.gov/faqs.html`.

[Park and Lee, 2001] Park, S.-T. and Lee, J. G. (2001). Improved Kalman Filter design for three-dimensional radar tracking. *IEEE Transactions on Aerospace and Electronic Systems*, 37(2).

[Qu and Hahn, 2009] Qu, C. C. and Hahn, J. (2009). Computation of arrival cost for moving horizon estimation via unscented Kalman filtering. *Journal of Process Control*, 19(2):358–363.

[Rao, 2000] Rao, C. (2000). Moving horizon strategies for the constrained monitoring and control of nonlinear discrete-time systems. Technical report, Ph.D. dissertation, University of Wisconsin-Madison.

[Rao et al., 2003] Rao, C., Rawlings, J., and Mayne, D. (2003). Constrained state estimation for nonlinear discrete-time systems: stability and moving horizon approximations. *IEEE Transactions on Automatic Control*, 48(2).

[Rawlings and Bakshi, 2006] Rawlings, J. B. and Bakshi, B. R. (2006). Particle filtering and moving horizon estimation. *Computers & chemical engineering*, 30(10).

[Rengaswamy et al., 2013] Rengaswamy, R., Narasimhan, S., and Kuppuraj, V. (2013). Receding horizon nonlinear Kalman Filter for state estimation. *IEEE Transactions on Automatic Control*, 58(8).

[Ristic et al., 2004] Ristic, B., Arulampalam, S., and Gordon, N. (2004). *Beyond the Kalman filter: Particle filters for tracking applications*. Artech house.

[Ristic et al., 2003] Ristic, B., Farina, A., Benvenuti, D., and Arulampalam, M. S. (2003). Performance bounds and comparison of nonlinear filters for tracking a ballistic object on re-entry. *IEEE Proceedings-Radar Sonar Navigation*, 150(2).

[Romanenko and Castro, 2004] Romanenko, A. and Castro, J. A. A. M. (2004). The unscented filter as an alternative to the ekf for nonlinear state estimation: a simulation case study. *Computer and Chemical Engineering*, 28(3).

[Sang et al., 2013] Sang, J., Bennett, J. C., and Smith, C. H. (2013). Estimation of ballistic coefficients of low altitude debris objects from historical two line elements. *Advances in Space Research*, 52(1):117–124.

[Schoenenberger et al., 2009] Schoenenberger, M., Dyakonov, A., Buning, P., Scallion, W., and Norman, J. V. (2009). Aerodynamic challenges for the mars science laboratory entry, descent and landing. *AIAA*, 2.

[Simon, 2010] Simon, D. (2010). Kalman filtering with state constraints. A survey of linear and nonlinear algorithms. *Control Theory Applications, IET*, 4(8).

[Smits and Dussauge, 2006] Smits, A. J. and Dussauge, J.-P. (2006). *Turbulent Shear Layers in Supersonic Flow*. Springer, New York, NY.

[Sui et al., 2010] Sui, D., Johansen, T., and Feng, L. (2010). Linear moving horizon estimation with pre-estimating observer. *IEEE Transactions on Automatic Control*, 55(10).

[Suwantong et al., 2012] Suwantong, R., Bertrand, S., Dumur, D., and Beauvois, D. (2012). Space debris trajectory estimation during atmospheric reentry using moving horizon estimator. In *51th IEEE Conference on Decision and Control*.

[Suwantong et al., 2014] Suwantong, R., Bertrand, S., Dumur, D., and Beauvois, D. (2014). Moving Horizon Estimation with Pre-Estimation (MHE-PE) for 3D Space Debris Tracking during Atmospheric Re-entries. In *2014 IEEE 53rd Annual Conference on Decision and Control (CDC)*.

[Suwantong et al., 2013] Suwantong, R., Bui Quang, P., Dumur, D., Beauvois, D., and Bertrand, S. (2013). Robustness analysis of a moving horizon estimator for space debris tracking during atmospheric reentry. *52th IEEE Conference on Decision and Control*.

[Ungarala, 2009] Ungarala, S. (2009). Computing arrival cost parameters in moving horizon estimation using sampling based filters. *Journal of Process Control*, 19(9):1576–1588.

[Von Neumann and Goldstine, 1947] Von Neumann, J. and Goldstine, H. H. (1947). Numerical inverting of matrices of high order. *Bulletin of the American Mathematical Society*, 53(11):1021–1099.

[Zavala, 2008] Zavala, V. (2008). A fast moving horizon estimation algorithm based on nonlinear programming sensitivity. *Journal of Process Control*, 18.

[Zhang et al., 2012] Zhang, W., Su, H., Zhu, F., and Yue, D. (2012). A note on observers for discrete-time lipschitz nonlinear systems. *IEEE Transactions on Circuits and Systems II: Express Briefs*, 59(2).

[Zolfagharifard, 2014] Zolfagharifard, E. (2014). Available at `http://www.dailymail.co.uk/sciencetech/article-2596500/Space-station-sidesteps-space-junk-again.html`.

Résumé

L'estimation de trajectoires de débris spatiaux pendant la rentrée atmosphérique est un défi majeur pour les prochaines années, renforcé par plusieurs projets liés à l'enlèvement de débris établis par des agences spatiales de plusieurs pays. Cependant, ce problème s'avère complexe du fait des erreurs de modèle et des difficultés d'initialisation des algorithmes d'estimation induites par une mauvaise connaissance de la dynamique des débris suite à leur désintégration pendant la phase de rentrée atmosphérique. Tout estimateur choisi doit donc être robuste vis-à-vis de ces facteurs. L'estimateur à horizon glissant (MHE) est reconnu dans la littérature pour être robuste vis-à-vis d'erreurs de modèle et de mauvaise initialisation, et les travaux de thèse ont montré qu'il était adapté en termes de performances à la problématique de l'estimation des débris en phase de rentrée. En revanche, il se fonde sur une stratégie d'optimisation qui requiert de fait un temps de calcul important. Pour pallier ce problème, une nouvelle structure d'estimation à horizon glissant a été développée, impliquant un temps de calcul faible nécessaire à l'application envisagée. Cette stratégie, appelée « estimateur à horizon glissant avec pré-estimation (MHE-PE)», prend en compte les erreurs de modèle via un estimateur auxiliaire, plutôt que de chercher à obtenir les estimées du bruit d'état sur l'horizon d'estimation, comme le fait la structure de l'estimateur MHE standard. Un théorème garantissant la stabilité de la dynamique de l'erreur d'estimation du MHE-PE a par ailleurs été proposé. Enfin, les performances de cette structure dans le cadre de l'estimation en trois dimensions des trajectoires de débris pendant la phase de rentrée se sont avérées meilleures que celles observées avec des estimateurs classiques. En particulier, sans dégrader la précision et la convergence de l'estimation, l'estimateur MHE-PE requiert moins de temps de calcul du fait du nombre réduit de paramètres à optimiser.

Abstract

Space debris tracking during atmospheric re-entries will be a crucial challenge in the coming years, emphasized through many projects on space debris mitigation established by space agencies worldwide. However, this problem appears to be complex, due to model errors and difficulties to properly initialize the estimation algorithms, as a result of unknown dynamics of the debris and their disintegrations during the re-entries. A-to-be used estimator for this problem must be robust against these factors. The Moving Horizon Estimator (MHE) is known in the literature to be robust to model errors and bad initialization, and the PhD work has proved its ability to satisfy performances required by the debris tracking during the re-entries. However, its optimization-based framework induces a large computation time. To overcome this, a new MHE structure which requires smaller computation time than the classical MHE has been developed. This strategy, so-called "Moving Horizon Estimator with Pre-Estimation (MHE-PE)" takes into account model errors by using an auxiliary estimator rather than by searching for estimates of the process noise sequence over the horizon as in the classical strategy. A theorem which guarantees the stability of the dynamics of the estimation errors of the MHE-PE has also been proposed. Finally, performances of this structure in the context of 3D space debris tracking during the re-entries have been shown to be better than those obtained with classical estimators including the MHE. In particular, without degrading accuracy of the estimates and convergence of the estimator, the MHE-PE estimator requires smaller computation time than the MHE thanks to its small number of optimization variables.